International Workshop

New Models and Hydrocodes for Shock Wave Processes in Condensed Matter

Edinburgh, Scotland

19-24 May, 2002

AD NUMBER	DATE	DTIC ACCESSION NOTICE
1. REPORT IDENTIFYING INFORMATION		REQUES
A. ORIGINATING AGENCY Inst. of Chemical Physics, Russia		1. Put your on revers 2. Complete
B. REPORT TITLE AND/OR NUMBER New Models of Hydrocodes for Shock Wave Processes in Condensed Matter		3. Attach fo mailed t 4. Use unc informa 5. Do not o for 6 to
C. MONITOR REPORT NUMBER R&D 9218-AN-03		DTIC:
D. PREPARED UNDER CONTRACT NUMBER N68171-01-M-6177		1. Assign 2. Return

2 APPROVED FOR PUBLIC DISTRIBUTION

DISTRIBUTION UNLIMITED

PROCEEDINGS

DTIC Form 50
JUL 96

PREVIOUS EDITIONS ARE OBSOLETE

International Workshop

NEW MODELS AND HYDROCODES FOR SHOCK WAVE PROCESSES IN CONDENSED MATTER

Edinburgh, Scotland, 19-24 May, 2002

DISTRIBUTION STATEMENT A
Approved for Public Release
Distribution Unlimited

Edited by:

Vladimir Yu. Klimenko

High Pressure Center
Institute of Chemical Physics
Moscow, Russia

20020731 061

ORGANIZING COMMITTEE

Chairman	- Klimenko V Y	Russia
Vice-Chairman	- Coffey C S	USA
Vice-Chairman	- Rajendran A M	USA
Vice-Chairman	- Swift D C	UK

Birukov A L	Moscow, Russia
Bourne N K	Cranfield, UK
Chhabildas L	Sandia, USA
Field J E	Cambridge, UK
Gray I N	Aldermaston, UK
Haskins P J	QinetiQ, UK
Hertel E S, Jr	Sandia, USA
Hixson R S	Los Alamos, USA
Klimenko I Y	Moscow, Russia
Krivchenko A L	Samara, Russia
Kuropatenko V F	Chelyabinsk-70, Russia
Llorca F	Dijon, France
Makarov P V	Tomsk, Russia
Saurel R	Marseille, France
Sheffield S A	Los Alamos, USA
Urtiew P A	Livermore, USA

Sponsored by:

Russian Ministry of Industry, Science and Technologies
US Army Research Office

© 2002 High Pressure Center

SESSION "Numerical Methods for Hydrocodes"

Chairmen:
E. Caramana - Los Alamos National Laboratory, Los Alamos, USA
V. Kuropatenko - Russian Federal Nuclear Center, Chelyabinsk-70, Russia

Methods of Shock Wave Calculations

V.F. Kuropatenko

Russian Federal Nuclear Center - VNIITF, Snezhinsk (Chelyabinsk-70), Russia

The laws of conservation on the surface of a strong discontinuity have the form of non-linear equations relating different quantities on both sides of the discontinuity to its velocity. These equations are such that energy dissipates and entropy increases in the jump over the discontinuity even in an ideal medium. This is the main difference between shock waves and continuous solutions where entropy of each particle is conserved. Therefore, unlike methods for continuous motion, those for shock waves are to involve energy dissipation mechanisms.

Shock-wave calculation methods that differ in energy dissipation mechanisms are analyzed. Each method can be implemented with different difference schemes. The work discusses shock-wave methods and particular difference equations proposed by their authors, and compares approximation, stability, destruction, monotony and energy dissipation.

Compatible Hydrodynamics Algorithms: Discrete Vector Identities, and Conjugate Force/Work, Formulations

E. J. Caramana and M. J. Shashkov

Theoretical Division, Los Alamos National Laboratory, Los Alamos, USA

The principal goal of all numerical algorithms is to represent as faithfully and accurately as possible the underlying continuum equations to which a numerical solution is sought. However, in the transformation of the equations of fluid dynamics into discretized form important physical properties are either lost, or obeyed only to an approximation that often becomes worse with time. This is because the numerical methods used to form the discrete analog of these equations may only represent them to some order of local truncation error without explicit regard to global properties of the continuum system. Although a finite truncation error is inherent to all discretization methods, it is possible to satisfy certain global properties, such as conservation of mass, momentum, and total energy, to numerical roundoff error. These properties are often expressed/derived by means of the identities of vector calculus. The purpose of the body of work referenced herein is to show how equations can be differenced "compatibly" so that they obey the aforementioned properties ([1]-[9]). The important interconnection of vector identities and conservation laws in discrete form is stressed.

The basic theoretical ideas developed can be viewed as an extension to discrete form of the principle of virtual work and the principle of least action as they are known in classical mechanics. The principle of virtual work has been used in the finite element context to connect the discrete equations for a force and the work that it produces. The method of support operators gives results that can be shown to be directly obtainable from the discrete form of the principle of least action [1],[2]. The essential idea is that a force and the work that it produces should be conjugate quantities in discrete form just as they are in the usual Lagrangian or Hamiltonian formulation of classical mechanics. The mathematical relations that must be obeyed to achieve this are the discrete analogs of the vector identities (relations between the operators DIV, GRAD, and CURL). Numerical algorithms constructed in this manner are said to be "compatible", in that the forms of the discrete terms that compose them are not specified independently. They can be shown to mimic to the degree possible the properties of the continuum system [3], [4].

It is shown how conservation of total energy can be utilized as an interme- diate device to achieve this goal for the equations of fluid dynamics written in Lagrangian form, and with a staggered spatial placement of variables for any number of dimensions and in any coordinate system [5]. How the momentum equation and the specific internal energy equation can be derived from each other in a simple and generic manner by use of the conservation of total energy is given. This allows for the specification of forces that can be of an arbitrary complexity, such as derive from an artificial viscosity [6] or sub-zonal pressures [7]. These forces originate only in discrete form; nonetheless, the change in internal energy caused by them is still completely determined. This allows the flexibility needed to construct an "edge-centered" artificial viscosity that can distinguish between adiabatic and shock compression so that overheating does not occur for compressible, high speed flow simulations. The subzonal pressure forces are necessary in order to resist unresolved and spurious grid distortion that often destroy the calculations prematurely. Numerical examples of the effectiveness of these methods will be given for high speed flow calculations in three dimensions, and where it is also important to preserve the limit of one dimensional cylindrical, or spherical, flow [8],[9].

References

[1] A. P. Favorskii, "Variational-Discrete Models of Hydrodynamics Equations" , Differential Equations, 16 (1980) 834.

[2] A. A. Samarskii, V. F. Tishkin, A. P. Favorskii, and M. J. Shashkov, "Operational Finite Difference Schemes", Differential Equations, 17 (1981) 854.

[3] J. M. Hyman and M. J. Shashkov, "Natural Discretizations for the Divergence, Gradient, and Curl on Logically Rectangular Grids", Int. J. of Computers and Math. with Applications, 33 (1997) 81-104.

[4] M. J. Shashkov and J. M. Hyman, "The Orthogonal Decomposition Theorems for Mimetic Finite Difference Methods", SIAM J. Numer. Anal., 36 (1999) 788-818.

[5] E. J. Caramana, D. E. Burton, M. J. Shashkov, P. P. Whalen, "The Construction of Compatible Hydrodynamics Algorithms Utilizing Conservation of Total Energy", J. Comp. Phys. 146, 227-262 (1998).

[6] E. J. Caramana, M. J. Shashkov, P. P. Whalen, "Formulations of Artificial Viscosity for Multi-Dimensional Shock Wave Computations", J. Comp. Phys. 144, 70-97 (1998).

[7] E. J. Caramana, M. J. Shashkov, "Elimination of Artificial Grid Distortion and Hourglass-Type Motions by Means of Lagrangian Subzonal Masses and Pressures", J. Comp. Phys. 142, 521-561 (1998).

[8] E. J. Caramana, P. P. Whalen, Numerical Preservation of Symmetry Properties of Continuum Problems", J. Comp. Phys. 141, 174-198
(1998).

[9] E. J. Caramana, C. L. Rousculp, D. E. Burton, "A Compatible, Energy and Symmetry Preserving Lagrangian Hydrodynamics Algorithm in Three-Dimensional Cartesian Geometry", J. Comp. Phys. 157, 89-119 (2000).

Computation of Thermodynamics Parameters for Mixed Cells in Gas Dynamics

Yu.A.Bondarenko, Yu.V.Yanilkin

Russian Federal Nuclear Center - VNIIEF, Sarov (Arzamas-16), Russia

The paper studies methods to close difference equations of Lagrangian multifluid gas dynamics in mixed cells, where the method of concentrations or similar methods are used for the gas dynamics computation. Three methods are discussed: (1) the condition of equal constituent compressibility /1/, (2) the condition of equal constituent pressures + viscosities, and (3) a new method assuming equal constituent pressure increments.

It is assumed that in the mixed cells constituent volume concentrations β_i, densities ρ_i, internal energies e_i, and artificial viscosities q_i are assumed known for each of the constituents and the equation of state can be used to determine pressures P_i and sound speed c_i individually for each component numbered

i. Average cell pressures and viscosities used in the difference scheme to calculate the grid point accelerations are determined with formulas

$$\bar{P} = \sum_i \beta_i^n \xi_i^n P_i, \qquad \bar{P}_i = P_i^n - \tau\chi\left(c_i^n\right)^2 \rho_i^n div_i^n \overset{0}{U}{}^n,$$

where the unknowns are constituent "compressibilities" $div_i^n \overset{\psi}{U}{}^n$ and positive normalization factors ξ_i^n, which have to be introduced for the difference law of conservation of total energy to be met. The constituent compressibilities are related with the cell "compressibility" through the equation of conservation of volume

$$div^n \overset{\psi}{U}{}^n = \sum_i \beta_i^n div_i^n \overset{\psi}{U}{}^n.$$

The condition of equal compressibility, $div_i^n \overset{\psi}{U}{}^n = div_k^n \overset{\psi}{U}{}^n, \forall i,k$ gives $\xi_i^n = 1, \forall i$.

The condition of equal constituent pressures + viscosities, $\bar{P}_i + \bar{q}_i = \bar{P} + \bar{q}, \forall i$, also gives $\xi_i^n = 1, \forall i$, but these equations have to be solved simultaneously with the equations for constituent internal energies and the equation of conservation of volume with any iterative method.

The condition of equal constituent pressure increments, $\bar{P}_i - P_i^n = \bar{P}_k - P_k^n, \forall i,k$, is substituted on the linearization for the following equations (continuous analogs of the equations correspond to the features of the gas dynamics differential equation solutions in the vicinity of the different materials' interface):

$$\left(c_i^n\right)^2 \rho_i^n div_i^n \overset{0}{U}{}^n = \left(c_k^n\right)^2 \rho_k^n div_k^n \overset{0}{U}{}^n, \forall i,k,$$

which, simultaneously with the equations of conservation of volume, give explicit formulas

$$div_i^n \overset{\psi}{U}{}^n = \xi_i^n div^n \overset{\psi}{U}{}^n, \qquad \xi_i^n = \frac{1}{\left(c_i^n\right)^2 \rho_i^n} \cdot \frac{1}{\sum_k \frac{\beta_k^n}{\left(c_k^n\right)^2 \rho_k^n}}.$$

Results of test and methodological computations are presented implying that the method of equal constituent pressure increments is no worse in its accuracy than the method of equal constituent pressure + viscosity, but is much simpler in its implementation and more space-efficient. The assumption of equal constituent compressibility results in a considerably lower accuracy.

The paper focuses on explicit difference schemes with pre-computed pressure, but the methods used and principal results can be also extended to other difference schemes.

1. Bakhrakh S.M., Spiridonov V.F., Shanin A.A. A method for computing 2D axisymmetric gas-dynamical heterogeneous medium flows in Lagrangian-Eulerian variables// DAN SSSR. –1984. –V.276, No.4.

A Semi-Implicit Numerical Algorithm for a Rate-Dependent Ductile Failure Model

Marvin A. Zocher

Los Alamos National Laboratory, Los Alamos, NM, USA

When ductile metals are loaded to capacity, the following sequence of events is often observed. Localized regions of large deformation and associated plastic flow begin to form on a microscopic level. Then as the deformation proceeds, these localized deformation regions spawn damage in the form of voids, which with further loading grow and coalesce to produce cracks and ultimate material failure. The formation of these localized regions of deformation and damage formation introduces a physical length scale to the problem within which localized material softening occurs. The presence of this localized softening phenomenon has important ramifications for the analyst who wishes to predict the deformation and damage evolution process. In dynamic loading problems, the impact is manifested in an ill-posedness of the initial boundary value problem as the governing equations become elliptic. Classical

rate-independent numerical schemes applied to this problem are inadequate in that they exhibit an unacceptable mesh sensitivity.

To adequately model the above described processes, a numerical scheme must introduce an appropriate characteristic length scale to the mathematical formulation which will remove the potential numerical ill-posedness. This might be accomplished through the use of higher order temporal derivatives which are associated with rate-dependent methods, or through non-local schemes which introduce higher order spatial derivatives. A rate-dependent model that is formulated to address this issue has been proposed by Addessio and Johnson[1]. This model successfully removed the ill-posedness and exhibited reasonable predictive capability, but because of its explicit nature required a time step so small as to render the model impractical for some applications. The present work describes a semi-implicit reformulation of the model of Addessio and Johnson which allows for a much larger time step. The reformulation that is to be described was influenced by some unpublished work of Q.H. Zuo. The reformulation will be described and some results which demonstrate the model's predictive capabilities will be presented.

1. Addessio, F.L., and Johnson, J.N., "Rate-dependent Ductile Failure Model", Journal of Applied Physics, Vol. 74, No. 3, 1993, pp. 1640-1648.

A Method for Treatment of Dynamic Contact-Impact in Multi-Material Frameworks

D.L. Littlefield

Institute for Advanced Technology and
Texas Institute for Computational and Applied Mathematics
University of Texas at Austin, Austin, USA

Realistic and accurate treatment of contact-impact is crucial to a large class of problems that involve highly dynamic solid mechanics applications, such as vehicle crash dynamics, vulnerability and failure analysis, orbital debris simulation, and ballistic penetration. When appropriate, the Lagrangian finite element method is often the technique of choice for this group of problems, due to its natural ability to represent material boundaries and to apply the appropriate constraints there. However, many of these applications involve deformations that are well beyond the ability of Lagrangian finite elements to model them; the finite elements can develop large aspect ratios, twist, or even invert. A variety of alternative methods have been developed in an attempt to alleviate some of these difficulties; included among these are SPH and other meshless methods, Eulerian methods, and arbitrary Lagrangian-Eulerian (ALE) methods. Eulerian and ALE methods in particular have gained popularity over the past decade, especially in ballistic penetration and orbital debris simulations.

A complication that accompanies Eulerian or ALE approaches, however, is the introduction of multi-material elements into the computation, which makes the treatment of contact-impact difficult. Traditionally, the treatment of contact-impact in multi-material frameworks involves a series of approximations aimed at replacing the contacting materials in an element by an equivalent, single material – and the approximations used often have little or nothing to do with the actual physics taking place at the contact boundary. For example, for J_2-type materials the flow stress in a mixed material element is usually assumed to be a volume-weighted average of all J_2 materials in that element.

Approach

Consider the contact of two bodies defined by the volumes Ω_1 and Ω_2 as shown in the figure. The computational volume is denoted as Ω_d. The boundaries on the contacting bodies are denoted as $\Gamma_{c,1}$ and $\Gamma_{c,2}$, respectively. The equations governing the momentum conservation in the two bodies can be represented as

$$\int_{\Omega_i}\left[v\rho\left(\partial_t \mathbf{v}+\mathbf{w}\cdot\nabla\mathbf{v}\right)+\nabla v\cdot\sigma-\mathbf{b}\right]dx=\int_{\Gamma_{c,i}} vt\,ds \qquad \forall v\in V \tag{1}$$

where **v** and **w** are the material and advection velocities, respectively; σ the Cauchy stress, **b** is a body force, **t** is the traction along the contact boundary, and the subscript *i* takes on the value 1 or 2 for bodies 1 and 2, respectively. The contact traction **t** and displacement field **u** on the contact boundary must satisfy the constraints

$$\left.\begin{array}{c} g-\mathbf{u}\cdot\mathbf{n}\geq 0 \\ \mathbf{t}\cdot\mathbf{n}\leq 0 \\ (\mathbf{t}\cdot\mathbf{n})(g-\mathbf{u}\cdot\mathbf{n})=0 \end{array}\right\} \text{ on } \Gamma_c \tag{2}$$

where g is a gap function and **n** is the outward unit normal vector along Γ_c. Eqs. (1) and (2) do not represent a true variational statement of the contact problem, since these equa-tions can also be combined and expressed as a single variational inequality (e.g. see Kikuchi and Oden [1]). However, this is a convenient form for the development explicit contact relations.

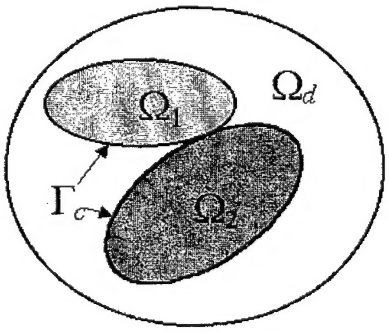

Figure 1. Representation of contact.

In this work a technique is des-cribed for treatment of contact-impact in a multi-material framework. This work differs from traditional approaches in that no mixed-element thermodynamic or constitutive models are used in the formulation. Instead, the governing equations in the form of Eq. (1) are solved for each material, with the appropriate traction integrals included. What arises from this is a set of coupled equations that are approximated by an uncoupled, reduced form. The traction and position along the contact boundary arise naturally from this formulation. Two-dimensional numerical examples for frictionless contact are shown which illustrate the superiority of this technique when compared to traditional mixed-element methods.

1. Kikuchi, N. and Oden, J. T., *Contact problems in elasticity: A study of variational inequalities and finite element methods*, SIAM Publications, Philadelphia (1988).

Hydrocode Modelling of Dynamic Friction Experiments

Andrew Barlow

Atomic Weapons Establishment, Aldermaston, UK

Most hydrocodes define the tangential force that acts across a material interface by assuming either that the material are locked (high friction) or allowed to slide freely over one another (zero friction). In reality the magnitude of the tangential force acting across the interface probably lies between these limits and a better model for use within a hydrocode may take the form of an interface constitutive law. The physics that this law would describe is often termed dynamic friction to distinguish that this refers to the interface dynamics when shock waves are present. The physics involved is however not well understood. If either of the materials involved are relatively weak then slip or zero friction is clearly a good approximation, however if both materials are strong then significant sensitivity can be observed to the interface treatment used in calculations.

This paper will discuss some of the work that has been carried out at AWE to investigate dynamic friction. Two types of dynamic friction experiments have been performed to both measure material slip and provide data for direct code and model comparison, and recovery experiments designed to improve understanding of the underlying physics of dynamic friction. The 2D multi-material Arbitrary Lagrangian Eulerian (ALE) code CORVUS [1] has been used to perform pre-shot and post shot calculations for the code comparison experiments. CORVUS is well suited to modelling such experiments as it allows two different interface treatments to be used. The slide line algorithms in CORVUS [2] provides a natural framework for the addition of interface physics such as dynamic friction, while the robust and accurate interface reconstruction technique [1,3] is well suited to modelling interfaces that may undergo high deformation. A simple empirical dynamic friction model has also been developed at AWE by the author and has been implemented in CORVUS to allow sensitivities to dynamic friction to be inferred [4].

The code comparison experiments that have been performed to date involve steel and aluminium plates in contact and under shock loading. Thin metal foils were placed within each plate and perpendicular to the common interface. These foils were then radiographed after the passage of a shock. The relative curvature of these foils gives an indirect measure of the frictional force, the amount of slip between the plates and the distribution of plastic work near to the interface. A similar approach has also at LANL in dynamic friction experiments performed by Hammerberg et al [5]. However, as the LANL experiments employed a pulsed power drive they have been limited to small target sizes. In contrast the AWE experiments [6] employ a high explosive drive and use flash X-ray radiography and so can employ larger target geometries, which should improve the resolution that can be obtained.

An example CORVUS calculation of one of the dynamic friction experiments that has been performed is given below. Figure 1 shows the initial t=0 μs computation mesh and Figure 2 shows the ALE mesh at t=25.0 μs when the radiograph was taken. Calculated fiducial positions are also presented in Figure 3 for the two limiting boundary conditions of true slip (zero friction) and a locked interface for 5.0 μs time intervals from 5.0 to 30.0 μs. This clearly indicates that at 25.0 μs when the radiograph was taken it should be possible to discriminate radiographically between these two limits.

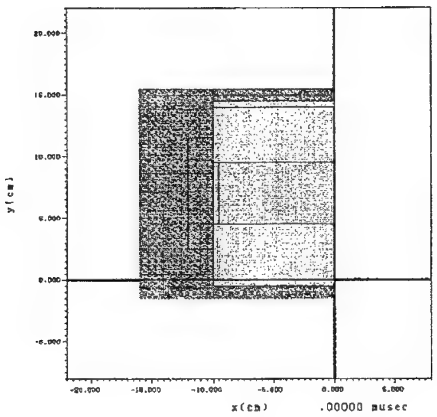

Figure 1. Initial mesh for CORVUS calculation of FN1/2 Dynamic Friction Experiment

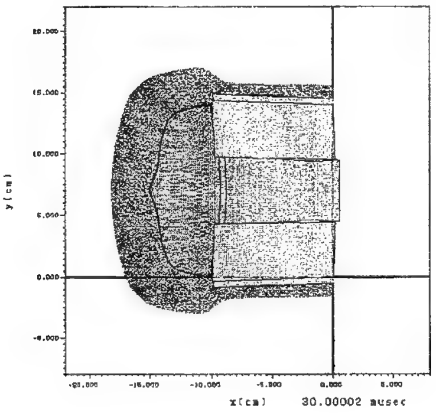

Figure 2. CORVUS calculation of FN1/2 Dynamic Friction Experiment at 25.0 μs.

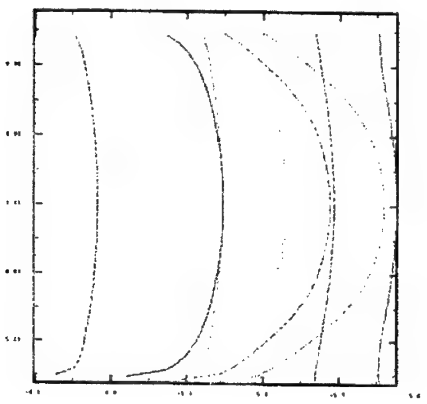

Figure 3. Calculated fiducial position for FN1/2 Dynamic Friction Experiment

The paper will present the calculational methodology that has been developed for modelling dynamic friction experiments using CORVUS ALE capability and discuss the strengths of the multi-material ALE code CORVUS for modelling dynamic friction experiments. The results to date from both the code validation and recovery experiments will also be presented and the former will be compared against CORVUS calculations. Future work will then be discussed including future experiments, plans for direct numerical simulation and possible refinements of the current simple empirical friction model.

References

1. A. J. Barlow, "ALE in CORVUS", Proceedings of New Models and Numerical Codes for Shock Wave Processes in Condesed Media, Oxford, 1997, pp.581-596.

2. A. J. Barlow and J. Whittle, "Mesh Adaptivity and Material Interface Algorithms", Chem. Phys. Reports, 2000, 19(2), pp.233-258.

3. A. J. Barlow, "A new Lagrangian scheme for multi-material cells", Proceedings ECCOMAS CFD 2001, University of Wales Swansea , 2001.

4. A. J. Barlow, "Friction in CORVUS a 2D ALE code", Proceedings of the 22nd International Symposium on Shock Waves, Imperial College, London, 1999, pp. 653-657.

5. J. E. Hammerberg, G. A. Krala, D. M. Oro, R. D. Fulton, W. E. Anderson, A. W. Obst, H. Oona, J. Stokes "A PEGASUS Dynamic Liner friction Experiment.", Shock Compression of Condensed Matter – 1999, p.1217.

6. R. E. Winter., P. Taylor., D. J. Carley, A. J. Barlow, H. Pragnell, "Strain Distribution at High Pressure, High Velocity Sliding Interfaces.", Proceedings of the American Physical Society meeting on materials under high strain rate, Atlanta, USA, 2001.

On Rules for Grid Motion in 3D ALE Codes

Gabi Luttwak

RAFAEL, Haifa, Israel

The rules of grid motion in three-dimensional Arbitrary Lagrangian Eulerian (ALE) codes[1-5] are discussed. Techniques for both grid smoothing and dynamic adaptive mesh refinement are considered. Looking at the motion of interface points, we look for the conditions when it is necessary to pass from

single material ALE to multi-material ALE calculations. While, some of the results would apply also for general connectivity, the actual examples shown used blocks of structured IJK mesh and were carried out in Autodyn-3D with additional external routines.

In an ALE code the grid points can move in any prescribed way. Any advantage the ALE technique might have on a purely Lagrangian, or multi-material Eulerian calculation depends on the right choice of the grid motion. This freedom can be exploited to achieve several goals. The most common purpose is to prevent mesh deformation of an otherwise Lagrangian grid. In the original ALE codes[1], boundary points were left moving with their material velocity following the position of the interfaces. This is equivalent to an authomatic and continuous rezoning of a Lagrangian calculation. However, when the boundary surfaces get distorted, such a calculation will obviously fail. In the multimaterial ALE technique[2-4], the position of interface points can also be adjusted. The boundary surfaces will cut through the zones. Several materials may share the same zone, and like in multi-material Eulerian codes, the challenge is to adequately follow such an interface. With the right ALE grid motion prescription, the advection terms will be much smaller than in a pure Eulerian calculation. Additionally, the ALE grid motion can help us to obtain a finer mesh in regions of interest[2,5], and to pass with a continuous mesh[3] from an almost Eulerian to an almost Lagrangian calculation.

A good computational mesh should have convex cells, so that it is reasonable to estimate the values inside a zone by interpolating the corresponding vertex values. An orthogonal mesh produces convex zones. The solution of the Laplace equation ($\nabla^2 f = 0$) generates orthogonal meshes. Solving the Laplace equation by iterations moves each zone toward an weighted average of its neighbors:

$$(1) \qquad \tilde{r}_k = \frac{\sum_{i=1}^{n} \omega_i r_i}{\sum_{i=1}^{n} \omega_i}$$

At singular points or near large curvatures at a boundary the Laplace solution may produce zones with decreasing mesh size. In an explicit scheme, the time step depends on the size of the smallest zone. This size should be determined only by the required resolution of the problem. Solving a Poisson equation ($\nabla^2 f = Q$), with appropiate source terms, Q, can prevent this thrinking in the size of the zones. On the other hand, these source terms can be also used to produce finer meshes in regions of interest. Alternatively we can directly control the mesh shape and size by altering the definition of the weights ω in (1).

The ALE grid motion prescription should be flexible. For problems involving only small material deformations the calculation should remain Lagrangian. For larger deformations, interior points are moved toward an weighted average of their neighbor positions, while the ALE grid motion will only move boundary points on the boundary itself. In the normal direction these points retain their material velocity. This way, the boundary surface remains fitted to the mesh. However, as the zones near the boundaries deform further or they limit the time step, the boundary points are moved toward the average position of their neighbors on both sides of the interface. At this stage, the boundary surface starts to cut through the zones of the mesh and a full multi-material ALE calculation is required.

References

1. Hirt C.W., Amsden A. A. ,Cook J. L., J.Comp.Phys., **14**, p.227,(1974)

2. Luttwak G., "Numerical simulation of jet formation using an adaptive grid in the multi-material ALE code, MMALE", p45 in Proc. of the 3rd HDP (High dynamic Pressure) Symp., LaGrande Motte, France, (1989)

3. Luttwak G., Florie C. , Venis A. ,"Numerical Simulation of Soft Body Impact", Shock Compression of Condensed Matter-1991, Schmidt S.C. et al Eds, p.999 , (1992)

4. Peery J. S.,Caroll D.E. ,"Multimaterial ALE Methods in Unstructured Grids", Comp.Meth.Appl.Mech.Eng.**187,** P.591,(2000)

5. Brackbill J.U.,Saltzman J. S. , J.Comp.Phys, **46**, p.185, (1982)

6. Luttwak, G., Cowler, M. S., "Advanced Eulerian Techniques for the Numerical Simulation of Impact and Penetration, using AUTODYN3D", Proc. 9th Int. Symposium on "Interaction of the Effects of Munitions with Structures", Berlin, May 1999

Adaptive Mesh Refinement in the CTH Shock Physics Hydrocode

D.A. Crawford*, P.A. Taylor*, and E.S. Hertel**

**Computational Physics and Simulation Frameworks Department*
***Thermal and Reactive Processes Department*
Sandia National Laboratories, Albuquerque, USA

Adaptive mesh refinement (AMR) has been widely hailed for improving computational resolution when resources are limited and has been used for hyperbolic problems on an experimental basis for years. For a mature Eulerian multi-material shock-physics code family like CTH and its predecessors, adaptivity is considered a natural next step in code development. It is a capability that allows full exploitation of today's limited computational resources and efficient use of tomorrow's substantial resources. Here we report on recent code development activity that is implementing an adaptive mesh refinement strategy in CTH otherwise known as AMRCTH.

In order to achieve adaptivity yet retain the man-years of effort that have been expended on the development of physics routines, the refinement is block-based, where each block consists of a small patch of cells. The refinement is isotropic with a maximum 2:1 resolution difference across block boundaries. Blocks are not allowed to overlap. In multiprocessor AMRCTH calculations, blocks are dynamically load-balanced among processors and CPU loading is optimized.

Block-based AMR appears to be a practical extension to CTH. At least a factor of three improvement of performance and memory utilization is achievable and, there is evidence of improved scaling for large problems (Fig. 1). Two-dimensional problems begin to scale as if they were 1.5D and three-dimensional problems begin to scale as ~2.4D.

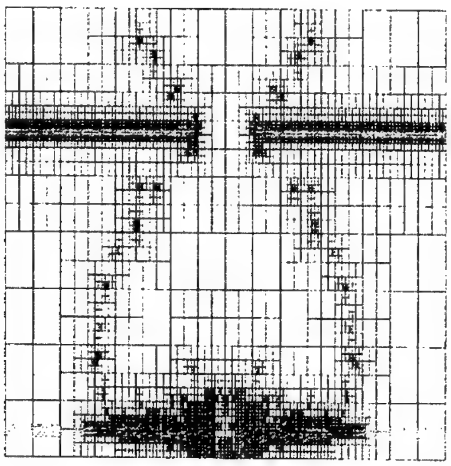

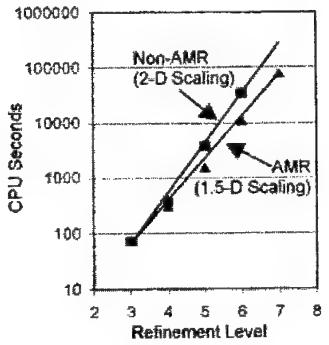

Figure 1. A two dimensional calculation of a copper ball striking a steel bumper shield. On the left, the outline of each block (6x12 cells per block) is shown. To perform this calculation without AMR would require 1.2 million cells. Including ghost cells, this seven level AMR calculation requires 277,312 cells. On the right, the CPU time required to perform this calculation with and without AMR at 5 different refinement levels is shown (each increment in refinement level equals a factor of two in linear resolution). Evidence of improved problem scaling is shown.

A "Dual Particle" Meshfree Discretization for Solid Dynamics

Larry Libersky

Los Alamos National Laboratory, Los Alamos, USA

We will give an update on our work on a meshfree particle method that we call Dual Particle Dynamics. A brief history of meshfree methods will be given, focusing on Smoothed Particle Hydrodynamics. The potential of meshfree methods for problem solving is huge, but so are the problems incurred by discarding the mesh.

We will talk about difficulties that have been overcome and those that remain. Specifically, we will address questions of stability. It is shown that DPD and SPH are conditionally stable for Eulerian kernels and linear fields. This result is important because it is highly desirable to move and change neighbors where the material deformation is large. For higher dimensions (than 1D), stability for general neighborhoods is shown to require a two-step update, such a predictor-corrector.

Performance of DPD on several test problems is presented.

A Method for Computation of Heat Conduction with Taking into Account Inter-Material Heat Exchange Inside Mixed Cells

Yu.A.Bondarenko, A.R.Shagalieva, Yu.V.Yanilkin

Russian Federal Nuclear Center - VNIIEF, Sarov (Arzamas-16), Russia

The paper proposes a new multicomponent heat conduction method that does not assume equal constituent temperature, but implies that in mixed cells inter-constituent heat exchange occurs according to the same heat conduction laws as for average energy of ordinary heat conduction.

The principal idea is division of the heat conduction process to two scales, the principle of splitting by physical processes is used for separately accounting the two scales. The "large" scale, inter-

cell heat exchange, is included in the ordinary implicit 2D difference scheme. Here (at the first stage) an ordinary implicit difference scheme is used, where average mixed cell parameters are calculated with any appropriate method.

Then the "small" scale heat exchange works, i.e. heat exchange among the constituents inside mixed cells, which uses heat flows through cell sides calculated at the first stage as input data. Properly speaking, it is only here (at the second stage) that the individual temperatures of the mixed cell constituents are calculated.

At the second stage of the program the flows through cell sides are distributed among the constituents, and the problem of distribution of the energy increment due to heat conduction among the constituents present in the mixed cells is solved independently in each mixed cell. This process is approximated with the following system of two equations (for two constituents in one cell):

$$M_1 \frac{e_1^{n+1} - e_1^n}{\tau} = S_{12}\chi_{12} \frac{U_2^{n+1} - U_1^{n+1}}{L_{12}} + \sum_{j=1}^{4} S_{1,j} q_{1,j} + M_1 f_1;$$

$$M_2 \frac{e_2^{n+1} - e_2^n}{\tau} = -S_{12}\chi_{12} \frac{U_2^{n+1} - U_1^{n+1}}{L_{12}} + \sum_{j=1}^{4} S_{2,j} q_{2,j} + M_2 f_2.$$

Here M_i denotes constituent masses; S_{12} is constituent contact area; χ_{12} is average heat conductivity for constituent heat exchange, L_{12} is the distance between the centers of the volumes occupied by the constituents: $S_{k,j}$ is area on the side numbered j=1,...,4 of a given quadrangular cell "occupied" by the constituent numbered k=1,2; $q_{k,j}$ is heat flux coming through the side numbered j=1,...,4 of a given cell into the volume occupied by the constituent numbered k=1,2; e_k^n is internal energy of constituent unit mass at time t^n; $e_k^{n+1} = E_k(U_k^{n+1})$ is internal energy of constituent unit mass at time t^{n+1}; f_k is energy source. The system is solved to find new temperatures and new constituent energies, which completes the computation of one timestep.

Results of test and methodological computations are given. Accuracy of the proposed method is shown to be considerably higher than that of the method assuming equal temperatures of the constituents inside a mixed cell.

A New Slide-Line Algorithm for Lagrangian Hydrocodes

E. J. Caramana

Los Alamos National Laboratory, Los Alamos, NM, USA

A new formulation of the long-standing slide line approach to handling material interfaces in Lagrangian hydrocodes is presented. The corner mass/force representation is used to construct the effective force across a slide line/surface in a natural manner that maintains only one scalar mass in the momentum equation. This allows friction forces to be included in a simple manner since the proper normal and tangential surface force needed to complete the one-sided momentum equation is automatically computed. The only information needed from each opposite side is the location of the single nearest neighbor point making elaborate neighbor searches, or ghost cell constructions, unnecessary.

The interpenetration problem is solved by defining the normal velocity to a surface point (no master/slave or penalty functions are needed). This normal velocity is found from the time advanced momentum equation but must be made consistent across the surface by means of a 1D inelastic collision. Forces of constraint are then implicitly added (but never directly calculated) when the coordinates are advanced in time; here it is required that the vector point-velocity be consistent with the scalar normal velocity using the time advanced coordinates to calculate new surface normals. This constraint produces a change in the direction, but not magnitude, of the vector velocity of all points on the slide surface. (This is iterated to convergence at roundoff level by an explicit line/surface iteration that converges quickly.)

Total energy is conserved to roundoff level; the partitioning of energy as well as the construction of "goodness" criteria are discussed.

Numerical examples are presented.

Implementation of Strength Models in the Eulerian Godunov Framework

I. Lomov

Lawrence Livermore National Laboratory, Livermore, USA

High order Eulerian Godunov methods are well known to give high quality solutions for compressible fluid dynamics problems [1]. Combination of this numerical approach with volume of fluid and interface reconstruction techniques has been shown to be successful for simulating multimaterial problems including liquids and solids when strength effects are insignificant [2].

An Eulerian frame of reference provides the significant advantage of relative ease of incorporation of adaptive mesh refinement (AMR) into the algorithm [3]. AMR provides significant speed advantages for a wide range of problems where a large region needs to be calculated, and it is necessary to resolve small portions with very fine zoning. Considering all these factors, it was very attractive to apply these methods for the solution of solid mechanics problems where strength effects are important. Several issues had to be resolved during implementation.

First, the full system of equations had to be formulated as a first order system of hyperbolic partial differential equations. On top of the usual conservation laws for mass, momentum and energy, and the equations for volume fraction, there need to be equations for the calculation of elastic shear deformation and history dependant variables like porosity, plastic strain, damage, etc.

A second issue is that the full system can be written in conservative form, required for finite-volume methods, only at additional cost (for example, consideration of the full nonsymmetric deformation tensor and complementary plastic deformation tensor). However, highly nonlinear behavior of shear stresses (like shear shock waves and rarefaction fans) is very rare and a divergent formulation does not have simple and clear physical meaning. Hence, our approach is as follows: We store the symmetric unimodular tensor of elastic distortional deformation [4]; then we calculate the velocity gradient tensor (based on the Riemann solver described below) and update elastic distortional deformation tensor in nondivergent formulation.

A third difference from the Eulerian formulation for fluids is that the plasticity equations have right parts, which could be singular for a rate-independent formulation of plasticity. We describe inelastic behavior with a general viscoelastic Maxwell model. Rate-independent behavior can be expressed as a limit of this model.

Characteristics analysis and the Riemann solver play a significant role in the accuracy of Godunov codes. Characteristics tracing for the full system of equations, including shear stresses, was performed similar to [1,2]. The Riemann solver calculates shear waves in the acoustic approximation and longitudinal waves in a manner similar to [1] without compromising the quality of solution for strong shock waves and rarefaction fans.

Multimaterial aspects were implemented similar to [2], distributing and averaging properties within multimaterial cells based on the bulk modulus of the corresponding material. The velocity gradient required for updating shear deformations is distributed between materials based on the shear modulus. The shear stress is also averaged based on the shear modulus. Some modifications to the algorithm in [2] were made to handle interfaces between materials with large density differences (like gases and solids).

The described implementation of material strength was used to simulate rate-dependent inelastic behavior in the framework of porosity and general plasticity models, including effects of pressure and strain dependent hardening, Lode angle, thermal and structural softening, bulking, dilatancy, shear enhanced compaction and fluid-filled porosity.

This approach was implemented in the Eulerian Godunov framework "BoxLib" [5] which provides transparent capabilities for adaptive mesh refinement and parallel execution. A number of problems was solved, including wave propagation, surface explosions, and impacts. Results of these simulations will be presented at the conference.

References

[1] Colella P., Glaz H. Efficient Solution Algorithms For The Riemann Problem For Real Gases. *J Comput Phys*, **59** (2), 264-289, 1985

[2] Miller G.H., Puckett E.G. A high-order Godunov method for multiple condensed phases. *J Comput Phys*, **128** (1), 134-164, 1996

[3] Berger M.J., Colella P. Local Adaptive Mesh Refinement for Shock Hydrodynamics. *J Comput Phys*, **82**(1), 64-84,1989

[4] Rubin M.B., Vorobiev O.Y., Glenn L.A. Mechanical and numerical modeling of a porous elastic-viscoplastic material with tensile failure. *Int J Solids Struct*, **37** (13), 1841-1871, 2000

[5] Rendleman C.A., Beckner V.E., Lijewski M., Crutchfield W.Y., Bell J.B., Parallelization of Structured, Hierarchical Adaptive Mesh Refinement Algorithms. *Computing and Visualization in Science*, 3, 2000

Session "Hydrocodes and Applications"

Chairmen:
A. Barlow - Atomic Weapons Establishment, Aldermaston, UK
D. Benson - University of California, San Diego, USA

Application of Eulerian Hydrocodes to Mesoscale Material Modeling

David J. Benson

Dept. of Mechanical and Aerospace Engineering
University of California, San Diego, CA, USA

Eulerian hydrocodes are useful for modeling mesoscale phenomena in materials because of their ability to accommodate large strains, the change in morphology due to material failure, and the introduction of new materials due to chemical reactions and phase changes. Applications in materials science and mechanics include void growth and coalescence, shock compression of powders, detonation in polymer-bonded explosives, and the synthesis of intermetallics through shock-initiated chemical reactions. Example calculations will be presented with a discussion of the challenges to Eulerian hydrocodes presented by these applications.

Adaptation of EGAK Code System to Simulation of 2D Flows Using an Adaptively Embedding Fragmented Grid

Yu.V. Yanilkin, S.P. Belyaev, V.I. Tarasov, Yu.A. Bondarenko, A.V. Gorodnichev, L.I. Degtyarenko, N.A. Hovrin, A.L. Stadnik, A.V. Volgin, G.V. Zharova

Russian Federal Nuclear Center - VNIIEF, Sarov (Arzamas-16), Russia

The paper describes the 2D code system with irregular dynamic data structure for simulating different-scale and concurrent physical processes in a multicomponent medium. Numerical techniques using both typical regular grids and adaptively embedding fragmented grids are being developed within the code system. The fragmented grid is created by multi-level fragmentatuion of movable quadrangular computational cells of the main grid in the vicinity of specific features, whose simulation requires considerably finer grids. The idea of the fragmentation is that each cell is divided into 4 smaller ones by straight lines going across the middles of the mother cell sides. These smaller cells can be further divided using the same algorithm. Thc maximum permissible fragmentation level is 5. Codes for automatic creation and deletion of fragmented grids during the specific feature motion in space are developed.

The code system along with relevant numerical codes using the fragmented grids allows simulation of problems requiring higher accuracy of description of a number of spatially small-scale specific features, such as a shock wave, interfaces, HE and gas mixture burning and detonation fronts, turbulent mixing, material fragmentation, etc. In the code system, each of above features can be simulated using its own grid, that is for each feature its own level of fragmenting the main grid can be given.

The code system features are as follows:

- use of the arbitrary Lagrangian-Eulerian (ALE) approach when developing computational modules;
- use of EGAK code system techniques [1] as a basis for further development of new numerical methods basing on fragmented grids; full succession of grids is provided, if a regular computational grid is used;
- use of an object-oriented approach and the C++ programming language.

The paper discusses principal features of the difference schemes for the fragmented grid and presents results of several gas-dynamic flow computations that include elastic-plastic properties of materials and HE detonation using the fragmented grid and compares them to analytical solutions and results of computations on the regular grid. Estimates of the C++ code performance are also presented in comparison with the Fortran-77 code.

1. Yanilkin Yu.V., Shanin A.A., Kovalev N.P. *et al.* EGAK code system for 2D multicomponent flow simulations. VANT, Ser.: MMPhP, Iss.4, 1993, pp.69-75.

New Generation Hydrocode Developments including Parallelisation for Heterogeneous Systems

C.J. Hayhurst, R.A. Clegg, M.S. Cowler

Century Dynamics Ltd. Horsham, West Sussex, UK

Computer simulations of nonlinear transient dynamic events such as impact, penetration and blast have become important tools for understanding and predicting the consequences of such events. Many real problems in this application area can often be approximated using 2D axial symmetry, thus enabling efficient simulation. Typically a practical/desired elapsed time for a hydrocode simulation would be of the order hours, and not usually more than two days. In many instances an axisymmetric approximation is insufficient and increasingly there is the need to simulate full three dimensional problems, often with complex geometry. Although the significant increase in computing power over recent years has helped to make such simulations a viable option, runtimes are often of order days, weeks or even months on the fastest single CPU's available. An approach to overcome this practical limitation of full three-dimensional simulation is to parallelize.

This paper provides an overview of the latest generation of features of the AUTODYN-3D code that facilitate parallelisation over homogeneous and heterogeneous, shared and distributed memory parallel systems. The object orientated nature of the algorithms allows the same basic coding to be used on many different parallel platforms including shared memory and distributed clusters of PC's running Windows NT/2000, Unix workstations and PC's running Linux. In particular, it is shown that good parallel performance can be achieved even on standard local area networks of PC's that can be found in most office environments - making efficient three-dimensional hydrocode simulations a practical and cost effective option for most users.

A series of benchmark calculations are presented highlighting the relative performance of AUTODYN-3D on various Windows NT/2000, Unix and Linux parallel systems. The main parameters influencing the efficiency of parallel hydrocode simulations will be highlighted and discussed.

Parallelization of 2D Gas Dynamics Problem Computation on Unstructured Grids on Distributed-Memory Computer System MP-3

R.A. Barabanov, O.I. Butnev, V.A. Pronin, I.D. Sofronov, S.G. Volkov, B.L. Voronin, B.M. Zhogov

Russian Federal Nuclear Center - VNIIEF, Sarov (Arzamas-16), Russia

Numerical computations with grid methods employ both regular grids, where information about computational data is stored as matrices, and irregular (unstructured) grids, in which that is stored as lists. Lagrangian algorithms and techniques have been developed to solve gas dynamics equations with difference methods both for regular [1-3] and irregular grids [4-6]. The irregular explicit free-Lagrangian technique MEDUZA [6] developed by VNIIEF Mathematics Division worked well at solution of gas-dynamical problems with complex-geometry initial and boundary conditions and severe shear flows [7,8]. The principal features of the technique are: all cell-centered grid values (both scalar and vector), a

variable difference template for numerical integration of differential equations and possibility to change the grid topology during the problem solution.

In this technique a set of grid points (nodes) are considered, which are assigned values of all thermodynamic and kinematics values to. The initial distribution of the points is given reasoning from initial and boundary conditions of the problem and from a priori considerations in regard to the occurring processes. For each point a set of its "neighbors" is specified basing on the Euclidean metric using triangulation method [6]. The point set with an established neighborhood correspondence generates the problem grid. An explicit free-Lagrangian code, which is an extension of code Meduza [6], was used to solve 2D gas dynamics equation system on the produced grid. Using a one-domain problem solution model leads to appearance of mixed cells on media interfaces, whose solution is sought using a multicomponent approach without explicit separation of the interface.

During the problem solution, at each timestep the neighborhood is re-specified basing on the Dirichlet principle, new points are removed or added, and grid functions are re-computed from the old grid to the new through their superposition.

Thus, the problem computation step can be conventionally divided into two phases: at the Lagrangian phase the grid state and grid values are computed using the explicit Lagrangian technique; at the Eulerian phase the neighborhood is re-specified, new points are removed or added, the grid is "expanded" by certain criteria, and then grid and grid values are re-computed.

The modern high-performance computers are multiprocessor computer systems with shared or distributed memory or combining the shared and distributed memory. Employment of computer power of hundreds or even thousands of processors for computation of a single problem is only possible, provided specialized algorithms and programs have been developed that not only ensure a high parallelization efficiency, but also are essentially free of crash. The code Meduza, by virtue of its irregularity and local regridding at each step, has the property of being essentially free of crash, even when computing complex eddy or shear flows. Moreover, by virtue of its explicit nature, the code is quite readily parallelizable.

The method of problem solution in the parallel mode uses domain geometry decomposition to fragments (problem subdomains with partial overlapping) and then computation of each fragment on its processor. Each fragment is covered with an irregular (unstructured) grid. In the fragment overlaps the grids are identical. A feature of code /6/ is performance of regridding, which can be necessary because of the need to change the "neighborhood" of the grid nodes basing on the Dirichlet principle. From the standpoint of parallel computations, this can lead to "transition" of the cells from one processor to another, i.e. to a decrease in the number of computed cells on one processor and increase on another (or others). Program implementation of the inter-processor cell migration is a fairly complicated problem and has to be paid a special attention to when developing a parallel program.

Upon the unstructured grid construction, identical points, triangles, and edges (intersecting part) appear in neighboring fragments on boundaries. Hereafter we refer to the fragment, in which the unstructured grid is formed, as a compact. The number of the processors determines the number of asynchronously operating branches. All compacts are processed by the same algorithm, each on its processor.

At the initial data computation phase the source domain decomposition is performed. The decomposition type and contact distribution by processors are given in the input flow. At each computational step the inter-processor data passing is performed using asynchronous communications by the principle of concurrent computation and communication. The computational step is composed of three phases, in each of which communication arrays are generated, data is transferred in accordance with the communication card, data is received, and the received data is analyzed. Moreover, the value of the computational step for the whole problem is computed with using a single global communication.

The presented program version implements the parallel algorithms for the Lagrangian phase computation, moving-apart, and grid value re-computation. The regriddings are performed only within one compact. It is planned that the parallel algorithm for regridding, point removal and addition, including with inter-processor point migration, would be implemented later on.

For testing the developed parallel program in order to assess the computation accuracy and parallelization efficiency, the problem of Richtmyer-Meshkov instability evolution [9, 10] was selected.

Taylor was the first to consider the interface gravitational instability for two fluids of different density moving from light fluid to heavy in the case, where acceleration is directed along the normal to

the interface [11]. The case, where the acceleration is of pulsed nature and, in particular, where the interface is driven by a shock wave, is considered by Richtmyer [9]. In [10] E.E.Meshkov presents results of the experimental study for instability of two gases interface passed through by SW. The two gases interface is found to be unstable, the interface perturbation increases linearly with time in the first approximation. The results of the experiments proved qualitatively agreeing with theory [9], however, it was impossible to detect finer effects predicted by Richtmyer because of a low resolution of the optical system. The measuring accuracy was noticeably improved through increasing the initial perturbation amplitude and image scale, and existence of weak oscillations in the perturbation growth rate was confirmed.

In Ref. [12] K.A.Meyer and P.J.Blewett present results of some numerical computations using Meshkov's experiments [10]. In particular, the program for solution of 2D gas dynamics problems in Lagrangian variables was used to study instability of two gases interface passed by SW. Setting up the problem appears in Ref. [12] concludes that the computed data agrees both with the linear theory of Richtmyer [9] and with the experimental data. The weak oscillations $\frac{da}{dt}$ predicted by Richtmyer were not estimated numericaliy, however the authors surmise the possibility to detect them at a finer analysis of the data.

The purpose of this paper is development of algorithms and a parallel program for solving 2D gas dynamics problems on an unstructured grids, demonstration of their serviceability, accuracy, and assessment of parallelization efficiency on distributed-memory computer system MP-3 [13].

The following conclusions are made from the results of the computations:

- when the points on the processor are more than 3000 in number, the parallelization efficiency is higher than 90%;
- the maximum efficiency of 92.5% is achieved on the 8-processor computer system MP-3 at the total point quantity 192*192=36864 and the "strips" decomposition by columns (i.e. at uniform distribution of mixed cells among the processors);
- for the considered problem the decomposition by columns is preferable, as when all the mixed cells are located on one processor, it is given a larger computational load (computation of mixed cells), which leads to its disbalance.

References

1. Sofronov I.D., Dmitriyev N.A., Dmitriyeva L.V., Malinovskaya E.V. A technique for computing 2D time-dependent gas dynamics problems in Lagrangian variables. IAM Preprint No.59. Moscow, USSR Academy of Sciences IAM, 1976.
2. Sofronov I.D., Dmitriyev N.A., Dmitriyeva L.V., Malinovskaya E.V. A technique for computing 2D time-dependent gas dynamics problems in Lagrangian coordinates// Theoretical fundamentals and designing of numerical algorithms for computational physics problems. Moscow, Nauka Publishers, 1979. Pp. 175-200.
3. Batalova M.V., Bakhrakh S.M., Vinokurov O.A. et al. System SIGMA for computing 2D gas dynamics problems// Proceedings, All-Union Seminar on Numerical Methods for Viscous Fluid Mechanics. Novosibirsk, Nauka Publishers, 1969. Pp. 283-288.
4. Sofronov I.D., Rasskazova V.V., Nesterenko L.V. The use of nonregular nets for solving two-dimensional nonstationary problems in gas dynamics //Numerical Methods in Fluid Dynamics Ed.by N.N. Yanenko, Ju.I. Shokin. M.:Mir Publishers. 1984. P.82-121.
5. I.D.Sofronov, V.V.Rasskazova, L.V.Nesterenko. Irregular grids in methods for computing 2D time-dependent gas dynamics problems// Issues of computer simulation, computational mathematics, and informatics. Moscow – Arzamas-16, 1994. Pp. 131-183.
6. Glagoleva Yu.P., Zhogov B.M., Kiryanov Yu.F. et al. Fundamentals of code MEDUZA for numerical computation of 2D time-dependent gas dynamics problems// Chisl. Met. Mekh. Splosh. Sredy. Novosibirsk, 1972, V.3, No. 2. Pp. 18-55.
7. Glagoleva Yu.P., Zhmailo V.A., Kiryanov Yu.F. et al. Formation of ring vortex at buoyancy of light gas in heavy// Chisl. Met. Mekh. Splosh. Sredy. Novosibirsk, 1974, V.5, No. 1. Pp. 38-52.
8. Glagoleva Yu.P., Malshakov V.D., Rodigin V.N. et al. Numerical solution to the problem of channel closure in

a wall under action of gas pressing on it// Chisl. Met. Mekh. Splosh. Sredy. Novosibirsk, 1976, V.7, No. 4. Pp. 48.

9. Richtmyer R.D. Taylor Instability in Shock Acceleration of Compressible Fluids. Communications on Pure and Applied Mathematics, vol.XIII, 1960, p.297-319
10. Meshkov E.E. Instability of two gases interface driven by shock wave. Izv. AN SSSR. Mekhanika Zhidkosti i Gaza, No.5, 1969, pp.151-158
11. Taylor J. The instability of liquid surfaces when accelerated in a direction perpendicular to their planes, I. Proc. Roy Soc., 1950, J. Lond. Ser. A, vol. 201, No. 1065, p.192
12. Meyer K.A., Blewett P.J. Numerical Investigation of the Stability of the Shock-Accelerated Interface between Two Fluids. The Physics of Fluids, vol.15, number 5, May 1972, p.753-759
13. Stepanenko S.A., Gusev V.A., Lyakishev A.M. et al. Multiprocessor computer systems MP-X-Y. In: Issues of computer simulation, computational mathematics, and informatics. Moscow – Arzamas-16, 1994. Pp. 101-103

The Code for Solution of Molecular Dynamics Problems at Parallel Computers with Distributed Memory

A.Yu. Aleynikov, R.A. Barabanov, O.I. Butnev, A.N. Bykov, R.A. Veselov, B.L. Voronin, N.S. Ganchuk, V.I. Delov, A.M. Erofeyev, V.A. Pronin, N.M. Rudko, A.A. Selezenev, S.I. Skrypnik

Sarov Open Computer Center, Sarov (Arzamas-16), Russia

Introduction

The report describes the method and the code for modeling of materials properties on the basis of the classical molecular-dynamic approach at highly parallel computational systems with distributed memory. The method and the code are oriented at solution of modeling problems of 3D particle ensembles over the wide range of atoms and molecules: from 10^3 to 10^6 –10^8. This requires high effectivity of the code both in memory and code operation speed.

Characteristic features of the code are:

- ✓ the code is run on MIMD-architecture distributed-memory parallel computers supporting interprocessor communications in accordance with the Standard MPI. This is validated by the code testing on a number of parallel computers;
- ✓ the code combines the grid method and Verlet method;
- ✓ developed methods for dynamic balancing of the processor load are used for uniform loading of the processors;
- ✓ problem dimensions: 2D and 3D;
- ✓ permissible domains of solution: coordinate parallelepiped set;
- ✓ crystal lattice types: body-centered (BCC) and face-centered (FCC), and diamond;
- ✓ boundary condition types: free surface, movable rigid wall, periodic boundary conditions; types of potentials: paired (Lennard-Jones, Morse) or unpaired (Stillinger-Weber).

Molecular Dynamics Parallel Code MDP-SOCC

Description of algorithm and optimization methods. Formally each particle (atom or molecule) is influenced by all particles of the ensemble being considered. However the interaction potential between two particles quickly tends to zero while the distance between them grows. To reduce the computations of almost zero interaction forces between the remote particles the r_{coff} parameter is introduced (the so-called cut-off radius). The comparison of this radius with the distance between particles allows computation of interaction force of the current particle only with particles, which are within r_{coff} radius. Nevertheless, computation of distance between each pares of particles (in case of pare potentials) causes huge computational costs and limits the allowable ensemble size to several thousands (tens of thousands particles). Presently the computations of interacting particles are reduced mainly through application of gridless methods (algorithms for development of Verlet lists or its versions), or grid methods.

Development of Verlet lists (lists of particles interacting with a current particle during a certain number of steps) causes the necessity of their storage and periodic update. If the lists are updated through search of all particle pares, this step will require computations, which according to square law will grow with growth of ensemble.

The grid approach is based on localization of interacting particles search zone. Decomposition of solution region into coordinate parallelepipeds (cells) with edge length a bit over r_{coff} allows limitation of search zone for the current particle of the given cell with particles of the given cell and in 3D case with particles of 26 neighboring cells. In this case the number of search operations for interacting particles is proportional to n^2, where n is the number of particles in a cell. Increase in ensemble size causes the increase in number of cells, while the number of particles in a cell is almost the same. Thus, the application of grid approach allows achievement of computations linear growth when increasing the ensemble size. On the other hand application of grid facilitates the solution of the problem of the geometric decomposition over processors. Using the data overlap (two layers of particles are simultaneously available on two neighboring processors) allows dividing computation steps and data exchange steps among processors. In doing this number of exchange steps is minimized. Besides there is a possibility to use asynchronous exchanges and combine computation with exchanges.

The report describes several ways to increase the code operation speed used by the authors.

Data decomposition over processors. Similarly to classic grid approach we will look for solution of the problem in a region of space, which is a parallelepiped with edges parallel to reference axis. Denote this region by Ω. Decompose the region Ω into cells – parallelepipeds with edges close to cut-off radius r_{coff}. When using the grid approach it seems most natural to use geometric decomposition when each processor must process a certain number of grid cells.

Depending on the geometry of region being calculated, the number of particles and processors, three ways of particles distribution over processors at the initial time moment are used: "lines", "columns", "cubes" (Fig. 1).

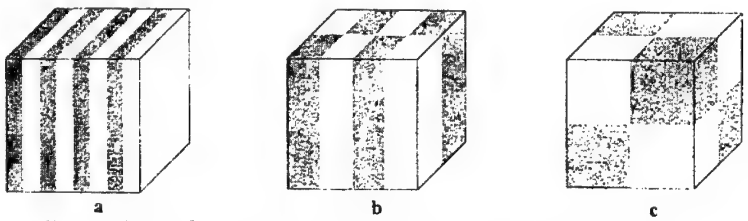

Figure 1. Types of geometric decomposition: a – "lines", b - "columns", c - "cubes".

Organization of parallel computations. To organize the parallel computations it is proposed to use the method of cell sets overlap on processors. The scheme of overlaps for 2D case is given in Fig. 2. The whole cell set on processor inwards is divided in four subsets:

- external cells,
- shell cells,
- preshell cells,
- internal cells.

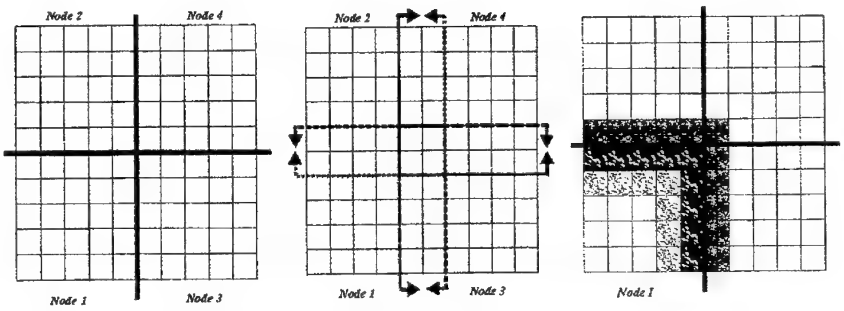

Figure 2. The scheme of overlaps organization for 2D case: a- cells decomposition over 4 processors, b- the scheme with one layer superposition, c- division of cell set a nod into 4 subsets.

The accuracy of the program developed was examined by a number of test problems (one-dimensional motion of 3D system of 7 atoms (the problem has analytical solution), compression of aluminum cluster, modeling of shock wave in aluminum cluster, collision of aluminum and iron clusters). The report contains the comparison of analytical and numerical results, as well as animation of clusters collision processes.

Examination of parallelization efficiency

The parallelization efficiency of the developed code was initially examined at Sarov Open Computer Center parallel computer (SOCC1) that comprises 16 nodes connected by Giganet commutator. Each node consists of two Pentium II processors with clock speed 450 MHz.

The developed molecular dynamics code was tested at a number of computational systems in the USA. The objective of these tests was to examine the code efficiency at computational systems with the number of processors (Np) up to 1024. The examination was conducted at the following computational systems:

SUN (Lawrence Livermore National Laboratory), $Np \leq 20$;
Blue Pacific (Lawrence Livermore National Laboratory), $Np \leq 1024$;
Cray T3E (San Diego Supercomputer Center), $Np \leq 128$;
Blue Horizon (San Diego Supercomputer Center), $Np \leq 512$.

The limitation of processors number (Np) was determined not by the maximum capabilities of computational system but by the number of processors provided for testing.

The parallelization efficiency was examined in two modes:

- mode 1 - with increase in processors number the number of particles in the whole problem did not change (i.e. the number of particles at each processor decrease);
- mode 2 - with increase in processors number the number of particles in the whole problem increased proportionally to processors number (i.e. the number of particles at each processor did not change).

The report contains the comparison of efficiency examination results at computers mentioned above. The Table 1 represents computation times and maximum particles number for each of the parallel computers.

Table 1.

Computer	N proc	N particles	Efficiency [%]	Speed Up	Time per Step [sec]	Particles per sec
SUN	20	26,926,740	99.16	19.8	895.1	30,081
Cluster SOCC	32	21,549,056	98.31	31.5	106.5	202,375
Golden (Cray T3E)	128	37,024,928	99.12	126.9	137.4	226,845

Blue Horizon (IBM)	400	307,903,920	97.68	390.7	139.2	2,212,487
Blue Pacific (IBM)	1024	788,234,784	94.70	969.7	107.0	7,365,000

Thus, the results obtained suggest that the investigators managed to develop an efficient parallel code for studying material properties with the molecular dynamics method.

Prediction of Hypervelocity Impacts on Silica Phenolic Using CTH

R.P. Nance, J.R. Cogar, L.C. Chhabildas*, W.D. Reinhart*, T.G. Thornhill*

Naval Surface Warfare Center, Dahlgren, USA
** Sandia National Laboratories, Albuquerque, USA*

Introduction

Shock-physics codes, or hydrocodes, are widely used to perform numerical predictions of high-strain-rate events, including ballistic impacts and shock initiation of high explosives. The accuracy of such predictions hinges largely on the quality of material models employed in the simulations. In hypervelocity impacts, for instance, the large amount of energy transferred from the impactor to the target, as well as the subsequent rapid expansion of the shocked material, can lead to a significant degree of vaporization. Proper characterization of this material state is very important if we are to make valid assessments of overall target response in hypervelocity impacts.

In the proposed paper, we will use a proven shock-physics analysis tool to examine a series of recent gas-gun experiments at very high impact velocities. A key question in this study is the role of equation of state (EOS). Existing and newly developed tabular EOSs will be compared for the same impact conditions.

Approach and Preliminary Results

A number of hypervelocity-impact experiments has recently been conducted at Sandia National Laboratories using the gas-gun facility described by Chhabildas *et al.*[1] In this setup, a two-stage gas gun in conjunction with a graded-density impactor is used to accelerate a flyer plate to speeds over 10 km/s. Use of a graded-density impactor imparts shock-free acceleration to the flyer, thereby preventing fracture or melting of the flyer plate.

This facility was used to propel Ti-6Al-4V flyer plates into silica phenolic targets at speeds between 8 and 11 km/s. Figure 1 shows a typical experimental setup, as well as an X-ray radiograph of the flyer plate just prior to impact. As this photo shows, the launch process can produce some deformation of the flyer; however, the distortion is considerably less than may be expected from more conventional hypervelocity-launch techniques. Figure 2 shows the target debris cloud generated during the impact. The time interval between the frames is approximately 1 microsecond; hence, the average debris-cloud velocity may be estimated from these photos as 16 km/s.

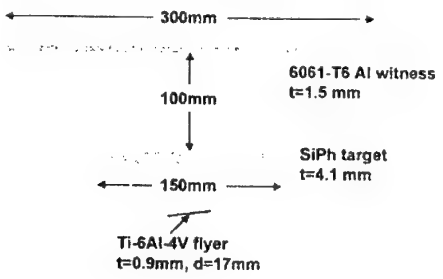

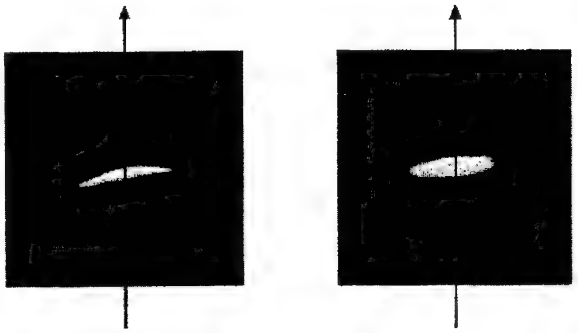

Figure 4. Test setup and top view of flyer prior to impact.

Sandia's CTH hydrocode[2] was used to perform pre-test analyses to drive target setup, and to conduct post-test predictions at the actual test conditions. CTH utilizes an Eulerian multimaterial algorithm in conjunction with a variety of equations of state (including the SESAME tabular EOS library[3]) to simulate high-strain-rate phenomena. The CTH runs conducted for this work utilize tabular EOSs for the titanium-alloy flyer, the phenolic target, and the aluminum witness plate, thereby accounting for thermodynamic phenomena such as melting, ionization, and vaporization. Figure 3 illustrates representative results from one such calculation, which employs 50 million zones. The average debris-cloud velocity in the computation is about the same as that observed experimentally; however, the debris cloud itself is clearly much narrower than that shown in Fig. 2.

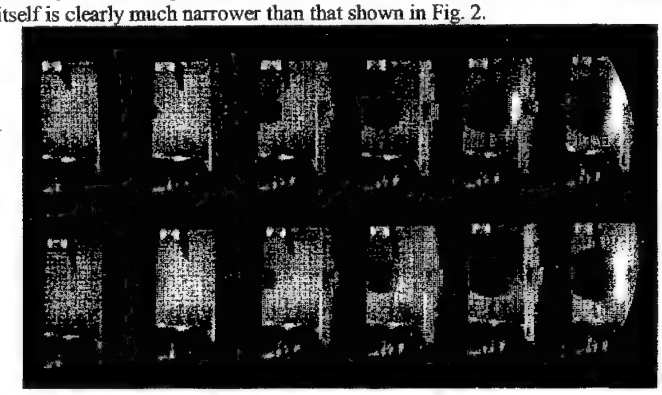

Figure 5. Formation of target debris cloud.

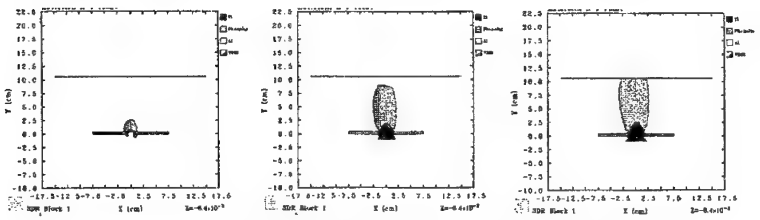

Figure 6. CTH debris-cloud predictions for case shown in Fig. 2.

Conclusion and Future Efforts

This study provides an important opportunity to study the physics of hypervelocity impact from both a computational standpoint and an experimental standpoint. Future work will include additional CTH calculations to examine the effects of equation of state on the results, analysis of the predicted motion of the witness plate, and comparison of these predictions to VISAR velocity records from the tests.

References

1. Chhabildas, L. C., Dunn, J. E., Reinhart, W. D., and Miller, J. M., "An Impact Technique to Accelerate Flier Plates to Velocities over 12 km/s", *Int J. Impact Engng.*, Vol. 14, pp. 121-132, 1993.
2. McGlaun, J. M., and Thompson, S. L., "CTH: A Three-Dimensional Shock Wave Physics Code", *Int. J. Impact Engng.*, Vol. 10, pp. 351-360, 1990.
3. Hertel, E. S., and Kerley, G. I., "CTH Reference Manual: The Equation of State Package", Sandia National Laboratories Report SAND98-0947, 1998.

Physics of (1) Multiple Initiation Points in Fragmentation Warheads and (2) Explosive Forming of Metal Parts

R.H.B. Bouma, M. Stuivinga, A.C. van der Steen, H.J. Verbeek

TNO Prins Maurits Laboratory, Rijswijk, The Netherlands

TNO Prins Maurits Laboratory is applying a number of different numerical codes in order to understand the physics behind observations in a variety of shock wave experiments. In this paper two typical examples will be shown in which the hydrocode Autodyn has been used in completely different applications. In the first example the effect of multiple initiation points on the fragmentation behaviour of a warhead is studied. In the second example the processes occurring during the explosive forming of metal plates are studied. For both examples several computer animations will be shown, from which data then have been extracted to give insight into the effectiveness of multiple initiation points, and in the fundamental processes underlying the explosive forming process.

The initiation of explosives and munitions typically occurs with use of a single detonator. In case where initiation of the explosive load at multiple points is required, until recently the use of complicated and expensive devices was needed since the response of standard detonators is not accurate enough to fulfil the requirements.

With the new initiator technology available (e.g. exploding foil initiator), one may explore the possibilities of using multiple initiation points in a warhead in order to improve its performance, while maintaining the same explosive main charge.

The effect of single and multiple initiation points, at various positions in a fragment accelerating warhead, on the angular distribution of fragment velocity will be described. Furthermore, the effect of timing accuracy between the firing of several initiators will be discussed.

Explosive forming of metals is a well-known technique. A metal plate is clamped into a mould, and then immersed in a water basin. The metal forming involves the detonation of an explosive charge causing a shock wave and a large momentum in the water, the expansion of detonation gases, and the subsequent interaction with the metal plate.

A mathematical description can only be given in the simplest of cases, and one is able to design the experiment given a certain application, and fine-tune the settings empirically. With numerical simulations it is possible to describe the full history of the explosive forming process. Due to the complexity and dimensions of the experimental set-up, however, a numerical simulation run implies a large computational effort.

A simulation has been performed to simulate the detonation of the explosive, momentum transfer by the water medium, and of course the detailed movement and deformation of the metal plate. Information has been obtained on the detailed processes occurring during explosive forming which are not covered by forementioned mathematical descriptions, e.g. cavitation, influence of mould and design of water basin, complex interactions of shock and release waves and water hammering.

Modeling the Oblique Impact of Yawed Projectiles on Ceramic Target

V.A. Gorelski

Tomsk State University of Control Systems and Radioelectronics, Tomsk, Russia

The investigation of three-dimensional problem of oblique interaction of yawed projectiles with ceramic plates in a velocity range up to 4000 m/s was carried out by the finite element method. The paper also presents an advanced constitutive model of AD995 Alumina. The model of damaged medium is used; it is characterized with possibility of crack initiation and propagation under impact loading. A kinetic fracture model of the active type developed earlier for the simulation of fracture in various materials is used for numerical modeling of ceramic failure at high velocity impact [1]. Temperature effects are taken into account in the constitutive model.

To investigate the effects of fracture and temperature in ceramic target during oblique impact of yawed projectiles in a range of velocities up to 4000 m/s a number of simulations was performed. The interaction of steel cylinder with 7.6 mm in diameter and 50.8 mm in height with AD995 plate with 10 mm in thickness was modeled. The model parameters for AD995 ceramics were adjusted using the data of impact experiments [2,3]. Computations have been done for yaw up to 10^0. Figure 1 shows configurations of projectile and plate during interaction at 4000 m/s impact velocity for obliquity 45^0 and yaw 10^0 at 10 μs. In this case the computation evidences that process of perforation is observed and one completed up to 15 μs.

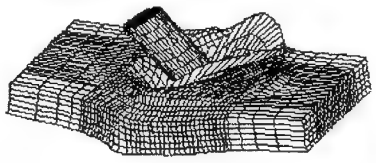

Figure 1. Penetration process at 4000 m/s impact velocity for obliquity 45^0 and yaw 10^0

Figure 2 shows the histories of components of forces of resistance during penetration at 4000 m/s impact velocity for obliquity 45^0. Curves show that at the initial moment the vertical components of forces of resistance are greater. After 6 μs the horizontal components of the forces of resistance are greater for both angles of yaw.

The histories of temperature near contact surface in target and in projectile also were investigated. Results evidence that temperature effects are important for the impact velocity range over 4000 m/s and they are more expressed for ceramic target. To further investigate the ceramics model the contours of specific volume of cracks were generated. The computations show that the maximum values of damage occurred in the bottom of ceramics near axis of impact for both angles of yaw and only for yaw 10^0 in the upper layers of ceramics near the leading edge of the projectile-target interaction region. Effect of yaw on the fracture was clearly expressed.

In summery it may be said that results of numerical simulations using the shock-wave propagation based finite element code revealed that both temperature effects and fracture of ceramics are important at 4000 m/s velocity. Stages in the penetration process, surfaces and contours of temperature and specific volume of cracks were generated for different moments of time. Results evidence that temperature effects in ceramic targets for impact velocity of 4000 m/s are clearly expressed .It was revealed that values of the horizontal components of the forces of resistance are greater than the values of the vertical components of forces of resistance during second stage of penetration. It results in normalization of velocity vector of mass center of projectile during the second stage of the process of the penetration.

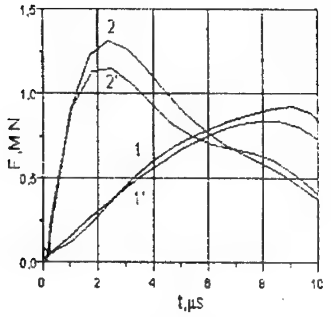

Figure 2. Histories of components of forces of resistance during penetration at 4000 m/s impact velocity for obliquity 45°:1–F_2, Yaw=0°;1^1– F_2, Yaw=10°;2–F_3, Yaw=0°; 2^1– F_3, Yaw=10°.

References

1. V.A. Gorelski and S.A. Zelepugin, "Mathematical simulation of a ceramic plate failure under an axisymmetrical high-velocity impact", *Strength of Materials*, No 5-6, pp. 87-94 (1995).

2. A.M. Rajendran, "Modeling the impact behavior of AD85 ceramics under multiaxial loading", *Int. J. Impact Engng.*, **15**, pp. 749-768 (1994).

3. R. Subramanian and S. J. Bless, "Penetration of semi-infinite AD995 Alumina targets by tungsten long rod penetrators from 1.5 to 3.5 km/s." *Int. J. Impact Engng.*, **17**, pp. 807-816 (1995).

Session "Physics of Detonation Processes"

Chairmen:
S. Coffey - Naval Surface Warfare Center, MD, USA
P. Haskins - QinetiQ Company, Fort Halstead, UK

Three Main Mechanisms of Detonation Decomposition of Heterogeneous HE

V.Yu. Klimenko

High Pressure Center, Institute of Chemical Physics, Moscow, Russia

20 years ago Tarver [1] had proposed the famous Ignition and Growth model of detonation that is based on hot-spot mechanism. It was great jump in development of detonation models. Time was going, we has obtained many important results about detonation processes and could hope to develop more perfect numerical model of detonation. However, we could not do it.

Detonation process is a very complex process. It is complex mixture of different physical and chemical elementary processes. It is impossible to study all these processes, but it is not necessary to do this. It is necessary to study only most important processes and try to prepare numerical model based on these governing processes.

All current numerical models of detonation are based on the hot-spot mechanism. But, is it right to use the same mechanism to describe behavior of explosive in great pressure range from 20 to 500 kbar? We made sure that this mechanism is a governing mechanism at low pressures 20-100 kbar and it describes (as it is incorporated into hydrocode) very well detonation processes at these pressures. But, we cannot use the hot spot mechanism for high pressures 400-500 kbar. Why?

P ~ 50 kbar

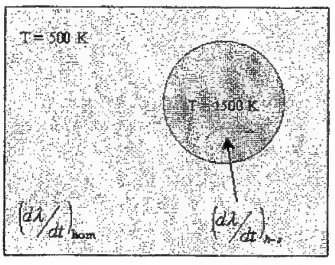

$$\frac{\left(d\lambda/dt\right)_{h-s}}{\left(d\lambda/dt\right)_{hom}} = \frac{\exp\left(-\frac{40000}{2*1500}\right)}{\exp\left(-\frac{40000}{2*500}\right)} = 10^{11}$$

P ~ 500 kbar

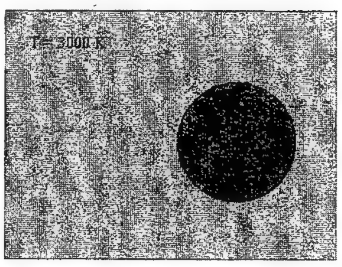

$$\frac{\left(d\lambda/dt\right)_{h-s}}{\left(d\lambda/dt\right)_{hom}} = \frac{\exp\left(-\frac{40000}{2*4000}\right)}{\exp\left(-\frac{40000}{2*3000}\right)} = 5$$

Figure 1. Hot spot and homogeneous decomposition rates in heterogeneous HE.

Firstly, rough estimation shows that this mechanism cannot ensure fast decomposition of explosive in detonation wave during 1-10 ns. It is necessary time more than 100-200 ns to do it. Secondly, at high pressures (when bulk temperature of explosive becomes very high) rates of decomposition in hot spot and outside of hot spot (i.e., in homogeneous part of explosive) become comparable. Figure 1 gives rough demonstration of rate constants at low pressure (left picture) and at high pressure (right picture). Thus, rates are comparable at high pressure. Since volume of pores is usually small - 1-5 %, we can conclude that main part of explosive (80-90 %) is decomposed outside of pores by

homogeneous mechanism. I.e., at high pressures homogeneous mechanism is governing in detonation decomposition of heterogeneous HE.

After that it is important to clear up what exact homogeneous mechanism operates in this case. There is well known standard thermal mechanism (thermodecomposition). However, it cannot be used for description of decomposition of HE with low porosity (PBX-9404, PBX-9501, EDC37, etc with ϕ = 1-2 %). If we use standard kinetic parameters E = 40-60 kcal/mol and Z = 10^{13}-10^{15} s^{-1} for the Arrhenius kinetics K=Z*exp(-E/RT), we cannot realize enough large reaction rate to ensure decomposition during 1-10 ns. We obtain small rate (see point B at Figure 2). Even if we increase artificially value of Z at 3-5 orders of magnitude to fit our rate to real rate of decomposition in vicinity of von Neumann spike (P ~ 500 kbar) (point A at Figure 2), this kinetics does not reproduce well rate at more low pressures P = 300-400 kbar. To reproduce "experimental" rate we need to use very low activation energy E = 5-10 kcal/mol.

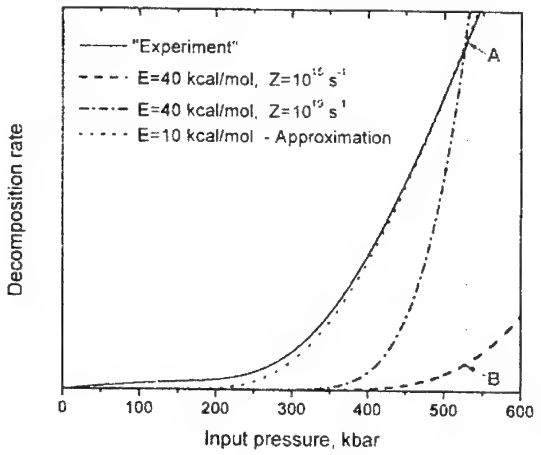

Figure 2. Rates of decomposition in HE with small porosity.

How could we explain so small activation energy? The so-called frontal mechanism was developed exactly for this 20 years ago [2-4]. A kernel of this homogeneous mechanism consists in formation of overheated temperature (in other words extreme translational energies, high energy phonons [5]) in narrow shock wave front. Belak [6] has confirmed this overheating effect in direct MD simulation of shock wave propagation in HMX monocrystal. This overheating (T ~ 10000-30000 K in HMX, RDX, TNT) causes electronic excitation of explosive molecules with subsequent instantaneous decomposition of molecules to radicals. A big concentration of these primary radicals ensures great reaction rate and fast decomposition during 1-10 ns.

There exist direct experimental results that support this nontrivial mechanism. Delpuch [7] detected phenomenon of electronic excitation of RDX molecules in front of shock wave (P=100 kbar) in RDX monocrystal. In other important experiment [8] he found that laser beam of specific wave length (which corresponds exactly to energy of electronic excitation of HMX molecule) causes acceleration of the shock-to-detonation transition in HMX.

Thus, one would think that all is clear: the frontal mechanism works at high pressures, the hot-spot mechanism - at low pressures and their joint action ensure proper decomposition of explosive at any pressure from 20 to 500 kbar (see Figure 3). But, it is necessary to emphasize that this is true for heterogeneous HE with low porosity (ϕ=1-2 %).

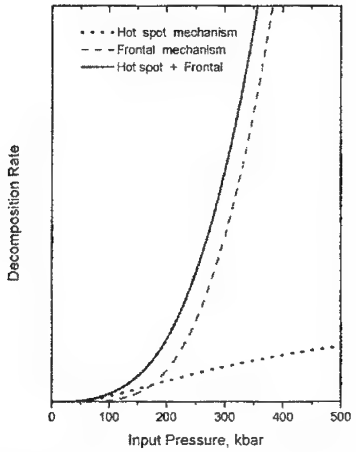

Figure 3. Rates of hot spot and frontal decomposition mechanisms in heterogeneous HE.

Last time there appeared some experimental results [9-11] that give very interest and important data on decomposition of explosives with variable porosity in detonation regime, i.e., at high pressures. Take, for example, data from [9] and analyse them. We obtain the following important dependence of decomposition rate vs porosity (Figure 4). We see two qualitatively different rates of decomposition (fast decomposition and slow decomposition) that clearly are combined with different mechanisms. How could we explain this curve?

Since the effect is combined with porosity, it is necessary to study carefully process of interaction of shock wave with pore. Earlier Taylor [12] and Chou [13] investigated this process in numerical simulations by 2D-hydrocode. However, these simulations had one defect, namely, width of shock front was comparable with pore size. As a result pore was loaded in quasi-shock regime, i.e., smoothly. In hydrodynamic simulations width of shock front is determined by artificial viscosity or by real viscosity as in [13]. Chou used real viscosity (μ = 100 poise in HMX). This viscosity describes well process of pore collapse. But, it cannot give narrow shock front. It spreads shock front up to 1 μm. It is not good.

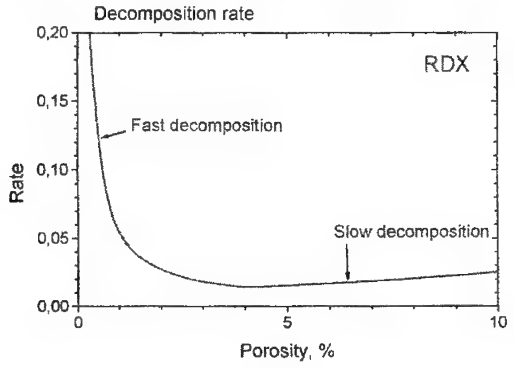

Figure 4. Decomposition rate in RDX.

As early as in 60-s researchers from Arzamas-16 [14] had investigated experimentally width of shock wave front in liquids and monocrystals. They used very original method. Light beam is sent under some angle to shock front and reflects from front. If retio of intensities of incident and reflected beams corresponds to Frenel formula, it means that the width of density jump (i.e., shock front) is more than order of magnitude smaller than the light wave length. Using this method they had determined that the width of shock front in liquids and monocrystals is smaller than 100 angstroms. It is very important fundamental result. It follows that "effective" viscosity inside shock front is as much as one or two orders of magnitude smaller than viscosity before and after front. We do not discuss nature of this effect. It is subject of special report. Most important for us is that for description of shock wave front in hydrodynamic simulations we have to use not real viscosity, but effective viscosity (or mathematical viscosity) that gives narrow front.

In our hydrodynamic calculations we simulated interaction of shock wave with the pore (d_{pore} = 5 μm) in HMX monocryctal and used real viscosity (30-50 Pa*s as it is recommended in [15]) for all volume of simulated explosive and used effective viscosity for shock front. Numerical calculations were performed by the RUSS-2DE hydrocode [16]. The initial stage of simulations is presented at Figure 5.

Here we do not consider events inside the pore. It is subject of next report. Now we are interested by process of explosive decomposition in all volume of explosive. Rate of the frontal mechanism depends from pressure at front of shock wave. This dependence can be presented schematically as it is shown at Figure 6. We recorded pressure at shock front in each point of explosive during passing front through this point. As a result in the end of numerical experiment (when shock front crossed all explosive) we have obtained the following picture (see Figure 7).

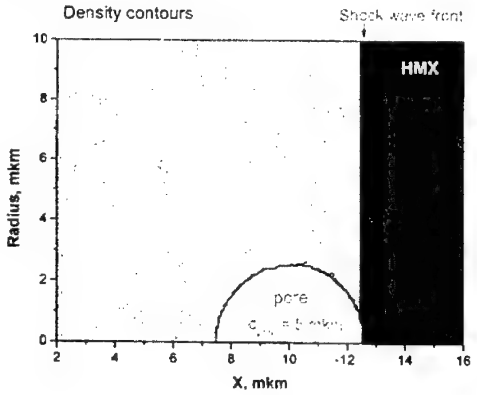

Figure 5.

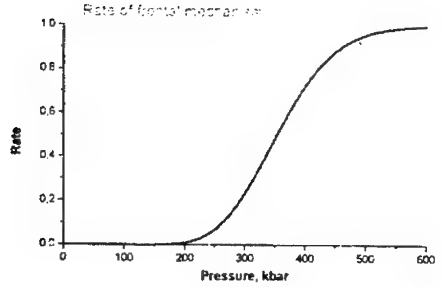

Figure 6.

Now we can conclude that in regions marked by dark color decomposition proceeds by the frontal mechanism. It is very fast decomposition. Depending on specific HE (HMX, RDX or TNT) decomposition time is about 0.1-0.5 μs. And in regions marked by light color fast frontal mechanism does not work. Here a standard thermal mechanism works. It is much more slow mechanism than the frontal one. Here explosive is decomposed during typical time 10-50 μs. The volume (in which slow thermal decomposition occurs) is approximately 5-10 times greater than the pore volume. It is clear that the same process is realized around each pore and gives some set of meso-regions of thermal decomposition. Therefore, if total volume of pores in explosive is, for example, 1 %, then total volume of explosive where thermal decomposition is realized, i.e., sum of meso-regions, is 5-10 %.

Thus, at high pressures we can mark out in explosive two typical volumes: (1) volume of decomposition by the fast frontal mechanism and (2) volume of decomposition by the slow thermal mechanism. If porosity is 1 %, then volume of thermal decomposition is 5-10 %. If porosity is 5 %, then volume of thermal decomposition is 25-50 %. At further increase of porosity the meso-regions of thermo-decomposition come into contact and as a result of their hydrodynamic interaction shock front is spread - its width becomes comparable with pore size. In this case the frontal mechanism does not work and all explosive is decomposed by the thermal mechanism.

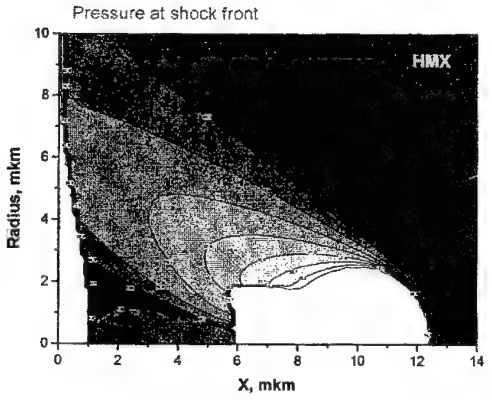

Figure 7.

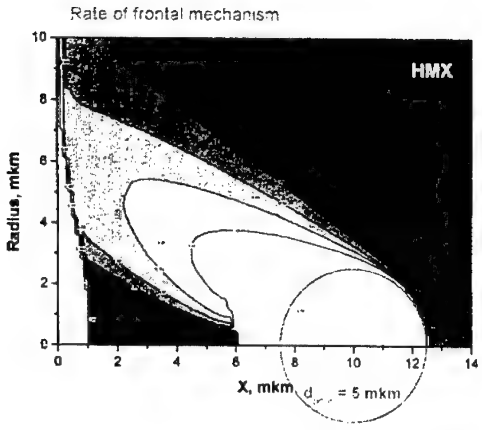

Figure 8.

Now we can explain the curve of Lubyatinsky (see Figure 4). At very small porosity decomposition proceeds by the fast frontal mechanism during time ~ 0.1 ns. At porosity increase a portion of explosive decomposed by the slow thermal mechanism rises and as a result total decomposition is delayed to time 1-5 ns. At some critical porosity (ϕ = 4 %) decomposition becomes entirely thermal and characteristic decomposition time is equal ~ 50 ns. From this moment shock front is transformed from narrow to wide. Further rise of decomposition rate is caused by increase of bulk temperature of explosive, because increase of porosity gives rise of temperature.

Thus, there are three main mechanisms of decomposition of heterogeneous HE: (1) the frontal mechanism, (2) the hot spot mechanism and (3) the thermal mechanism. At low pressures HE decomposition proceeds by the hot spot mechanism. At high pressures decomposition proceeds by the frontal mechanism (if porosity is small) or by the thermal mechanism (if porosity is large).

References

1. E.L. Lee, C.M. Tarver, "Phenomenological Model of Shock Initiation in Heterogeneous Explosives", Physics of Fluids, v. 23, p. 2362 (1980).
2. V.Yu.Klimenko, A.N. Dremin, "On Decomposition Reaction Kinetics in Shock Wave Front", VI All-Union Symposium on Combustion and Explosion, Alma-Ata, USSR, 1980, p. 69.
3. V.Yu. Klimenko, O.N. Davidova, A.N. Dremin, "Multiprocess Model of Detonation", IV All-Union Symposium on Detonation, Telavi, USSR, 1988, v.2, p. 261.
4. V.Yu. Klimenko, "Multiprocess Model of Detonation (Version 3)", Shock Compression of Condensed Matter - 1995, Seattle, USA, p. 361.
5. C.M. Tarver, L.E. Fried, A.J. Ruggerio, D.F. Calef, "Energy Transfer in Solid Explosives", X Int. Detonation Symposium, Boston, USA, 1993, p. 3.
6. J. Belak, "Atomic-Scale Computer Simulation of the Behaviour of High Explosives Molecules at Shock Front", Gordon Conference on Energetic Materials, New Hampton, USA, 1994.
7. S. Dufort, A. Delpuech, "A Molecular Mechanism for the Initiation of Secondary Explosives", VIII Symposium (Int.) on Detonation, Albuquerque, USA, 1985, p. 847.
8. A.E. Delpuech, "The Use of Time-Resolved Spectrometries in the Study of Initiation of Explosives at Molecular Level", IX Symposium (Int.) on Detonation, Portland, USA, 1989, p. 172.
9. S.N.Lubyatinsky, B.G. Loboiko, "Density Effect on Detonation Reaction Zone Length in Solid Explosives", Shock Compression of Condensed Matter - 1997, Amherst, USA, p. 743.
10. A.V. Fedorov, A.V. Menshikh, N.B. Yagodin, "On Detonation Wave Front Structure of Condensed High Explosives", New Models and Hydrocodes for Shock Wave Processes in Condensed Media,

Oxford, UK, 1997, p. 830.

11. A. Utkin, S. Kolesnikov, S. Pershin, "Reaction Zone Transformation for Steady-State Detonation of High Explosives under Initial Density Increase", Shock Compression of Condensed Matter - 2001, Atlanta, USA.
12. P.A.Taylor, "The Effect of Material Microstructure on the Shock Sensitivity of Porous Granular Explosives", VIII Symposium (Int.) on Detonation, Albuquerque, USA, 1985, p. 26.
13. P.C. Chou, D. Liang, Z. Ritman, "The Viscoplastic Hot Spots in Pore Collapse", X Int. Detonation Symposium, Boston, USA, 1993, p. 979.
14. K.B. Yushko, G.V. Krishkevich, S.B. Kormer, Journal of Experimental and Theoretical Physics (Russian), N 7, p. 12 (1968).
15. B.A. Khasainov, A.V. Attetkov, A.A. Borisov, "Shock-Wave Initiation of Porous Energetic Materials and Viscoplastic Model of Hot Spots", Chemical Physics (Russian), v.15, N 7, p. 53 (1996).
16. G.S. Romanov, A.E. Suvorov, I.M. Kozlov, V.Yu. Klimenko, "RUSS-2DE Hydrocode with the TVD Procedure", New Models and Hydrocodes for Shock Wave Processes in Condensed Media, Oxford, UK, 1997, p. 401.

Mechanism of Shock Propagation in Porous Materials at Mesoscale Level

J. Ribeiro, J. Campos, I. Plaksin, and R Mendes

Laboratory of Energetics and Detonics, Mechanical Engineering Department
University of Coimbra, Coimbra, PORTUGAL

It is believed that many of the macroscopic aspects of the shock wave [SW] propagation in heterogeneous materials are due to the SW interaction with the heterogeneities – grains, crystals, particles or pores. Even being very different in their nature, at this scale level – the mesoscale level – we think that the process of SW propagation presents significant similarities for almost all kinds of heterogeneous materials. This idea have taken us, in the past, to propose the use of Syntactic Foam [SF] samples - Hollow Glass Microspheres [HGMS] within a binder – as an ideal media to obtain experimental details of the SW propagation process in heterogeneous materials at mesoscale level[1]. Some of the essential features of this material are the possibility to control, in wide limits, and with a good precision, the size, the amount and even the relative position of the HGMS.

The results already obtained show a non-monotonous emission of light from the compressed material, presenting a surprising and remarkable regularity for some of the situations in which we have worked with SF samples prepared with sieved HGMS[2,3]. It is clear that the nature of these oscillations is related with the nature of the heterogeneities because they change with the size and the amount of the HGMS. Nevertheless, some attempts to relate the regularity in the light oscillations with the distribution of the HGMS in the binder failed. In the Figure 1,a it is possible to observe a typical streak record obtained for a SF sample prepared with sieved HGMS (d_{50} = 92 μm) and with an initial density of 0.64 g/cm^3, shock loaded with a PBX cylindrical charge – details of the experimental set-up can be found elsewhere[2]. In the Figure 1,b is possible to see an optical microscope photo taken from a transversal section of a sample identical to the one used to obtain the streak record. In fact when we compare both pictures it is not possible to find a degree of order in the HGMS distribution in the binder that can justify the regularity in the light oscillations observed in the streak record.

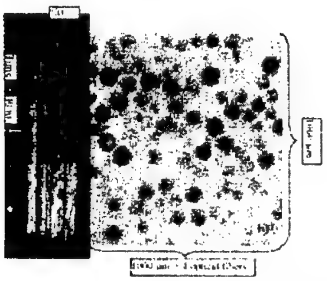

Figure 1. a) Typical streak record obtained for a SF prepared with HGMS presenting a mean diameter of 92 μm, an initial density of 0.64 g/cm^3 and a thickness of 1000 μm. b) Optical microscope photograph of a transversal section of a SF identical to the one used to obtain the streak record.

These results, together with preliminary numeric simulations of the SW interaction with two layers of HGMS, allowed us to say that the redistribution of kinetic energy over the entire SW front is the main mechanism in the observed SW behaviour. From the numeric simulations it was possible to see that the release waves beginning at the internal surface of each of the HGMS tends to redirect the particle velocity, in the space between the HGMS, toward the centre of the collapsing HGMS. This process removes the energy from the back of the SW that is sweeping around each of the HGMS, and even if this SF reaches the second layer of HGMS first that the one going through the collapsing spheres doesn't have the strength enough to proceeds with the collapse.

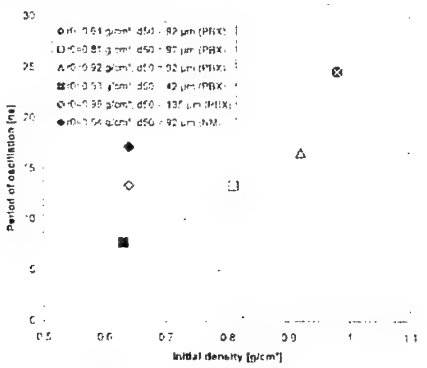

Figure 2. Characteristic period of light oscillations as a function of the initial density for the several studied situations.

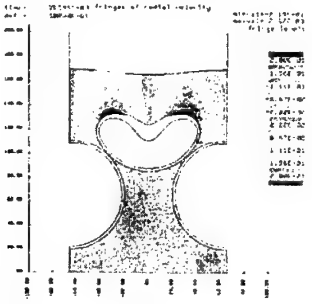

Figure 3. Simulation of the collapse of a HGMS from a idealized layer of a $\rho_0 = 0.64$ g/cm^3 and $d_{50} = 92$ μm SF sample. Fringes of radial velocity – horiz. direction in the picture [cm/μs].

Even not having a layer-by-layer distribution of the HGMS in the binder, or a constant inter-particle distance, it is possible to say that the release waves (dissipative structures) coming from the internal surface of the HGMS tend to act together, in a cooperative/synergetic way making the re-distribution of the kinetic energy, slowing down the wave in some parts and accelerating in others, being responsible for a layer-by-layer way of propagation compatible with the observed experimental behaviour.

Table 1. Physical characteristics of the studied SF samples

Mean diameter of the HGMS [μm]	Effective density [g/cm^3]	Characteristic distance between two homologue points in idealized successive layers of HGMS [μm]
92	0.64	66
92	0.81	82
92	0.92	88
42	0.75	35
135	0.98	143

Another experimental evidence of the existence of this mechanism of propagation can be found in the relation between the characteristic period of light oscillations and a typical inter-particle distance. The values of the characteristic period of light oscillations, as a function of the initial density of the samples, for each of the studied situations are presented in Figure 2. The typical values of the inter-particle distance, together with other physical characteristics of the samples can be found in Table 1.

It was found that the quotient of the inter-particle distance versus characteristic period of light oscillation is very close to the measured values of SW velocity as it can be seen in the graphic of the Figure 3.

REFERENCES

1. Ribeiro, J., Campos, J., Plaksin, I., and Mendes, R., "Process of Shock Wave Attenuation Inside a Hollow Glass Microshpere/Polymeric Composite Material" Shock Compression in Condensed Matter-1999, edited by M. D. Furnish, L. C. Chhabildas, and R. S. Hixson, AIP Conference Proceedings 505, New York, 2000, pp. 559-562.
2. Ribeiro, J., Campos, J., Plaksin, I., and Mendes, R., "Microscopic Aspects of the Shock Wave Propagation in Epoxy Syntactic Foams", presented at the International Conference of Shock Waves in Condensed Matter, St. Petersburg, September 2000, to be publish in the Chem. Phys. Reports.
3. Ribeiro, J., Campos, J., Plaksin, I., and Mendes, R., "Shock Wave Propagation Process in Epoxy Syntactic Foams" to be published in Shock Compression in Condensed Matter-2001, edited by M. D. Furnish, L. C. Chhabildas, and R. S. Hixson, AIP Conference Proceedings.

Experimental Investigation of Heterogeneous HE Decomposition Mechanism in Detonation Wave Front

A.V. Fedorov

Russian Federal Nuclear Centre – VNIIEF, Sarov, Russia

Heterogeneous HE decomposition mechanism in hot spots in detonation wave front is considered. Investigation of detonation wave structure of HE (HMX, RDX, PETN, a.o.) with different porosity values (1-10%) was performed. U(t) profile was recorded at the HE-(LiF) window interface of Fabry-Perot laser interferometer with nanosecond time resolution [1,2,3]. Between HE and window a thin foil or a layer sprayed on LiF covering was placed which reflects laser beam. The experimental set-up is depicted in Fig. 1.

It is recorded in a number of experiments that just before detonation wave arrival HE-window interface starts smoothly accelerating during 5-7 ns up to velocity of v≈100 m/s. Then recording is broken. The reason of such acceleration can be microjets that overtake detonation, front, accelerate LiF surface, and destroy Al-covering (recording break). The jets occur due to HE cavities collapse.

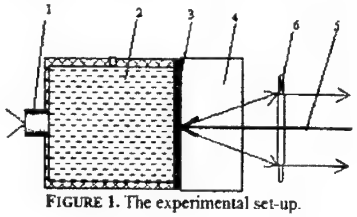

1.- detonator;
2 - liquid HE in cylindrical cell or sample of solid HE;
3.- Al covering (0.2-1.5 μm) or Al foil (5-10 μm),
4.- crystal of LiF;
5.- laser beam (λ=694.3 nm);
6.- focusing lens

FIGURE 1. The experimental set-up.

In a number of model experiments, conical cavities were formed in plastified PETN with depth of 0.3-4 mm and vertex angle of 30-60 degrees. HE in these tests came in contact with thick (20…50 mm) aluminum plate. Figure 2 shows schematically the results of the model experiments The size of the cavity, that was formed in the Al plate due to the impact of jets is approximately equal to the size of conical cavity in HE. In case when not an aluminum plate but HE is opposite the jets, the latter will influence the front HE layers, i.e. the jets make an impact on unreacted HE.

In the case, when the cavity is filled with glue (that is simulator of binder in HE), size of the cavity in the Al plate approximately 3-4 times decreases. If to make a conical cavity not in HE, but in aluminum plate, then under the impact of explosion products the size of this cavity 3-4 times increases. Thus the jet forms a small cavity in front and explosion products 3-4 times increase its diameter and depth.

Velocity of jets in these conical cavities was measured. The jet head part velocity was 9-12 km/s which is higher than detonation velocity (7.8 km/s).

In different HEs at porosity changing from 1 to 10% it is determined that HE being in contact with Al-covering (1 μm) destroys the covering, and recording is broken. The higher HEs porosity, the higher the number of recording breaks in the experiments. At porosity of 7% microjets destroy the whole surface of Al covering and close LiF layers. Recording is broken in 100% of cases. In liquid homogeneous HEs, where voids are absent recording breaks (Al covering destruction) are practically not observed.

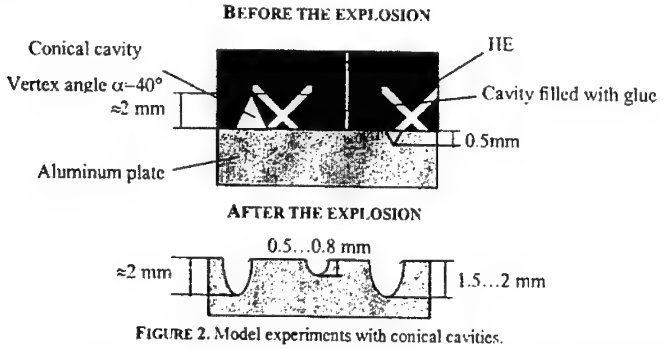

FIGURE 2. Model experiments with conical cavities.

We suppose, that if the jet is decelerated in the layer of high-density (93-99% TMD) HE and the window is situated just behind the HE layer, then the jet influences HE, and in the falling profile U(t) at the boundary HE-window we record velocity oscillation up to ±100 m/s and with duration up to 20 ns. In our U(t) recordings together with smooth profiles there are profiles with damping oscillations.

The profiles with velocity oscillations are depicted in fig. 3. The higher porosity, the more often is such oscillations in profiles. In cases when HE has high porosity and cavities size is large the jet can induce very large perturbations in U(t) profile. In [9] for HMX with porosity 35% and average particle

size =10 μm, velocity oscillations reach 300...400 m/s, at particle size of 120 μm they are up to 800-1000 m/s.

In [8], it is shown that during pressing in HMX crystals appear cracks and average particle size decreases from 192 μm to 131 μm at density change from 70% TMD to 95% TMD. It is known that if a crack is perpendicular to detonation front then at the initial moment of detonation wave arrival the crack plane turning occurs for the angle $\alpha \approx 5°$ [10], i.e. at crack collapse at the angle $2\alpha \approx 10°$, the jet can also be realized.

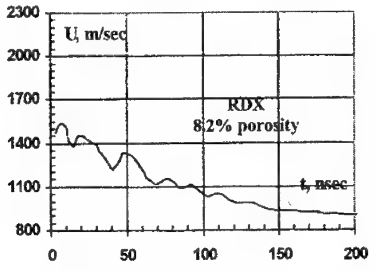

FIGURE 3. Profiles of particle velocity with decelerated oscillations.

It should be noted that in high-density HEs at cavities size of 5...10 μm, detonation wave passed these cavities at times of 0.5-1 ns, where according to [4,6], HE has not yet started decomposition (active particles storage is on), i.e. the beginning of jets formation takes place even in solid HE. Besides, the beginning of jets formation occurs not at Chapman-Jouguet (C-J) pressure, but at Neumann spike pressure, the value of which is ≈30% more than C-J pressure [2,3], hence either jet parameters or its influence on unreacted HE will be significantly higher.

According to [4,6], shock front width is 1 ns. After this, HE starts decomposing, pressure falls and in cavities collapse of HEs take part at the stage of decomposition, reaction products, active particles (radicals, ions, etc.) are involved into the jet.

Most HEs cavities have the view of long polyhedrons, cracks, gaps which produce many microjets and introduce turbulence into detonation front.

Simple evaluations show that in heterogeneous HEs even of very high density (99% TMD) in 1 mm^3 (10^9 μm^3) HE contains 10^7 μm^3 air and 10^7 voids at void size ≈1 μm (1 μm^3) and 10^4 voids at voids size ≈10 μm (10 μm^3).

As it is followed from the experiments, the reason of local heated zones (hot spots) formation in detonation wave front is, apparently, microjets that overtake detonation front, penetrate into unreacted HE, turbulize the front and increase HE decomposition velocity.

In [11,12], it is shown at initiation of HE, where pressure is significantly lower (tens kilobar) cavities collapse is also one of the reason of hot sports formation. The ignition of material at the point at which the jet hit was found to be the principal ignition mechanism.

The investigation of detonation wave structure recording in single crystals PETN was performed. Samples of single crystal were pressed into composition of plastified PETN. Detonation wave from plastified PETN (C-J pressure P=25.6 GPa) entered single crystal. Detonation parameters of single crystals PETN are: ρ=1.77/cm^2, D=8.3 km/s, $P_{(C-J)}$=33.5 GPa [7]. Thickness of single crystals was in the range of 4...6 mm. Particle velocity recording was performed at the boundary single crystal – (LiF) window. Falling from spike concave profile U(t) was recorded. The recorded states in LiF were recalculated into states in single crystal. LiF spike value was 2...2.2 mm/μs, whish corresponds to the spike in single crystal PETN P=35...37.5 GPa.

We have recorded that the spike in single crystal is 5-12% higher than detonation pressure (33.5 GPa). Earlier it was determined [2,3] that Neumann spike for most solid heterogeneous HEs 1.3 times exceeds C-J pressure in average. Hence, the expected value of Neumann spike in single crystal PETN is 43.5 GPa, but we have recorded 35-37.5 GPa. Thus, on thickness of single crystal 4...6 mm

Neumann spike has not yet formed. It is also recorded that just after the spike velocity decrease gradient in profile U(t) in single crystal differs from the gradient for plastified PETN, where it is significantly higher.

For single crystals, gradient of velocity change was $\approx 30 \frac{m/s}{ns}$, and for plastified PETN (1% porosity), it was $180 \frac{m/s}{ns}$. Evaluations show that at the expected in single crystal Neumann spike (43.5 GPa) velocity decrease gradient will be $\approx 60 \ldots 80 \frac{m/s}{ns}$. The higher velocity gradient is, the higher HE decomposition rate is in chemical reaction zone (CRZ). Before this, in plastified PETN, duration of chemical reaction zone was defined as 3±1 ns. And though Neumann spike on thickness 4-6 mm has not reached its maximum value, it shall be expected that CRZ duration in single crystal will be several times higher than in plastified PETN.

It should be noted that in liquid homogeneous HEs of monolithic initial velocity exists either stable front (in accordance with ZND model) mirror reflecting light (tetranitromethane – TNM, nitroglycerine) or unstable front with pulsing detonation [5].

In mixed composition of liquid HEs (TNM/NB) (where nitrobenzene – NB was more than 25%) we also have found unstable pulsing detonation front [2]. And though these mixtures have very high sensitivity (critical diameter of mixture TNM/NB 74/26 is 0.03 mm) detonation in them can not develop in stable mode according to ZND model. Moreover, detonation parameters for composition TNM/NB 74/26 (P_{C-J}=21 GPa, D=7.5 km/s) are higher than those for TNM (P_{C-J}=15.9 GPa, D=6.4 km/s), where detonation is stable. Hence, detonation wave structure and detonation development selection to stable or unstable mechanism is not linked with HE sensitivity and critical diameter.

Dremin [4,6] explained it by the failure of chemical reaction In the front of detonation wave the same as in theory of thermal explosion, first comes the induction period and after this self ignition. For HE with slow energy release kinetics, the induction period is the basic part of explosion time and self ignition in Neumann spike can not exist (failure of chemical reaction) [4,6]. Detonation occurs later and passed along compressed HE catching up with the front, in this way occurs three-shock wave configurations (pulsing, unstable detonation front). Apparently, adding NB into TNM rises its energy and sensitivity, but makes energy release kinetics slow and detonation front – pulsing. In [2] the difference between maximum (41.6 GPa) and minimum (17 GPa) pressure in unstable pulsing front for TNM/NB 74/26 was 2.45 times. Besides, the minimum pressure was reached immediately in the shock discontinuity zone, and maximum pressure fast increased during 20-25 ns [2]. We proposed that this fast smooth increase is caused by collision of cross waves.

We suppose that in single crystal HEs in which energy release kinetics is slower than in heterogeneous HEs, one can find such HEs in which detonation will start to unstable pulsing mode as it does in liquid HEs. Among heterogeneous HEs it is impossible to face HEs with unstable pulsing mode as the voids inside HE and jets appearing in them introduce turbulence in detonation front, carry ahead intermediate and final reaction products and by this the produce fast energy release kinetics, where reaction rate is maximum just after von Neumann spike.

In TNM the shock front has the view of a mirror [4,5]. We have reflected light from metal samples of different roughness and noted that already at roughness $l \leq 0.1$ μm (100 nm and less) the samples reflect the light mirror. Taking for evaluations detonation velocity D=10 km/s=10 nm/ps we see that the duration of shock discontinuity zone l/D=10 ps and less can produce mirror reflection. Considering molecule size ≈1 nm for width of shock discontinuity zone is 100 nm, we see that increase of parameters in shock discontinuity zone to maximum values can occur on a chain of ≈100 molecules. Other authors [4,6] suppose the duration of shock discontinuity zone to be ≈1 ps (10 nm) then parameter increase will occur in a chain of ≈10 molecules.

Thus, molecule #1 in this chain is in maximum compressed state and has very high temperature and starts to ignite, and molecule #11 in the chain has zero pressure and normal temperature. Nobody can imagine what will occur to it in a small share of picosecond.

Author greatly appreciate the help of Davidov V.A., Men'shikh A.V., Nazarov D.V. and Finyushin S.A. in realization of this work.

References

1. Fedorov A. V., Menshikh A. V., Yagodin N. B. Chemical Physics (Russian), #11, pp. 64-68, 1999.
2. Fedorov A. V. et al. Detonation front in homogeneous and heterogeneous High Explosive, Shock Compression of Condensed Matter, Snowbird, USA, pp. 801-804, 1999.
3. Fedorov A. V., Menshikh A. V., Yagodin N. B. Chem Phys. Repots, vol. 18 (10-11), pp. 2129–2138, 2000.
4. Dremin A. N. Towad Detonation Theory. Springier, 1999.
5. Dremin A. N., Savrov S. D., Trofimov V. S., Shevedov K. K. Detonation Waves in Condenced Media. (Russian), Moscow, Nauka, 1970.
6. Dremin A. N. Discoveries in the investigation of the detonation of molecular condensed explosives in the XX century. Fizika gorenia i vzryva (Russian), v. 36, #6, pp. 31-34, 2000.
7. Mader C. L. Numerical modeling of detonations, University of California Press, 1979.
8. Burnside N. J. et al. Shock Compression of Condensed Matter , Amherst, USA, pp. 571-574, 1997.
9. Gustavsen R. L., Sheffield S. A., Alcon R. R. Progress in measuring detonation wave profiles in PBX9501, Proceedings of XI Symposium on Detonation, Snowmass, USA, 1998.
10. Deribas A. A. Applied Mechanic and Technical Physics. (Russian) vol. 41, #5 (243), pp. 68-74, 2000.
11. Bourne N. K., Field J. E. Shock-induced collapse of single cavities in liquids, J. Fluid Mech., vol. 244, pp. 225-240, 1992.
12. Bourne N. K., Field J. E. Explosive ignition by the collapse of cavities. Proc. R. Soc., Lond. A455, pp. 2411-2426, 1999.

Initiation of Crystalline Explosives Using the Sakharov Corrugated Shock Experiments

C. S. Coffey

Indian Head Division, Naval Surface Warfare Center, Indian Head, USA

Recent theoretical calculations have predicted the behavior of the plastic deforma-tion rate and the viscosity of crystalline solids as they undergo plastic deformation due to shear resulting from very high level shocks.[1,2,3] The magnitude of the plastic deformation rate and the viscosity have been determined and compared with experimental data obtained by A. D. Sakharov and co-workers.[4,5,6] The comparisons between these fundamental calculations and the results of the corrugated shock experiments of Sakharov and co-workers is very good and extend over a range from about 5 GPa to greater than 200 GPa.

Only inert materials were used in the Sakharov experiments while the theoretical calculations are entirely general and can be applied equally to energetic materials as well as to inert materials. The current paper will focus on applying the shear stress generated by the Sakharov corrugated shock experiment to study the processes of initiation of crystalline explosives at low shock pressures, .1 GPa to 5 GPa. The theory makes definite predictions about the processes of plastic flow and energy dissipation during the plastic flow. The shear stress results from pressure gradients that occur in the shock wave.[3,7] The Sakharov corrugated shock front can be written as

$$P(x, y, z) = P_{0z}u(t - \{.5a_0 / U_0\}\{1 + \cos 2\pi x / \lambda\}),$$

where z is the direction of shock wave propagation. P_{0z} is the pressure amplitude in the z direction of the steady shock wave, $u(t-t_0)$ is a step function and a_0 is the amplitude of corrugated sine wave. The cosine term describes the corrugation at the front end of the shock. Let x be the direction perpendicular to the corrugation and lambda the wavelength of the sinusoidal perturbation in this direction. The y axis lies along the length of the corrugations. The shear stress at the corrugated shock front is just the gradient of P(x,y,z),

$$\tau(x, y, z) = (\frac{\pi a_0}{\lambda}) P_{0z} \sin 2\pi x / \lambda .$$

A lower limit of the amplitude of the pressure perturbation at which initiation occurs in RDX can be estimated since it is known that initiation in RDX occurs at shear stress amplitudes of about 20 to 30 MPa. Let lambda equal 10^{-2}m (as in the Sakharov Expt.) and let $a_0 = 10^{-3}$ m. so that P_{oz} is approximately 60 MPa to 100 MPa. This represents a lower limit because for this case the maximum shear occurs only instantaneously along a line in the y direction where x = an odd multiple of lambda / 4. The location x = 0

is the point of maximum pressure so that the locations of maximum pressure and of maximum shear stress are easily distinguished. To achieve initiation of chemical reaction locally in the explosive the shear has to persist for a time long enough to allow plastic flow and energy dissipation to occur. If to achieve sufficient plastic flow and energy dissipation the threshold pressure for reaction occurs at x = lambda / 12, then P_{0z} is approximately 120 MPa. to 200 MPa. which is an entirely reasonable range for the shock threshold for RDX in experimental conditions for which plastic flow is allowed to occur.

. The locations of the first initiation sites are predicted not to be in the regions of highest pressure but rather to be in the regions of highest shear and plastic deformation. On the corrugated surface of the Sakharov experiment, the surfaces of peak pressure will appear as narrow regions along the direction of the y axis. The regions of maximum shear deformation and maximum energy dissipation and consequentially first initiation will be located parallel to the regions of pressure but shifted in the x direction a distance of + / -lambda / 4 = .25 x 10^{-2} m from the lines of maximum pressure.

The condition where grad $P_0 = 0$ describes the case of a completely "Dead Pressed" explosive in which the porosity of the charge is zero and its inertial confinement so great that no plastic deformation and consequently no energy dissipation can occur in the explosive. Actually, because a finite amount of energy is required to cause initiation of chemical reaction in a shocked or impacted explosive, the definition of a dead pressed explosive can be relaxed somewhat so that 0 < grad P_0 < the critical pressure gradient level required for initiation , grad $P_{0,crit}$. An example of this broader definition of dead pressing where heating due to sub threshold plastic deformation-energy dissipation is observed without initiating chemical reaction is to be found in Figure (4) of Reference (8).

This analysis of the Sakharov Corrugated Shock Experiment ascribes initiation to the energy dissipated due to plastic flow arising from the applied shear stress generated by the corrugated shock. In this way it should be possible to relate initiation due to impact, where shear is the only plausible means of achieving the necessary energy dissipation, with initiation due to shock.

References

1. C.S. Coffey, Phys. Rev. B **49**, 208 (1994).
2. C.S. Coffey, in **Mechanics of Deformation at High Rates**, edited by R. Graham (Springer-Verlag, Berlin, 1996), Vol. 3.
3. C.S. Coffey, "Quantum Limiting Behavior of High Rate Deformation in Solids and Liquids", Submitted to Phys. Rev. B August 2001.
4. A.D. Sakharov, R.M. Zaidel', V.N. Mineev and A.G. Oleinik, Soviet Physics-Doklady, **9**, 1091, (1965).
5. V.N. Mineev and E.V. Savinov, Soviet Physics JETP, **24**, 411, (1967).
6. V.N. Mineev and R.M. Zaidel', Soviet Physics JETP, **27**, 874, (1968).
7. C.S. Coffey, in **Decomposition, Combustion and Detonation Chemistry of Energetic Materials**. Editors, T. B. Brill, T. P. Russell, W. C. Tao and R. B. Wardle. Mat. Res. Soc. Symp. Proc. Vol. 418, p. 331, (1996).
8. C.S. Coffey and J. Sharma, J. of Appl. Phys. **89**, 4797, (2001).

Model Study of Crystal Size Influences on Impact/Shock Initiation of Energetic Materials

R.W. Armstrong

AFRL/MNME, Eglin Air Force Base, USA

The dislocation pile-up avalanche model of deformation-induced "hot spot" generation[1], as applied to drop-weight impact sensitivity results[2], is examined for two opposite limiting size-scale applications: (1) for the transition from micro-to-nanometric crystal sizes; and, (2) for analogy with micro-to-macroscopic crack initiation on a fracture mechanics basis. These extensions compare to the intermediate mesoscale at which the pile-up avalanche model provides a fundamental explanation of the shear banding susceptibilities of materials[3]. Connection is examined also with predictions of the pore-collapse model for hot spot generation[4]. Interesting connection is made too with the modeled greater (impacting) piston speed required to reach a sustained combustion threshold during compressive compaction of smaller reactive particles[5].

1. R.W. Armstrong, C.S. Coffey, and W.L. Elban, "Adiabatic heating at a dislocation pile-up avalanche", Acta Metallurgica, Vol. 30, pp. 2111-2116 (1982).
2. R.W. Armstrong, H.L. Ammon, W.L. Elban and D.H. Tsai, "Investigation of hot spot characteristics in energetic crystals", in Energetic Materials, Thermochimica Acta, 6871, pp. 1-11 (2001).
3. R.W. Armstrong and F.J. Zerilli, "Dislocation mechanics aspects of plastic instability and shear banding", Mechanics of Materials, Vol. 17, pp. 319-327 (1994).
4. C.M. Tarver, "Next generation experiments and models for shock initiation and detonation of solid explosives", in CP505, Shock Compression of Condensed Matter -- 1999, edited by M.D. Furnish, L.C. Chabbildas, and R.S, Hixson, Amer. Inst. Phys., N.Y., 2000, pp. 873-977.
5. K.A. Gonthier, "Modeling and analysis of reactive compaction for granular energetic solids", Report AFRL-MN-EG-TR-7091, 20 pages, 2001 NRC/AFOSR Summer Faculty Fellowship Program.

The Decomposition of HMX at Extreme Conditions

M. Riad Manaa [1], Laurence E Fried [1], Jack Reaugh[1], and Marcus Elstner [2]

[1] Lawrence Livermore National Laboratory,L-282, Livermore, USA
[2] Universität-GH, Paderborn, Germany

Detailed description of chemical reaction mechanisms of solid energetic materials at high-pressure and temperatures is essential for understanding events that occur at the reactive front of these materials and the subsequent building of predictive models of materials properties. We report the results of our ongoing *ab initio* based molecular dynamic simulation of the chemistry of HMX, at density of 1.9 g/cm^3 and temperature of 3500 K; conditions similar to CJ point.

The molecular forces are determined using the self-consistent-charge, density-functional - based tight-binding method. Following the dynamics for a time scale of up to forty picoseconds allows the construction of approximate rate laws for typical products such as H_2O, N_2, and CO_2. The concentration of these species is fit to a functional form $C(t)= C\ (1- e^{-at})$, where C is the concentration at time t and C is the equilibrium concentration. From this fit, we estimate the reaction rates of these products to be 0.5, 0.05, and 0.16 ps^{-1}, respectively.

The simulation results of product formation are also compared to those obtained from thermochemical calculations. We find good agreement for the existence of dominant species, despite the different theoretical approaches. We also show how these rates are being used in hydrocode modeling of flame propagation.

This work was performed under the auspices of the U.S. Department of Energy by the Lawrence Livermore National Laboratory under contract number W-7405-Eng-48.

Equation of State of Unreacted High Explosives as a Function of Porosity

B.D. Lambourn and H.R. James

AWE Aldermaston, Reading RG74PR, United Kingdom

INTRODUCTION

For the majority of the run to detonation during the SDT process, the explosive near the shock front is in its unreacted state, and the remainder is in a partially reacted state, one component of which is unreacted HE. Hence to understand the SDT process it is important to model the equation of state of the unreacted HE as accurately as possible, where the key parameter is the porosity of the explosive. However, there are a number of problems of modelling the available experimental data as a function of porosity. The Hugoniot data is relatively sparse, and often only available at one mean density. What is required is a 'hydrodynamic' EOS, yet the explosives have finite strength and visco-plastic properties. At

the higher porosities the data tends to be well scattered. Finally, there is a question as to whether the Hugoniot measurements at the higher shock strengths have been affected by fast energy release.

The aim in this paper is to develop a plausible EOS for unreacted HEs at their theoretical maximum density, and then to use the Snowplough and p-α models to define the EOS as a function of porosity. The first step is to extrapolate experimental Hugoniot data for porous explosives to a best estimate for the fully dense Hugoniot. This involves choosing a plausible form for the variation of Gruneisen Gamma with volume, and, at least for some explosives, taking account of a finite yield strength.

EXTRAPOLATION OF HUGONIOT DATA TO TMD

Assuming a Gruneisen EOS for the fully dense material at initial specific volume v_{0s}, the Hugoniot for porous material initially at v_0 is

$$p = p_H(v)\frac{(\Gamma+2)v - \Gamma v_{0s}}{(\Gamma+2)v - \Gamma v_0} \qquad (1)$$

where $p_H(v)$ is the Hugoniot for the fully dense material.

Given a suitable function for Gruneisen Gamma, equation (1) can be inverted, so that for every experimental (p,v) state on a porous Hugoniot, a corresponding data point on the fully dense Hugoniot can be evaluated.

A specific value of Γ is known for most materials at NTP. In the absence of other data, it is frequently assumed that Γ or ρΓ is constant. However, for conventional HEs such as PBX9404 and PBX9501, it will be shown that neither assumption leads to a sensible pattern of porous Hugoniots in the p - v plane. The way to overcome the difficulty is to ensure that the porous and fully dense Hugoniots tend to an asymptote at the same volume v_*. For a linear shock velocity - particle velocity fully dense Hugoniot, this leads to a second specific value of Gamma, Γ_*.

$$\Gamma_* = 2(b-1) \quad \text{at} \quad v_*/v_{0s} = (b-1)/b \qquad (2)$$

Given the two values of Gruneisen Gamma, a plausible function is taken for Gamma that tends to a low value as v tends both to zero and to infinity, with a single maximum between.

APPLICATION TO CONVENTIONAL HEs

The method of extrapolating the porous Hugoniot data to form a Hugoniot at TMD has been applied to a number of explosives. Except for very weak shocks for which the Snowplough model is inappropriate, the method works well for porosities less than 10%. For larger porosities, the errors in the porous data are over-amplified.

For PBX9404, PBX9501 and EDC37 the shock velocity – particle velocity Hugoniots at TMD are linear and closely similar. Combining the data together gives

a W u relation

$$W = 2.8 + 1.95\,u \text{ mm/}\mu\text{s} \qquad (4)$$

The slope is at the upper end for inorganic materials, but still plausible. The higher slope of 2.4 that is often used for ~2% porous PBX9404 and PBX9501 arises from the porosity of the samples used.

PETN and Tetryl both have curved W -- u relations, which have been fitted by a quadratic form at low pressures and a linear form at high pressures. The porous data for Tetryl can be fitted by the snowplough model down to densities of 1.5g/cc. In general the snowplough model gives adequate fits to data at porosities less than ~15%.

The problem with the Snowplough model is that contrary to the experimental evidence, shock velocity tends to zero at low pressures. This can be overcome by using a p α model of porosity, where α, the ratio of the porous specific volume to the specific volume of the fully dense material surrounding the pores, is assumed to be a function of pressure. At a pressure when all the pores have closed, α tends to one and the p-α model reverts to the Snowplough model.

EVALUATION OF TEMPERATURE

Temperature is most easily evaluated from a Gruneisen form of EOS if the reference curve is chosen to be the principal isentrope. Estimates for the values of parameters in the pressure-volume relation for the principal isentrope can be found from the Hugoniot. A finite strain form has been used. The resulting temperatures are sensitive to the assumed form for the specific heat as a function of temperature, which is again constrained by the limited amount of data available.

Analysis of Some Ratios of Detonation Parameters by the Zeldovich -Von Neumann - Doring Theory in Acoustic Approximation

A.L. Krivchenko, A.A. Krivchenko, D.A. Krivchenko

Samara State Technical University, Samara, Russia

The question about correlation of parameters of detonation front and parameters in the Chapman-Jouguet (CJ) plane in the Zeldovich - von Neumann -Doring (ZND) hydrodynamic theory is not viewed but postulated that the parameters on the front should be higher. In the researches of the last years [1-3] the question about given ratios and about possible abnormalities (including even complete disappearance of chemical spike) is often sold [3].

In the given work there carried out thermodynamic and acoustic analysis of the ZND model with the aim to reveal the main regularities of parameters changes in the zone of chemical reaction. The main conservation laws for the classical and modern hydrodynamic theory of detonation are described only by the segment of Reiley - Mikhelson straight line on the segment from Jouguet point to the initial state. That is why it seems to be quite expedient to view the segment of the given straight line from the state on the front (f) to the CJ plain, which, due to the equality of propagation rates, can be described by the following expression:

$$D^2=V^2\frac{P_f-P}{V-V_f} \qquad (1)$$

Given equation defines the correlation of parameters on the front and on the CJ plain.

Analysis of the equation of energy conservation between the front and the CJ plain shows that kinetic front energy (chemical reaction is absent) should be equal to the sum of kinetic energy and change of inner energies of the products of detonation and initial explosive, which for the mass unity can be expressed in the following way:

$$\frac{1}{2}U^2=\frac{1}{2}(P-P_0)(V_0-V) \qquad (2)$$

$$\varepsilon-\varepsilon_0=\frac{1}{2}(P+P_0)(V_0-V) \qquad (3)$$

Rejecting P_0 as a small quantity we may present the full energy change on P-V diagram as a square with diagonal PV- P_0V_0, and energy change on the front as a triangle with diagonal P_fV_f - P_0V_0

Equality of floor spaces of the triangle and square are correspondent to the ratio

$$\frac{P_f}{P}=\sqrt{2}\approx 1.4142$$

Thus, this correlation defines the parameters of the process for ideal detonation or extremal diameter of the charge. In case if charge diameters are smaller than extremal diameter, the correlation will decrease due to dissipative losses of the process.

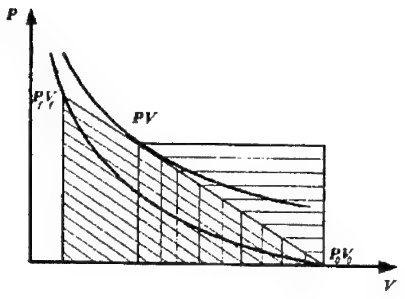

Figure 1.

Reiley - Mikhelson straight line, which is tangent to the adiabat of detonation products, simultaneously defines their sound speed:

$$C = \sqrt{\left(\frac{\partial P}{\partial \rho}\right)_S}.$$

Tangent to point P_fV_f on the adiabat of the initial explosive is also sound speed on the front of detonation process, and as a result of chemical reaction absence the entropy is also constant, thus $C = \sqrt{\left(\frac{\partial P_f}{\partial \rho_f}\right)_S}$. As in many experiments resilient acoustic precursor of detonation is not seen, thus $C_f = D$.

According to acoustic correlations during substance compression, its sound speed is defined by the following expression:

$$C = C_0\left(\frac{\rho}{\rho_0}\right)^3 \qquad (4)$$

From this it follows

$$D = \left(\frac{\rho_f}{\rho_0}\right)^3 \qquad (4')$$

Using mass conservation during compression law in the form of the expression

$$\rho_0 D = \rho C \qquad (5)$$

and substituting D from the expression (4') by way of simple transformations, we receive the ratios between the initial density, density of detonation products and explosive on the front of detonation process:

$$\rho_f = \frac{\rho^2}{\rho_0} \quad \text{or} \quad \rho = \sqrt{\rho_0 \rho_f} \qquad (6)$$

Substituting ratio (6) into the expression for sound speed in detonation products and detonation speed, we receive tangency condition in the following way:

$$C_0\left(\frac{\rho}{\rho_0}\right)^4 - C_0\left(\frac{\rho}{\rho_0}\right)^3 = U \qquad (7)$$

which is at the same time represents the equation of state.

Finding the function of mass speed from maximal exothermicity of reaction with the help of equation (7), it is possible with high level of precision to calculate detonation parameters of practically all explosive in the whole range of densities and explosive mixtures containing up to 40% of coolants in some diapason of substances sizes, as well as those explosives (ZOX and TNETB) where chemical spike at high densities was not found [3] .

References

1. A.L. Mikhailov, A.V. Fedorov, *International Conference III Khariton's topical scientific reading. Extreme states of substance. Detonation. Shock waves.* February 26 - March 2, 2001, p. 43.
2. L.V. Altshuler, G.S. Doronin, V.S. Zhuchenko, *Physics of Combusion and Explosion (Russian)*, 1989, N2, pp. 84-103.
3. A.V. Utkin, S.A. Kolesnikov, S.V.Pershin, *International Conference III Khariton's topical scientific reading. Extreme states of substance. Detonation. Shock waves,* February 26 - March 2, 2001.

Thermodynamic Detonation Conditions and Performance of Low Density Explosive Compositions

N.A. Imkhovik, V.S. Soloviev, I.P. Machneva

Bauman Moscow State Technical University, Moscow, Russia

Application of HE of low density in systems of "soft" shock-wave loading and high-velocity safe accelerating of low-strength structures including ones charged with HE or pyrotechnic compounds and in mine clearing devices is based on comparatively high performance of Low Density HE (LDHE) and lower loading level on environment in comparison with brisant HE and ability to control the energy release and impulse transfer processes. Experimental investigations [1-8] and theoretical studies [9, 10] deal with features of detonation waves propagation and detonation initiation in LDHE, detonation parameters and LDHE explosion work determination.

LDHE with additives of high energy such as aluminum and HE-oxidizers are particularly interesting in terms of gas-dynamic impulse device charge performance increase. However today there are no reliable methods of detonation parameters calculation and estimation criteria of ballistic properties of compounds, which take into account the real device dimensions, because detonation regimes differ essentially from ideal ones due to heterogeneity (porosity) of LDHE charges and presence compounds with essentially different physical mechanical and thermodynamic properties in them. In addition compounds of low density are usually applied in specific schemes of loading and accelerating, in which it is not always affordable to use accelerating ability estimation methods designed for HE of high density. The main reason is that the parameters of detonation products (DP) of LDHE as the working body at accelerating are balancing for a comparatively long period, and existing experimental evaluation methods of process characteristics of energy transfer-obtaining, in particular, ballistic pendulum method, impulse meter, side accelerating of plate and cylinder test [11], are designed for more intensive loading.

The results of theoretical study and experimental data are presented in the paper for the wide range of LDHE on the base of RDX with urea-formaldehyde resin (microporous rubber or MR), phenol-formaldehyde micro spheres (PMS), bakelite filler and energetic additives: aluminum (ASD-1) and HE oxidizers (ammoniac niter (AN), potassium perchlorate (PP), ammonium perchlorate (AP)). Mixtures on the base of TNT/RDX 40/60 with expanded polystyrene (EP) and aluminum have been considered. Initial characteristics and composition of LDHE under consideration are presented in Table.

Features of LDHE detonation parameters calculation. The range of initial densities of LDHE, which can be obtained by application in such compounds fillers of low densities, is from 200 to 800

kg/m^3 [1-4, 8, 12], that is essentially low than gravimetric densities of powdery HE. ρ_0 = 50 - 200 (700) kg/m^3 which is characteristic for explosive foams [5 - 7], and the range ρ_0 = 300 - 900 kg/m^3 for aerated systems [9]. Practically lower level of density values as a rule is determined from detonation limits of a system taking into account the real device charges dimensions and technological possibilities, when upper level is determined from permissible values of loading on accelerating and elements under shock wave action.

In contrast to gas-drudges with DP pressure at Chapmen-Jouget plane p_H lower than units of megapascals, p_H of LDHE is 0,1-10 GPa depending on initial charge density. At such pressures it is already impossible to use the equation of state of ideal gas, and real gas models [11, 13 - 16] designed for HE of high density on the analogy of condensed materials are not still applicable. So it is impossible to neglect neither thermal, nor elastic components of pressure and energy [11, 16].

For the thermodynamic calculation of detonation parameters for LDHE real gas models are the most acceptable, which take into account contributions of separate components of DP mixture and corresponding virial and covolume equations of state. The paper [9] has applied an equation with five virial coefficients, but the complexity in determination of dependencies of these coefficients on temperature for every single DP makes difficult application of this equation despite its realistic form. Theoretically rigorously proved virial Boltzmann-Hirschfelder equation, produced in accordance with the kinetic gas theory for rigid spherical molecules, as well as Abel equation with constant covolume appeared to be inapplicable for the description of the real DP state of LDHE at $\rho_0 \geq 500$ kg/m^3 [11, 16].

For calculation HE detonation parameters within the range of densities $200 \leq \rho_0 \leq \rho_{max}$ in the paper [14] both virial equation in the VLW form obtained with the help of Lennard-Jones potential of intermolecular interaction, and equation with variable covolume in the BKW form [11, 13, 16], obtained by introduction of repulsive potential corresponding to the model of "soft" spherical molecules in the equation with virial coefficients and substitution of power series with exponential function have been used.

Calculation results presented in the paper [14] for LDHE based on RDX, PENT and TNT showed, that both the equations VLW and BKW describe satisfactory parameters corresponding to the limit detonation regimes and their dependencies on initial charge densities in the range of LDHE. At that the BKW equation used values of α, β, γ, θ coefficients obtained by Mader [13] for HE of high and poured densities. The restriction of experimental base for ideal (limit) detonation parameters of LDHE didn't afford to correct fitting coefficients of BKW equations as applied to LDHE. Nevertheless regularities of DP LDHE behavior at ideal detonation regimes can be studied with even incompletely calibrated parameters of equation of state (at least for said and analyzed in the paper [14] LDHE).

We should consider dependencies $D(\rho_0)$ and $p_H(\rho_0^2)$ representing liner functions for the most LDHE as the features of LDHE DP behavior established on the base of thermodynamic calculation analysis (this fact is usually used in express methods of evaluation of these HE detonation parameters [11]). But these dependencies are not linear in the range of low density $\rho_0 \leq$800-1000 kg/m^3. The last phenomenon is connected with the change of DP composition, reducing of thermal effect of chemical reaction HE Q_{pT} and energy redistribution between elastic and thermal components. DP adiabatic index decreases with ρ_0 reduction from typical for the most poured HE $k \approx$2,5 to 1,5-1,7 (at ρ_0=200 kg/m^3) approaching to corresponding values k =7/5-9/7 for ideal gas. When using the BKW equation, the calculation DP temperature as a rule increases with ρ_0 reduction, which qualitatively corresponds to test data [11, 13].

Modeling of detonation and energetic characteristics of LDHE. Numerical method, algorithm and code [10, 14, 15,17] have been used to determine LDHE ideal and non-ideal detonation parameters, presented in Table 1, composition and thermodynamic DP characteristic at Chapmen-Jouget plane and at expansion isentrope. Composition, initial density ρ_0 and enthalpy of production ΔfH^0_{HE} of studied HE were posed as input data for the calculation.

As LDHE have large values of limit diameters d_{lim}, at which ideal regimes of charge detonation and ratio $D_{cr}/D_{lim} \approx 0,5$ are achieved according to the papers [1,12], the comparison of thermodynamic calculation with test data should be carried out taking into account the dependencies of detonation velocity on charge diameter $D(d)$. For determination of $D_{lim}=D(d_{lim})$ test data for RDX/MR and poured RDX have been extrapolated to infinitely large charge diameter $D(d \to \infty)$. At ρ_0 = 400 kg/m^3 and in

charges of 30 mm diameter even contained in massive steel shells steady non-ideal detonation regimes occur owing to curvature of detonation wave front (DW) and "delayed" energy release at DW, at that "shortage" of detonation velocity (D_{exp} in Table) is more than 10% relative to D_{lim} [12, 14]. For TNT/RDX/EP at the same initial density as for RDX/MR (ρ_0 = 400 kg/m^3) limit diameter achieves already 300 mm, and ration $D_{cr}/D_{lim}\approx 0.4$ [8].

Thus thermodynamic balance in DP of HE mixtures containing aluminum, HE-oxidizer and inert frame filler of low density may not be achieved even at sufficiently large charge diameters (more than 100 mm providing flat surface of detonation front) owing to difference of kinetic characteristic of decomposition of such composition components and influence of diffusion factor (incomplete mixing of decomposition products). Parameters of non-ideal steady detonation regimes have been determined on the base of Gibbs energy minimization at given particular thermal and chemical non-equilibrium with the method presented in the papers [10, 15]. In common case three calculation variants have been used corresponding to ideal (variant I) and non-ideal (variants II, III) detonation regimes:

I - complete thermodynamic equilibrium of DP at Chapmen-Jouget plane, at which all the components (in common case up to 45 gaseous substance and 5 *k*-phases) are in mechanical, chemical and phase equilibrium;

II - at Chapmen-Jouget plane aluminum stays hard, chemically inert and has internal energy in accordance with its Hugoniot, i.e. particular chemical and thermal non-equilibrium of PD mixture of LDHE with aluminum takes place;

III - decomposition products of base explosive component – RDX are in mechanical equilibrium with other initial components (aluminum, oxidizers, TNT, inert fillers), which are considered as non-reacting before Chapmen-Jouget plane and are pressed along their Hugoniots, that corresponds to more realistic degree of non-ideality in comparison with variant II.

Results of thermodynamic calculation are shown in Table and demonstrate essential influence of composition and degree of non-ideality of detonation (calculation variant) on detonation and energetic characteristics of LDHE. At equal values of ρ_0 the highest levels of detonation velocity D and pressure at Chapmen-Jouget plane take place ρ_H in RDX/MR compositions containing in comparison with other compositions maximum quantity of the base explosive – RDX and minimum quantity of inert filler. The influence of initial HE density ρ_0 and aluminum additives on detonation parameters of RDX/MR has been studied in the papers [10, 15, 18]. At that it has been shown, that in contrast to HE of high density, for which aluminum oxidation (in case of negative oxygen balance of HE) reduces D and ρ_H, for LDHE (at $\rho_0\approx 500$ kg/m^3) ideal detonation velocity stays practically constant, and PD pressure increases with increase of aluminum mass ratio in the mixture and achieves maximum at 10-15% of Al. If there is more aluminum, D and ρ_H decrease, although thermal effect of reaction Q_{pT} at constant pressure and temperature continues growing. The same calculation dependencies for mixture of TNT/RDX/EP with aluminum. At that the optimum ratio of aluminum additive calculated for these compositions are in a good agreement with the real values.

Table. Thermodynamic calculation of detonation conditions and DP LDHE characteristics

№	LDHE, Composition, (ρ_0, kg/m^3 /D_{exp}, m/s)	Calcul. variant	D, m/s	P_H, GPa	Q_{pT}, MJ/kg	k	k^*	V^0_{DP}, m^3/kg
1	RDX/MR 92/8 (400/3740±50)	I	4010	2.12	4.54	2.04	1.67	0.96
	RDX/MR 92/8 (500/4000±50)	I	4373	3.03	4.60	2.15	1.76	0.96
	RDX/MR 92/8 (600/4360±50)	I	4724	4.12	4.65	2.25	1.85	0.95
2	RDX/Al/PMS/bakelite	I	3723	2.55	5.02	2.10	1.54	0.73
	62/10/14/14	II	3573	2.22	3.34	2.27	1.71	0.73
	(570 / 3400±100)	III	3670	2.30	3.19	2.34	1.57	0.56
3	RDX/AN/Al/PMS/bakelite	I	3528	2.49	6.34	2.06	1.41	0.63
	40/15/20/12/13	II	3373	2.16	2.75	2.22	1.75	0.67
	(610 / 3245±100)	III	2950	1.52	2.05	2.49	1.77	0.36

4	RDX/AP/Al/PMS/bakelite 40/15/20/12/13 (610 / 2820±150)	I II III	3510 3470 2920	2.47 2.24 1.50	6.62 2.86 2.05	2.05 2.27 2.47	1.39 1.76 1.75	0.59 0.66 0.36
5	RDX/PP/Al/PMS/bakelite 40/15/20/12/13 (610 / 2350±100)	I II III	3166 3261 2838	2.01 1.98 1.44	6.69 2.78 2.05	2.04 2.25 2.41	1.32 1.70 1.72	0.51 0.64 0.36
6	TNT/RDX/EP 38/58/4 (540 / 3950±50)	I II	4250 3360	3.06 1.87	4.17 2.97	2.20 2.27	1.78 1.70	0.90 0.52
7	TNT/RDX/Al/EP 35/51/10/4 (590 / 3550±100)	I II III	4160 4080 3227	3.31 3.00 1.84	5.53 3.72 2.62	2.08 2.25 2.34	1.60 1.80 1.73	0.77 0.80 0.46

The introduction to these LDHE 15% additive of HE-oxidizer (AN, AP, PP) leads to further increase of Q_{pT} owing to aluminum and condensed carbon oxidation and decrease of average molecular mass of gaseous DP and adiabat index $k=\rho_0 D^2/p_H-1$, that, however, doesn't give considerable gain of $D \sim (Q_{pT})^{1/2}$, as it may be from the classical theory and assumption about constancy of polytrope index $k^*=(D^2/2\ Q_{pT}+1)^{1/2}$, which is valid for ideal gaseous systems. It has been explained in papers [10, 15, 18] as change in DP composition owing to decrease the total mole quality of gaseous DP at Chapman-Jouget plane and DP volume when expanding to normal conditions V^0_{DP} as a result of production of k-phases Al_2O_3 and C_k of high density. Detonation imperfection of LDHE with aluminum and oxidizers at calculation on variants II and III without taking into account the burnout of energetic additives results in sharp (2-3 times) decrease Q_{pT} at Chapman-Jouget plane, considerable recession of pressure p_H and to lower extend reduction of detonation velocity D (approximately 5-20%).

The velocity of DP ($W^*=(2\ E_{Gurni})^{1/2} = (2(E_H-E_S))^{1/2}$) during isentropic expansion and evolved isentropic volume internal energy ($E^* = \rho_0(E_H - E_S)$) are taken as criteria of ballistic of LDHE [17, 19]. The characteristics W^* and E^* also show the specific area of using and ability to make analytical calculation of throwing velocity for some geometrical shames. For charges of same density the most high means of W^* and E^* characteristics realize for explosive mixture RDX/MR. The explosive mixture TNT/RDX/polystyrene and this mixture with aluminum (with 10 % Al) in the case, when all aluminum is oxidized, demonstrated close means of W^* and E^*. The addition of 20 % Al and 15 % explosive-oxidizer simultaneously (AN, APC), which give the essential increasing of the heat of explosive transformation Q_{pT} , don't give visible increasing of W^* and E^*. This fact shows the influence of lowering parameters of detonation, which, in their turn, is consequence of amount of moles of gaseous DP in Chapmen - Jouget plane.

We put LDHE in the line of throwing ability, but this line transforms according to limitation of pressure of load in living detonation wave and to limitation in the sizes of charges in throwing devises. These limitations show high effect in explosives with ammonium and potassium perchlorate. The comparison of the result of calculation and experimental dates in the different conditions of using LDHE shows conformity between calculated and experimental lines of pressure and throwing ability.

References

[1] V.S. Soloviev, S.G. Andreev, K.N. Shamshev et al., «Optical and X-ray photographic investigations of detonation properties of HE of low density on the base of RDX», Proc. of the III All-Union symposium on burning and explosion., Moscow, Nauka, 1972, P. 451.

[2] M.M. Boiko, V.N. Kramarenko, V.S. Soloviev, «Detonation features of HE of low density with open porosity», Chimfizika processov gorenia i vzryva. Detonacia., Chernogolovka, 1977, P. 58.

[3] L.N. Akimova, M.F. Gogulya, V.N. Galkin, «Detonation parameters of low density condensed HE», *Rus. J. Fizika gorenia i vzryva*, 1978, V. 14, No. 2, P. 135.

[4] K.K. Shvedov, S.A. Koldunov, T.P. Gruzdeva, A.N. Dremin, «Study of detonation and explosive work of mixed HE of lower density with expanded polystyrene», Preprint OIHF AN SSSR, Chernogolovka, 1984.

[5] J.L. Austing, A.J. Tulis, C.D. Johnson, «Detonation Characteristics of Very Low Density Explosive Systems», Proc. of the Fifth Symposium (Intern.) on Detonation, ACR-184, ONR, 1970, P. 47.

[6] L. Xueguo, «Detonation Characteristics of Polyurethane Foamed Explosives», Proc. of the International Symposium on Intense Dynamic Loading and Its Effects, Beijing, China, 1983, P. 173.
[7] C.J. Anderson, K.V. Rosen, A.W. Gibb, I.O. Moen, «Detonation properties of explosive foams», Proc. of the Ninth Symposium (Intern.) on Detonation. Portland, 1989, P. 601.
[8] I.F. Kobylkin, I.P. Machneva, N.I. Nosenko, V.S. Soloviev, «Low density explosive compound TNT/RDX/EP», Proc. of the X Symposium on combustion and explosion, Chernogolovka, 1992, P. 31.
[9] S.A. Gubin, V.N. Michalkin, V.V. Odintzov et al., «Calculation of detonation parameters and composition of detonation products of low density mixtures of various state», *Rus.J. Chemical Physics*,1983,No.3,P. 420
[10] N.A. Imkhovik, V.S. Soloviev, «Thermodynamic calculations of detonation parameters in mixtures of HE with aluminum», Chemical physics of transformations in shock waves. Detonation, (Proc. of the IX All-Union symposium on combustion and explosion), Chernogolovka, 1989, P.33.
[11] F.A. Baum, L.P. Orlenko, K.P. Stanukovich et al., Physics of explosion, Moscow, Nauka, 1975.
[12] V.A. Pyriev, V.S. Soloviev, «Detonation characteristics of HE», *Rus. J. Fizika gorenia i vzryva*, 1992, V. 28, No.3, P.69.
[13] Mader C. L., Numerical modeling of detonation , Univ. of California Press, Los Angeles, CA 1979.
[14] N.A. Imkhovik, V.S. Soloviev , «Calculation of equilibrium thermodynamic parameters and composition of detonation products of condensed HE»,*Rus.J. Vestnik MGTU, Seria "Mashinostroenie"*, 1993,No.2, P. 53.
[15] N.A. Imkhovik, V.S. Soloviev, «Thermodynamic calculation of detonation parameters of multi-component mixed explosive compositions», *Rus. J. Vestnik MGTU, Seria "Machinostroenie"*, 1994, No. 3, P. 95.
[16] N.A. Imkhovik, S.G. Andreev, V.S. Soloviev, «Equation of state of detonation products of condensed HE» Mechanika impulsnych processov, Trudy MGTU No. 557, 1992, P. 17.
[17] N.A. Imkhovik, V.S. Soloviev, G.G. Shevelenkov, «Calculation of isentropic expansion of detonation products of condensed HE», *Rus. J. Oboronnaya technika*, 1993, No. 9, P. 3.
[18] N.A. Imkhovik, V.S. Soloviev, «Oxidation of aluminum particles in products of condensed explosive detonation», Proc. of the XXI Intern. Pyrotechnics Seminar, Moscow, 1995, P.316.
[19] N.A. Imkhovik, I.P. Machneva, V.S. Soloviev, «Thermodynamic calculations of detonation parameters and estimation of the throwing ability of the low-density explosives», Proc. of the XI Symposium on combustion and explosion, Chernogolovka, 1996, V. 2, P.66.

Study of Heterogeneous Explosive Decomposition at Pressure Decrease after Shock Wave Front

S.G.Andreev, N.V.Paliy

Bauman Moscow State Technical University, Moscow, Russia

Heterogeneous explosives decomposition at rarefaction after front of initiating shock wave has some features. Explosive decomposition can stop (after partial development) at the pressure decrease. But, under certain conditions the decomposition rate increases because of pressure decrease after initiating shock wave [1] or because of increasing of specific volume of reacting flow [2]. Nontrivial behavior of decomposition rate at detonation initiated by short initial pressure impulse had been discussed in [3].

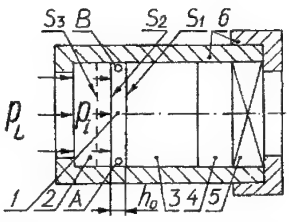

Figure 1. Generalized scheme of QTL experiments:
1 – explosive layer under consideration; **2** – facial shield; **3** – rear shield; **4** – gap for regulation of residual pressure; **5** – arrangement for braking and comparison of final hydrodymamic effects; **6** – body and cover; S_1 – arrangement surface for pressure sensor and foil for electric conductivity measurement; S_2 – arrangement surface for foil; S_3 – arrangement surface of pressure sensor for $p_L(t)$ calculation (without usage supplementary experiment)

The present paper is intended to formulate and to improve views about processes accompanied explosive decomposition in weak shock wave and contributes to development of reaction kinetics equations allowing to model these features. The results of original experiments and decomposition

modeling under pressure changing in time in various ways have been compared and possible reasons of divergence have been analyzed in the paper.

In spite of traditional method for Lagrangian analysis of reacting flow we use some another method that we named the "method of quasi thin layers" (QTL method). The method allows to study the explosive decomposition at pressure changing law $p(t)$ close to dependences given by researcher before the experiment.

The experiment scheme for the QTL method is shown in Figure 1. The explosive charge under consideration is made in the form of layer of $h_0 << l_1$ thick (here l_D – distance to detonation at the initial impulse pressure $p_1(t)$). The material of rear shield has the same dynamic compressibility as the tested explosive. The simplest (but not the best) way to define $p_1(t)$ is pressure measurement in subsidiary experiment without explosive between rear and facial shields. In order to carry out the hydrodynamic analysis of QTL decomposition, the impulse $p_L(t)$, creating flat-symmetrical flow, is applied to butt-end of facial shield. The construction with braking mechanism of rear shield allows to obtain explosive specimens partly decomposed and been under the residual pressure p_r in adiabatic conditions or to obtain hot-spot decomposition image. At hydrodynamic analysis and decomposition modeling we use the system of equations, obtained at assumption of homogeneous distribution of state characteristics and linear distribution of mass velocity through the thick of expanding explosive layer.

$u_- = [F(p)-1](\alpha/2\beta)$;

$u_- = u_{c1} - (p-p_{c1})/(\rho c)$;

$u_{c1} = u_- + (p_1-p_{c1})/(\rho c) - h_{t1}$; $p_{c1} = \rho_0 u_{c1}(\alpha + \beta u_{c1})$

$u_+ = [F(p_1)-1](\alpha/2\beta)$; $h_{t1} = (h_1/v_{e1})(dv_e/dp_1)dp_1/dt$;

$dh/dt = u_+ - u_-$; $h = h_0 v/v_{e0}$; $v_{e0} = 1/\rho_{e0}$;

$d(e+e_k)/dt = -pdv/dt$; $e_k = [(u_-^2 + u_+^2 + u_- u_+) - (3u_{t1}^2 + h_{t1}^2 - 3u_{t1}h_{t1})/6$;

$v = wv_g + (1-w)v_e$; $e = we_g + (1-w)e_e$;

$v_e = v_e(p)$; $e_e = e_e(p, v_e)$; $e_g = e_g(p, v_g)$; $T_g = T_g(p, v_g)$; $p_1 = p_1(t)$.

where v, e, p, T - specific volume, specific energy, pressure, temperature; u_- and u_+ – the velocities of explosive layer planes directed to rear and facial shields accordingly; h thickness of explosive layer; ρ_0, α and β - density and parameters of shock adiabat ($D = \alpha + \beta u$) for rear shield with the same form as explosive under consideration; ρc – acoustic impedance of facial shield concerned in acoustic approximation; w – decomposition fraction; e and g – indexes for explosive and its reaction products; 0 – index of standard initial state; e_k – kinetic energy; $F(x) = (1+(4\cdot\beta\cdot v_0\cdot x/\alpha^2))^{0.5}$. Index c means calculated correction of the loading impulse $p_L(t)$, necessary so that at homobaric model the dependencies $v_e(p)$ and $p_1(t)$ would be the same as at QTL compression by wave.

The system is closed by experimentally obtained laws $p(t)$ and $p_1(t)$ and is used for extracting of reaction kinetics $w = w(t)$ and $\eta = dw/dt$.

The system closed by $p_1(t)$ and reaction kinetics is used for modeling the process. The value of h_0 is so that difference between $p(t)$ and $p_1(t)$ would be not great, but enough to obtain reaction kinetics.

The reaction kinetics system used in modeling is based on idea about explosive decomposition after shock wave front as laminar burning. The topology of the combustion is defined by spherical hot-spots concentration – N_{cr}, by distribution law of sizes of cubical cells (modeling microstructure of explosive), by distribution regularity of hot-spots on the cells surface of explosive structure (the cells are some models of explosive grains or conglomerations of explosive grains), by specific volumes of reaction products and matrix explosive. The dependence N_{cr} upon front pressure p_f of initiating shock wave is calculated with the use of rules of viscous-plastic mechanism of active hot-spots formation from spherical pores with given distribution of size. The model of quasi-stationary burning with front rate is used.

$$U_B = [Bp^{\nu}][\psi_1(\overline{T_g})]\cdot[\psi_2(p_f, w, \ldots)]$$

where B, ν – parameters of explosive burning law with standard initial temperature T_0^{ST} = 298 K in standard conditions of burning in which reaction products are not cooled because of adiabatic expansion. It is assumed that U_B is defined by reaction zone of intermediate heat-release with the temperature T_{fl0}. The function ψ_1 describes the influence of dependency $\overline{T_g}$ of reaction products temperature T_g adiabaticaly changing of specific volume v_g and temperature T_{fl0} of intermediate heat-release zone that

defines the burning rate of explosive heated higher than T_o^{ST} at v_g = const. The function ψ_2 describes the influence of heating heterogeneity of porous explosive at shock wave compression.

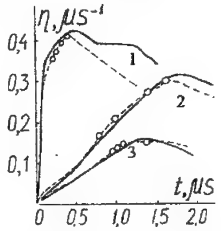

Figure 2. Comparison of η(t) at stepped initial pressure impulse:
1 – PETN ρ_{co}= 1,67 g/cm^3 p_f = 2,2 GPa;
2 - RDX_{ad} ρ_{co} = 1,60 g/cm^3 "damaged structure" p_f = 23 kbar;
3 - RDX_{ad} ρ_{co} = 1,63 g/cm^3 p_f = 22 kbar
(here RDX_{ad} means RDX +5% of wax-like additive)

The main condition of burning existence is defined by the model, in which governing parameter is $\bar{\tau} = \tau_\chi/\tau_p$. Here τ_χ is time of relaxation of temperature gradient in explosive from value, which corresponds to burning at pressure p, to value, which is necessary for burning at pressure p-Dp. It is necessary to emphasizes that temperature gradient is considered at the surface of transition of explosive to gas phase. And τ_p is time of pressure decrease from value p to value p-Dp. If $\bar{\tau}$ is greater than critical value τ_{crit}, then we have initial failure of burning. It occurs because of great heat conducting from reaction zone, i.e., because of cooling this zone. Value τ_{crit} is selected on the base of experimental data on critical conditions of burning failure at pressure decrease.

The additional condition of burning existence assumes the possibility of repeated explosive ignition at certain stock of heat in reaction products of extinguished hot-spot and intensity of its heat exchange with surrounding explosive.

The parameters of reaction kinetics system sorted out taking into account the results of extraction of decomposition kinetics at stepped initial impulse with $p_f \approx 20$ kbar (Fig.2). The quasi-thin layers of explosive with h_0 = 0,4 – 0,6 m and with various degree of explosive grain damage (given by the way of quasi-thin layers preparation) have been investigated. Circles show the calculated contact moments of burning spherical surfaces and topology changing for each fraction of explosive structure cells. The hot-spots contact begins in big fraction and defines calculating value of delay of electric conductivity appearance between opposite quasi-thin layer planes t_s^C. The relation $t_s^{EX} < t_s^C$ (where t_s^{EX} – experimental value of electric conductivity appearance) is observed for most explosive compositions with large content of wax-like binders excluding influence of connected pores.

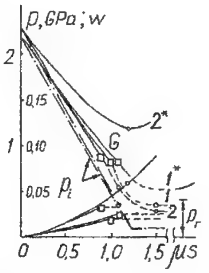

Figure 3. Results of RDX_{ad} decomposition modeling at T_{flo} = 1100 K.
1 and 1* - "undamaged structure";
2 and 2* - "damaged structure";
1 - h_0 = 0,6 mm;
1* - h_0 = 2 mm;
2 - h_0 = 0,4 mm;
2* - h_0 = 2 mm.

The obtained reaction kinetics is used for calculation of quasi-thin layer decomposition dynamics at various $p_f(t)$, for example in form shown in Fig.3. Squares with index G (failure) show the moments of initial failure of burning. The critical degrees of decomposition W_G^{cr} have been calculated. Its achievement to the moment of initial failure of burning allows repeated explosive ignition with the delay depended upon the level of residual pressure p_r (Fig.4). The transition of mixture of reaction products and explosive from p_G to p_r=*const* is suppose to be isentropic. The relation $W_G^{cr}(p_f)$ depends upon the process history before the initial failure of burning.

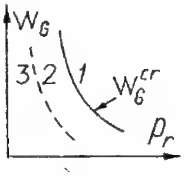

Figure 4. Evolution variants of process
after the initial failure of burning:
1 – continuation of burning with delay;
2 – thermal decomposition of condensed explosive
(thermal explosion);
3 – "final freezing" of decomposition.

The decomposition modeling is accompanied by estimation of explosive deformation velocity $\dot{\varepsilon}$ just before spherical burning surface. In quasi-thin layer of RDX_{ad} at the p_f=23 kbar $\dot{\varepsilon}$ decreases from ~10^8 1/s at the decomposition beginning up to ~10^6 1/s at the $W \sim 10^{-2} \div 10^{-1}$ achievement.

The calculated results (Fig.3) are confirmed with experiment results to define the critical condition of reaction failure. The Figure 5a shows the results of simple experiment for estimation of critical condition of reaction failure in RDX_{ad} ρ_{00} = 1,63 g/sm^3 with initial "undamaged" structure. The facial shield loading creating monotonous parameters changing $p_f(t)$ in direction from A to B has been used (Fig.1). The amplitude of the first pressure peak and average rate of the pressure decrease after initiated shock wave front were: 10 kbar and 5 kbar/mks in zone A; 25 kbar and 20 kbar/mks in zone B. The pressure relaxation oscillations are followed after the first pressure peak (the parameters of $p_f(t)$ were obtained by calculation).

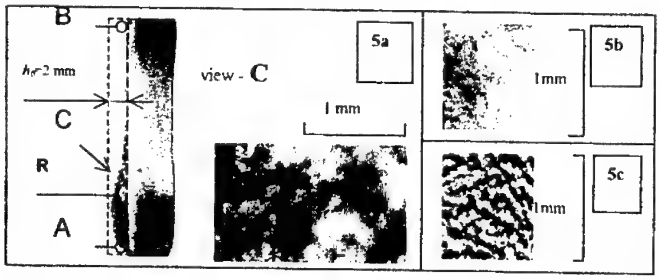

Figure 5. The results of simple experiments for estimation of critical conditions of "final freezing"of decomposition. (R is the rest of RDX_{ad} and wax-like casing of quasi-thin layer).

The dark background in photorecording of surface of residual explosive layer in direction of zone C is shady image of cavity between grains and conglomerates of explosive grains produced by reaction products. The Figure 5b shows image of reaction zone with subcritical degree ($10^{-4} \div 10^{-3} \sim W < W_G^{cr}$) of decomposition of RDX_{ad} ρ_{00} = 1,5 g/sm^3 (dark zones – shady image of micro cavities filled with light reaction products without any dark products). After achievement of the supercritical decomposition degree the same quasi-thin layer continues to decompose up to W~1. In this case the flouroplastic rear shield (Fig.5c) registers the reaction zones at shock-wave stage (dark – reaction products, light – copy of RDX grains).

The used reaction kinetics system allows to predict existence of the two regimes of initial failure of explosive burning at the pressure decrease. The first regime is typical to explosive with T_{fl0} close to maximum value for explosive with the temperature of adiabatic burning equals, for example, to 3300 K for RDX. In this case the initial failure of burning and final failure of reaction can occur directly after hot-spots burn-out as a result of reaction products cooling at expansion up to $T_g < T_{fl0}$ and sharp decrease of burning rate.

The second regime is typical to explosive with low value T_{fl0} (at the limit equals to explosive gasification temperature). In this case the initial failure of burning occurs in absence of influence of reaction products temperature on burning rate.

It is assumed that large explosive deformation and its rates at the beginning of decomposition can essentially influence on topology of burning and mechanism of reaction evolution. The topological features can be concerned with violation of media continuousness in explosive cell structure after the beginning of burning and also with the instability of surface between reaction products and initial

explosive in burning front. The reason of decomposition intensification can be superposition of mechanism of reaction expansion on account of heat-transfer from reaction products and mechanism (and also the initiation [4]) of reaction acceleration by deformation wave, which is generated by expansion of reaction products. If the burning rate is determined by thermal decomposition of condensed phase of explosive then the deformation influence on U_B can be conditioned by changing the pre-exponent factor and the activation energy in generation of critical cores (embryons) of new gas phase.

References

1. Andreev S.G., Boyko M.M., Lazarev V.V., Solovjev V.S., Chernov A.I., *Fizika gorenia i vzryva (Russian Journal of Combustion and Explosion)*, vol.21, N 3, p.80 (1985).
2. Trofimov V.S., Trofimova G.P., *Fizika gorenia i vzryva (Russian Journal of Combustion and Explosion)*, vol.26, N 1, p.136 (1990).
3. J. Wackerle, R. Rabie, M. Ginsberg, A. Anderson, *Symposium on High Dynamic Pressure - H.D.P.*, Paris, 27-31 August 1978.
4. Coffey C.S., *Chemical Physics (Russian)*, vol.17, N 1, p.4 (1998); *Chemical Physics Reports*,

Insights into the Shock Initiation/Detonation of Homogeneous and Heterogeneous HE

S.A. Sheffield, R.L. Gustavsen, L.G. Hill, R. Engelke, R.R. Alcon, and L.L. Davis

Los Alamos National Laboratory, Los Alamos, USA

It has long been known that there are fundamental differences between homogeneous and heterogeneous high explosives. The shock initiation behavior of these materials was first described in the literature by Campbell et al. in 1961.[1,2] Chaiken was also involved in describing this process for liquid nitromethane.[3] Since then, there have been a number of studies which have added considerable insight into the shock initiation/detonation behavior of these materials. We only give a few references here (Refs. 4 – 11) and these should be considered representative; e.g. they do not represent an exhaustive list of references available. Many of these studies were done on homogeneous explosives, most often nitromethane (NM) and include particle velocity gauge measurements, optical temperature measurements, VISAR measurements, as well as streak camera measurements of interfaces. In some cases NM was heterogenized by gelling and adding silica particles.

Homogeneous materials are typically liquids or single crystals in which there are a minimal number of physical imperfections (e.g. bubbles or voids) that can cause perturbations in the input shock and the flow behind it. Homogeneous materials viewed with macroscopic probes characteristic of detonation physics experiments appear uniform. Heterogeneous explosives are generally all other types; these are usually pressed, cast, machined, or extruded into the shapes or parts desired. These materials contain imperfections of a variety of types that cause fluid-mechanical irregularities (called hot spots) when a shock or detonation wave passes over them. Such hot spots cause associated localized space/time fluctuations in the thermodynamic fields (e.g., the pressure or temperature fields) from which reaction spreads in the material. These local thermodynamic variations affect the chemical-heat-release rate – they produce an average heat-release rate that is a combination of chemistry and mechanics. Hot spots could be the result of voids, shock interactions, jetting, shock impedance mismatches, etc.

Shock initiation of homogeneous explosives is due to a thermal explosion that occurs in the material shocked the longest. This reaction produces a reactive wave that grows behind the front and eventually overtakes the front. The reactive wave may grow into what is called a superdetonation before it overtakes the initial shock and settles down to a steady detonation. A superdetonation is a detonation in the precompressed (higher mass density) explosive. The shock initiation process in heterogeneous explosives differs a great deal. The steps are roughly as follows: 1) the shock passes through the explosive heating most of the material to a uniform temperature but also creating hot spots with various sizes and temperatures (the size and temperature of the various hot spots is dependent on the explosive composition and the shock strength); 2) some hot spots release their energy quickly and feed energy forward to the shock front amplifying it (these are typically formed by strong shocks and/or large irregularities; 3) other hot spots react slowly and have a delay before releasing their energy which causes growth considerably behind the shock front (these are typically formed by weak shocks and/or small irregularities). Most

initiating solid explosive materials include both fast and slow hot spots, so the initiation process produces waves that grow both at the shock front and behind it. This leads to a relatively smooth growth of the initiating shock to a detonation, in contrast to the abrupt changes that occur in the homogeneous case. These differences are apparent in both the in-situ reaction wave profiles and the acceleration of the shock front.

In addition to differences in the shock initiation behavior, there are also differences in the diameter-effect curve (i.e., the relationship between detonation velocity and inverse charge diameter) and the Pop-plot (i.e., the relationship between the logarithm of the input shock pressure and the logarithm of the distance or time to detonation). In general, a homogeneous explosive has a shallow diameter-effect curve with very little decrease in detonation velocity before the failure diameter is reached (called the velocity deficit). NM has a velocity deficit of about 1%. Heterogeneous explosives have diameter-effect curves that curve downward as the diameter decreases and can have velocity deficits that are much greater. As an example, heterogenized NM has a velocity deficit of 10%; i.e., an order of magnitude greater than homogeneous NM.

With respect to Pop-plot differences, the initiation behavior of homogeneous explosives is very state sensitive; e.g., small changes in input shock pressure result in large changes in the time or distance to detonation. This is expected because the chemistry depends on a thermal explosion, an inherently state-sensitive process. In the case of heterogeneous materials, hot spots develop at the heterogeneities, stimulating chemical energy release locally and making the explosive initiate at much lower pressure inputs than would otherwise be the case. For example, pure liquid NM can be made to initiate, with a sustained shock input of about 8 to 9 GPa, in approximately 1 μs, whereas the same material with a large number of corundum heterogeneities will initiate in the same time interval with 2 to 3 GPa inputs. Because the hot spots produce reaction locally, heterogeneous explosives have much less-sensitive state-dependent heat-release rates than homogeneous materials. The dependence of the energy release on the bulk material pressure and temperature produced by the initiating shock (which is all important in the homogeneous case) is secondary.

Many of the common explosives used (PBX9501, PBX9502) have initiation/detonation properties that fall in between the purely homogeneous and purely heterogeneous cases. We have made a number of multiple magnetic gauge particle velocity measurements on these materials; some will be presented and discussed. These are all gun experiments in which the input to the explosives is well known because the projectile velocity is precisely measured and the impactor materials are well characterized. Examples of these measurements are shown in Figs. 1 and 2; the waveforms in these figures are particle velocity measurements at discreet Lagrangian positions in the flow. There are eleven separate gauges in Fig. 1 and ten in Fig. 2. In Fig. 1 it is clear that the PBX9501 growth to detonation results from some growth in the front and considerable growth behind the front. We take this to mean that there is some evidence of both a homogeneous and a heterogeneous nature to this reactive wave. In Fig. 2 the waveforms show much more growth in the front and less behind the front. We interpret this to mean that the PBX9502 initiation appears to be more heterogeneous than is the case for the PBX9501. This is interesting and will be discussed in relation to some earlier diameter effect data on PBX9502 of Campbell and Engelke that suggests it has a more homogeneous nature.

The magnetic gauges we use have several "shock trackers" that track the shock front and can be plotted in a distance-time (x-t) diagram to give information about how the shock front accelerates during the initiation process. These data are plotted for Shot 1133 in Fig. 3. The shape of the curve indicates the acceleration is relatively rapid at the time the wave turns over to a detonation. This can be contrasted to the buildup in the PBX9502 experiment of Fig. 2; the x-t data are shown in Fig. 4. The acceleration is much more gradual for the PBX9502, the result of more reaction in the front and less behind the front. We present an empirical form for fitting to the x-t data and use this to compare the nature of the buildup process for these two materials.

We have also completed an experiment where the initiation process in isopropyl nitrate (IPN) has been measured with in-situ magnetic gauges. IPN is a relatively low energy liquid explosive. The data from this experiment are shown in Fig. 5. These profiles show the superdetonation forming and it appears to have reached a near steady state before it overtakes the initial shock. This buildup process occurs faster than that observe in chemically sensitized NM. It appears that the exact details of the buildup process depend on the particular material and the chemistry that is going on during the initiation.

In any case, these waveforms support the modified classical homogeneous initiation model[9]. Details of the wave growth and superdetonation velocity will be discussed in detail.

In summary, these new measurements and analysis add to the knowledge base for homogeneous/heterogeneous initiation and detonation phenomena. However, much more work will be required to work out the details relating to these processes. The solid composite HEs routinely used have both a heterogeneous and a homogeneous nature to them and the differences are measurable and can be quantified to some extent. The large number of in-situ measurements in a single experiment provides a body of data to challenge the reactive models being used in computations and provides a unique challenge for the modelers.

References

1. Campbell, A.W., Davis, W.C., and Travis, J.R., Phys. Fluids 4, p. 498 (1961).
2. Campbell, A.W., Davis, W.C., Ramsay, J.B., and Travis, J.R., Phys. Fluids 4, p. 511 (1961).
3. Chaiken, R.F., *The Kinetic Theory of Detonation of High Explosives*, M.S. Thesis, Polytechnic Institute of Brooklyn (1958); see also 8th Symposium (International) on Combustion, The Williams & Wilkins Co., Baltimore, p. 759 (1962).
4. Campbell, A.W. and Engelke, R., in Proceedings of the Sixth Symposium (International) on Detonation, Office of Naval Research Department of the Navy Report ACR-221, Washington D. C., pp. 642–652 (1976).
5. Engelke, R., Phys. Fluids 22, p. 1623 (1979); 23, p. 875 (1980).

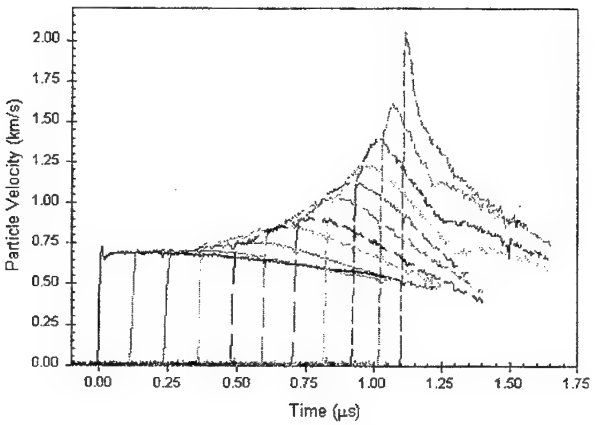

Figure 1. Particle velocity wave profiles from PBX9501 Shot 1133. The input was 5.15 GPa.

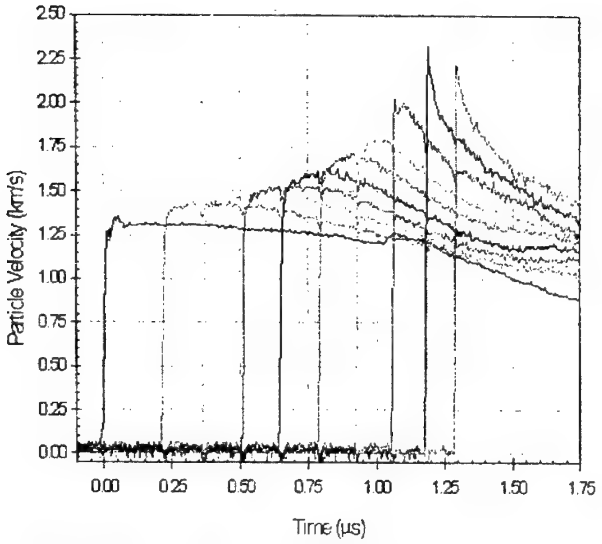

Figure 2. Particle velocity wave profiles from PBX9502 Shot 2s-40. The input was 13.5 GPa.

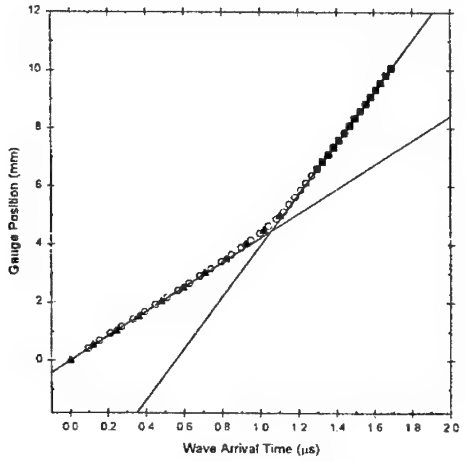

Figure 3. Distance-time (x-t) plot obtained from shock arrival at shock tracker points (before detonation--circles), shock tracker points (after detonation--squares) and particle velocity gauge points (triangles). Data are from Shot 1133, PBX9501.

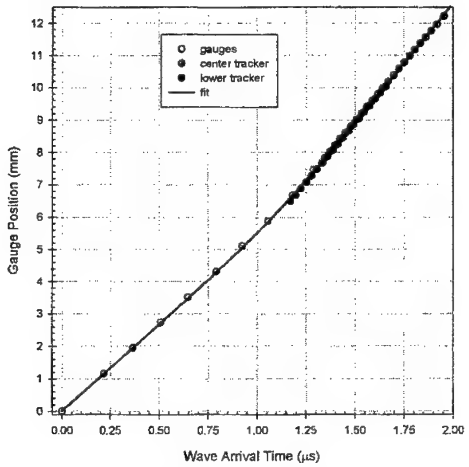

Figure 4. Distance-time (*x-t*) plot obtained from shock arrival at shock tracker points (close together circles), and particle velocity gauge points (far apart circle). Data are from Shot 2s-40, PBX9502.

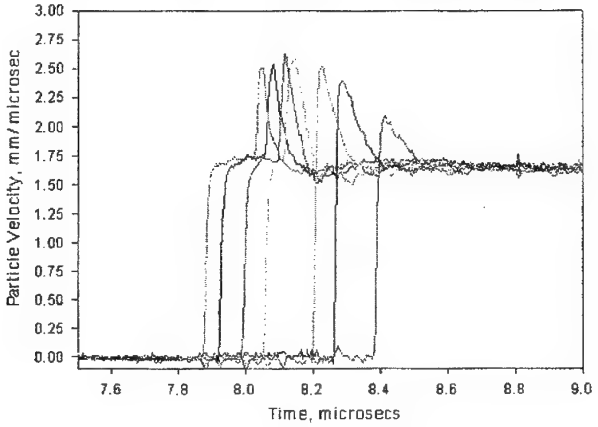

Figure 5. Particle velocity wave profiles from IPN Shot 2s-29. The input was 9.0 GPa.

6. Hardesty, D.R., Combustion and Flame 27, p. 229 (1976); see also Hardesty, D.R. and Lysne, P.C., *Shock Initiation and Detonation Properties of Homogeneous Explosives*, Sandia Laboratories Research Report No. SLA-74-0165 (May 1974).
7. Engelke, R. and Bdzil, J.B., Phys. Fluids 26, p. 1210 (1983).
8. Moulard, H., in Proceedings of the Ninth Symposium (International) on Detonation, Office of Naval Research OCNR 113291-7, pp. 18–24 (1989).
9. Sheffield, S.A., Engelke, R. and Alcon, R.R., in Proceedings of the Ninth Symposium (International) on Detonation, Office of Naval Research OCNR 113291-7, pp. 39–49 (1989).
10. Yoo, C.S. and Holmes, N.C., in Shock Compression of Condensed Matter – 1993, Ed. Schmidt, S., et al, AIP Conference Proceedings 309, p. 1567 (1994); see also Yoo, C.S., Holmes, N.C., and Souers, P.C., in Shock Compression of Condensed Matter – 1995, Eds. Schmidt, S.C. and Tao, W.C., AIP Conference Proceedings 370, p. 913 (1996).

11. Leal, B., Baudin, G., Goutelle, J. C., Presles, H.-N., in Proceedings of the Eleventh International Symposium on Detonation, Office of Naval Research Report ONR 33300-5, Washington D. C., pp. 353 361 (2000).

12. Klebert, P., Etude Experimentale et Theorique de la Transition Choc Detonation Dans les Explosifs Homogenes, These de Doctorat, Universite Paris VI – Pierre et Marie Curie (1998).

Molecular Modelling and Prediction of Explosives Properties

D. Mathieu, P. Simonetti

Commissariat a l'Energie Atomique – Le Ripault, Monts, France

The search for new energetic materials, with satisfactory chemical structures in relation to required specifications, is guided by a predictive approach at the molecular level. In this approach, we develop and we apply techniques to calculate the macroscopic properties, performances and safety, with the only knowledge of the molecular structure. Models are also useful to identify the relevant parameters that play a role in the macroscopic behaviour ; the property of interest is correlated with the adequate molecular features, when an explicit expression is available.

This paper is concerned with the prediction of density and enthalpy of formation of explosives. Indeed, these physico-chemical characteristics are used in the calculation of their performances, detonation velocity or energy released, by a thermochemical code based upon the CHAPMAN-JOUGUET model.

A number of procedures have been applied to calculate density of explosives : the ACD group contribution method [1], statistical techniques by QSPR, and a procedure requiring the 3D molecular geometry and the volume enclosed within atomic radii [2]. An other density estimation model with an explicit term for hydrogen bonds in the correlation is also described.

The solid-state formation enthalpies are obtained as the difference between gas-phase values and sublimation enthalpies. For gas-phase enthalpy formation, we apply either a model relying on empirical procedure and a simple Hamiltonian [3] or geometry optimization and electronic structure calculations using Density Functional Density (DFT) [4], to obtain more accurate results but at higher cost. To estimate sublimation enthalpy, we use an explicit model to describe the Van der Waals interactions at the molecular surfaces, the electrostatic energy and the hydrogen bonds contribution [5].

On a list of explosives with various chemical structures, we calculate detonation velocities with the thermochemical code and the physico-chemical characteristics estimated as above mentioned. Experimental data and theoretical results are compared to qualify the reliability and the accuracy of the methods.

[1] ACD/Chemsketch User's Guide, Version 4.5 , Advanced Chemistry Development Inc. 2000.

[2] G. Piacenza , G. Legsa, B. Blaive, R. Gallo.
J. Phys. Org. Chem. 1996, 9, 427.

[3] D. Mathieu, P. Simonetti, Mol Engin. 8 (1999) 121.

[4] E. Rousseau, D. Mathieu, J. Comput. Chem 21 (2000) 367.

[5] D. Mathieu, P. Simonetti, Thermochim. Acta. to appear.

Influence of High Explosive Initial Density on the Reaction Zone for Steady-State Detonation

A.V. Utkin, S.A. Kolesnikov, S.V. Pershin, and V.E. Fortov

Institute of Problems of Chemical Physics, Chernogolovka, Russia

According to the classical theory [1], the detonation wave consists of a shock jump and a chemical reaction zone, in which the pressure decreases and the matter expands, i.e. Von Neumann spike is shaped. Numerous experimental data confirm the validity of this model for heterogeneous high explosives (HE).

However, it was found [2] that in RDX and HMX at high initial density the pressure increases in the reaction zone and the spike does not form. The detonation wave without Von Neumann spike does not correspond to the classical model. Moreover, it is not clear, whether the Chapman-Jouguet state will be reached, and what the selection rule of detonation velocity is in this case. To solve these key theoretical problems the experimental investigation of the reaction zone transformation under initial density increase in pressed RDX ($C_3H_6N_6O_6$), HMX ($C_4H_8N_8O_8$), ZOX ($C_6H_8N_{10}O_{16}$, Bis (2, 2, 2 – Trinitroethyl - N - nitro) Ethylenediamine), and TNETB ($C_6H_6N_6O_{14}$, Trinitroethyl trinitrobutyrate) was conducted.

The laser interferometric system VISAR was used to investigate the detonation waves structure of pressed HE with different initial density. The laser beam reflected from a 100 - 400 μm aluminum foil placed between the charge and the water window. As the result of the experiment we have the velocity of the foil - water border, which represents all the details of the reaction zone structure in detonation wave.

Critical initial densities ρ_c at which the reaction zone structure changes crucially were found: Von Neumann spike was recorded if the density was less than the critical value, otherwise monotone pressure increase in the reaction zone was observed. The ρ_c is equal to 1.72 g/cm^3, 1.82 g/cm^3, 1.56 g/cm^3, and 1.71 g/cm^3 for RDX, HMX, TNETB and ZOX respectively.

The results obtained for RDX demonstrate that the ρ_c essentially depends on the sample structure and is determined not only by the HE particle size, but also by the pressing process. RDX sample pressing with a small quantity of acetone creates a lot of the potential centers of reaction, and the decomposition rate and explosive part reacting in a shock front increase. Therefore the detonation wave without Von Neumann spike is formed at $\rho_0 > 1.72$ g/cm^3. Pressing with a big quantity of acetone gives the same density at smaller damage of RDX particles, which decreases the decomposition rate and the spike is recorded.

The abnormal change of particle velocity at critical density was found for RDX and TNETB: nearly ρ_c the velocity does not increase with the increase of initial density. It can be explain by transition to underdriven detonation at the disappearance of Von Neumann spike.

The results of this work confirm the possibility of detonation wave propagation without Von Neumann spike in powerful HE. The reaction zone structure changes qualitatively at the critical initial density. It can be explained by growth of the initial decomposition rate of explosive with increase of density if it is assumed that the physicochemical transformations take place in the compression wave. Strong coupling between the shock and reaction zones was noted [3-5]. Moreover when the pressure increases in the reaction zone, the final state of detonation products can be on the weak part of detonation Huhoniot [4,5].

The work has been funded by Russian Fund for Basic Research, grant number 00-03-32308a.

References

1. Zeldovich Ya.B., *The theory of shock waves and introducing in gas dynamics*, Academy Science of USSR, Moscow, 1946, pp.45-98.
2. Ashaev V.K., Doronin G.S., Levin A.D., *Phys. of Combustion and Explosion*, **24**, N1, pp.95-101 (1988).
3. Dremin A.N. *Toward Detonation Theory*, Springer, New York,1999, pp.123-203.
4. Williams F.A., *Combustion Theory*, Addison-Wesley Publishing Company, London, 1964, pp.194-213.
5. W.Fickett. *Introduction to Detonation Theory*. University of California Press, Berkely - Los Angeles - London, 1985, pp.55-61.

Spatial-Temporal Structure of Plane Stationary Detonation Wave in Plasticized TATB and HMX- based Compositions

L.A.Gatilov, I.V.Kuz'mitsky

Russian Federal Nuclear Center - VNIIEF, Sarov (Arzamas – 16), Russia

The study of HE decomposition kinetics is an interesting problem important for practical applications. Typically, this is a function of variables: pressure P, density ρ, and burnup (mass fraction of EP in heterogeneous mixture) F. One seeks to simulate anticipated mechanisms of the physical processes that occur during detonation evolution by selection of a function for reaction kinetics leaning on a certain set of experimental data. A kind of "hierarchy" of the experimental data, which should be involved for the problem solution to be most successful, can be specified. Only one class of experiments will be considered here. These are experiments to determine the spatial-temporal structure of the stationary detonation wave (DW). Considered below are HE TATB (LX-17) and two domestic octogen base explosives VV-2 and VV-3, which are close analogs of HEs PBX-9404, PBX-9501, LX-14, etc. The data on pressure profile P(t) in the chemical reaction zone (CRZ) are obtained with the manganin sensor (MS) method.

Figs. 1 and 2 show the MS oscillograph traces for HEs TATB, VV-2, and VV-3.

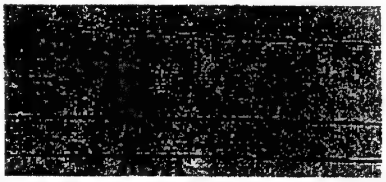

Figure 1. MS pressure oscillograph traces for HE TATB. The MS was located in teflon at a distance of 0.2 mm from the teflon-HE interface. The plane wave had traveled a distance of Δx= 80 mm. The measurement time interval is Δt = 40 ns.

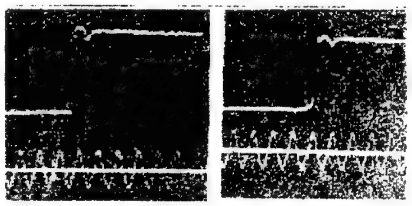

Figure 2. Pressure oscillograph traces. The MS was located in teflon at a distance of 0.2 mm from the teflon-HE interface. The measurement time interval is Δt = 40 ns.
a) VV-2. The wave had traveled a distance of Δx = 90 mm
b) VV-3. The wave had traveled a distance of Δx = 70 mm

Table 1 presents quantitative data for measured P(t) obtained from Figs.1 and 2 ([t]= ns, [P] = GPa).

The algebraic equation system with JWL form of EOS for stationary DW, which allows us to find all values as functions of burnup F in CRZ is:

$1/\rho = (1-F)/\rho_1 + F/\rho_2$	$P = (D_S\rho_0)^2(1/\rho_0 - 1/\rho)$	$\varepsilon = (1-F)\varepsilon_1 + F\varepsilon_2$
$\varepsilon = (D_S\rho_0)^2(1/\rho_0 - 1/\rho)^2/2 + FQ + \varepsilon_0$	$P1_X = A_1\exp(-R_{11}\rho_0/\rho_1) + B_1\exp(-R_{12}\rho_0/\rho_1)$	
$P2_X = A_2\exp(-R_{21}\rho_0/\rho_2) + B_2\exp(-R_{22}\rho_0/\rho_2)$		$P = P1_x + (\Delta P_S)(\rho_1/\rho_S)^{\omega 1+1}$
$\Delta P_S = \omega_1\rho_S\Delta\varepsilon_S - P_S - P_x(\rho_S)$	$\varepsilon_1 = \varepsilon 1_X + (P-P1_x)/(\omega_1\rho_1)$	$\varepsilon_2 = \varepsilon 2_X + (P-P2_x)/(\omega_2\rho_2)$
$\varepsilon 1_X = (A_1\exp(-R_{11}\rho_0/\rho_1)/R_{11} + B_1\exp(-R_{12}\rho_0/\rho_1)/R_{12})/\rho_0$		
$\varepsilon 2_X = (A_2\exp(-R_{21}\rho_0/\rho_2)/R_{21} + B_2\exp(-R_{22}\rho_0/\rho_2)/R_{22})/\rho_0$		

The reaction rate in DW CRZ for various reaction kinetics approximations depends, as a rule, on local parameters P, ρ, and F:

$$dF/dt = K(P, \rho, F).$$

Coordinate function of burnup, $\xi = \xi(F)$, is determined by integral:

$$\xi(F) = \int_0^F dF \frac{(D_S - U(F))}{K(P(F), \rho(F), F)}$$

The reaction zone length, ξ_S, at F = 1.0 is: $\xi_S = \xi(F=1)$, $t_S = \xi_S/D_S$

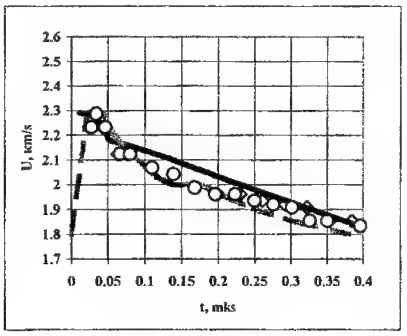

Figure 3. HE TATB

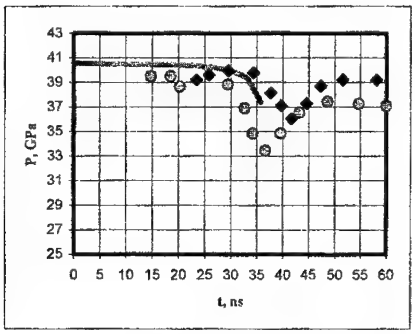

Figure 4. HE VV-2 and VV-3

Figs. 3 and 4 present calculated CRZ structure for HEs TATB, VV-2, and VV-3 with LLNL kinetics from [1,2] and experimental points from Table 1.

In Fig.3, the solid line is self-similar computation, rhombs are the data from Lagrangian manganin sensor in teflon, the circles are manganin sensor data re-calculated to the "Eulerian" sensor in HE, the dotted line represents the data of Heiss sensor (LLNL). Time interval for chemical zone width (UJ = 1.842 km/s) - computation "Ignition / Growth" - is 387 ns, zone width is 2.91 mm.

Fig.4 plots the calculated profile for DW CRZ pressure in HE PBX-9501 (solid line), experimental data for VV-2 (curcles), VV-3 (rhombs) re-calculated to the "Eulerian" sensor in HE. Time interval for chemical zone width - computation "Ignition / Growth" - is 35.8 ns, zone width is 0.317 mm.

Table 1

HE TATB				VV -2				VV -3			
T	P_{HE}	t	P_{HE}	t	P_{HE}	t	P_{HE}	t	P_{HE}	t	P_{HE}
0	0	168.7	28.82	0	0	33.85	33.5	0	0	41.9	36.1
24.1	32.36	199.5	28.44	3.85	45.06	38.5	34.8	14.8	39.2	47.1	37.3
30.3	33.15	230.3	28.44	8.46	33.97	44.6	36.6	18.1	38.3	52.3	38.7
42.6	32.36	261.0	28.05	10.8	38.65	54.6	37.4	23.3	39.9	60.65	39.2
62.6	30.78	291.8	27.83	23.1	38.8	67.7	37.3	30.3	39.8	76.1	39.2

76.4	30.78	322.6	27.66	27.7	36.9	81.55	37.1	35.5	38.2	90.3	38.9
107.2	30.00	353.3	26.88	30.0	34.8	93.85	37.1	38.7	37.1		
138.0	29.60	384.1	26.88								

References

[1] C.M. Tarver, J.W. Kury and R.D. Breithaupt // J. Appl Phys 1997.V. 82 №8 P. 3771.

[2] S.K.Chidester, C.M.Tarver, and R.G.Garza //11th Internat. Detonation Symp. 1998. P. 331

Session "Numerical Models for Detonation Processes"

Chairmen:
V. Klimenko - **Institute of Chemical Physics, Moscow, Russia**
C. Tarver - Lawrence Livermore National Laboratory, Livermore, USA

Current Status of the Non-Equilibrium Zeldovich - Von Neumann - Doring Theory and Reactive Flow Modeling of Detonation Waves

C.M. Tarver, J.W. Forbes, P.A. Urtiew

Energetic Materials Center
Lawrence Livermore National Laboratory, Livermore, USA

Understanding the underlying chemical reaction mechanisms and measurement and numerical prediction of the performance of steady detonation waves in solid high explosives have long been the ultimate goals of energetic material research. The Non-Equilibrium Zeldovich - von Neumann - Doring (NEZND) theory has extended the classical ZND theory to include the non-equilibrium excitations processes which precede and follow the exothermic chemical energy release within the detonation wave reaction zone. NEZND theory has successfully explained the induction times required for chemical reactions behind each shock wavelet in the complex three-dimensional leading shock front of gaseous, liquid, and solid explosives. The formation of the reaction products in highly vibrationally excited states and their subsequent relaxation toward the equilibrium Chapman-Jouguet (C-J) state has been shown to be the fundamental mechanism by which the chemical energy release sustains the leading shock front at a constant velocity. The current understanding of these processes will be discussed.

Through the implementation of embedded pressure and particle velocity gauge and laser interferometric experimental techniques, the unreacted von Neumann spike state, the exothermic chemical reaction zone, the Chapman-Jouguet (C-J) or sonic state, and the subsequent adiabatic expansion of the reaction products has been measured for many explosives with nanosecond resolution by several laboratories. The Ignition and Growth reactive flow model has been implemented in many one-, two- and three-dimensional hydrodynamic computer codes and normalized to this experimental data.

The current status of both the experimental techniques and the reactive flow modeling efforts at LLNL and prospects for future research will be reviewed.

Shock Wave Sensitivity Model "Growth and Coalesce" for Solid Heterogeneous HE

V.G. Morozov, I.I. Karpenko, L.V. Dmitriyeva, N.V. Korepova, S.S. Sokolov, T.L. Grebennikova, B.N. Shamraev

Russian Federal Nuclear Center-VNIIEF, Sarov (Arzamas-16), Russia

Phenomenological Growth and Coalesce model (GC model) and its verification as applied to TATB-based HE was described in [1] in 1993 and also in [2] in 1995. Concepts of "hot spots" (HS) generation in a shock wave front area, their growth and coalesce (if $\int p^2 dt$ value is sufficient) form the model basis. During coalesce process the induction period passes to the next phase, a short and high peak of the major energy release.

The whole process is drawn out in time and depth by the hydrodynamic flow passage behind the shock wave front. Simple models of separate phases were considered and used to construct macroscopic energy release equations. One of the GC model's specific features is a capability of taking into account a high negative dependence of HE sensitivity on the density before the shock wave front (both in statics and dynamics). This allowed reproduction of multiple phenomena occurring in HE application experience and

related to sensitivity changes because of shock wave and unloading wave interference, or when changing the initial density. For the past period, GC model was used to solve a great number of one-dimensional and multidimensional application problems. The model was also extended to a number of other solid HE compositions. The model validity was experimentally proved by comparing calculations and results of experiments.

The first goal of the presentation is to demonstrate some of the results obtained for the period of its use: HE sensitivity dependence on the initial density, initiation of the unloaded HE, detonation extinguishing by the first weak compression, initiation during a shock wave release from HE to the gap between HE and a barrier and the unloaded HE impact on a barrier (if there is no gap, initiation is not observed), initiation by impacting using thin slabs, spatial picture of initiating and extinguishing detonation under the interference of shock waves from several sources. A profound enough phenomenological model should include assumptions giving information for future studying physics of the phenomenon. These are the second goal of the presentation. The model assumes that a thermal conductivity coefficient χ which determines HS growth is proportional to p^2 (where p is pressure). This accounts for the well-known initiation criterion $p^2t=const$.

It also follows from the analysis of an experimental induction time value that χ value at hot spot front exceeds its value under standard conditions by a factor of 2 to 3 orders of the magnitude and even more. A turbulent mechanism of energy transport is a most natural explanation to the fact. To fortify this hypothetical assumption, we evaluate the energy flow density dependence on p. According to Ref./2/, the material expansion velocity v inside hot spots rapidly increases from the center towards the boundary, where energy transport takes place, and then decreases in a surrounding cold HE. According to Ref./4/, hydrodynamic instability occurs in a near-boundary region that satisfies the criterion $div_v\, a > 0$, where $div_v\, a$ is divergence of acceleration in the velocity space. The above criterion is more demonstrative for a one-dimensional flow: $da/dv > 0$, i.e. acceleration increases with the increasing velocity. The flow becomes turbulent. According to Ref./4/, vortex formations are generated, i.e. particles that transport mass (EP mixing with HE), pulse, and energy. Special studies are required for the role of shear flows (turbulence) within the mechanism of initiating HE. Here we only consider their contribution to energy transport. The major turbulence contribution to the energy flow equation is about $v\psi u^2$, where v is a medium velocity, ψ is density of vortical particles (g/cm^3), $u^2 \sim p/\rho$ is an average squared turbulent velocity (to within a factor which is slightly dependent on p).

The equation for ψ looks like $\partial\psi/\partial t=(da/dv)\,\psi$; $\psi=\exp(\int da/dv\, dt)$ (see Ref.[4]).

When substituting $a \approx v(dv/dr)$,

we evaluate $\int \approx \int (dr/v)\,(d\,(v(dv/dr))/dr)\,(dr/dv) = \ln 0{,}5(dv^2/dr)$.

This means $\psi \sim d\,v^2/dr$.

In general, a turbulent energy flow density is $J \sim v\psi u^2 \sim v\,(d\,v^2/dr)\,p/\rho$.

Since v^2 is also proportional to p/ρ, it can be written as $J \sim (p)^{3/2}d\varepsilon/dr$. To specify the dependence of χ on p, more accurate though time consumable calculations are required. It should be kept in mind that the empirical criterion $p^n\, t=const$ is an approximate one (n=1,5 to 2). Now we can only say that the above calculations show the turbulent nature of energy transport and more profound studies are required to understand the role of shear flows during chemical decomposition of solid HEs, explosion product transport and mixing, especially with low-velocity effects on HE. Possibly, this is the way to bring together standpoints of advocates of the thermal and the shear detonation theories.

References

1. V.G.Morozov, I.I.Karpenko, O.V.Olkhov, S.S.Sokolov, I.E.Plaksin, A.A.Evstigneev, A.D.Kovtun, V.E.Gerasimenko, A.N.Shuikin, V.A.Komrachkov, J.M.Makarov, V.M.Gerasimov, V.I.Shutov. Experimentally Proved Numerical Modeling of Detonation Initiation and Development in Solid HE in terms of Desensitization by Shock and Detonation Waves Interaction. – The 14th International Colloquium on Dynamics of Explosions and Reactive Systems, University of Coimbra, 1993.
2. V.G.Morozov, I.I.Karpenko, S.E.Kuratov, S.S.Sokolov, B.N.Shamraev, L.V.Dmitriyeva. Theoretical Proves for Phenomenological Model of TATB-based HE Sensitivity to Shock Waves. – Chemical Physics, Vol.14, p.203, 1995.

3. V.G.Morozov, I.I.Karpenko, L.V.Dmitriyeva, N.V.Korepova. Numerical simulation of TATB-based HE detonation initiation by impacting a thin volant slab using D techniques. – VANT, Ser.:Mathem.Model.Phys.Process., Iss.2, 1999, Moscow.

4. V.G.Morozov, O.V.Olkhov. On Corpuscular Approach to Modeling a Turbulent Flow. - VANT, Ser.: Mathem. Model. Phys. Process., Iss.3, 1999, Moscow.

A New Reaction Rate Equation For Simulating the Ignition and Growth of Reaction in High Explosives

M.J. Murphy, J.J. Hsu, A.L. Nichols

Lawrence Livermore National Laboratory, Livermore, USA

We describe a new reaction rate equation for simulating the ignition and growth of reaction in high explosives. The new reaction rate equation has been implemented into an arbitrary Lagrange Eulerian hydrocode as an alternate rate equation in the baseline the Lee-Tarver reactive flow model. The reactive flow model treats the explosive in two phases (unreacted/reactants and reacted/products) with a reaction rate equation to determine the amount of material that has reacted (fraction reacted).

The new rate equation uses a cosine function in the form factor of the ignition term and a sine function in the form factor of the growth and completion terms. The new rate equation is simpler and has fewer parameters while providing the same functionality as the baseline rate equation. Hydrocode simulations of embedded gage shock to detonation experiments using the new rate equation will be presented.

Baseline rate equation

The utility of the baseline reaction rate equation has been demonstrated for a wide range of energetic materials. The two-term form of the baseline reaction rate equation is shown in Eq. 1.

$$dF/dt = Freq \cdot (1-F)^{Frer} \cdot (\rho/\rho_0 - 1 - Ccrit)^{Eeta1} + Grow \cdot (1-F)^{Es} \cdot F^{Ar} \cdot p^{em}$$

There are several factors that make it difficult to parameterize the reaction rate equation for new materials:

- There is a discontinuity in dF/dt from the ignition term when F exceeds the ignition limit.
- The maximum values of the growth and completion form factors vary as Es and Ar are varied.

New Rate Equation

The two term form of the new reaction rate equation is described in Equation 2. Note that the ***Frer*** and ***Ar*** parameters and not used in the new form of the rate equation.

$$dF/dt = Freq \cdot 0.5 \cdot (1 + Cos(\pi F / figmx))(\rho/\rho_0 - 1 - Ccrit)^{Eeta1} + Grow_2 \cdot (Sin(\pi F^{Es})) \cdot p^{em}$$

This form of the reaction rate equation has fewer parameters and several advantages over the baseline form of the rate equation:

- The ignition term is continuous and smoothly goes from a value of 1.0 to 0.0 as the fraction reacted, F, goes from 0.0 to the ignition limit, ***figmx***.
- The growth and completion term form factors go from 0.0 to 1.0 and back to 0.0 as the fraction reacted, F, goes from 0.0 to 1.0.
- The maximum value of the growth and completion term form factors is always 1.0.

Comparison of ignition terms

A comparison of the ignition term portions of the baseline and new rate equations is shown in Figure 1. This figure shows how the baseline ignition term is discontinuous when the fraction reacted (***F***) reaches the ignition limit (***Figmx***). The new ignition term is continuous and smoothly approaches a value of 0.0 as ***F*** approaches the ignition limit (***Figmx***).

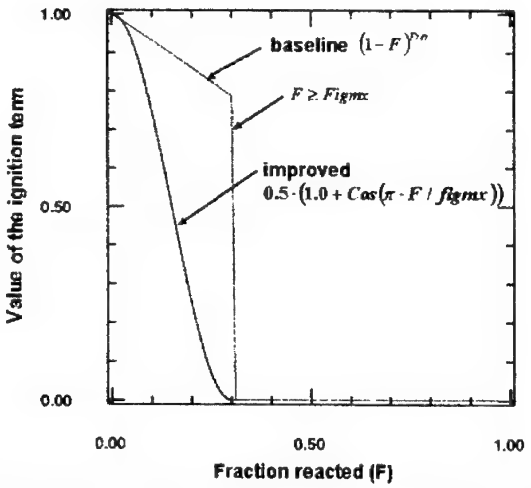

Figure 1. Comparison of the baseline and new ignition terms of the rate equation.

Comparison of completion terms

The baseline growth and completion term form factors are given in Equation 3. Three curves showing the value of the form factor as a function of the fraction reacted, *F*, are shown in Figure 2. These curves are for three sets of *Es* and *Ar* values. Note that the peak value of the form factor is different for each set of *Es* and *Ar* values. Changes in the value of *Es* or *Ar* in order to affect a shift in the shape of the form factor curve will usually require a change in the growth or completion term prefactor because of the change in the maximum value of the form factor.

$$(1-F)^{Es} \cdot F^{Ar} \qquad \text{Eq. (3)}$$

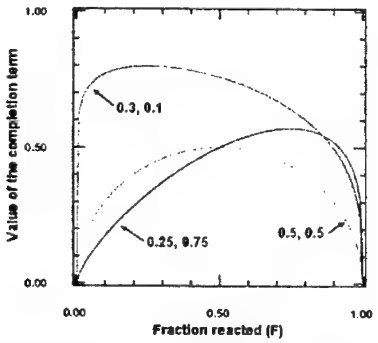

Figure 2. Three curves of the baseline completion term form factor as a function of the fraction reacted.

Equation 4 describes the new growth and completion term form factors. This form factor equation has one less parameter and always has a maximum value of 1.0. Three curves showing the value of the new growth or completion term form factor as a function of the fraction reacted, F, are shown in Figure 3. These curves are for three values of Es (0.5, 1.0, and 2.4). Note that each curve goes from 0.0 to 1.0 and back to 0.0 as F goes from 0.0 to 1.0. Since the peak value of the form factor is always 1.0, the paramcterization process is simplified. Note also that the parameter Ar is not required.

$$\left(Sin\left(\pi F^{Es}\right)\right) \qquad \text{Eq. (4)}$$

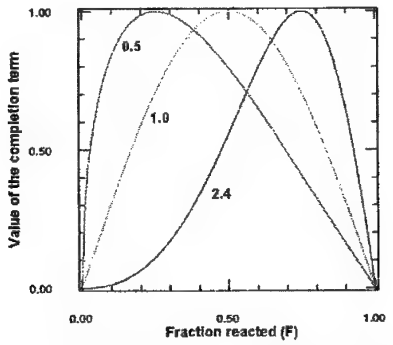

Figure 3. Three curves of the new completion term form factor as a function of the fraction reacted.

Summary

The new rate equation is simpler, has fewer parameters, and maintains the functionality of the baseline rate equation.

Simulations of Plastic Bonded Explosives: Bridging Mesoscopic to Macroscopic Length Scales

B.E. Clements, E.M. Mas

Los Alamos National Laboratory, Los Alamos, USA

A general theory is put forth to model the sub-detonation thermal mechanical response of plastic bonded high explosives (PBX). Because most PBXs are comprised of explosive grains of varying sizes we use a hybrid composite theory to handle the size distribution of the explosive grains. It is speculated that the role of the small grains is to mechanically stiffen the en-coating polymeric binder but they are not involved in the fracture properties of the entire explosive composite.

It is then natural to treat the mechanical response of the smaller grains at a cruder but more efficient level than the larger grains and for that we use the Eshelby-Mori-Tanaka (EMT) effective medium theory. This small grain-binder mixture is referred to as the filled binder. The larger grains are know to experience micro-crack growth when the composite is dynamically deformed.

The large grain and filled-binder composite is treated using the Method of Cells (MOC) composite theory. The rate and temperature dependence of the binder is accounted for by using a Generalized Maxwell viscoelasticity analysis. The constitutive behavior of the large grains is assumed to be elastic-plastic, and to damage by brittle fracture. Only elasticity of the small grains is considered here. Interfacial debonding between the filled binder and the large grains is included.

The MOC/EMT theory is homogenization technique and can be implemented in a finite element method (FEM) computer code. This allows simulations to be carried out for macro-length scale dynamic

integrated experiments. As an example, we apply this theory to model experiments done on the explosive PBX 9501.

Modeling of Double Shock Initiation of TATB-Based Explosives

Yu.A. Aminov, N.S. Es'kov, Yu.R. Nikitenko

Russian Federal Nuclear Center-VNIITF, Snezhinsk (Chelyabinsk-70), Russia

The paper presents a kinetics model that describes basic features of the detonation development in the heterogeneous explosives. The results of numerical simulation of the experiments with a TATB-based composition are presented for the case when initiation was caused by two sequential shock waves.

Model description

Presented semiempirical macrokinetics detonation model was developed at Institute of Technical Physics to simulate behavior of condensed heterogeneous explosives. The model is based on the "hot spots" concept and describes a wide class of experiments on shock initiation. The proposed model contains the following kinetic equation:

$$\frac{d\xi}{dt}=\begin{cases}-W_0\cdot\dfrac{\rho_{BB}}{\rho_{0k}^{1/3}\cdot\rho_{HB}^{2/3}}\cdot\left(\dfrac{1-\xi}{\theta^*}\right)^{2/3}\cdot\exp\left(-E_a/3E_i^*\right)\cdot U(\sigma), & \dfrac{\theta^*\cdot\xi}{\rho_{BB}}>\dfrac{1-\xi}{\rho_{HB}};\\ -W_0\cdot\left(\dfrac{\rho_{BB}}{\rho_{0k}}\right)^{1/2}\cdot\xi^{2/3}\cdot\exp\left(-E_a/3E_i^*\right)\cdot U(\sigma), & \dfrac{\theta^*\cdot\xi}{\rho_{BB}}\le\dfrac{1-\xi}{\rho_{HB}}.\end{cases}$$

Here ξ is a fraction of unreacted explosive; W_0 is a constant; ρ_{0k} is crystal density of explosive; $\sigma=P/P_{CJ}$; E_a is the effective activation energy; E_i^* is a thermal component of specific internal energy at the initial shock front; $U(\sigma)=arc\ tan(a\sigma+b\sigma^m)$ is the non-dimensional "velocity" of combustion front and is a smooth step-wise function of pressure. Such dependence of $U(\sigma)$ allows to qualitatively simulate the following basic features of heterogeneous HE decomposition: a leading role of the hot-spot mechanism at low pressures and transition to the homogeneous mechanism at high pressures.

The first stage of model describes the ignition of hot spots, the second one describes the surface combustion after merging of hot spots. The factor $exp(E_a/3E_i^*)$ depends on a number of the hot spots activated by the initial shock wave. θ^* controls the transition to a surface combustion stage under the assumption that the hotspots emerge on the HE grain surfaces. If the shock forms only few hot spots located far from each other, their spatial distribution can be considered as uniform. In this case transition to the second stage can take place only at equal volumes of the unreacted explosive and explosion products, i.e. $\theta^*=1$. If there are a lot of hot spots they cover the whole surface of each grain thus leading to an instantaneous transition to the second stage, i.e. $\theta^*=0$. The following formula is selected to satisfy these boundary conditions for function θ^*:

$$\theta^*\left(E_i^*\right)=1-\exp\left(\frac{-\beta\cdot E_a}{E_i^*}\right).$$

Thus, there are six reaction rate parameters: W_0, E_a, β, α, a, b, m.

Double-shock experiments with LX-17

LX-17 is a low-sensitive composition (ρ_0=1.905 g/cm^3), containing 92.5 % TATB. The set-up and the results of double-shock experiments with LX-17 are given in [1]. A 20 mm thick explosive sample was shocked by a steel flyer plate accelerated by a 4-inch gas gun. The flyer velocity varied in the range of W=(0.75÷1.23) km/s, that corresponds to the values of pressure in HE at the leading shock front P_1=(4.4÷8.6) GPa. This is insufficient for shock initiation in the sample under study. After propagation through the explosive the wave was reflected from the metal plate (aluminum, copper or tantalum) behind HE, making a stronger shock wave to run through the shocked LX-17 in the opposite direction. The

pressure profiles were recorded by the manganin gauges embedded in the explosive charge at the depth of 5, 10, and 15 mm.

The experimental profiles shown in Figs. 1-6 imply that pre-shocking by a weak shock wave decreases the explosive sensitivity (desensitization). In particular, with cooper backing plate the gauges show the decay of the shock wave and no detonation at the velocity W=1.0 km/s (P_1=6.8 GPa), though the pressure on the reflected wave front was P_2=14 GPa (Fig. 1). According to [1], such single shock would cause a detonation of LX-17 at the depth no more than 10 mm. When the flyer velocity was increased up to W=1.14 km/s (P_1=7.6 GPa), detonation on the second wave developed very fast (Fig. 2). A similar situation is in systems with the aluminum backing plate (Figs. 3, 4). Thus, in the considered experiments the critical initiation pressure of pre-shocked explosive turns out to exceed that of the initial explosive.

Simulation results

The double-shock experiments were simulated with one-dimensional hydrodynamic code VOLNA, permitting calculations with precise fronts of shock and detonation waves.

TABLE. **The reaction rate parameters for HE LX-17.**

W_0	E_a	β	a	B	m
91.1714 μs^{-1}	0.5 kJ/g	0.15	0.165	8.418	8.9659

The calculated results are shown in Figs. 1-6, where they are compared to the experimental data [1] obtained for different back plate materials and 3 gauge locations in LX-17. The good agreement is observed, though presented model has fewer empirical parameters than "Ignition and Growth" model.

References

1. C.M. Tarver, T.M. Cook, P.A. Urtiew, W.C. Tao. Multiple Shock Initiation of LX-17. Proceedings of the Tenth Symposium (International) on Detonation, 1993.

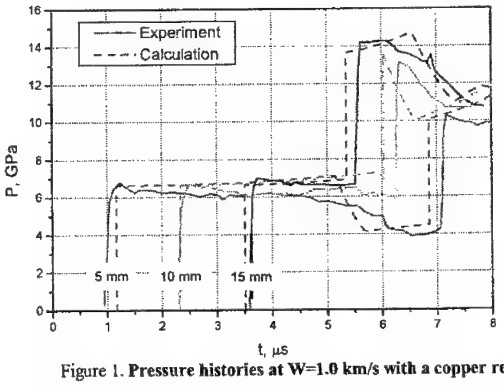

Figure 1. **Pressure histories at W=1.0 km/s with a copper reflector plate.**

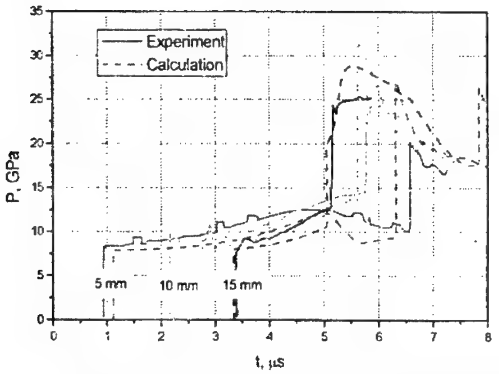

Figure 2. **Pressure histories at W=1.14 km/s with a copper reflector plate.**

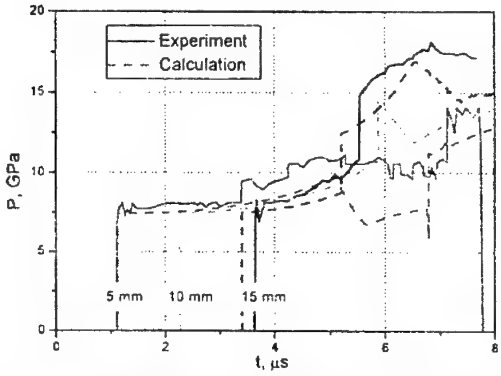

Figure 3. **Pressure histories at W=1.09 km/s with an aluminum reflector plate.**

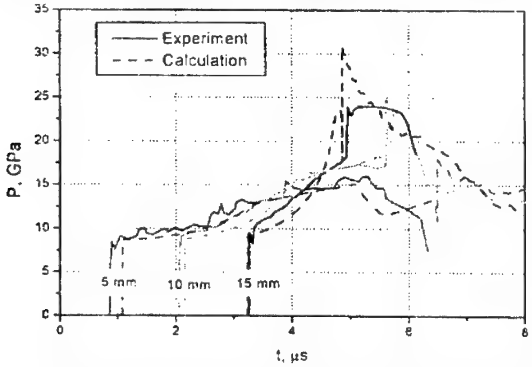

Figure 4. **Pressure histories at W=1.23 km/s with an aluminum reflector plate.**

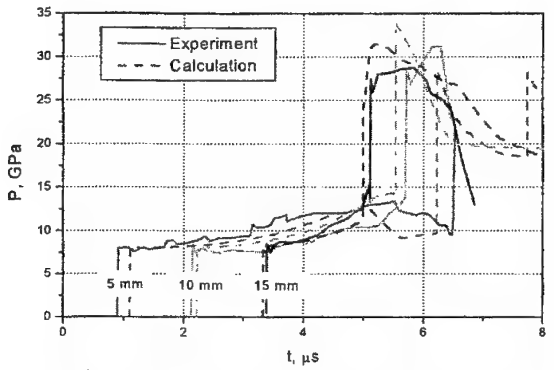

Figure 5. **Pressure histories at W=1.15 km/s with a tantalum reflector plate.**

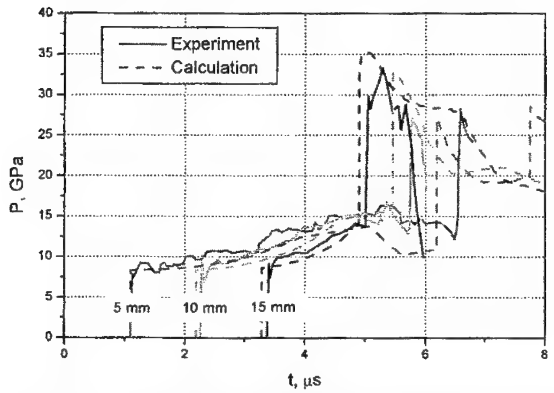

Figure 6. Pressure histories at W=1.19 km/s with a tantalum reflector plate.

A Continuum-Based Reaction Growth Model for the Shock Initiation of Porous Explosives

H.R.James, B.D.Lambourn

Atomic Weapons Establishment, Aldermaston, Reading, UK

A one-dimensional, semi-analytic, continuum-based model has been developed [1] that can quickly calculate reaction growth in shocked explosives. As such it can predict initiation patterns in Monte Carlo assessments of events such as multiple fragment attack scenarios. The model, SCORE (Simple Computation of Reaction Evolution), will be briefly described and shown that, with two adjustable coefficients, it can successfully predict both the patterns of shock wave growth for a single sustained pulse, and Pop Plots for a variety of explosives. In addition it can produce a reaction rate curve similar in form and amplitude to that required as input to a widely used [2] hydrocode-based reaction model.

The current paper will show that porosity in the explosive is an important parameter in any calculation of reaction growth, and in SCORE it enables the adjustable coefficients to be closely allied with the coefficients required to describe the thin pulse initiation threshold. This goes a long way towards removing the need for anything other than measured coefficients to be used in the predictions of Pop Plots etc. by this model. In addition it will be shown that one of the major assumptions behind SCORE leads to a theoretical description of behaviour which closely matches that observed in conventional explosives with densities near to their Theoretical Maximum Density (TMD).

SCORE assumes during the initiation process that a reactive wave can be identified such that it contains at every step all the necessary conditions for both triggering reaction, and describing the subsequent reaction growth to detonation. It also assumes there is a minimum energy within this wave that is coupled to a maximum efficiency in converting chemical energy into power. The minimum energy in the pulse corresponds to that required to just trigger initiation at that pressure. The maximum efficiency is based on adopting a ZND-type structure for the wave, but with the rear of the wave identified as the maximum internal energy that is present on the Rayleigh line. This condition corresponds to the rate at which chemical energy is completely converted to mechanical work. These assumptions, combined with a mix model in which both solid and gas are on their respective Hugoniots, provides a closed set of ordinary differential equations. From the energy considerations SCORE can be considered as corresponding to the most efficient summation possible of any hot spot growth that eventually leads to detonation.

In previously using SCORE, the near fully dense explosive was treated as a non-porous solid. In that treatment it was noted that the two coefficients, which should correspond to the shock initiation threshold parameters, needed to have values which were often different to those given by experiment in order for the model to fit the Pop Plot. An examination of the pattern of wave growth given by SCORE, and confirmed by experiment, indicated that the overwhelming majority of the run distance is carried out at or near non-reactive conditions. As such this (and any other reactive growth method) is very sensitive to the non-reactive Hugoniot used. This can significantly vary depending on the degree of porosity. Either a Hugoniot is required which has been measured at the exact degree of porosity (which is rarely the case), or a model, such as the Snowplough model, is needed to convert a reference Hugoniot to one at the required porosity. Only once these conditions are met can consideration be given to adjusting sensitivity parameters.

SCORE, modified to accept the Snowplough model, shows in the few experimental datasets where exactly the same explosive was used to determine both threshold and Pop Plot, that the two coefficients now tend to apply to both conditions. Fits to experimental data also show that SCORE confirms a fairly abrupt change in sensitivity behaviour for conventional explosives as their initial density goes below about 98% of TMD. In the explosives examined, SCORE indicates that this change is due to the disappearance of the coefficient associated with an energy cut-off term. This term is also associated with homogeneous behaviour [3] which, in quantitative terms may well indicate the increased dominance of hot spots as porosity increases. It will be shown that the use of the maximum internal energy criterion in the model leads to a theoretical cut-off term for materials at TMD, but disappears once the Snowplough model is used. Cut-off values from the theory are very similar to those obtained by just fitting SCORE to the experimental Pop Plots near TMD. A better porosity model such as p,α [4] leads to a rather less abrupt disappearance of this term.

1. H.R.James and B.D.Lambourn, *Propellants, Explosives, Pyrotechnics* 26, 246 (2001).
2. E.L.Lee and C.M.Tarver, *Phys.Fluids*, 23, 2362 (1980).
3. H.R.James, M.D.Cook and P.J.Haskins, *11th International Detonation Symposium*, 581 (1998).
4. W.Herrmann, *J.Appl.Phys.*, 40, 2490 (1969).

Comparison of Different Reactive Flow Models for Nitromethane

R.N. Mulford, D.C. Swift

Los Alamos National Laboratory, Los Alamos, New Mexico, USA

Reactive flow models for explosives are usually developed by choosing an empirical form for the reaction rate and calibrating parameters against initiation experiments. In shock wave initiation, experimental data almost always comprise mechanical measurements such as shock speed, material speed, compression, and pressure. However, we know from chemistry that reaction rates depend on temperature as well as on the mechanical state. This is one reason why mechanically-based reaction rates do not extrapolate well outwith the range of states used to normalize them. For instance, mechanical

reaction models which match single-shock initiation generally fail to reproduce multiple-shock initiation phenomena.

We have previously developed reactive flow models for explosives which include temperature as well as the mechanical state. These models reproduced multiple-shock initiation behavior much more accurately than did reactive flow models with a purely mechanical reaction rate, and they were also capable of being used to simulate cook-off problems.

We have recently extended the temperature-based model for use with nitromethane. A quasi-harmonic equation of state is used to predict the temperatures of states, from the cold curve and the explicit molecular vibrations of the molecule. The nitromethane reacts with a rate that depends on its thermodynamic state. Porosity may be introduced, and contributed to heating. A finite-rate equilibration model is used to determine the overall response of the material to dynamic loading. Pressure and temperature are equilibrated separately.

The model is compared with data for nitromethane initiation, and with predictions made using other types of equation of state for nitromethane.

Hydro-Reactive Computations with a Temperature Dependent Reaction Rate

Y. Partom

Rafael, Haifa, Israel

Hydro-reactive computations are usually performed with a reaction model containing a pressure dependent reaction rate (PDRR). A well-known example is the "Ignition & Growth" (I&G) reaction model introduced by Lee and Tarver some twenty years ago. Performing such computations it has become evident that in many cases the results obtained seem unreliable.

For these cases using a temperature dependent reaction rate (TDRR) may produce better results. We're using a surface burn reaction model that we've developed some twenty years ago. Originally we used it with a TDRR. Some years ago we introduced it into the PISCES code and used it with a PDRR.

In this work we reintroduce the TDRR into the model with the purpose of comparing the performance of the two reaction rates. We first calibrate the rates to reproduce the pop-plot of PBX-9502. We then run the code with the two rates for several 1D and 2D situations. The resulting differences are qualitatively as expected, but previously we could not have estimated them quantitatively.

Modelling of Detonation Features of Metallized High Ezplosives as Systems with Non-Monotonous Energy Release

N.A. Imkhovik

Moscow State Technical University, Moscow, Russia

The addition of metals to explosives has been well studied for many years. When summarizing the results of these works it is possible to come to the following conclusions. The addition of powder aluminum to a condensed phase HE leads to considerable increase of its heat of explosion Q as measured in calorimetric bomb (end HE shock wave performance). However detonation performance from detonation velocity D and pressure in detonation products (DP) p remains the same contrary to the increase ($D \sim Q^{1/2}$ and $p \sim Q$) as theoretically expected. Aluminum addition in certain condition reduces detonation performance to greater extent, than chemically inert additives, such as NaCl, SiO_2, LiF, talcum etc. Moreover, it is known, that in certain conditions the addition of aluminum reduce detonation performance to greater extent, than chemically inert additives. However, an increase of HE detonation velocity is observed for additive of fine aluminum powder, but for some low-sensitive HE's with positive oxygen balance. These HE's have comparatively low detonation conditions and wide zone of chemical

reaction (ZCR) of detonation wave (DW) (for example, ammonium nitrate and ammonium and potassium perchlorate) for their low density.

The increase of speed of non-ideal detonation D of real charges of aluminized industry HE with limited diameter d ($d_{lim} < d < d_{cr}$) and approximation of the detonation regime to ideal one $D_{id} = D(d \to \infty)$ says, that exothermal combustion of aluminum takes place in the chemical reaction zone of a DW before C-J point, i.e. fine aluminum is oxidized completely of partially by HE decomposition products for 0.1…1 μs. However, in this case (even for charge diameter of 10^1 cm and the most favorable condition of aluminum oxidation) the increase of detonation speed of non-organic HE's with positive oxygen balance above 6 km/s has not been obtained in practice. For high-energy brisant HE's with detonation conditions higher, than for HE's with positive oxygen balance, and narrower zone of chemical reaction of HE decomposition (units and tens of nanoseconds) numerous attempts to increase the detonation speed and other detonation wave front conditions by adding aluminum (in various ways) has not succeeded.

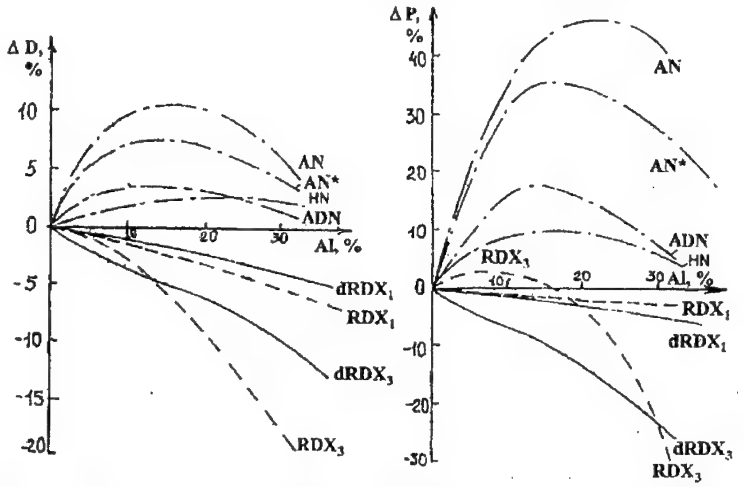

Figure 1. Change of speed and pressure of ideal detonation of mix HE as function of aluminum fraction, charge density and Al behavior in C-J plane (cases of calculation: case 1 - aluminum remains inert at DW front and is compressed according its Hugoniot; case 3 - aluminum fully reacts at DW front with the formation of equilibrium reaction products at C-J plane including the oxide Al_2O_3):

- AN, AN*, ADN, HN - case 3 calculations for mixtures on the base of ammonium nitrate ($\rho_{HE} = 1050$ and $\rho_{HE} = 1725$ kg/m^3), ammonium dinitramide ($\rho_{HE} = 1700$ kg/m^3) and hydrazine nitrate ($\rho_{HE} = 1630$ kg/m^3);
- RDX_1, RDX_3, $dRDX_1$, $dRDX_3$ - cases 1 and 3 calculations for mixture on the base of poured (low-density RDX) ($\rho_{HE} = 1140$ kg/m^3) on the base of RDX with paraffin ($\rho_{HE} = 1650$ kg/m^3).

A number of hypotheses regarding the impossibility to increase the high-energy HE detonation conditions by adding aluminum powder has been made. These hypotheses have been also tried to explain the difference between the nature of shock wave and acceleration effect from aluminized HE explosion and influence of fine aluminum on detonation properties and sensitivity. They are presented in reviews including [1-2] by the author, in which the influence of aluminum additives on detonation performance of different high explosives with varied chemical composition and initial density has been studied within the framework of thermochemical equilibrium. It has been determined, that partial or (in hypothetical case) complete reaction of fine-dispersed aluminum at the detonation wave front influences the detonation wave speed and Chapman-Jouget pressure in condensed HE in a variety of ways: for high-density brisant HE (such as composition based on RDX, HMX, RDX-TNT mixtures) having negative oxygen balance both the wave speed and pressure decrease, whereas they increase for HE's with positive oxygen balance (AN, HN, ADN). Fig. 4 (where $\Delta D = (D_{HE/Al} - D_{HE})/D_{HE}$ and $\Delta p = (p_{HE/Al} - p_{HE})/p_{HE}$) clearly demonstrates the fact, that the introduction of aluminum additive (in the case of its oxidation) influences detonation HE

conditions in the different ways depending on their oxygen balance, initial HE density and aluminum fraction.

New data gave rise to a large wave of discussions and interest to this problem. These data present investigation results from test on compositions with nano-size aluminum particles [3], aluminum powder ALEX [4], and metal hydrides [5]. These particles are of 50...100 nanometer size, that is finer, than studied earlier aluminum particles (250...1000 nanometers). Thus one can expect higher oxidation degree for these fine and active when applying modern technologies to produce maximally uniform heterogeneous mix structures in comparison with 0.25...1.0 μm size particles studied earlier. Therefore the problem of correct thermodynamic prediction of influence of these particles on HE detonation conditions for different compositions is realizable.

However, more actual and the most disputable is a question on metal oxidation kinetics in DP and energy release in DW. Moreover, conclusions by different authors on detonation ability of Al in DW (from the viewpoint of its influence on DW front conditions and HE accceleration ability) don't match each other and do cover all the range: from practically instant oxidation of 5 micron particles in the CRZ before C-J point (C. Mader, 1979; R.R. McGuire, D.L. Ornellas e.a., 1981), to completely chemically inert behavior of metal particles in CRZ (A.I. Aniskin, K.K. Shvedov, 1978, and other) and slow (for tens of microseconds) oxidation following the DW front in the rarefaction wave. Aside from polar opinions on question of completeness of aluminum oxidation in CRZ, there are also a lot of contradictory intermediate estimations of metal fraction reacted before C-J point: 70% of aluminum particles of 40 μm from (M. Cowperthwaite, 1993) and 40% for 5-10 μm particles from (M.L. Hobbs, M.R. Baer, 1993). One of the causes of such disagreement consists in the incorrect detonation front velocity usage, first, as a parameter poorly depending on aluminum fraction reacted (this feature for compositions on the base of high-energy HE with negative oxygen balance was shown by R. Cheret's results of thermodynamic modeling even in 1971) and, second, as a parameter determined by the feature of detonation regime for metallized HE (normal or under-compressed).

On the other hand, attempts to find the parameters of Al oxidation macro-kinetics following the DW front (in the rarefaction wave) on the base of comparative analysis of particle velocity profiles or plate (or shell) acceleration diagrams by HE charges containing Al or its inert substitute LiF (as for example in (M. Finger, H.C. Hornig, E.L. Lee, J.W. Kury, 1970; G. Baudin, D. Bergues, 1993; W.C. Tao, C.M. Tarver, etc., 1993) are also incorrect.

Investigations performed by the author have shown, that the increase of kinetic energy of an accelerated body is not proportional to the release of chemical heat ΔQ_{pT} from the secondary reaction of Al oxidation, and change according to more complex ("abnormal") dependence. This is conditioned by the fact, that if reacted (to the highest oxide) Al fraction increases and additional heat ΔQ_{pT} releases (and DP temperature increases), there is a considerable (in tens of percents) decrease of the total mole fraction of gaseous DP components, that results in decrease of the DP pressure p for the constant specific volume v. The last phenomenon is equivalent to the condition of decrease of isobaric-isochoric heat effect Q_{pv} (or $\Delta Q_{pv}<0$). This fact results in the specific position of Hugoniots and isentropes of expansion for equilibrium (with condensed Al_2O_3) and partially non-equilibrium (with Al compressed by shock) detonation products in p-v plane, when a equilibrium adiabat is matched by lower C-J conditions (pressure and detonation velocity), than for a partially non-equilibrium one. However, the isentrope starting at C-J point of the non-equilibrium adiabat is steeper and crosses the equilibrium adiabat of smoother pressure decrease character at DP expansion degree $v/v_0 \approx 1.5 - 2.0$.

Thus, the main part of aluminized HE energy can release at the stage of DP expansion to lower pressures. Even more complete oxidation of the Al additive in the DW front for high-energy brisant HE with negative oxygen balance cannot provide the increase of the acceleration rate at the initial stage of the DP expansion. At the same time, the considerable difference between plate and shell acceleration diagrams observed in many tests since 3-4 μs is connected with no beginning of Al oxidation, but with achievement of such expansion degrees, the extra heat energy from its oxidation can effectively transfer into work to accelerate plates and shells. In the general case, the effect from the addition of Al to HE is defined by a number of thermodynamic, gas dynamic and time-scale factors, which should be included when studying behavior of fine metal additives in DW and estimation of kinetic characteristics of their oxidation.

This conclusion is obviously approved by the results of pyrometric investigations of fine structure of a DW front in mixtures on the base of HMX with Al and LiF of different particle size, which were performed at Institute of Chemical Physisces of Russian Academy of Sciences [6]. The results show very complicated character of pressure and temperature profile change for mix compositions of different Al mass fraction. They haven't given a final answer on the question of Al oxidation kinetics, but have only shown, that the interaction of fine Al with DP already takes place near a DW front (for 50-100 nanoseconds).

The second conclusion from the analysis of p-v adiabats for DP [2,7] is the possibility to detonate metallized HE (with equilibrium adiabat matching the complete Al oxidation is placed lower, that intermediate one, which is typical for partial Al reaction) in self-sustaining under-compressed regime. According to Zeldovich theory, this regime can take place, "if in reacting system there are two independent chemical reactions with heat release of different sign, the endothermic reaction having lower rate". For the detonation of metallized compositions on the base of high-energy HE, the aluminum oxidation plays a role of "endothermic reaction" (in the CRZ of HE for DP pressure higher, than points of intersection of isentropes of intermediate and equilibrium DP compositions on p-v plane. If certain conditions are achieved during DP reaction following the DW front, the energy release function ΔQ_{pv} becomes zero and then positive.

In this case according to Zeldovich theory the speed of self-sustaining detonation is to be determined from the condition of Michaelson line contact to Hugoniot of DP (containing aluminum unreacted still) and pressure DP from the intersection of the line with the final equilibrium Hugoniot (containing aluminum oxidized and placed below the intermediate one). The transfer from the upper adiabat to lower one is possible either along this line (with the formation self-same propagating plato), or in rarefaction wave (in any case the detonation velocity for high-performance HE is not dependent on the reacted aluminum fraction). The main necessary condition for the detonation of the aforementioned undercompressed regime is a non-monotonous movement of detonation DP Hugoniots in p-v plane, that is true for aluminized HE of high performance.

The report presents to discuss the physical model and thermo-gas-dynamic calculation method allowing to provide an adequate description of the detonation process and acceleration ability of aluminized HE [7-8]. On the basis of the developed model and experimental data (in particular [9]) the acceleration ability analyzes of the homogeneous and heterogeneous explosives in detonation products hydrodynamic flow of different types and throwing shims of different energy accommodation conditions is performed. The influence of chemical compositions of single explosives, dispersed Al additives to HE and combustion time after detonation front on the plates acceleration dynamics (see Fig. 2, *a*), one dimensional cylinder expansion (see Fig. 2, *b*) and shaped charge linear collapse (see Fig. 2, *c*) has been considered. On the basis of the comparison of experimental data and calculation results (Fig. 3), aluminum combustion energy release and its contribution to acceleration has been defined. The approximate functions of the fine Al particle oxidation rate on time for different particle size and RDX and HMX mix HE have been obtained. The scale effect value has been estimated when accelerating palates and shells using mix HEs.

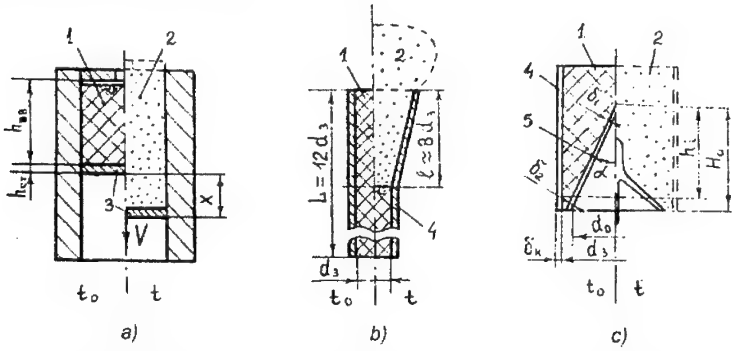

Figure 2. Calculation schemes: 1- HE, 2-DP, 3-plate, 4-cylinder, 5-shaped charge linear.

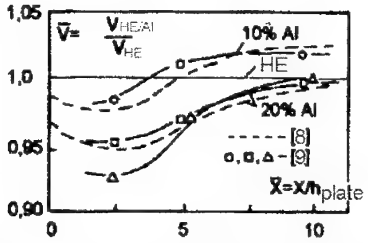

Figure 3. Dependence of relative plate velocity of acceleration distance.

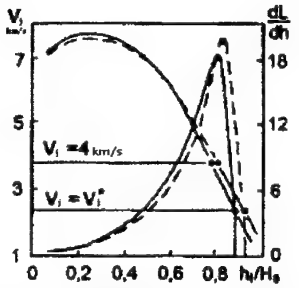

Figure 4. Predicted influence of Al additive on shaped charge elements velocity and their contribution to armor perforation: — - HE, ----- - HE/Al.

Al addition influence on kinematical parameters of conical liner collapse and efficiency of shaped HE charges has been considered. The increase of collapse velocity of tail ($h_i \geq 0.5H_0$) linear elements (when introducing less than 10% Al and HE charge diameter d_3 less than 100 mm) can lead to increase of V_j of corresponding shaped charge jet elements and their contribution to armor perforation dL/dh (Fig. 4). However, due to the decrease of V_j for head elements and V_j velocity gradient, the increase (or even conservation) of L/d_3 for mixture HE with Al needs additional optimization of geometry of the shaped charge linear: δ_1/δ_2, α, d_0, δ_K (see Fig. 3, *e*).

This work was supported by Russian Foundation for Basic Researches (Grant is № 00-03-32231a).

REFERENCES

1. Imkhovik N.A., Soloviev V.S. Thermodynamic calculations of detonation parameters in mixtures of HE with aluminum // Proc. of the IX All-Union symposium on combustion and explosion, Chernogolovka, 1989, P.33. (Russian)

2. Imkhovik N.A., Soloviev V.S. Oxidation of aluminum particles in products of condensed explosive detonation // Proc. of the XXI Intern. Pyrotechnics Seminar, Moscow, 1995, P.316

3. Miller P.G., Bedford C.D., Davis J.J. Effect of Metal Particle Sice on the Detonation properties of Various Metallised Explosives // Proc. of Paper Summaries the XI (Intern.) Detonation Symposium, Colorado, 1998.- P. 302.

4. Ivanov G.V., Tepper F. Activated Aluminum as Stores Energy Source for Propellants // Fourth Intern. Symp. On Special Topics in Chemical Propulsion.- Stockholm, Sweden, May 27-28, 1996.

5. The Comparative Analysis of Influence of Aluminum and Aluminum Hydride on the Detonation Parameters and Performance of the Mixed Explosives/ A.A.Selezenev, D.A.Kreknin, V.N.Lashkov, A.V.Fedorov, N.A. Imkhovik // Proc. of Paper Summaries the XI (Intern.) Detonation Symposium, Colorado, 1998.- P. 309.

6. Detonation Waves in HMX/ Al Mixtures (Pressure and Temperature Measurements) / M.F.Gogulya, A.Yu.Dolgoborodov, M.A.Brazhnikov, G. Baudin // Proc. of Paper Summaries the XI (Intern.) Detonation Symposium, Colorado, 1998.- P. 127.

7. Imkhovik N.A., Soloviev V.S. Numerical Modeling of Aluminum Additive Influence on Projection Velocity by Detonation Products of Mix HEs// Proc. of the X All-Union symposium on combustion and explosion, Chernogolovka, 1992, P. 37.(Russian)

8. Imkhovik N.A., and Soloviev V.S. Mathematics modeling of acceleration dynamics for elements casting by detonation products of aluminized HE. // Oboronnaya Tehnika, 1995, No 1, p.5 (Russian).

9. Davydov V.Yu, Grishkin A.M., Muryshev E.Yu. Influence of Gas-Dynamic Conditions on Release Degree of Secondary Reaction Energy in Accelerating Ability//Fizika gorenia i vzryva.-1993.-V.29,No. 2.-P.109 (Russian).

A Hydrocode Energy Release Method for the JWL Equation of State

S.J. White

Atomic Weapons Establishment, Aldermaston, UK

A method of adjusting the Equation of State of EDC37 to account for detonation wave curvature is presented. By 'tuning out' the predicted steady-state pressure given by the EoS, an attempt is made to account for the real behaviour seen in a diverging detonation wave without recourse to a reaction rate form. This makes the method suitable for implementation in hydrocodes where burning is pseudo-instantaneous.

A Unifying Model of Hot Spots and the Ignition of Energetic Materials

Y. Horie

Los Alamos National Laboratory, Los Alamos, USA

A one dimensional model of hot spots is proposed to consider various regimes of gnition scenarios on a common platform.

The model contains the most advanced features of spherical pore-collapse models. They include viscoplastic heating, phase change, gas-phase heating, finite rate chemical reactions, heat transfer between the locally heated zone and the surrounding mass.

Test calculations, based so far on RDX data, show that chemical initiation under various mechanical excitations as well as thermal heating can be understood in a unified fashion.

Results also show that the complex phenomena of initiation influenced by a variety of factors such as porosity, grain size, physical properties, and chemical kinetics may be modeled by a fewer parameters than the number that is anticipated. In fact, ignition thresholds are summarized in a single chart in terms of total energy deposition, the rate of energy deposition and the size of hotspots.

Multi-Shock Initiation of Heterogeneous Explosives

R. Belmas

Commissariat a l'Energie Atomique, Le Ripault, Monts, France

Multi-shock initiation is one of the most interesting features of heterogeneous explosives behavior which allows to analyze the complex mechanisms at work during shock-to-detonation transition (SDT).

Many experimental results are now available which show, as a function of the multi-shock profile either complete or partial desensitization (in the case of a continuous pressure profile or in the case of a ramp wave), or significant sensitization (in some configurations where the different shocks are separated by release waves). This last phenomenon is currently named XDT and is interpreted as a damage (due to a first shock) followed by defects expansion (due to release) and recompression (due to a second shock). In this case, the second shock compresses a medium the heterogeneity of which is significantly enhanced by defects expansion.

In this paper, we focus on the case where the pressure shock profile is continuous, that is to say where no release wave follows a first compression. The result of such a stimulus is generally desensitization.

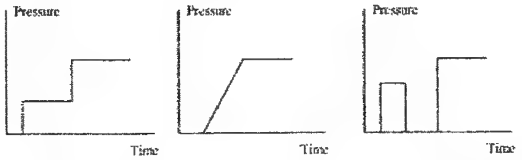

Continuous multishock profile *Ramp wave* *Separated shocks*

Many studies have been conducted which shows that hot spot formation due to the interaction of a shock wave with the explosive microstructure defects is the mechanism governing the initial stage of SDT. The analysis and the comparison of the efficiency of possible mechanisms for hot spot formation suggest explosive heating due to viscoplastic work at the vicinity of microstructure defects.

Several authors proposed more or less complex models based on this interpretation which leads often to good agreements when faced to the experimental results.

The most classical models allow to calculate porosity collapse, surrounding explosive heating and decomposition, and cooling due to thermal conduction. These three phenomena seem to be the key of a hot spot model efficiency but some refinements can be introduced as pore size distribution, complex decomposition kinetics, reactions in gas phase...

However, even the most refined models come to term with several approximations : the geometry is supposed spherical and kinetics constant, burning velocities and mechanical and thermal parameters take most often the values which were determined at ambient pressure and temperature. Moreover at less one (even more) fit parameters are necessary to get agreement with experiments.

As a conclusion on this kind of models, they should not be considered as an accurate representation of what happen at the microstructural level under the effects of a shock wave but more as a global description of an initial SDT stage governed by mechanical and thermal processes in the grain structure.

We use such a model to interpret single and multi shock initiation experiments with three explosive compositions :

1. a pure HMX based one (X1),
2. a pure TATB based one (T2),
3. a mixed TATB-HMX based one (TX1).

Single shocks experiments on these explosives allow to determine indirectly some parameters of the model as explosive viscosity.
Then, it can be observed that multi-shock stimuli lead to different effects as a function of :

1. the shocked explosive composition,
2. the pressure profile (shock pressure values and duration).

In pure HMX or TATB based compositions, total or partial desensitization are observed and it is obvious that desensitization has its own kinetics. For example, if a complete desensitization is observed, after a first pressure plateau with given duration, it can be noticed that decomposition gradually starts again as the duration of this plateau becomes shorter.

These features are in good qualitative agreement with the theory and the model fitted on single shock experiments leads to a correct prediction of the observed phenomena. Particularly, it can be noticed that explosive viscosity is a very important parameter as it governs the pore collapse duration and then the desensitization kinetics.

But more complex phenomena are noticed in the mixed HMX-TATB composition. Once again, partial or complete desensitization are observed but the influence of the first pressure plateau duration is more curious. Indeed, delayed initiations are observed in shock configurations where (according to the theory) hot spots could not ignite neither in HMX (due to the fact that the pores in this explosive should

be closed and cooled when decomposition is observed) nor in TATB (because shock pressures are too low to generate hot spot ignition in this material).

A deepened analysis of these phenomena, by the means of shock experiments and of calculations with the hot spot model suggests that, in this configuration, HMX is initiated by hot spots generated in TATB. The temperature of these hot spots is not high enough to ignite TATB but is sufficient to ignite HMX grains in close contact with TATB ones.

From this study, we can deduce that :

1. A "good" hot spot model (as to be introduced in an efficient SDT kinetics) must take into account, at the very least, pores collapse and heat generation due to viscoplastic work, thermal conduction explosive decomposition and pore size distribution.
2. The complexity of microstructural mechanisms in the case of multicomponents explosives shows the difficulty of representative models development for these compositions.
3. It must be kept in mind that such models are very useful (and sometimes predictive) tools but that they are not a precise representation of the explosives microstructure behavior.
4. The need for a good microstructure description (pore size distribution) grains morphology...) is an additional difficulty for this kind of physical modeling.

A Multifluid Reaction Zone Description Based New Model for Shock-to-Detonation Transition and Non Stationary Detonation Wave Propagation in Reactive Materials

Alain FROGER

Commissariat à l'Energie Atomique, Centre d'Etudes du Ripault, Monts, France

This paper is concerned with a new model developed for studying the propagation of non-stationary detonation waves and shock-to-detonation transition (SDT) in reactive materials, for any given geometry and confinement. In particular, the model is suitable for non ideal explosives. For SDT and detonation propagation in non ideal explosives the reaction zone behind the shock front is relatively thick. This implies that pressure, celerity, curvature, ... at the shock front are strongly dependant on the flow divergence just behind it. So a precise physical description of both thermodynamic phenomena and mechanical properties in the reaction zone is absolutely necessary to perform accurate computations of SDT and non stationary detonation waves.

The model is based upon the following physical considerations : 1) the reaction zone is a close mixture of non reacted material and decomposition products. 2) the energy release appears on the decomposition products only. 3) the energy release ΔQ by mass unit of material is not a constant but depends on the local thermodynamic state.

So the fundamental features of this model are : 1) use of the reaction enthalpy balance ΔH, which is a physical constant, to determine $\Delta Q(x,t)$ in space and time. 2) the two components of the mixture have the same material velocity, the same pressure, but different temperatures. The model also involves a realistic behaviour of the materials : equation of state of each component, induction time and chemical kinetics of the reaction, possible energy exchange between the two components by molecular collision process.

From a theoretical point of view, it appears that it is not possible to build an equation of state for the mixture and that the meaning of the so-called CJ-point is to be reviewed.

Note that our model is suitable for both homogeneous or heterogeneous reactive substances. Moreover, it can be straightforwardly extended to multifluid composition of the reaction products if required, each component having its own temperature.

The model is complete, in the sense that it does not need any adjustment (e.g. ΔQ in standard models), nor any phenomenological sub-model (e.g. celerity/curvature relationship at the front shock), which is a considerable advantage.

Computations were carried out to demonstrate the capability to simulate SDT, highly non-stationary detonation propagation, superdetonation phenomenon and diameter dependence of propagation

experiments in standard cylindrical cartridge test. A very good agreement was obtained by simulating some experiments reported in open literature.

From a numerical point of view it was pointed out that the model is not scheme dependent : it works with the old lagrangian Richtmyer scheme, with a lagrangian Godunov-type scheme or with an eulerian Godunov-type scheme. At the moment (May 2001), it works on a pseudo-2D hydrocode with a sophisticated Godunov-type scheme (optionally Lagrangian or Eulerian).

The accurate simulation of the reaction zone needs fine cells near the shock front. So the present model is being currently introduced in a complete 2D AMR code with highly sophisticated Godunov-type scheme developed at CEA/DIF.

Chéret R. (1999), *Chapman-Jouguet hypothesis 1899-1999: One century between myth and reality*, Shock Waves (1999) vol 9.

Jourdren H, Ballereau P., Commissariat à l'Energie Atomique – Centre d'Etudes DIF.

B. Léal-Crouzet, G. Baudin, H.N. Presles , *Shock initiation of detonation in nitromethane*, Combustion and Flame, vol. 122 (2000)

Application of a Multiphase Mixture Theory with Coupled Damage and Reaction to Impact Hazards

R.G. Schmitt, P.A. Taylor, E.S. Hertel

Sandia National Laboratories, Albuquerque, USA

A multiphase continuum mixture theory is presented that couples the mechanical response, damage evolution, and combustion of energetic materials. The model is demonstrated to capture shock-to-detonation transition, deflagration-to-detonation transition and response due to low velocity impact. The modeling approach has also been demonstrated to simulate delayed detonation for rocket propellants and to investigate the violence of reaction in thermal explosion experiments. Traditional models for shock to detonation transition are not appropriate when the processes that lead to reactive waves are not initiated directly by mechanical shock. Most shock-to-detonation models are empirically based with input parameters fit to pop-plot data. The fits are not unique and several sets of reaction rate parameters will yield similar results. These models are often applied in situations that may not be appropriate. One example is low velocity impact. In a low velocity impact the stress wave from the impact propagates through the material several times before a violent reaction occurs. During this phase of the impact the energetic material response exhibits damage evolution and reaction. A key aspect of the multiphase mixture model is that the damage evolution interacts with combustion and the resulting enhanced surface area burning will accelerate to shock induced reactions if sufficient damage develops.

Computation of Detonation Waves in Multiphase Multispecies Multimaterial Flows

A. Chinnayya, E. Daniel, R. Saurel

IUSTI, Université Aix-Marseille I, Marseille, France
INRIA Projet SMASH, Sophia Antipolis, France

Computation of detonation waves in condensed energetic materials involves several fundamental problems related to the presence of different compressible fluid mixtures: physical and artificial multiphase mixtures. The first type of mixture involved in these applications is due to the decomposition of the condensed phase into product gases. Thus, this mixture has a physico-chemical origin. Knowing the basic thermodynamic properties of this mixture raises several problems. Let us briefly recall the approach usually employed.

Detonation physics codes are based on the Euler equations augmented by several species conservation equations. An equation of state (EOS) for the mixture is necessary to close this type of model.Equations of state for mixture are built on the basis of pure materials EOS's.

Usually, the equation of state for the condensed (inert) material is a Mie-Gruneisen EOS, whose parameters are determined from the experimental Hugoniot curve. This equation of state is in principle accurate enough. A first difficulty appears from the determination of the EOS of the gaseous products. When the reaction is very fast, i.e. when the reaction zone is very thin (a few microns), for most applications it is not important to have an accurate determination of the flow variables in this zone. Only the gas dynamics outside the reaction zone plays an important role for propulsion. The gas follows a thermodynamic path closed to an isentrope. Along such a thermodynamic path it is possible to compute the equilibrium gas composition and to determine a reduced Mie-Gruneisen-*like* equation of state. Many thermochemical codes are devoted to such purposes (Baudin, 1995, Fried 1997).

When both equations of state for pure substances (solid and gas) are available, it is possible to build a mixture equation of state, by using two equilibrium assumptions between the two phases: pressure and temperature equilibrium, pressure and density equilibrium, etc. These closure assumptions suffer from a lack of physical validity. We will show in this paper that these two closures laws are not valid.

For specific applications, accurate determination of the reaction zone is necessary. Indeed, there exist explosives whose reaction zone is very thick (of the order of 1m). The explosive contains several reactants, which consume with very different characteristic times, yielding a gas mixture whose composition varies strongly. Of course, this phenomenon is out of equilibrium, non isentropic, and cannot be computed with thermochemical codes. The thermodynamic gas properties must be computed with theoretical equation of state (BKW, virial expansions) that requires knowledge of the gas composition (mass fractions) and thermodynamical variables (internal energy, density). These thermodynamic variables are not available when the Euler equations are used as hydrodynamic model: only mixture energy and density are computed. Thus, it is necessary to adopt another hydrodynamic model. On the other hand, building a *mixture equation of state* when the solid phase is governed by its own EOS and the gas by another EOS function of gas thermodynamic variables and gas composition is quite impossible so that the Euler model cannot be used any more.

So our first motivation for a multiphase flow model is based on mixture thermodynamics considerations. This type of approach was adopted in the papers of Butler *et al.* (1982), Baer and Nunziato (1986), Kapila *et al.* (1997), Saurel and Abgrall (1999), Kapila *et al.* (2000), Saurel and LeMetayer (2001).

Our second motivation is related to the computation of interface problems between compressible materials and boundaries between pure fluids and mixtures. Indeed, an explosive is always confined by other materials and it is important to determine accurately the propulsive effects, that have strong coupling effects with the detonation dynamics. This second topic poses another fundamental computational challenge related to the creation of artificial fluid mixtures. These artificial mixtures are created by the numerical diffusion at the interfaces when eulerian methods are used. This problem is known as "mixture cells" computation.

In the past decades, there have been considerable efforts to deal with the computation of flow with interfaces. We refer to the papers by Benson (1992), Saurel and Abgrall (1999) and the references herein for an overview.

For an efficient and simple computationnal methodology, our strategy relies on full eulerian methods without front tracking or interface reconstructions. This way has been initiated by Karni (1993), Abgrall (1996), Karni (1996), Shyue (1998), Saurel and Abgrall (1999a), Fedkiw et al. (1999), Fedkiw et al. (1999), Saurel and Abgrall (1999b), Saurel and Le Metayer (2001), Abgrall and Saurel (2001).

Among these approaches, two of them are particularly interesting for our applications. In the Fedkiw's method a unique strategy is employed for the resolution of interface problems and detonations.

This is particularly interesting for a code development. This method is based on level set ideas, and ghost cells, mimicking boundary conditions on discontinuities. Although non-conservative, it has shown interesting features.

The other approach is based on a multiphase modeling of the entire flow (Saurel and Abgrall (1999b), Saurel and Le Metayer (2001), Abgrall and Saurel (2001)). This approach is more complicated that the previous ones, in the sense that the PDE system is more heavy and non-conservative terms are present in the equations. However, this approach is conservative regarding the mixture and allows a determination of the thermodynamic state of each component of the mixture. In particular, this method is able to deal with the first goal of this paper, i.e. physical fluid mixtures due to chemical decomposition (Saurel and Le Metayer (2001)), as well as with numerical mixtures (Saurel and Abgrall (1999b)).

In these references, an unconditionally hyperbolic model able to deal with physical mixtures as well as with numerical ones was proposed. The non-conservative terms were considered and approximated according physically fundaments. The numerical approximations were derived by considering a uniform flow with respect to velocities and pressure, and the idea was to keep such wave structure invariant by the scheme. Such approximations are valid for interfaces, which correspond to volume fraction discontinuities in this context, except when a shock wave interacts with them. In Saurel and Le Metayer (2001), the difficulties that appear when mass transfer occurs at shock front in the context of detonation waves were explained. Also, the method developed in these references was dissipative for contact discontinuities. Indeed, the Riemann solver only considered two waves instead of seven.

To summarize, the model and the method were suffering of some imperfections:

* The closure laws for the average interfacial velocity and pressure were unclear.
* The numerical method was too much dissipative for contact and volume fractions discontinuities.
* The approximation of the non-conservative terms was carefully done for contact discontinuities, but was left unclear for shock interaction with volume fraction discontinuities.

In a recent paper by Abgrall and Saurel (2001), these difficulties have been solved. The key idea is to discretise the multiphase mixture at the microscopic level and then to average the discrete equations. This provides a new discrete model as well as the numerical method. This is done in the opposite way than before. Indeed, it was conventional to obtain a system of PDE on the basis of averaging procedures, and then to discretise the corresponding PDE system.

With the concept of Abgrall and Saurel (2001), robustness and accuracy are such that it seems possible to solve complex situations involving compressible mixtures under strong shock wave and with complex chemistry couplings. It is the goal of the present paper.

Of course, the method of Abgrall and Saurel (2001) needs a lot of extensions to deal with the applications of multiphase detonations and interfaces:

* The materials are reactive and it is necessary to adapt the model to such situation.
* The equations of state are complex and chemical kinetics effects need to be modeled and solved accurately.
* Multiphase mixtures encountered in the physics of detonation waves are specific. The mixture mainly flows with a single velocity and pressure (Kapila et al. (2000)). We propose to adopt a description of the microstructure of the mixtures that relaxes intrinsically toward equilibrium, in order to model the effects that render the various velocities and pressures close to each other.
* The overall model and method needs to be extended to an arbitrary number of fluids.
  In Abgrall and Saurel (2001) the method was developed for two fluids only.
* When dealing with interfaces and mixtures, all fluids are present in the entire computational domain, with variable proportions. For example, the confining material of the explosive will contain a negligible amount of gas products of the explosive, as well as a negligible quantity of the condensed state of the explosive. The presence of these negligible quantities poses many computational difficulties, like the choice of the integration time step for example. These difficulties are explained here and solved.
* The method is extended in two-dimensions under operator splitting and special treatment of slip lines.
* The extra computational difficulties due to mass transfer, stiff chemical kinetics, and their couplings with the pressure relaxation are explained and solved.

The paper is organized as follows. First the reactive multiphase model is developed under conventional averaging procedure and with the help of continuous differential operators. Then a modification of the Abgrall and Saurel (2001) method is developed for modeling mixtures that

intrinsically relax toward pressure and velocity equilibrium. This provides the basic hyperbolic solver, for an arbitrary number of fluids, in absence of mass transfer and chemical reactions. The difficulties related to the presence of negligible amount of materials in computational zones are then addressed. The next section is devoted mass transfer and finite rate reactions resolution. Finally a set of validation is proposed as well as illustrative computations.

Acknowledgments

This work was partially supported by DGA / CEG Gramat. The authors are particularly grateful to Dr. Gérard Baudin.

References

Baer, M.R. and Nunziato, J.W., (1986) A two-phase mixture theory for the deflagration-to-detonation transition (DDT) in reactive granular materials. *Int. J. of Multiphase Flows*, **12**, pp 861 - 889

Bdzil, J.B., Menikoff, R., Son, S.F., Kapila, A.K., Stewart, D.S. (1999) Two-phase modeling of a deflagration-to detonation transition in granular materials: A critical examination of modeling issues. *Physics of Fluids*, **11:2**, pp 378-402

Kapila, A, Son, S, Bdzil, J, Menikoff, R and Stewart, D (1997) Two-phase modeling of DDT: structure of the velocity-relaxation zone. *Physics of Fluids*, **9 : 12**, pp 3885-3897

Massoni, J., Saurel, R., Baudin, G. and Demol, G., (1999) A Mechanistic model for shock to detonation transition in solid energetic materials. *Physics of Fluids*, **11: 3**, pp 710-736

Saurel, R. and Abgrall, R. (1999) A simple method for compressible multifluid flows. *SIAM Journal of Scientific Computing* **21 (3)**, 1115

Saurel, R. and Abgrall, R. (1999) A multiphase Godunov method for multifluid and multiphase flows. *Journal of Computational Physics* **150**, 425

Saurel R. and Le Metayer, O. (2001) A multiphase model for compressible flows with interfaces, shocks, detonation waves and cavitation, *Journal of Fluid Mechanics*, **431**, pp 239-271

A Model of Hot Spot Ignition and Heat Release Rate in Porous Composite Explosives

B.A. Khasainov, B.S. Ermolaev, H-N. Presles*, P. Vidal*

Institute of Chemical Physics, Moscow, Russia
**Laboratoire de Combustion et de Detonique ENSMA-Poitiers, France,*

A new physical model is proposed to simulate detonation build-up and propagation in composite explosives, particularly in binary HE/metal compositions of arbitrary density and particle-size distribution. Some formal attempts to model such explosives are already known. For example, Leiper and Cooper [1] successfully described charge diameter effect in commercial explosive made of ammonium nitrate (AN) and aluminium by means of a slightly divergent one-dimensional detonation model. Their formal kinetic law takes into account particle size distributions of AN and Al. However, in general, such formal laws are only valid for the particular gasdynamic models used to derive them, and only for the studied composition. Thus, one cannot rely on such formal models when considering other charge density, metal content or equation of state.

DESCRIPTION OF THE MODEL

The model summarized in the present work relies on macroscopic gasdynamic conservation equations which explicitly take into account effect of charge porosity. The model considers three components, namely fresh HE, fresh metal (aluminium) and reaction products. Every component is described by its own equation of state. All the components are assumed to have the same particle velocity. For solid components we use HOM equations of state (EOS) corresponding to theoretical maximum

density respectively of HE and metal. Hence, there is no need to recalibrate coefficients of EOS of the mixture when porosity of the mixture or content of metal is modified. This is a significant advantage of the proposed approach.

Dynamics of void collapse behind a shock was described in the framework of a visco-plastic model [2]. This dynamics controls variation of charge porosity in the governing conservation equations. Formation of reaction products begins when ignition criterion of HE at the void surface is satisfied, i.e. when local thermal explosion takes place at the surface of voids in spite of cooling of HE at the void surface by heat conduction. According to the surface burn concept the burn rate of explosive $r=bPA_s$ is controlled by the product of the linear regression rate bP and of the specific surface area A_s of ignited grains. Also taken into account is the bulk Arrhenius reaction, which becomes important after shock front pressure attains the detonation level. For simplicity, and better agreement with experimental data [1,3], we assume that the specific surface area A_s of ignited grains remains constant after the shock. In single-component case, this area is close to the initial specific surface area of heterogeneous HE [3], while for binary mixture we assume that A_s is an initial void-faced specific surface area of HE grains in mixture with metal powder whose mean size is of the same order of magnitude as that of HE (specific surface area is inversely proportional to a mean particle size).

Aluminium particle behind a shock front are assumed to be in thermal and mechanical equilibrium with detonation products and their ignition occurs when particle temperature attains some threshold temperature. Characteristic time of aluminium oxidation rate is reciprocally proportional to a square of initial particle diameter. However, we assume that conversion of aluminium is slower than that of HE.

Since shock sensitivity parameters of heterogeneous explosives such as critical detonation diameter and run distance to detonation are controlled by initial specific surface area of HE [3], the decomposition rate of heterogeneous HE is also controlled by the specific surface area or the mean size of HE particles. Apparently, this rate is very slow in comparison with that of the chemical reactions in «gaseous» phase, so that the composition and state of «gas» surrounding HE is in thermodynamic equilibrium. Then, as soon as, say, 3% of HE is burnt, we switch from HOM equation of state for HE to the equilibrium thermodynamic equation of state [5] to calculate pressure, temperature and composition of detonation products at given burnt fractions of HE and metal and specific volume and energy of the mixture given by the solution of gasdynamic equations at every instant of time for every particle trajectory behind the shock. The considered equilibrium chemistry approach provides correct energetics of the mixture while heat release rate is controlled by decomposition rates of HE and metal which can be varied to cover all the range between ideal high explosives and nonideal ones. This approach can be easily generalized to a larger number of components.

Finally, to model qualitatively the charge diameter effect on detonation velocity, we use a quasi-one-dimensional approximation, valid for relatively small lateral expansions of charge confinement and small thickness of confining tube. With such an approximation, we cannot have a perfect agreement between calculations and observations, especially in the case of thick tubes. However, the approach appears quite reasonable because it takes into account competitions between heat production (chemical kinetics) and losses, both at the macroscopic (adiabatic expansion) and microscopic (heat conduction) levels.

RESULTS OF CALCULATIONS FOR LOOSE-DENSITY AMMONIUM NITRATE

Here we consider experiments of Miyake [4] who has measured effects of charge-diameter and thickness of a 1-m long tube on the detonation velocity and pressure in pure ammonium nitrate (AN) at density ρ_o=0.85 kg/m^3 (porosity $\phi_o=1-\rho_o/\rho_{TMD}=0.507$). Detonation was initiated by means of a PETN/oil booster (66-mm length pellet). Miyake reports on diameters of AN prills (between 1 and 2.8 mm) but, unfortunately, does not report on either specific surface area of AN prills or mean void size. Therefore, we have had to select some representative value of the product $b\cdot A_s$ which is thus a best-fitting parameter of the proposed model. Specifically, we have assumed that $b\cdot A_s=7\cdot10^{-5}$ l/s/Pa.

Figure 1 shows results of numerical simulations of detonation build-up in a tube with inner diameter of 10 cm at different wall thickness. One can see that the final detonation velocity increases with tube thickness and that there exists a critical tube thickness below which detonation propagates in an irregular low-velocity detonation mode. Thus, detonation velocity is controlled by competition between chemical heat release rate and heat losses rate, which increases as tube thickness decreases. Transition

distance to quasi-steady detonation agrees with that reported by Miyake. Decrease of wall thickness from 30 mm to 8 mm decreases velocity and peak pressure of the detonation wave along with completion of AN conversion. As a result, the specific amount of oxygen containing species in detonation products also decreases (these species are important for aluminium oxidation in the case of AN/Al mixtures). Hot-spot ignition becomes a rate-controlling factor in low-velocity detonation case (at smallest h_o=6 mm). Incompleteness of AN conversion in nonideal detonation amounts to about 30% (instead of about 15% at h_o=8 mm).

Figure 2 compares calculated and experimental detonation velocities in 100-mm diameter tube at different wall thickness h_o. At high h_o we overestimate detonation velocity by 200 m/s (~ 7%). In view of the simplicity of the quasi-1D approximation, the agreement can thus be considered as reasonable. However, in contrast to the observed trend, which exhibits a plateau at h_o>20 mm, the calculated detonation velocity D keeps growing with h_o, even at higher h_o. This difference is due to the fact that we voluntarily neglected Arhenius reaction to isolate it from the effect of surface burn rate.

As a whole, and in spite of a simplified description of the tube expansion, the considered model of detonation initiation and propagation in porous AN seems to be quite reasonable. It also gives a good agreement between the calculated pressures and the experimental ones reported by Miyake. With the pre-estimated «representative» value of surface burn rate characteristic bA_s of pure AN we are now simulating detonations in ammonium nitrate/aluminium mixtures.

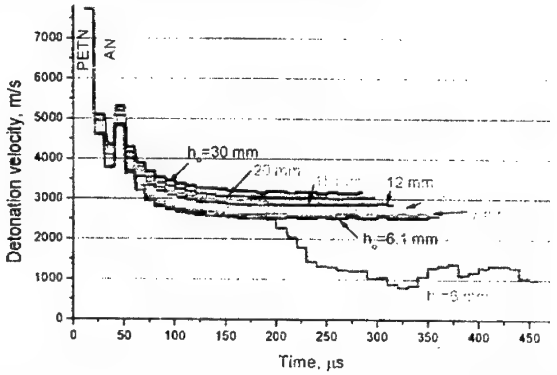

Figure 1. Effect of steel tube thickness (h_o) on detonation velocity evolution in porous AN in 1-m long tube with i.d. 100 mm (in calculations detonation velocity was «measured» every 10 μs)

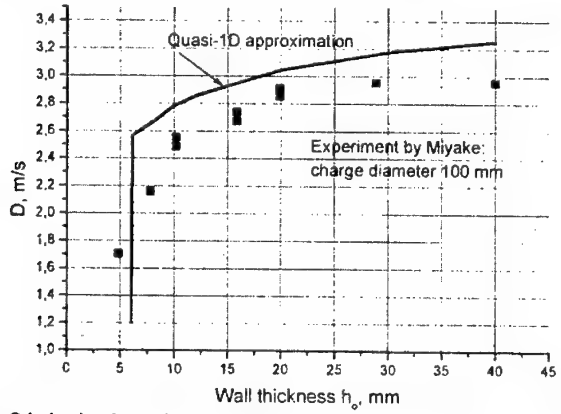

Figure 2. Calculated and experimental effect of tube thickness on detonation velocity in porous AN at constant tube diameter of 100 mm.

References

1. Leiper G.A.,Cooper J. (1993) *Reaction of aluminium and ammonium nitrate in non-ideal heterogeneous explosives.* Proceedings Tenth International Detonation Symposium, Office of Naval Research, Arlington, Virginia 22217-5000, ONR 33395-12, p.267-274.
2. Khasainov B.A., Borisov A.A., Ermolaev B.S., Korotkov A.I. (1981) *Two-phase viscoplastic model of shock initiation of detonation in high density pressed explosives.* Seventh Symp. (International) on Detonation: Proceedings. Annapolis. USA. NSWC MP 82-334. pp. 435-447.
3. Khasainov B.A., Ermolaev B.S., Presles H.-N., Vidal P. (1997) *On the effect of grain size on shock sensitivity of heterogeneous high explosives.* Shock Waves, V. 7, pp. 89-105.
4. Miyake A. (1991) *Detonation velocity and pressure of the non-ideal explosive ammonium nitrate.* The Ninth Symp. (Int.) on Detonation. v.1, p.253-256.
5. Khasainov B.A., Ermolaev B.S., Borisov A.A., Baudin G., Presles H.-N. (1998) *Numerical Modeling of effect of aluminum particles on detonation performance of model high explosive based on equilibrium chemistry approach.* International Conference on Shock Waves in Condensed Matter. St.Petersburg, Russia, 12-17 July 1998.

Numerical Simulation of Intermediate Stages of DDT in Confined Charges of Grained Single-Based Propellants

B.S. Ermolaev, A.A. Belyaev, A.A. Sulimov

Institute of Chemical Physics, Moscow, Russia

According to recent knowledge, the transition of deflagration to detonation (DDT) goes through several stages, which sequentially change each other and have different temporary and spatial scales and mechanisms both of initiation of chemical conversion and transport of energy to the wave front. The key intermediate stages of the DDT are convective combustion and low-velocity detonation (the latter sometimes is named as compressive burning). Properties of these stages, conditions of their origination and dynamics of their development determine propensity of energetic material to the DDT and its behavior, including run distance to detonation.

For the theoretical consideration of the DDT the different groups of investigators have developed a few models, which, however, differ from each other only in not so essential details. All these models are based on equations of mechanics of multiphase reactive media. They also assume that the heating of energetic material to temperatures providing beginning of exothermal conversion takes place on a pore surface due to two possible mechanisms, i.e., convective heat transfer from hot gases filtering through pores and visco-plastic dissipation of energy during pore collapse and neglect effects of finite rates of chemical reactions in the flame. The last assumption allows one to consider only two phases (solid phase as an initial EM, and gas phase as products of its conversion), and to define the bulk rate of energy release as a product of specific surface of pores or grains, normal regression rate and heat effect.

In the literature there are impressive examples of coincidence between numerical modeling and experimental data both on the behavior of DDT as a whole, and characteristics of its intermediate stages. However comprehensive comparison was conducted only for separate particular runs. Variation of material properties was studied only in a few cases but attention was paid solely to run-to-detonation distance. As a result, a few important questions including the range of validity of the models and even relationships between governing parameters of the porous charge and DDT parameters remain uncertain. Besides, some details of DDT mechanisms, in particular, role of so called "plug" of compacted material generated in front of the wave

during convective burning stage together with possibility of low-velocity detonation without participation of the "plug" need further consideration.

Here we present the results of parametric study of the convective burning and LVD in loose-packed and compacted beds of grained single-based gun powders. The study has been conducted using quasi one-dimensional computer code we have developed for simulating intermediate stage of DDT process. One of the problems hampering analysis of DDT is the uncertainty in size of material particles formed after possible crush of original grains into fragments before ignition front during deformations under increasing stresses. The grained single-based gun powders allows one to ignore crushing effect in a wide pressure range. Parameters varied in a wide range in our calculations were grain diameter, initial charge porosity, constant in the law of normal regression rate, parameters determining dynamics of charge compaction and a few other material properties. Effects of changes in charge diameter and confinement properties were considered in frame of quasi one-dimensional approximation assuming inertial expansion of confinement after the local stress in energetic material exceeds yield strength of the confinement.

The calculation results are presented separately for convective burning and low velocity detonation stages. The phases of development of convective burning stage are analyzed, particularly, the phase of the "plug" generation together with evolution of profiles of pressure and other parameters and front velocity. The conditions at which the convective burning terminates and compressive burning arises are considered in detail.

Transition from convective burning to compressive burning means that visco-plastic pore collapse under the developed stresses provides heating of a pore surface layer sufficient for ignition of material. In the case of charges of low density close to the loose-packed density, the change of the stages takes place when maximum pressure attains 230 - 250 MPa and particle velocity in the "plug" 200 - 230 m/s. The change is accompanied by noticeable increase in the velocity of the flame front from 400 - 500 up to nearly 800 m/s, that is manifested in a break of the flame front trajectory

Evolution of the low velocity detonation stage goes through two phases. In the course of the first phase the wave propagates without noticeable acceleration. The pressure profile of triangular shape is gradually developing, the maximum pressure in spike grows, reaching 1 GPa and more. In the course of the second phase which has much smaller duration than the first one, 10-fold increase in the rate of growth of pressure in spike takes place, the profiles of pressure and particle velocity look as typical profiles of detonation wave with "chemical spike". The wave velocity sharply increases and the process changes into the stage of formation of the normal detonation wave.

The increase of grain size results in the slower development of the process; the distances traveled by the flame front during both stages proportionally increase, but the aforementioned wave characteristic attained at the moment of the stage change remains almost invariable. Besides, the effect of deformation of confinement manifests itself more and more noticeably. As a result, in the case of grains of 3.3 mm in diameter the stage of low velocity detonation does not result in formation of a normal detonation even if the charge is confined into the steel casing. Here, the quasi-steady low velocity detonation is observed that propagates along considerable length of the charge keeping almost constant parameters. Reducing initial porosity (in the range from 0.48 up to 0.1) results in acceleration of the rate of development of process. The change of the stages takes place at higher maximum pressure but lower particle velocity in the "plug". The first phase of low velocity detonation has the higher wave velocity and is easier stabilized due to the casing deformation.

The calculations performed for coarse-grained charges of loose-packed density have revealed also essential difference in the mechanism of low velocity detonation in comparison to fine-grained charges. So, if in the last case the controlling role of dissipative heating during the pore collapse is kept at all phases of low velocity detonation, in charges with coarse grains a bit later after the origin of low velocity detonation, the wave undergoes a structural transformation. As a result, a new spatial structure is formed that provides conditions when the energetic material grains are ignited without participation of the pore collapse by means of convective heat transfer from shocked and strongly heated gas. This mechanism of low velocity detonation is referred to as "gas-compression" one. This process is considered in detail.

The simulation results are compared to the experimental data obtained for grained gun-powders. There is good agreement both for behavior and characteristics of the stages. As well as in calculations, the

experimental data demonstrate two phases of the development of convective burning and low velocity detonation, slower evolution of the process in the case of coarse-grained powders, quasi-stabilized propagation along considerable part of the charge length, and the spatial pattern adequate to the gas-compressive mechanism in the coarse-grained charges. However a few differences are revealed, which we shall pay special attention to.

A 1D Computational Fluid Dynamics and Radiation Heat Transfer Solver for Modeling Shock-to-Detonation Transition of Nitromethane

G. Baudin[1], V. Bouyer[1,2], I. Darbord [2], R. Saurel [3]

[1] DGA/Centre d'Etudes de Gramat, Gramat, France
[2] Laboratoire d'Energétique et d'Economie d'Energie, Ville d'Avray, France
[3] Institut Universitaire des Systèmes Thermiques Industriels, Marseille, France

1. Introduction

Luminance temperature measurements have been performed to study the rapid phenomena of shock-to-detonation transition (SDT) in nitromethane (NM), using a time-resolved six-wavelength pyrometer in the range 1500-6000 K [1]. The experiments consisted in plane shock impacts on explosive targets: the impactors used were copper disks with a 80 mm diameter and the NM was confined in a polyethylene chamber (70 mm inside diameter, depth ranging from 15 to 25 mm), enclosed by a 4 mm thick copper transfer plate. The optical pyrometer recorded the explosive luminance history during the SDT through a LiF window. Complementary information, required to read the luminance signals, were obtained from other sources: a Fabry-Perot Interferometer to record the transfer plate velocity history during initiation and piezo-electric pins located at measured depths in the explosive to measure the shock and detonation velocities.

Both spectral distribution of the luminance signals and velocity records of the transfer plate highlight semi-transparent reaction products prior to the detonation formation. The semi-transparency of the reaction products is a real problem to determine the emissivity and the temperature of the nitromethane reacted layers, using the luminance signals recorded by the six-wavelength pyrometer. To obtain more information on the spectral absorption coefficients of the reaction products,a spectral analysis was performed in the visible range, 0.3-0.85 μm wavelength, using a time resolved emission spectroscopy technique [2].

Both pyrometer and spectroscopy techniques give several radiance intensity values depending on wavelength and time. They can be used as data to solve the reversal mathematical problem of the radiation equation transfer in a semi-transparent medium for each stage of the SDT to evaluate the optical properties of the reaction products and the parameters of the forward chemical kinetics. The direct problem, using computational fluids dynamics and radiation heat transfer 1D code, is a first step of such approach to evaluate the sensitivity of the physical parameters on the luminance signals.

2. The physical system

The basic equations are the one-dimensional Euler fluid dynamical conservation equations and the heat transfer equation for the mixture of liquid nitromethane and gaseous reactions products. The heat transfer equation is used in a differential form and the Euler equations are written in an integral form over an arbitrary volume. The thermodynamics of the liquid-gas mixture is described using simple mixing rules and complete equations of state for the liquid and the gas phases.

[1] B. LEAL-CROUZET, G. BAUDIN, H.N. PRESLES, « Shock Initiation of Detonation in Nitromethane », Combustion and Flame 122:463-473, 2000

[2] V. BOUYER, G. BAUDIN, C. LE GALLIC, « Emission Spectroscopy Applied to Shock to Detonation Transition in Nitromethane », Shock Compression of Condensed Matter, The American Institute of Physics, 2001

One of the main complications in the system of equations is the source term arising from the chemical mass production. Several models exist in the literature for the chemical mass production of the NM reaction products, without certainty on the reaction mechanisms under shock waves. However, it is well known that the chemical mass production is very sensitive to the temperature, and that the chemical characteristic time is less than the hydrodynamic characteristic time.

Another complication in the system of equations is the unknown optical characteristics of the liquid-reaction products mixture at high pressure and high temperature.

The chemistry is treated using one single forward chemical kinetics based on the theory of the transition state. The rate coefficients $k = \frac{k_B T}{h} e^{\frac{Sa}{R}} e^{-\frac{Ea+PVa}{RT}}$ is a function $k(P,T)$ with dEa = -PdVa + TdSa. The equality of the second partial cross derivatives of $k(P,T)$ gives a useful relation-ship between Ea and Va which can be used to determine their T and P dependence, assuming simple hypothesis. The classical Arrhenius law is a particular case of this model.

3. Numerical method

The solver is based on a one-dimensional Lagrangian finite-volume numerical scheme. The strategy adopted is the Strang splitting into two integration subproblems: (i) the source terms arising from the chemical mass production and (ii) the Euler equations without the source terms.

For the time integration of the source terms, a second order Euler step is used. For the Euler equations without source terms, a Godunov's second-order numerical method is used with a MUSCL Hancok approach for the predictor, a Minmod slope limiter to preserve the solution monotonicity, and a characteristics PVRS (Primitive Variable Riemann Solver) to solve the Riemann problem at the cells interfaces.

The luminance temperature histories are directly calculated, integrating the radiative flux transfer equation along the axis. The parametric representation of the spectral absorption coefficient adopted is $\kappa_\lambda = Y_{liq}\rho\kappa_{liq}(\lambda) + Y_p\rho\kappa_p(\lambda,T)$ where λ is the wavelength, ρ the density, T the temperature and Y_i the mass fractions of NM and reaction products. κ_{liq} and κ_P are mass absorption coefficients of the liquid NM and reaction products.

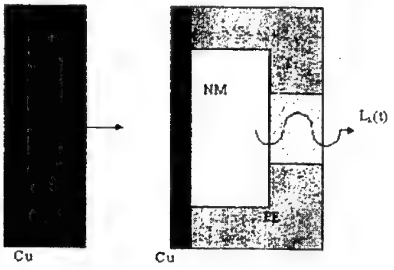

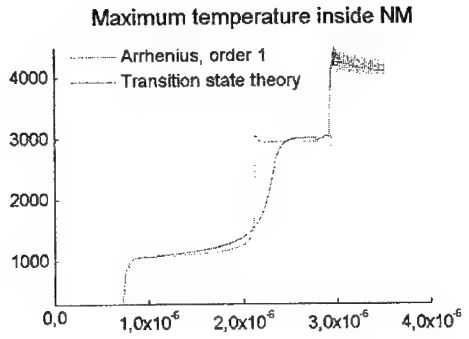

4. Some results

- *Sensitivity of the spectral absorption parameters on the luminance signals*

The linear absorption coefficient $\kappa_{liq}(\lambda)$ of the liquid NM is determined using transmission spectrometry experiments at 298K-1atm. Several functions $\kappa_P(\lambda,T)$ for nonscattering and scattering reaction products, due to the solid carbon ($\approx$ 7% volume fraction), were used. The luminance signals are sensitive to the parametric representation of the spectral absorption coefficient $\kappa_P(\lambda,T)$. Finally, the unknown optical characteristics of the reaction products at high pressure and high temperature lead to retain a simple gray media hypothesis to study the influence of the chemical kinetic on the luminance temperature signals.

- *Influence of the chemical kinetic on the luminance temperature*

The 850 nm luminance temperature signals measured with the optical pyrometer and simulated with a classical first order chemical reaction NM $\rightarrow$ P using an Arrhenius law, are displayed on the figure 1 for a 9 GPa shock pressure. An induction delay corresponding to the beginning of the exothermic reactions leading to superdetonation formation can be seen on these signal. During this induction delay, the explosive remains transparent. Unlike the numerical simulation, the temperature measured by the pyrometer exceeds 1500 K far before the superdetonation formation and increases regularly up to 2500 K. Large differences are obtained between the experimental and the calculated luminance temperatures prior to the superdetonation formation. The differences between the experimental and numerical detonation temperatures are due to the equation of state chosen for the reaction products. The calculation of the induction delay versus the pressure fails for a pressure lower than 9 GPa using this classical model.

Let us consider a single two-molecular forward chemical kinetic 2NM $\rightarrow$ P deduced from a more complex chemical reactions pattern proposed by Bardo et al. If we assume that the temperature dependence of Ea is negligible compared to its pressure dependence, and that Ea and Va are linear in P, we obtain a model which allows the calculation of the induction delay for a large pressure range. However, large differences are also obtained between the experimental and the calculated luminance temperatures prior to the detonation formation.

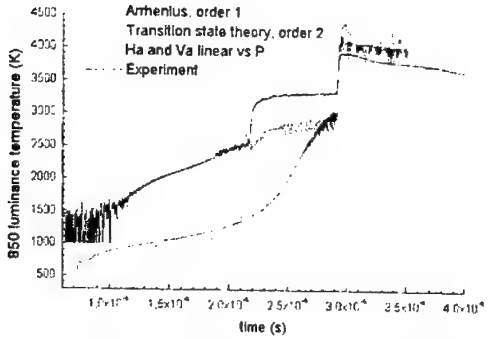

Figure 1: Sensitivity study of the luminance temperature signals to the chemistry model.

5. Conclusion

The unknown optical characteristics of the reaction products at high pressure and high temperature lead to retain simple hypothesis to study the influence of the chemical kinetic on the luminance temperature signals. Large differences are obtained between the experimental and the calculated luminance temperatures prior to the detonation formation, using a single forward chemical kinetic. Two parallel forward chemical kinetics could reduce the error between the experimental and the calculated luminance temperature signals prior to the superdetonation formation. However, the identification of the activation parameters are more difficult, and solving the reversal mathematical problem of the radiation equation transfer is a better way to determine these parameters.

SESSION "Physics of Shock Wave Processes in Inert Materials"

Chairmen:
N. Bourne - **Cranfield University, Shrivenham, UK**
W. Thissell - Los Alamos National Laboratory, USA

High Rate Deformation Processes in Solids

C.S. Coffey

Indian Head Division, Naval Surface Warfare Center, Indian Head, USA

Plastic deformation in solids during high amplitude shock loading is examined. Previous theoretical results that treat the quantum mechanical nature of plastic flow in crystals are extended to high deformation rates due to high amplitude shocks.[1-6] It is shown that the quantum processes responsible for plastic flow limit the maximum rate of plastic deformation. Further, at the high shear stress levels created by strong shocks the plastic deformation behavior of crystalline solids asymptotically approach a steady state. The predicted behavior of these quantities at very high pressure and deformation rates are uniquely and sharply defined by the quantum processes responsible for plastic flow and can not be obtained from a classical analysis.

Predictions are obtained for crystal strength, maximum plastic deformation rate and viscosity. For several different materials, the maximum plastic deformation rate ranged from about 10^5 s^{-1} to a few times 10^6 s^{-1} and the viscosity from about 10^4 to 10^5 poise. This limiting behavior begins at shock pressures between 5 and 10 GPa, depending on the material, and extends to all higher shock pressure levels. Both the limiting plastic deformation rate and the viscosity simplify to concise expressions that contain only a few terms relating to material properties.

These predictions are compared with results from the corrugated shock wave experiments of A. D. Sakharov and co-workers.[7-9] These leading experiments provide insights into the fundamental physical processes responsible for the plastic flow and energy dissipation that occur in solids during extremely rapid deformation due to very high shock levels. For the Sakharov experiments the shock pressure ranged from 5 GPa to more than 200 GPa. The results allowed the estimation of both the plastic deformation rate and the viscosity for a number of solids and liquids while they were subjected to very high level shocks. These experimental results and the above theoretical results are in substantial agreement both numerically and in describing the asymptotically limiting behaviors of the maximum deformation rate and the viscosity.

References

1. C.S. Coffey, Phys. Rev. B **24**, 6984 (1981).
2. C.S. Coffey, Phys. Rev. B **32**, 5335 (1984).
3. C.S. Coffey, Phys. Rev. B **49**, 208 (1994).
4. C.S. Coffey and J. Sharma, Phys. Rev. B **60**, 9365 (1999).
5. C.S. Coffey and J. Sharma, J. of Appl. Phys. **89**, 4797 (2001).
6. C.S. Coffey "High Rate Deformation Processes in Liquids and Solids", Submitted to Phys. Rev. **B**, May 2001.
7. A.D. Sakharov, R.M. Zaidal', V. N. Mineev and A. G. Oleink, Soviet Physics-Doklady, **9**, 1091 (1965).
8. V.N. Mineev and E.V Savinov, Soviet Physics JETP, **25**, 411, (1966).
9. V.N. Mineev and R.M. Zaidal', Soviet Physics JETP, **27**, 874, (1968).

Collective Properties of Mesodefect Ensembles and Shock Induced Plasticity and Failure: Models and Experimental Study

O.B. Naimark, A. Fanget*

Institute of Continuous Media Mechanics, Perm, Russia
**DGA/Centre d'Etudes de Gramat, Gramat, France*

Shocked materials exhibit unexpected indications of universal behavior in the range of stress amplitude and load durations where strength and relaxation effects due to structural changes have a considerable influence. Experiments on shock loading with pressure amplitudes less 100 GPa have established the existence of general deformation responses under condition such a governing role is played by the influence of the evolution of mesoscopic defects (dislocation pile-ups, microcracks, microshears). The density of these defects reaches $10^{12} - 10^{14} cm^{-3}$, but each mesoscopic defect consists of a dislocation ensemble and exhibits the properties of this ensemble. It was shown in the course of statistical and thermodynamic description of the behavior of the mesodefects ensemble that scenario of the defects ensemble evolution in the terms of macroscopic tensor parameter of the defects density (in fact, deformation caused by the defects) reveal the features of different non-equilibrium kinetic transitions. The specific non-linearity (attractors types) corresponds to the ability of plastic relaxation and damage localization.

The existence of characteristic self-similar solutions in the area of the corresponding attractor in the form of the orientation solitary waves, that is typical for dislocation plasticity, and the dissipative structure with the blow-up damage kinetics localized on the spectrum of spatial scales was shown. These self-similar solutions revealed the nonlinear resonance nature of main relaxation processes in solid (plasticity and failure) and the opportunity of the excitation of corresponding regimes in shocked materials. The subjection of shocked solid to the attractor type corresponding to the orientation transition in the microshear ensemble is observed for the strain rate range $\dot{\bar{\varepsilon}} \approx 10^3 - 10^5 s^{-1}$ and is realized as the nucleation and the propagation of the localized plastic waves. The existence of the orientation metastability area as the structural mechanism of the plastic strain instability allowed the determination of the nature of the Hugoniot elastic limits. The well-known phenomenon of adiabatic shear bands as the mechanism of plugging for the long rod penetration is linked with the resonance excitation of these solitary waves. The precise numerical studies of the influence of the defect orientation instability allowed us to propose the explanation of the viscosity universal limit $\eta \approx 10^4 Pz$ for $\dot{\bar{\varepsilon}} \to 10^5 s^{-1}$, that was observed first by Sakharov, and the four power law for stress amplitude established by Barker and Grady for the steady-state plastic shock front. The pronounced illustration of the failure resonance excitation for ceramics and glasses for the rise pulse time

$\sim 1\mu s$ was shown for the condition of spalling ("dynamic branch effect") both experimentally and theoretically as the nucleation of numerous mirror zones in different spall cross-sections and for the case of excitation of, the so-called, failure waves.

The observation of delayed failure allowed us to summarize the following features of failure waves in glasses: (i) failure waves propagates from the impact boundary at the impact pressure about $0.5\sigma_{HEL}$; (ii) the failure wave velocity in various glasses is 1.5-2.5 km/s; (iii) behind the failure wave the spall strength is lost and the shear stress decreases. The self-keeping features of failure corresponding to the condition of failure wave where observed in the condition of dynamic crack propagation. The framing of crack dynamics in the preloaded PMMA plane specimen was carried out with the usage of a high speed digital camera Remix REM 100-8 (time lag between pictures 10 μs) coupled with photo-elasticity method. The existence of three characteristic velocities was established: the velocity of the transition from the steady-state to the non-monotonic straight regime $V_S \approx 220\, m/s$, the transient velocity to the branching regime $V_C \approx 330\, m/s$ and the velocity $V_B \approx 600\, m/s$, when the branches behave autonomous. The low rise of velocity for $\sigma > 60 MPa$ reflects the stress independent character of failure. The pictures of stress distribution at the crack tip is shown in Fig.1 for slow ($V < V_C$), fast ($V > V_C$) and branching ($V > V_B$) cracks.

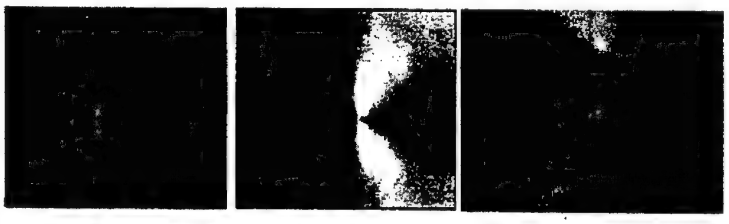

$V < V_C$ $V > V_C$ $V > V_B$

Figure 1. Different regimes of crack dynamics.

The study of failure wave initiation and propagation was studied using original finite element code. The simulation based on mentioned non-linear approach confirmed spontaneous propagation of the failure front behind the stress wave, Fig.6. We observed that the shear stress vanishes in the failure wave. The failure wave propagation leads to qualitative change in the transverse stress when this stress is approaching to the longitudinal stress level.

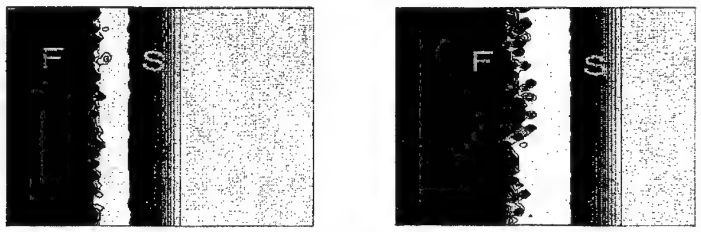

Figure 2. Propagation of stress (S) and failure (F) waves in a target.

The experimental study and numerical simulation allowed us to conclude that the ""failure waves" represent the dissipative structures with the blow-up damage kinetics and the pronounced front propagating with some group velocity.

The Effect of Pulse Duration Time on Damage Accumulation and Model Predictions in Incipiently Spalled Tantalum

W. R. Thissell[1], A.K. Zurek[1], D.A. S. Macdougall[1], C.P. Trujillo[1], D.L. Tonks[2] and T.A. Mason[1]

[1] MST-08: Structure Property Relationships
[2] X-7: Materials Modeling
Los Alamos National Laboratory, Los Alamos, NM, USA

The effect of pulse duration and shock amplitude on damage accumulation in incipiently failed flyer plate experiments in tantalum is described. Flyer plate experiments were performed at 5.6-7.4 GPa shock amplitude and 0.4-2.2 μs pulse duration. The back free surface velocities were recorded with a VISAR. The soft recovered specimens were sectioned and metallographically prepared and etched. The resulting damage was quantified using image analysis and optical profilometry and then subsequently statistically reduced.

The combination of free surface velocities, and spatially resolved void volumetric number densities and size distributions are used to calibrate damage model(s) and also compare to model predictions at conditions other than the calibration conditions.

Grain Size Dependence of Shock-Induced Twinning Stresses for ARMCO Iron

R.W. Armstrong, W. Arnold*, F.J. Zerilli**

AFRL/MNME, Eglin Air Force Base, USA
**TDW, Schrobenhausen, Germany*
***Naval Surface Warfare Center, Indian Head, USA*

Deformation twinning is an increasingly likely deformation mechanism in structural materials, such as body-centered-cubic metals and alloys, at lower temperature and higher strain rates, in the latter case, particularly, extending to shock loading conditions[1]. Here, measurements of the grain size dependence of the deformation twinning determined Hugoniot Elastic Limit (HEL) of ARMCO iron[2] are shown to compare favorably with other pioneering shock determinations at different single grain sizes

and, especially, are shown to compare favorably with a well-determined Hall-Petch (H-P) reciprocal square root of grain diameter dependence reported for collected conventional and split Hopkinson pressure bar (SHPB) measurements of deformation twinning stresses obtaining at different temperatures[3].

Model consideration of the H-P dependence is based on a very nearly athermal twinning stress being determined by dislocation pile-ups in pre-twinning microslip deformation. The comparison of conventional and SHPB results on an equivalent compressive stress basis with the HEL results, measured at pressures in the range of ~0.6 to ~2.0 GPa, are suggested to give a counterpart deformation stress analogy to the reference comparison of static and shock pressure results for the α - γ phase transformation in iron, corresponding to a volumetrically better-specified pressure of 13.5 GPa.

1. R,W. Armstrong and F.J. Zerilli, "Deformation twinning: from atomic modeling to shock wave loading", in Advances in Twinning, edited by S. Ankem and C.S. Pande, Minerals, Metals and Materials Society, Warrendale, PA, 1999, pp. 1-17.

2. W. Arnold, "Dynamisches werkstoffverhalten von Armco-Eisen bei Stosswellenbelastung", Fortschritt-Beriche VDI, Reihe 5, Nr. 247, VDI-Verlag, Dusseldorf, 1992, 242 pages.

3. R.W. Armstrong and F.J. Zerilli, "Dislocation mechanics based analysis of material dynamics behavior", in Second International Conference on Mechanical and Physical Behavior of Materials under Dynamic Loading, DYMAT 88, Journal de Physique-Colloque, Vol. 49, C3-529- (1988).

4. R.W. Armstrong and F.J. Zerilli, "Dislocation aspects of shock-wave and high-strain-rate phenomena", in Fundamental Issues and Applications of Shock-Wave and High-Strain-Rate Phenomena, edited by K.P. Staudhammer, L.E. Murr and M.A. Meyers, Elsevier Science Ltd, N.Y., 2001, Chapter 15, pp. 115-124.

Multi-Scale Modelling of Beryllium: Quantum Mechanics and Laser-Driven Shock Experiments Using Novel Diagnostics

D. Swift [1], D. Paisley [2], G. Kyrala [2], A. Hauer [2]and G. Ackland [3]

[1] University of Edinburgh, Scotland; presently at Los Alamos National Laboratory, USA
[2] Los Alamos National Laboratory, USA
[3] University of Edinburgh, Scotland

Ab initio quantum mechanics was used to construct a thermodynamically complete and rigorous equation of state for beryllium in the hexagonal and body-centred cubic structures, and to predict elastic constants as a function of compression. The equation of state agreed well with Hugoniot data and previously-published equations of state, but the temperatures were significantly different.The hexagonal / bcc phase boundary agreed reasonably well with published data,suggesting that the temperatures in our new equation of state were accurate.

Shock waves were induced in single crystals and polycrystalline foils of beryllium, by direct illumination using the TRIDENT laser at Los Alamos. The velocity history at the surface of the sample was measured using a line-imaging VISAR, and transient X-ray diffraction (TXD) records were obtained with a plasma backlighter and X-ray streak cameras. The VISAR records exhibited elastic precursors, plastic waves, phase changes and spall. Dual TXD records were taken, in Bragg and Laue orientations. The Bragg lines moved in response to compression in the uniaxial direction. Because direct laser drive was used, the results had to be interpreted with the aid of radiation hydrodynamics simulations to predict the loading history for each laser pulse.In the experiments where there was evidence of polymorphism in the VISAR record, additional lines appeared in the Bragg and Laue records.The corresponding pressures were consistent with the phase boundary predicted by the quantum mechanical equation of state for beryllium.

A model of the response of a single crystal of beryllium to shock loading is being developed using these new theoretical and experimental results. This model will be used in meso-scale studies of the response of the microstructure, allowing us to develop a more accurate representation of the behaviour of polycrystalline beryllium.

A. Koskelo[1], K. McClellan[2], J. Brooks[2], D. Paisley[3], D. Swift[3]

1: Chemistry Division (C-ADI), Los Alamos National Laboratory, USA
2: Materials Science and Technology Division (MST-8), Los Alamos National Laboratory, USA
3: Physics Division (P-24), Los Alamos National Laboratory, USA

Introduction

New models for the dynamic response of materials will be based increasingly on better understanding and representation of processes occurring at the microstructural level. These developments require advances in diagnostics and models which can be applied explicitly to microstructural response. Various phenomena occur at the microstructural level which are generally ignored or averaged out in continuum-level models. One example of such 'irregular hydrodynamics' is the roughness imparted to a shock wave as it propagates through a polycrystalline material.

We have developed imaging techniques to study spatial variations in shock propagation through polycrystalline materials. In order to interpret spatially-resolved data from polycrystal samples, we need to compare with simulations which represent the microstructure. Here we describe work undertaken to develop a model of the dynamic response of individual grains. The material chosen was Ni-Al alloy, because it exhibits a relatively large degree of elastic anisotropy, and it is relatively easy to manufacture.

Sample preparation

High purity Ni and Al pieces were mixed in proportions to give equal numbers by atom and fused. A single crystal was grown from the melt by directional solidification within a mold using a <001> oriented seed. The resulting crystal was in the form of a bar of about 10 mm diameter. The orientation was determined by back-reflection Laue diffraction, and the bar was sliced to obtain samples oriented parallel to (100) and (110) planes. Samples were cut to shapes suitable for the flyer experiments. They were then ground and polished to the desired thickness using diamond media to a 1 micron mirror finish.

Theoretical equation of state and elasticity

An ab initio equation of state (EOS) was calculated using quantum mechanics, by the method applied previously to several elements [Swift00,Swift01]. The frozen-ion cold curve was estimated for Ni-Al in the CsCl structure by finding the ground state energy of the outer electrons with respect to ab initio pseudopotentials for Ni and Al. Ab initio phonons were deduced by performing additional calculations of a supercell with atoms displaced from equilibrium. A rigorous thermodynamically complete EOS was then generated in tabular form.

Because of the intrinsic limitations of the local density approximation used to represent the exchange-correlation energy of the outer electrons, the ab initio EOS overpredicted the lattice spacing at STP by ~1%. This discrepancy was corrected by adding a constant pressure offset to the EOS.

The elastic response was predicted as a function of compression by performing further quantum mechanical calculations with the lattice cell compressed uniaxially or sheared.

Laser-launched flyer experiments

The theoretical EOS was tested, and a basic constitutive model obtained, by performing laser-launched flyer experiments with laser Doppler velocimetry (VISAR) diagnostics. Flyers were punched from copper foil and glued to a substrate consisting of PMMA coated with thin (~micron) layers of materials to absorb the laser energy, confine the plasma, and insulate the flyer from heating. The flyers were between 50 and 250 microns thick.

The TRIDENT laser at Los Alamos was used to launch the flyers. Pulses ~600 ns long in the infra-red were used, allowing the flyers to be launched without shocking up, spalling or significant ringing. Flyer speeds up to ~600 m/s were obtained.

The flyers were impacted against Ni-Al targets, attached to PMMA windows. The target typically covered half of the area of the flyer, giving space for the flyer speed to be measured with the VISAR. The surface of the target was also monitored with the VISAR. Wave profiles at the surface of the target provided EOS and strength information.

The Hugoniot data obtained were consistent with the ab initio EOS. The magnitude of the elastic precursor allowed an estimate to be made of the flow stress at different orientations.

Single-crystal plasticity model

The EOS, elasticity, and flow data were used to calibrate a continuum-type model for the response of a crystal of Ni-Al. The local state includes an orientation; plastic flow was based on the mechanical threshold stress (MTS) model [Johnson92,Goto00]. This model will be used for explicit microstructure simulations, complementing future experiments on bicrystals of Ni-Al.

Conclusions

The ab initio quantum mechanical method produced a complete EOS and elasticity model for Ni-Al alloy in the CsCl structure. The EOS was tested against laser-launched flyer experiments, which also allowed an orientation-dependent plastic flow model to be calibrated.

Acknowledgements

We would like to acknowledge the contributions of the TRIDENT team.
This project was funded under the LDRD-DR on Shocks at the Mesoscale, FY 2002-2004. The LDRD program is funded under the auspices of the U.S. Department of Energy under contract W-7405-ENG-36.

References

Miracle93 D.B. Miracle, *The physical and mechanical properties of NiAl*, Acta metall mater **41**, 3 (1993).
Swift97 D.C. Swift, *Ab fere initio equations of state for solids*, Proc 1997 APS Topical Conference on Shock Physics, held Amherst, Massachusetts, 28 Jul - 2 Aug 1997, AIP (1998).
Swift01 D.C. Swift, G.J. Ackland, A. Hauer and G.A. Kyrala, *First principles equations of state for simulations of shock waves in silicon*, Phys Rev B **64**, 214107 (2001).
Johnson92 J.N. Johnson, *Calculation of rate-dependent shock wave hardening*, J App Phys **72**. 2 (1992).
Goto00 D.M Goto, J.F. Bingert, S.R. Chen, G.T. Gray III, and R.K. Garrett Jr, *The mechanical threshold stress constitutive-strength model description of HY-100 steel*, Metall and Mat Trans A **31A**, 8 (2000).

Features of Static and Shock Compression of Some Ceramic Materials

B.A.Nadykto

Russian Federal Nuclear Center - VNIIEF, Sarov (Arzamas-16), Russia

Ceramic materials find a wide application in the action of high pulsed loads. So, it is of interest to study action of high static and shock-wave pressures on those materials. A change in phase state (either crystalline or electronic) under pressure can dramatically affect the material security or failure under shock loading.

We analyze the experimental data on ceramic material compressibility using model [1], [2], according to which the compression pressure is caused by compression of the external electronic shell of solid atoms. The model explicitly includes the quantum nature of the electron motion and allows clear-cut explanation of behavior features for many elements under pressure [2]. Model [1], [2] provides approximate analytic expressions that describe elastic energy and compression pressure well:

$$E(\sigma)=\frac{2E_nN_A}{A}\left(\frac{\sigma^{2/3}}{2}-\sigma^{1/3}\right),\qquad P(\sigma)=\frac{2E_nN_A\rho_n}{3A}\left(\sigma^{5/3}-\sigma^{4/3}\right)\qquad(1)$$

The equation of state parameters are material equilibrium density (at P=0, T=0), ρ_n, and outer electron energy, E_n, of atoms in the equilibrium state; A is atomic mass, N_A is Avogadro number, $\sigma=\rho/\rho_n$ is compression degree. In this paper we dwell on materials, which at high pressure transfer to a state with equilibrium density lower than the initial phase density.

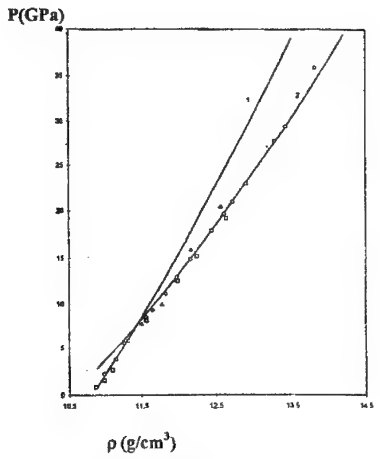

Fig. 1. P(ρ) on normal isotherm in YbO.

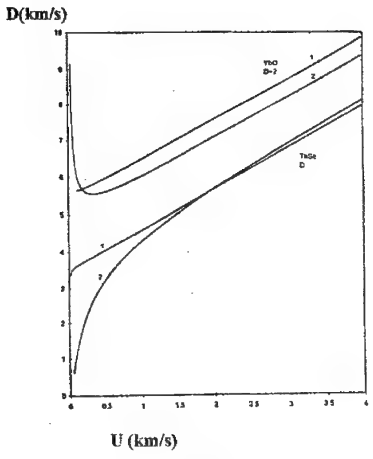

Fig. 2. Hugoniot of two phases of compounds YbO and ThSe

Fig.1 plots P(ρ) on the normal isotherm in ytterbium monoxide, YbO. The curves are results of the computation by (1) for two different phases of YbO. The computed phase parameters are: YbO(I) – ρ_0=10.87 g/cm^3, B_0=130 GPa; YbO(II) – ρ_0=10.63 g/cm^3, B_0=87 GPa. The experimental points are taken from ref. [3]. At pressure higher than 8 GPa YbO transfers to a state of an equilibrium density lower than that in the original phase and lower bulk modulus. Fig.2 presents computed Hugoniots D(u) for these two phases of YbO. For comparison the figure also presents computed Hugoniots for ThSe, in which at high pressure there is a transition to a harder phase of a higher equilibrium density. In the case of YbO, where during the phase transition at the shock front a phase forms, whose equilibrium crystalline density is lower than the initial phase density, the computation yields D(u) in the form of a curve with its convexity directed down, in contrast to porous material Hugoniots with their convexity directed upwards. Among the experimental data [4] it is easy to find D(u) having this shape, for example, B, BeO, SiC. So an unusual pattern of the D-u diagram with decreasing D at low values of u has been experimentally demonstrated most clearly for aluminum nitride, AlN, in ref. [5].

The run of D(u) Hugoniot as a function of specimen initial density in this kind of transition can be followed by the example of BeO (experimental data [6]). Fig.3 clearly shows the change in the shape of the curve D(u) from concave to convex as the specimen initial density increases.

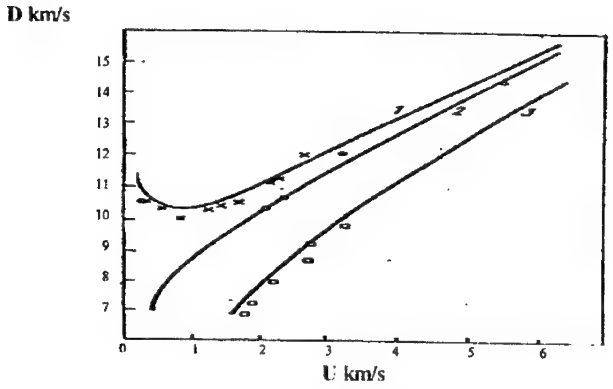

Fig. 3. Hugoniot D(u) for BeO. Points – experiment [3].
Curve 1 - computation for ρ_{00}=2.99 g/cm^3,
Curve 2 - ρ_{00}=2.86 g/cm^3,
Curve 3 - ρ_{00}=2.45 g/cm^3.

A similar compression behavior is demonstrated by a number of metals, for example, Ba, Sr, Ca, Nd. Barium is most characteristic in this regard. For a low equilibrium density phase the Hugoniot of P(ρ) essentially coincides with the normal isotherm. This is seen from the comparison of experimental data [4] for Ba shock loading and static compression data [7].

Several different phases with equilibrium density both lower and higher than the initial phase density occurring following the shock front at different pressures can lead to not uniquely defined Hugoniot P(ρ). One value of density can be correspondent with several values of pressure that correspond to different material phases following the shock front.

When the shock wave travels through material, which transfers to a state of a lower equilibrium density, the material structure changes, which may result in a considerable change in the initial phase defect structure. Micropore closure and decrease in the number of dislocations and point defects can be expected with this transition. All of this can lead to higher strength characteristics of material following the shock front.

References

1. Nadykto B.A. // UFN. 1993. V. 163, No. 9. P. 37-74.
2. Nadykto B.A. // VANT. Ser. Teor. i Prikl. Fizika. 1996. No.3. P. 58-73.
3. Jayaraman A. // Rev Mod. Phys. 1983. Vol. 55., N 1. P. 65-108.
4. Marsh S. P. LASL Shock Hugoniot Data. University of California, Berkley, 1980.
5. Kondo K., Sawaoka A., Sato K., Ando M. // In Physics of Solids under High Pressure, edited by W. J. Nellis. AIP Conf. Proc. N 78 (AIP, New York, 1981). P 325.
6. Marsh S. P.// High Temperatures-High Pressure// 1973. Vol. 5, N 5. P. 503-508.
7. Takemura K. //Phys. Rev. 1994. Vol. B50, N 22. P. 16238-16246.

A Cluster Model for Liquids and Melting

J. Moore[3]
AWE Aldermaston, UK
P.G. Parish
Mathematical Physics Associates Ltd, UK

[3] Now at Imperial College, London, UK

A cluster model of liquids, currently under development, is described. A cluster is defined as a physical grouping of atoms having correlated dynamical behaviour (vibration, translation and rotation). On this model, the liquid consists entirely of such ordered microdomains, which are in dynamic equilibrium while individually having only a transient identity. The partition function and grand partition function are constructed for an ensemble of N atoms consisting of interacting clusters having a spectrum of sizes $j = 1,2,3...$, such that there are n_j clusters of size j. The statistical mechanics then automatically dictates the equilibrium population spectrum n_j in the form:

$$n_j = \begin{cases} x_j, & 0 < x_j < \infty \quad (indistinguishable) \\ \dfrac{x_j}{1-x_j}, & 0 < x_j < 1 \quad (distinguishable) \end{cases} ; \qquad N = \sum_j j n_j ; \tag{1}$$

$$x_j \equiv q_j^{(rot)} q_j^{(trans)} \exp[-j(\tilde{f}_{sol} - \tilde{f}_{liq})/k_B T] ; \tag{2}$$

depending on whether j-sized clusters are mutually indistinguishable (in the more dilute liquid) or distinguishable (near melt). The $q_j^{(\cdot)}$ are rotational and translational partition functions for j-sized clusters. The quantities $\tilde{f}$ in the Boltzmann factor in (2) are "reduced" free energies per atom, defined by $\tilde{f} \equiv \mu - \overline{\psi} - pv \equiv (e - \overline{\psi}) - Ts$ in the usual notation, where all the quantities are defined for single atoms. $\overline{\psi}$ is the average configurational potential energy per atom. The appearance of the terms $(-\overline{\psi})$ and $(-pv)$ predicts the existence of a two-phase melt zone; without them liquidus and solidus would be co-incident.

Solutions (and therefore clusters) exist only for $\tilde{f}_{liq} < \tilde{f}_{sol}$, which is the condition for the liquid state. At the solidus, $\tilde{f}_{liq} = \tilde{f}_{sol}$ and eqs. (1) predict one cluster of size N, the solid state. The spectra (1) represent bell-shaped curves peaking at the most probable cluster size j_{peak}, which reduces with increasing temperature or volume.

The logical generalisation of eqs. (1-2) allows the liquid to consist of a mixture of clusters of different phases with a frequency governed by their respective reduced free energies and partition functions in eq. (2). This enables the theory to embrace substances which either expand or contract on melting. In the latter case the majority of clusters will be in phases denser than the expanded phase which melted to form the liquid. In the liquid, the clusters are unstable and transient. In the melt zone, clusters of the appropriate phase, that of the solidus, are stable and permanent (due to equality of chemical potential μ) and a true two-phase medium exists.

Predictions of cluster population spectra are given, showing variation with temperature and total volume. Equations are given for the internal energy and pressure in the liquid assuming the clusters are of one phase.

© Crown Copyright 2002. This document is of United Kingdom origin and contains proprietary information which is the property of the Secretary of State for Defence. It is furnished in confidence and may not be copied, used or disclosed in whole or in part, without prior written consent of the Director of Commercial 2 Defence Procurement Agency, Ash 2b, Mailpoint 88, MOD, Abbey Wood, Bristol BS34 8JH, England.

Elastic Instabilities in Uniaxial Compression

Damian Swift [1] and Graeme Ackland [2]

[1] *University of Edinburgh, Scotland; presently at Los Alamos National Laboratory, USA*
[2] *Department of Physics and Astronomy, University of Edinburgh, Scotland*

Relations between shear stress and elastic strain were predicted for silicon, beryllium, aluminium and copper by performing ab initio calculations of the electron ground states during uniaxial compression in the 001 direction. The face-centred cubic (fcc) materials (all except beryllium) exhibited significant structure, including extrema and zeroes in the stress-strain relation. One zero can be explained when the fcc structure becomes under body-centred cubic uniaxial compression; further explanation of the structure

would require more detailed analysis of the electron wavefunctions. The stress-strain relation for beryllium exhibited a maximum and a relatively shallow dip, but no zeroes for strains greater than zero. Such structure in the stress-strain relation would be important in the development of ab initio models of plasticity, since the shear stress is the driving force for dislocations and twinning.

The conventional decomposition of stress into an isotropic pressure (a function of mass density and temperature or energy, but not of shear strain) and off-diagonal stress deviators was investigated. According to the ground state calculations, the mean pressure varied significantly with shear strain for silicon and beryllium. The mean pressure appeared to be independent of shear strain in aluminium and copper, except at extreme strains. Any relevant dependence on shear strain should also be taken into account when developing models of material properties for use at macroscopic scales.

Non-Steady Waveforms and High-Rate Multiscale Energy Exchange in the Shock Compressed Matter

T. A. Khantuleva

Saint-Petersburg State University, S.-Petersburg,Russia

High-rate straining of materials is followed by multiscale and multistage energy exchange between the atom-dislocation and the macroscopic degrees of freedom. First fluctuations are exciting and as they are growing and can be referred to the so-called mesoscopic or intermediate scale level, they produce an essential dispersion of macroscopic variables. This assumes being an evidence of the macro-meso-energy transfer. The intensive process can result new internal structure formation at the mesoscopic scale level. Rotational and translational mesoscopic structures had been found out in series of experimental investigations on the shock loading of materials [1]. These mesoscopic structures are responsible for the macroscopic behavior of solids as new carriers of deformation. Experiments shows that the energy exchange between macroscopic and mesoscopic scale levels during the stress relaxation takes place before the dissipation into a heat and proceeds by two stages. If the macro-meso-energy exchange is equilibrium, its role is essential only inside a wave front. But in the non-equilibrium case when the relaxation isn't completed during the rise-time, mechanical properties of material can be considerably changed.

At present it is clear that a relaxation in a shock-compressed solid cannot be described in the framework of the traditional elastic-plastic theory. Unlike the quasi-static straining the most important feature of the high-strain-rate deformation of solids is the emergence of a space-time correlation among the elementary carriers of deformation. The collective effects cause a formation of new structure elements of larger scale than initial ones. Particularly, the origin of mesoscopic structure formation is the collective

effects during non-equilibrium process under high-rate loading conditions. So, the theory capable to describe high-strain-rate processes in solids should introduce correlation of macroscopic variables and the structure formation in dynamically deformed media. It means that it should be non-local in space and include memory effects.

A new self-consistent non-local approach developed by the author on the base of non-equilibrium statistical mechanics in [3-5] presents integral relaxation models for a medium with mesoscopic internal structures. The proposed relaxation model with internal parameters determining mesoscopic characteristics of a medium. in a kernel generalizes the well-known Maxwell model of elastic, plastic and viscous medium.

$$S_l = S_l^*(1+\alpha)k_o(x,t;\varepsilon,\gamma) + \frac{2}{3}\eta(1+\alpha)\int_o^\infty \frac{dx'}{\varepsilon}\exp[\frac{\pi}{\varepsilon^2}(x'-x-\gamma)^2]\frac{\partial}{\partial}\frac{u}{x'}(x',t). \qquad (1)$$

Here S_l , u denote deviator stress and macroscopic velocity in the x-direction, η is a viscosity, $_l^*$ is a yield limit and the coefficient k_o is

$$k_o(x,t;\varepsilon,\gamma) = (1/2)[\mathrm{erf}\left\{\frac{\sqrt{\pi}}{\varepsilon}(Ct-x-\gamma)\right\} + \mathrm{erf}\left\{\frac{\sqrt{\pi}}{\varepsilon}(x+\gamma)\right\}] \Big|_{\varepsilon\to\infty}^{\varepsilon\to 0} \begin{matrix}\longrightarrow 1\\ \longrightarrow 0\end{matrix}.$$

The non-local model (1) includes three internal parameters α , γ , ε :

1) ε is a typical correlation length ;

2) $(1+\alpha)$ is a relative effective viscosity of a medium with mesoscopic internal structure;

3) γ is a polarization parameter making the shear stress tensor asymmetrical.

As $\varepsilon\to\infty$ the model results the Hook's law for the stress deviator in an elastic solid. As $\varepsilon\to 0$ the newtonian liquid is resulted in the limit. In the resonance case ε determines a typical size of the medium internal structure element The other parameter γ is closely connected with a type of kinematic straining (rotation or translation). All the structure characteristics assume varying with time. The transition between the limiting cases is described for the more general conditions than the Maxwell model: for the higher rates, smaller rise-times and with accounting for the mesoscopic structure formation. Some nonlinear integral relationships derived from boundary conditions determine a discrete spectrum of the internal structure scales depending on time like the usual dispersion relationships determine wavelengths depending on a frequency. These additional relationships introduce a feedback into the system, make the model completed and self-consistent.

In scope of this theory the problem of the shock wave propagation in semi-space had been formulated as a nonlinear operator set with the branching solutions for the mesostructure parameters. An approximate analytical solution obtained to the problem has a two-wave form with an elastic precursor and a smoothed relaxing front moving at some delay after it. The plastic front retardation is related to the parameter γ. Herewith, a property of plasticity arises as a structure transition in a threshold way. Plastic flow of structured medium is initially non-steady and entirely determined by an effective multiscale energy exchange and mesostructure formation. Two relationships based on the momentum and energy balances at the distance x from the impact surface with respect to the two characteristics of the meso-macro- energy exchange D, δu had been derived using the obtained solution:

$$\delta u = D\frac{\eta \delta U}{\rho_0 \varepsilon}(t)\ \exp\left\{-\frac{\pi}{\varepsilon^2}(a_1 t - x - \gamma)^2\right\}, \qquad (2)$$

$$\delta E = \delta u \delta U - c_m D. \qquad (3)$$

The velocity dispersion D characterizes the velocity fluctuations at the mesoscopic scale level and the wave amplitude loss δu on account of the macroscopic kinetic energy transfer to the mesoscopic scale level is related to the non-equilibrium characteristics of the macro-meso-energy exchange δE. Both values D and δu can be measured experimentally [1]. Here δU denotes the plastic front amplitude and c_m is the specific mesolevel energy capacity. In general it is time-dependant function and characterizes dynamic properties of a given material. As $c_m \to 0$ the macro-meso-energy exchange is already completed, an equilibrium between the two levels is reached. In the opposite case $c_m \to \infty$ the macro-meso-energy exchange is frozen. It had been proved that in both limits energy exchange characteristics D, $\delta u = 0$. In the intermediate case two situations are possible: $\delta E > 0$ and $\delta E < 0$. The positive difference or the excess of mesoenergy goes to the mesostructure formation. The deficit energy can be taken only from the stored elastic energy inside the wave front due to the decreasing of the local potential. This very important conclusion can be confirmed by the physical investigations [ ] and experimental data [ ]. At time when δE changes the sign fluctuations become so large that a new meso-2 scale level is excited. It means that the value $\delta u \delta U$ have a sense of the velocity dispersion at the meso-2 scale level. Then it is possible to say that beginning from the instance when $\delta u \delta U \approx c_m D_2$ and until the mesoscale relaxation is finished the mechanical properties of material can be essentially different from that during quasi-static loading. In case when during the wave front propagation the relaxation is not completed the changed properties can conserve after loading.

An algorithm is obtained to calculate non-steady waveforms using the measured profiles of the velocity dispersion. The influence of the mesostructure parameters on the wave front shape is analyzed numerically. Also, the reverse problem of mesostructure determination via a measured wave front profile is under investigation. It has been calculated that the wave amplitude loss only due to the energy transfer to the fluctuations for copper in the range of impact velocities (100-300m/s} is about 10% in case where the velocity dispersion decreased up to zero and about 40% in case where it didn't reach zero. So, more 60% of macroscopic energy loss is conditioned by the structure relaxation.

The obtained solution describes three stages of the process.

1) During the first stage the velocity fluctuations begin growing. Their physical origin is unharmonic vibrations of the atom lattice during non-steady wave propagation. Until the structure relaxation initiated, the macro-meso-energy exchange is reversible and the energy from mesolevel can entirely come back without the mass velocity loss.

2) The structure relaxation begins at the second stage of a process. It determines the structure formation at the mesolevel that can be referred to the irreversible process. The scales and types of structures are defined by the spectrum resulted from the dispersion relationships. A step-wise appearance of a new scale or type of the structure considers being a structure transition. It has been shown that the typical size of the formed rotations and shear bands varies within the range $0.1 \div 10$ μm that corresponds to the experimental results. Besides it has been calculated that during local deceleration (velocity dispersion's rate is negative) there appears a new scale 4000 μm corresponding to the meso-2 scale level. A direct proportion between a size of rotations and a value of the local acceleration (velocity dispersion's rate is positive) noted experimentally has been derived in scope of the proposed relaxation model. At this stage due to the rotations the energy conserves at the mesolevel after the structure formation is already finished. Experimental results show that scales and types of the formed structures essentially influence on the strength and fracture properties of materials.

3) The third stage is quasi-static until the relaxation isn't completed. For the later stages with the relaxation being neglected Hugonio theory of shock waves propagation is adequate.

So, the developed non-local self-consistent theory allows calculating of non-steady waveforms propagation accounting for the non-equilibrium macro-meso-energy exchange and mesostructure formation. It must be noted that such mechanical property of materials as the spall strength can be correctly calculated on the proposed theoretical base.

[1] Mescheryakov Yu. I., Divakov. A. K. DYMAT J., 4 (1994), 271-287.
[2] Mescheryakov Yu. I., Makhutov N. I., Atroshenko S. A. J. Mech. Phys. Solids, (1994), 1435-1456.
[3] Khantuleva T. A., Mescheryakov Yu. I. Intern. J. Solids and Structures, 36 (1999), 3105-3129.
[4] Khantuleva T. A. CP505 Shock Compression of Condensed Matter-2000 Amer. Inst. Phys. 1-56396-923-8/00, 371-374.
[5] Khantuleva T. A. J. Phys. 4 France 10(2000) EDP Sci.., Les Ulis, 485-490.

Quantitative Analysis of Damage Accumulation in Spall

A.K. Zurek, W.R. Thissell, C.P. Trujillo, D.L. Tonks, D.A. Macdougall

Los Alamos National Laboratory, Los Alamos, New Mexico, 87544, USA

For dynamically loaded engineering systems to be successful, the materials they are made of must deform in precisely the right way. In the absence of capabilities to test entire engineering systems and/or materials in all possible configurations scientists and engineers are using sophisticated computer models and laboratory experiments to predict behavior of such systems and materials. A major challenge is to make sure the computer models take into account all of the relevant factors.

We performed a dynamic fracture test - spall experiments to understand exactly how materials fracture at very high impact velocities and we are using the results to improve the models for a variety of materials such as tantalum, copper, U-Nb 6%, uranium and others.

Present fracture simulation models use the initial porosity of the fracturing material and how it changes during the fracture as one of the few input parameters. The model is optimized to do the best job of matching the measured results for one sets of experiments - the calibration tests and than is used to predict behavior at other experimental conditions. The model validation and verification continues until a reasonable convergence is achieved between the model and experimental results.

In this work we will present a newly developed method for damage quantification and the statistical analysis of data from incipiently spall tests that is implemented into micro-mechanical, as well continuum ductile fracture models.

Effect of Instability in Metals under Impulse Loading

G.V.Stepanov, V.I.Zubov

Institute for Problems of Strength, Kiev, Ukraine

Enough experimental evidence is at hand for strain-rate effects on the strength of structural metals under such types of dynamic loading as impact, explosion, and others. This effect is quite pronounced in the region of high strain rates exceeding 10^4 s^{-1}. As follows from experimental results, at very high strain rate (above 10^5 s^{-1}), the strength in the region of small plastic strains exceeds its value under static loading tenfold and is close to a theoretical limit for metals. The effects of strain hardening, strain rate, pressure and temperature are usually accounted for in computer simulation deformation/fracture of structure elements using the equations of state for continuum in the general form, that do not allow for an explicit effect of a strain rate and pressure on strain hardening:

$$F_g(p, v, T) = 0; \quad F_i(\sigma_i, \varepsilon_i, \varepsilon_i', T) = 0. \qquad (1)$$

The first equation in (1) reveals a relation between mean stress (pressure p) and the specific volume v for a compact material (without porosity) at different temperatures T. For porous materials, this equation is valid only for the matrix one. The second equation in (1) is a simplified presentation of the rheological behavior of a metal, i.e. relation between stress $\sigma_i(t)$ and strain $\varepsilon_i(t)$ intensity histories with the account of a change in temperature accompanying adiabatic (for dynamic loading) plastic flow:

$$\sigma_i(t) = \varepsilon_i(t) \quad \text{for } T(t) = T(\varepsilon_i(t)). \qquad (2)$$

Under dynamic loading the system of equations (1) is complemented with the equation of heat generation and an increase in temperature $T(t)$ upon adiabatic plastic flow (for a material with the specific hea c_v and coefficient of heat generation λ):

$$\dot{T}(t) = \lambda \cdot \sigma_i(t) \cdot \varepsilon_i'(t_i) / c_v \qquad (3)$$

The instant strength σ_i is the result of the instant strain rate ε_i' as well as a previous history of loading $\sigma_i(t)$ or $\varepsilon_i(t)$. The latter determines increase in temperature with time.

The equations in (1) and (2) are valid for limited ranges of loading parameters corresponding to a small influence of damage/fracture in a metal. To account for the above processes equations (1) should be coupled with the equations of damage/fracture kinetics as well as with the criteria of transitions in the behavior of a material.

The equations of state usually used for computer simulations represent the simplified forms of the relation between stress-strain intensities, they take into account an influence of the instant strain rate intensity ε_i' but do not allow for an influence of loading history. The examples of such equations can be found in Johnson-Cook's, Armstrong's papers, in publications 0f the author of this paper, and others:

$$\begin{aligned} &\sigma_i = f_1(\varepsilon_i) \cdot f_2(\varepsilon_i') \cdot f_3(T), \\ &\sigma_i = \sigma_u(\varepsilon_i, T) + K(\varepsilon_i, T) \cdot \ln(\varepsilon_i') + \mu \cdot \varepsilon_i' \end{aligned}, \qquad (4)$$

where $\sigma_{st}(T, \varepsilon_i)$ and is the strength under static loading, μ is the linear viscosity factor, $K(T, \varepsilon_i)$ is the factor accounting for the nonlinear strain rate effect.

In some cases the effect of loading history on the strength under dynamic loading is quite pronounced. Intensive strain hardening on the surface of a metal plate subjected to impulse pressure due to high explosive detonation caused by an accelerated grow in dislocation density at a high strain rate and pressure is a well-known process widely used in technology.

The opposite effect of a high strain rate on the strength follows from impact indentation/penetration experiments. The development of shear bands at large strains in a metal under impulse loading can explain the mechanism of this effect. Such conclusion follows from the analysis of studies on shear strain localization [1], impact indentation/penetration, super-high penetration, and changes in a microstructure caused by impulse loading. The effects of a rapid decrease in stress intensity in metals are similar to the effect of a decrease in strength in brittle materials due to crack nucleation and growth. The behavior of a metal or a brittle material after the development of the system of shear bands/cracks is controlled by volume compression with stress intensity determined by the effect of viscosity or friction. The relation for stress-strain intensities for the behavior of a metal associated with a decrease in the nonviscous component of strength can be written as

$$\sigma_i = A(\varepsilon_i(t)) \cdot \left[\sigma_{st}(\varepsilon_i, T) + K(\varepsilon_i, T) \cdot \ln(\varepsilon_i')\right] + \mu \cdot \varepsilon_i'. \qquad (5)$$

The factor $A(\varepsilon_i(t))$ depends on loading history and tends to zero at large strain developed in a short period of time even at relatively low averaged temperatures, which is caused by the effect of hot layers of localized flow. Because of heat conduction this effect decreases with time.

The use of such equations of state in computer simulation is limited for lack of experimental data on the criteria of the above transformations in a metal, including the effect of further stiffening of the materials with time.

Experimental evidence of a temporary decrease in metal strength after intense loading is very scarce. This effect was demonstrated in G.Kanel's experimental studies on shock wave propagation in a

metal subjected to shock wave preloading, in Yu. Mescheryakov's publications devoted to specific changes in microstructure and in experiments on impact indentation [2], carried out by authors of this paper.

The latter experiments on indentation show the difference in dynamic hardness of mild steel plate just after its loading by plane elastoplastic wave and some time (3..10 μs) after loading. These experiments show clearly that hardness, decreased just after shock wave loading due to an unstable state in metal, increases with time.

Development of high temperature local bands in a shock wave loaded materials, leads to rapid stress relaxation (decrease of stress intensity). Further heat conduction from hot layers, leading to a uniform temperature distribution after some time (with relatively low average temperate and higher stress intensity), can explain strength regain with time.

Instability effects in metals induced by impulse loading can be taken into account in computer simulation of large-strains processes using modified equations of state (5).

For an example, the multiplier $A(\varepsilon_i(t))$, accounting for the instability effects in a metal, was taken in the form:

$$A(\varepsilon_i(t)) = 1/[1 + k \cdot \varepsilon_i^{nc} \cdot (\varepsilon')_i^{nt}] \qquad (6)$$

According to equation (6) in the range of small plastic strains and low strain rates the effect of instability is negligible (if $k\,\varepsilon_i^{nc}\,(\varepsilon_i')^{nt} \ll 1$). In the range of large plastic strains and high strain rates the multiplier is close to zero, that corresponds to a purely viscous component of strength.

Computer simulation of cylindrical cavity expansion at a constant velocity allowing for instability effects in a metal with equations (5) and (6), resulted in a decreased pressure for cavity expansion with an increase in an expansion velocity, is consistent with experimental results on impact indentation with a rigid cone indenter.

Stress components near the cavity surface in steel at its expansion are shown on Figure. 1. A pressure of volume compression with its thermal component prevail in the total radial compression stress on a cavity surface, due to decreased influence of a strength.

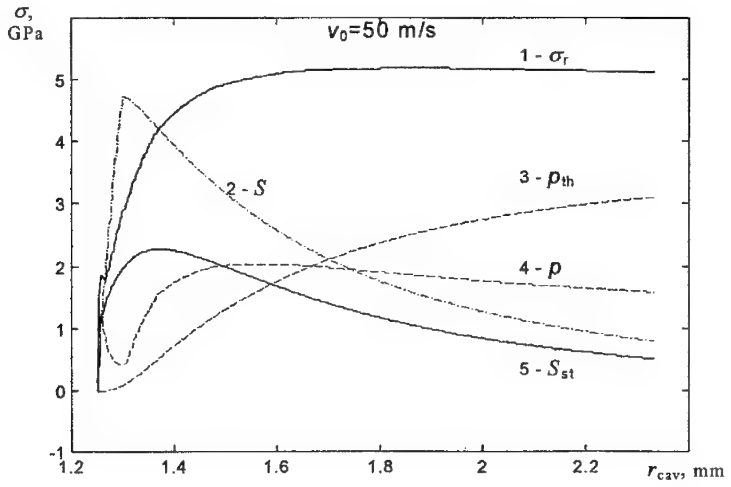

Fig. 1. Stresses in a metal near the cavity surface at its expansion at a constant velocity of 50 m/s: (1) is the total radial compression stress; (2) and (5) are the stress intensity and the static component of stress intensity; (4) and (3) are the pressure of isothermal volume compression and the thermal component of pressure.

1. G.Stepanov, V.Fedorchuk, Localized shear in metals under impact loading. *J. Phys. IV. (France)*, v.10, p.707-712 (2000).
2. G.Stepanov, V.Zubov, Dynamic hardness of high-strength steel and titanium alloy. *J. Phys. IV. (France)*, v.10, p.647-651 (2000).

4-th Level of a Numerical Model of Shock-Wave Synthesis of Diamond: Kinetics of Phase Transformations in Local Volume of a Calculated Cell

V.D. Andreyev

Institute for Superhard Materials, Kiev, Ukraine

The full scale computing experiment is the necessary element at development of a process engineering of shock-wave synthesis of diamond in a system Me-C with use of massive ampoules for preservation of yields of synthesis and, accordingly, large charges HE (more than 100 ÷1000 kg). It allows beforehand to complete a construction of an explosive device and to determine optimum parameters of a loading for deriving a maximum amount of a final yield etc. without inputs of realization of full-scale experiments, which practically do not give in to simulation on the samples, reduced in a scale.

For these purposes the 3-levels numerical model was developed (is reported by the author on the 1-st conference "New Models and Hydrocodes for Shock Wave Processes in Condensed Matter", St. Petersburg, 1995 [1]), which consist of:

— a numerical model, with the help of with which the fields of velocities, pressure and temperatures in an explosive at an axisymmetrical detonation of a charge on a surface of the flat or cylindrical liner were calculated (are the 1-st level of a total model);

— a numerical model, with the help of with which were calculated a character of a modification of the form of the liner in flying and at a collision with an ampoule of preservation, and also velocity and pressure on a surface of a collision (are the 2-nd level of a total model);

— a numerical model of an shock loading of a cylindrical ampoule of preservation and reactionary mixture, contained in it representing a bicomponent medium a matrix - inclusion (metal-graphite), simulated with the help of of modified method of particles (in the ratio percentage a carrying phase (the metal) is simulated by large particles, and inclusion — by particles). In this medium during a loading and unloadings both components undergo phase transformations: a melting - hardening of metal, and also direct and inverse solid-phase passages graphite→diamond. The fields of velocities, pressure and temperatures, and also the areas of phase passages in volume of a reactionary mixture with the help of of this model were calculated (are the 3-rd level of a total model).

The total model of the process of synthesis is received at a sewing together of results of calculations of a model of the previous level with the entry conditions of a model of the following level. Such sewing enables to receive a total technological picture of the process of synthesis.

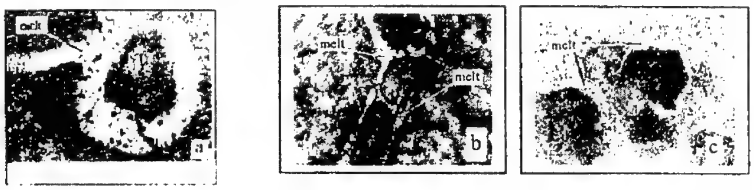

Fig. 1. Zones of a melting on the boundary line of inclusion-matrix after of shock loading (×540).

The necessity of development of a model of the 4-th level is stipulated by results of experimental researches of features of phase transformations of a matrix and inclusions in local volumes of a reactionary mixture, commensurable with sizes of inclusions. For example, in areas, where the parameters of a loading do not reach conditions of a melting of a matrix, the local zones of a melting of a various breadth round inclusions will be derivated (fig. 1, a-c) [2]. The located along traffic route of a shock wave plate-like inclusions of graphite not turning into diamond and same inclusions located in the same place, but is perpendicular to traffic route of a shock wave — completely turning in diamond in areas, where the parameters of a loading certainly meet to transformation of graphite → diamond and preservation the latter after unloadings, can be observed (fig. 2, a) [3].. Besides the relation of sizes of a saved after unloading of diamond inclusions and inclusions completely undergoing an inverse transformation of diamond in graphite illogical, on the first sight, from positions of the mechanism of graphitization is observed: the more small-sized grains (~10 μm) remain diamond, and the grains by a size ~50 μm completely are anneal back in graphite. The inclusions of intermediate sizes (~ 20 ÷ 40 μm) represent a yield a not full inverse graphitization as diamond-graphite formations with exotic, before a unknown structure — it is formations with an outside diamond envelope and graphite core (fig. 2, b-c) [4, 5].

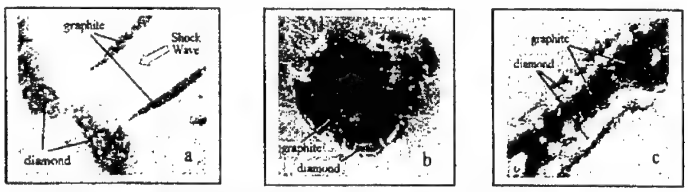

Fig. 2. Features of formation of diamond at a shock loading in a system metal - graphite: ×540 (*a*) , ×950 (*b*) и ×3000 (*c*).

Obviously, that the development of a numerical model of synthesis of the 4-th level pursues except for scientific interest in explanation of the enumerated facts also solution immediately of applied problems connected to optimization of the technological process.

The dynamic problem of formation and transition of the boundary line of two phases (Stefan's problem) : liquid and solid phases in a matrix and graphite-diamond phases in inclusion at a relaxation of an inhomogeneous field of distribution of temperatures in a heterogeneous medium (matrix-inclusion), described by presence of local zones of higher temperatures concerning to diamond (graphite) inclusions, and lower — to a metal matrix , is puted in a basis of this model (fig. 3). Such distribution of temperatures at a shock loading is stipulated by distinction of wave and thermodynamic characteristics of a matrix and inclusions.

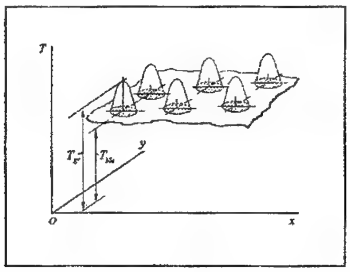

Fig. 3. Hypersurface of distribution of temperatures in a medium of matrix-inclusion after of shock loading.

Apporting local volume in a hand-picked calculated cell from a model of the 3-rd level it is supposed, that in this volume has a place a uniform distribution of inclusions of a specific size. In this case chosen volume one can to devide on identical cells, in which center the single inclusion places. Thus, being set a size of inclusion and knowing initial percentage of inclusions of graphite in a matrix, one it is possible to determine a size of a researched cell in a model of the 4-th level. For simplification of the problem the cell is adopted of the spherical form with volume equivalent to volume of a cube. At such statement the research is reduced to the solution of the one-dimensional spherical problem, in which the boundary conditions are determined by a heat rejection from inclusion in limited volume. The entry conditions are set from the solution of the 3-rd level.

The further construction of a model is reduced to breakdown of inclusion and matrix, enclosing it, on the spherical finite elements, in each of which the problem of distribution of temperature in time (heat conduction equation), melting of a matrix and graphitization of diamond (kinetics Arhenius's equation) is decided. The functional dependences of a heat capacity from temperature for metal, graphite and diamond were introduced into a model. That during magnification of concentration of a new phase (i.e. accumulation of a graphite phase in the element of diamond inclusion, or liquid phase in the element of a matrix) average values of a denseness, volume, heat capacity and the heat conductivity vary, in a course of the solution of the task it was taken into account (were used a mix model of two phases and model of interpenetrative lattices). At the sizing of temperature of the diamond elements during their graphitization was taken into account an additional increment of temperatures formed for a computation of evolve of the latent heat ΔQ of transformation diamond → graphite.

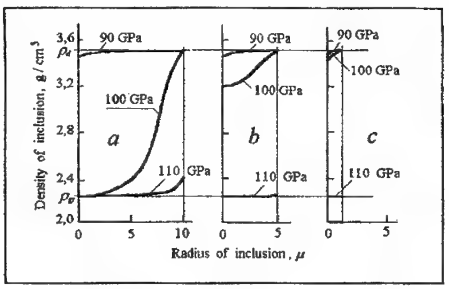

Fig. 4. A graphitization of inclusions by a diameter 20 μm (*a*), 10 μm (*b*) and 2 μm (*c*) after unloadings at various amplitudes of a shock loading.

The results of calculations have shown, that the developed model is adequate to physical analog. Practically all features of phase transformations in local volumes of a reactionary medium, obtained at metallographic researches, have found the physical explanation (except for a connection of transformation to disposition of plate-like inclusions of graphite concerning to traffic route of a shock wave). Thus the quantitative correlations between parameters of a loading and picture of formation of diamond-graphite inclusions (fig. 4, *a-c*) and zones of a melting of a matrix round inclusions were established. It was appeared, that the parameters of a loading determine a relation of permanent temperatures in a matrix and inclusion, and kinetics of processes a graphitization and the meltings are controlled by a velocity of a heat rejection. In this case at specific depending on parameters of loading initial relations of temperature of inclusion and matrix the given velocity of a heat removal allows to save small-sized inclusions of diamond, while larger partially or completely graphitize. Thus the graphitization is spreaded from a center of inclusion, where temperature is higher, to a periphery, where the diamond phase is cooled more heavily for a computation of a heat removing in contacting with inclusion a metal matrix. It explains formation of diamond-graphite inclusions with a diamond skin.

Thus, the model of the 4-th level has allowed to ascertain, that the preservation of diamond limits from above by some maximum parameters of a loading, which exceeding reduces in a graphitization of grains of any sizes. At the same time formation of diamond is limited from below to parameters of a loading, below which does not happen transformations of graphite in diamond. The same conditions determine the greatest possible sizes of grains of synthesized diamond.

References

1. *Andreyev V.D., Sandrakov G.V.* //Abstracts of the 1-st Conference "New Models and Hydrocodes for Shock Wave Processes in Condensed Matter", St. Petersburg, 1995.
2. *Andreyev V.D., Voloshin M.N., Klimenko T.P.*// Superhard Materials, 1979, № 3, p. 5 - 9.
3. *Andreyev V.D., Lukash V.A., Voloshin M.N.* // Superhard Materials, 1980, № 1, p. 13 - 17.
4. *Andreyev V.D., Voloshin M.N., Malik V.R.* // Superhard Materials, 1983, № 6, p. 5 - 9.
5. *Andreyev V.D., Voloshin M.N., Malik V.R.* // Superhard Materials, 1985, № 3, p. 9 - 14.

Model of Electrical Response of Piezoceramics to Shock-Wave Loading

V.D. Sadunov, M.V Antipov, A.L. Mikhaylov, E.Z. Novitsky, T.V. Trishchenko

Russian Federal Nuclear Center - VNIIEF, Sarov (Arzamas-16), Russia

In the paper the authors describe a numerical model of electrical response of piezoceramics to shock-wave loading. The model was developed with account for factors important for description of operation of the shock-wave converter of energy (SWCE). Properties of the model and results of its practical application for development of SWCE for various purposes are considered.

The following is shown within the frames of the considered model:

1. The same linear differential equation of the second order for current in RLC-loading of the converter can be used to describe operation of one-element and multielement, axial and cross SWCE.

2. Calculated relations obtained with the help of this equation are in good agreement with experiment, and they confirm practical suitability of the developed model for description of SWCE operation.

3. The cross and axial methods for loading of piezoelectric ceramics are not equivalent. Under axial loading electric fields always reach their maximum values. Under cross loading an electric field is controlled by sizes of a working body of SWCE and parameters of RLC-loading. The maximum intensity of electric field in cross SWCE is reached only in the electrometric regime of its operation.

4. Description of the mechanism of SW energy transformation into electrical energy is presented. The maximum efficiency of energy transformation is reached in design of cross SWCE. Limitation of efficiency of operation of axial SWCE is caused by losses of charge of depolarization in piezoceramics volume due to its insufficient electrical strength.

As an example of application of the numerical model, the authors performed analysis of operation of one-element axial and cross converter as a gauge of shock wave pressure. It is shown that only cross

converter can be used as a pressure gauge similar to the quartz gauge in characteristics. The operational range of such gauge is limited: from below – by manifestation of inertia of piezoceramics depolarization process, from above – by value of pressure of its total depolarization.

The paper presents calculated and experimental characteristics for a series of piezoceramic compositions used for development of shock-wave converters of energy in range of pressures of shock loading from 2 up to 20 GPa.

SESSION "Numerical Models for Inert Materials"

Chairmen:
A. Rajendran - US Army Research Office, NC, USA
D. Swift - University of Edinburgh, Edinburgh, Scotland

Current Status of Ceramic Damage Modeling under Shock and Penetration Loading

A.M. Rajendran

U.S. Army Research Office, NC, USA

Due to their high compressive strength, ceramic materials have been frequently employed in armor systems for vehicle and soldier protection. Ceramics are also candidate materials for ceramic engine components (turbine blades, etc.) and aircraft engine containment systems due to their high temperature properties. This paper presents the current status of modeling the brittle fracture of ceramics based on the recent high fidelity computational modeling of projectile penetration processes in ceramic plates.

Rajendran and Cook [1] presented a comprehensive review of modeling of impact damage in ceramics. Lawn and Wilshaw [2] reviewed the indentation fracture in detail. Hockey [3] reported dislocation networks in alumina at local indentation sites. Shockey et al [4] and Curran et al [5] address many of the deformation mechanisms in confined ceramics under ballistic impact loading conditions. These studies clearly established the presence of dislocations and twinning in the brittle ceramics due to high pressures and high strain rate loading conditions. Espinosa et al [6] reported evidence of inelastic deformation in compression due to microcracking at triple junctions of the grain boundaries in recovered alumina samples at velocities below the Hugoniot Elastic Limit (HEL). The microplasticity in a brittle solid is often attributed to the dislocation motions in the vicinity of microflaw tip regions. In brittle solids, large-scale grain distortions are usually absent. These microscopic investigations indicated that the various forms of inelastic strain in the brittle ceramics under shock and high strain rate of loading were caused by dislocations and twins, microcracking, and pore collapse.

In the phenomenological modeling, the material is assumed to behave as an elastic-plastic solid. This approach ignores the details of crack growth and concentrates on describing the effects of localized fracture on stress wave propagation. The stiffness of the ceramic is not degraded due to damage, but the strength is degraded due to plastic deformation induced damage. The concepts and equations are the same as those derived for metal plasticity. Johnson and Holmquist [7] modeled the strength of the ceramic as a function of pressure and strain rate through a two-surface approach. Basically, there are two surfaces: one corresponds to $D = 0$, and the other to $D = 1$. Steinberg [8] proposed a ceramic damage model that is very similar to his metal fracture model.

In a fracture mechanics based microphysical theory/model approach, the basic is to describe the apparent inelastic behavior while keeping track of the microstructural evolutions under a given set of loading conditions. For ceramics, the evolution laws for microcracking must incorporate the fracture mechanics theories that describe the conditions for crack growth. A statistical description of number of cracks per unit volume as a function of position, crack size, and orientation, is an example of a microphysical approach. The Hooke's law based elasticity equations are combined with an effective moduli description that relates the microstructure to the macroscopic material properties. The models by Rajendran and Grove [9,10] and Espinosa [11] follow this approach. During the past decade, several new ceramic damage models (Simha [12], Partom [13], Sadyrin, Ruzanov, and Podgornova [14], Riou, Cottenot, and Boussauge [15], and Malaise, Tranchet, and Collombet [16]) have been reported for hydrocode applications.

In summary, during the 1970's, the computational analysis of a projectile (metallic spheres and cylinders) impacting a brittle ceramic plate was mainly performed to gain a fundamental understanding of complex crack patterns developed due to the impact. A combined indentation-based experimental and

computational analysis approach was employed in the evaluation of hardness and compressive strength of ceramics. The response of the ceramic was assumed to be elastic in the indentation analysis. During the past decade, researchers realized an urgent need for a fully three-dimensional constitutive description of ceramic materials to perform realistic hydrocode analyses suitable for impact-resistance applications. Constitutive model formulations have mainly focused on incorporating the effects of pressure, defects (pores and microcracks), and strain rate on strength and stiffness of the ceramic. A few models have included the effects of flaw orientation and/or microplasticity (dislocations, twins, etc.) on the degradation of strength and stiffness. Those model parameters that cannot be directly measured from experiments are estimated (calibrated) based on their ability to reproduce or match the measured wave profiles. Most models use the Mohr-Coulomb law to describe the compressive/shear loading response of the comminuted ceramic. Generally, one or two parameters are needed for this purpose. Currently, there is no physics-based model to accurately describe the comminuted ceramic response.

Current models are incapable of describing the effects of grain size and grain boundary properties on the impact and shock resistance of ceramics. Recently, Zavattieri and Espinosa [17] presented a grain level analysis of ceramic microstructures subjected to impact loading. Through a two dimensional stochastic finite element analysis, they explicitly modeled the details of grain morphology and its effects on crack nucleation and propagation at grain boundaries. Though we have made significant progress in modeling the ceramic damage under shock and penetration loading conditions, there are still issues that need attention and additional research.

References

[1]A.M. Rajendran and W.H. Cook, "A Comprehensive Review of Modeling of Impact Damage in Ceramics," Technical Report AFATL-TR-88-143, Air Force Armament Laboratory, Eglin Air Force Base, Florida 32542-5434 (1988).

[2]B.R. Lawn and T.R. Wilshaw, "Review: Indentation Fracture: Principles and Applications," *Journal of Materials Science*, **10** 1049-1081 (1975).

[3]B. Hockey, "Plastic Deformation of Aluminum Oxide by Indentation and Abrasion," *Journal of the American Ceramic Society*, 54 [5] 223-31 (1971).

[4]D.A. Shockey, A.H. Marchand, S.R. Skaggs, G.E. Cort, M.W. Burkett, and R. Parker, "Failure Phenomenology of Confined Ceramics Targets and Impacting Rods," *Int. J. Impact Engng.*, 9, 263-275 (1990).

[5]D.R. Curran, L. Seaman, T. Cooper, and D.A. Shockey, "Micromechanical Model for Comminution and Granular Flow of Brittle Material Under High Strain Rate Application to Penetration of Ceramic Targets," *Int. J. Imp Eng.* **13**, 53-83 (1993).

[6]H.D. Espinosa, G. Raiser, R.J. Clifton, and M. Ortiz, "Experimental Observations and Numerical Modeling of Inelasticity in Dynamically Loaded Ceramics," *J. of Hard Materials* **3**, 285-313 (1992).

[7]G. Johnson and T.J. Holmquist, "An Improved Computational Constitutive Model for Brittle Materials," *in High-Pressure Science and Technology - 1993*, Part 2, AIP Press, 981-984 (1994).

[8]D.J. Steinberg, "Computer Studies of the Dynamic Strength of Ceramics," *Shock Compression of Condensed Matter*", Elsevier Science, 447-450 (1992).

[9]A.M. Rajendran, "Modeling the Impact Behavior of AD85 Ceramic Under Multiaxial Loading," *Int. J. Impact Engng.*, **15** (6) 749-768 (1994).

[10]A.M. Rajendran and D.J. Grove, "Modeling the Shock Response of Silicon Carbide, Boron Carbide, and Titanium Diboride," *Int. J. Impact Engng.*, **18** (6) 611-631 (1996).

[11]H.D. Espinosa, P.D. Zavattieri, and S.K. Dwivedi, "A Finite Deformation Continuum/Discrete Model for the Description of Fragmentation and Damage in Brittle Materials," *J. Mech. and Phys Solids*, 46 [10] 1909-1942 (1998).

[12]M. Simha, "High Rate Loading of a High Purity Ceramic – One Dimensional Stress Experiments and Constitutive Modeling," Ph.D Thesis, University of Texas at Austin, TX, 1998.

[13]Y.Partom, "Calibrating a Strength Model for AD995 Alumina from Plate Impact VISAR Profiles," *J. de Physique IV* c8-495 (1994).

[14]. N.Sadyrin, A. Ruzanov, and T. Podgornova, "Modeling Impact Loading and Failure of Brittle Solids; Constitutive Damage Model for AD995," Research Institute of Mechanics, State University of Nizhny Novgorod, Russia (1998).

[15]J.Riou, C.E. Cottenot, and M. Boussauge, "Steel Rod Impact on Silicon Carbide Beams: Experiments and Anisotropic Model of Damage," in "Structures under Shock and Impact," eds., N. Jones, C.A. Brebbia, and A.J. Watson, Computational Mechanics Publications, 533-541 (1996).

[16] F. Malaise, J-Y. Tranchet, and F. Collombet, "Effects of Dynamic Confinement on the Penetration Resistance of Ceramics Against Long Rods," *Shock Compression of Condensed Matter-1999*, Elsevier Science Publishers B.V. 1121-1124 (2000).

[17] P.D.Zavattieri and H.D. Espinosa, "Grain Level Analysis of Ceramic Microstructures Subjected to Impact Loading," a Chapter in PAC RIM IV proceedings, 2002.

Void Coalescence Models for Ductile Damage

D.L. Tonks*, A.K. Zurek**, W.R. Thissell**

Constitutive Modeling, D413; ** Structure-Property Relations, G755;
Los Alamos National Laboratory, Los Alamos, USA

A model for void coalescence for ductile damage in metals is presented. The basic mechanism is void linking through an instability in the intervoid ligament. The formation probability of void clusters is calculated, as a function of cluster size, imposed stress, and strain. Numerical approximations are validated in a 1 D hydrocode.

High strain rate ductile fracture is caused by the nucleation, growth, and link up of voids. We describe a model for microscale void cluster growth via the coalescence of initially existing voids, based on earlier work. [Tonks et al, 94,95,96]

The general phenomenology at high strain rates is that a random initial void configuration produces a spatially disordered damage morphology, where widely separated voids have little time to communicate with each other via stress waves. This inhibits the potential for large damage clusters to grow faster than the smaller ones. The sample breaks when widespread damage finally accumulates to the point where a damage surface forms. This fracture point is modeled with random percolation theory [Stauffer, 1985]. At lower strain rates, a sample breaks with less damage at smaller strains, when the biggest crack rapidly outstrips its neighbors. This occurs because there is time for the size enhancement of stress and strain fields to occur at its periphery. [Tonks 94, 95]. The fracture is modeled by refining a probabilistic theory for cluster growth [Domb, 1990].

Void linking occurs through a local plastic instability that thins out the intervoid ligament, unloading surrounding material. The stress conditions triggering the instability, which depend on cluster geometry and the applied stresses, were given by Thomason [1990] for arrays of voids for the quasistatic case. We have generalized this work to treat single voids linking to a growing disk of coalesced voids with range enhanced by the concentrated stress and strain fields at the disk periphery. We have included shear and tensile stresses and linking strain effects.

We assume that the most probable morphology of a damage clusters is a disk of linked voids that have their flat surfaces normal to the direction of greatest principal stress. This orientation, appropriate for plate impact spallation, intercepts the greatest applied stress and causes the greatest cluster size enhancement of the applied stress at the cluster periphery. The disks are assumed to be one void thick. The disks will be grown from the basic voids and will not interact. This should be accurate for the early and middle regions of damage growth. A disk is "grown" in a stepwise fashion by adding a ring of linked voids to a previously existing disk. $P(\beta)$, the probability for formation of a void disk of radius, r, from rings of voids, is obtained by multiplying together the probabilities of ring formation, for which an approximate formula of Domb [1990] is used. An approximation for the probability product is then derived by an integral approximation for its logarithm. This approximation allows one to write a closed form formula for the disk size probability function for a given external loading.

Another approach is to track the largest disk in a system. This method allows history effects to be more accurately included. Both approaches will be described and the resulting behavior illustrated under typical conditions occurring in gas gun plate impact experiments.

References

Tonks D. L., 1994, "Percolation and Void Link Up Effects in Ductile Fracture", J. Physique IV, **C8**, C8-665.

Tonks D. L., Zurek, A. K., and Thissell, W. R., 1995, "Ductile Damage Modeling Based on Void Coalescence and Percolation Theories", in Metall. and Materials Applications of Shock-Wave High-Strain-Rate Phenomena, ed. L. E. Murr et al, Elsevier, New York, NY, 171 – 178.

Tonks D. L., 1996, "Disorder, Percolation, and Wave Propagation Effects in Ductile Fracture", in High Pressure Shock Compression of Solids II, ed Davidson et al, Springer, New York.

Stauffer D., 1985, Introduction to Percolation Theory ,Taylor and Francis, London.

Domb C., 1990, "On Hammersly's Method for One-Dimensional Covering Problems", in Disorder in Physical Systems, ed G. R. Grimmett and D. A. Welsh, Clarendon, Oxford.

Thomason P. F., 1990, Ductile Fracture of Metals, Pergamon, New York.

Numerical Modeling of Elastic-Viscous-Plastic Properties, Phase Transitions and Fractures in Iron

G.V. Kovalenko, A.V. Petrovtsev

Russian Federal Nuclear Center -VNIITF, Snezhinsk (Chelyabinsk-70), Russia

A model is proposed for the dynamic response of iron to stresses of different intensity that considers elastic-viscous-plastic properties, phase transitions (polymorphic and melting) and spall fractures.

The model uses a multi-phase (α-, γ-, ε- and liquid) equation of state derived earlier on the basis of ab initio calculations and available experimental data. Polymorphic transitions are modeled with kinetic equations that take into account the metastable character and finite time of phase transitions. This allows simulating sophisticated changes in phase composition (several transitions) depending on the history of thermodynamic state of material particle.

The modeling of elastic-viscous-plastic properties considers the strain rate and strain hardening of the material and the Bauschinger effect in unloading. Fractures are modeled with equations describing the development of damages in the material material and also with limiting relations accounting for mechanisms of fracture from shearing and breaking strains.

Model parameters chosen through the numerical modeling of some experiments ensure the real structure of stress waves in iron including amplitudes in the multi-wave configuration (elastic precursor, phase precursor and main plastic wave) and strain rates on their fronts in loading and unloading. This allows the accurate calculation of changes in the state of material particles in the fracture zone.

The presentation discusses results obtained in the numerical simulation of several explosive and shock wave experiments and analyzes of processes responsible for the peculiarities on stress wave profiles in iron.

Hydrocode Simulation of Plate Impact on an Anisotropic Alloy

T. De Vuyst[(1)], R. Vignjevic[(1)], N.K. Bourne[(2)], J. Campbell[(1)]

[(1)] College of Aeronautics, Cranfield University, Cranfield, UK
[(2)] Royal Military College of Science, Cranfield University, Shrivenham, UK

I. Introduction

Spall caused by hypervelocity impacts at the lower range of velocities could result in significant damage to structures. A number of polycrystalline alloys exhibit a pronounced anisotropy in their mechanical properties. The aluminium alloy AA 7010, whose orthotropy is a consequence of the meso-scale phase distribution or grain morphology, has been chosen for this investigation. The material failure observed in plate impact was simulated using an explicit finite element code and a smoothed particle hydrodynamics (SPH) code, and their performance was compared. The Hugoniot Elastic Limit (HEL) and spall strength have been studied as a function of orientation and impact speed, and compared to experimental results.

II. Experiment

Experiments were performed on single stage gas guns. Samples of the aluminium alloy 7010-T6 were cut from a single hot rolled block. As a consequence of the hot working process the material has a characteristic pan-cake grain structure (with the long axis of the grains in the rolling direction), which shows dynamic recovery but not dynamic recrystallisation. Manganin stress gauges (MicroMeasurements LM-SS-125CH-048) were supported on the back of the alloy targets with 12 mm blocks of polymethylmethacrylate (PMMA). Calibration studies by Rosenberg *et al* [1] were used to convert voltage-time data from the gauges into stress-time. A dural (aluminium alloy 6082-T6) flyer was chosen as an impactor since it had a close similarity in acoustic properties to the target. The geometry of the target and the impactor was chosen so that the reflected complete releases from target and flyer would interact in the centre of the 7010 target plate.

III. Hydrocode Modelling

The main purpose of the modelling studies was firstly to compare the performance of explicit finite element codes and smoothed particle hydrodynamics (SPH) codes, secondly to investigate the capability of current constitutive models to accurately predict the material behaviour under high velocity impacts Thirdly, to obtain an insight into some of the experimental observations and attempt to explain their physical significance. It was clear that some of these observations challenged quite long-standing views of the physics of spallation. Modelling therefore provided a potentially powerful and independent approach to investigating the issues. The main reason for this is that hydrocodes do not make any pre-determined assumptions concerning the stress-system or wave propagation behaviour. They solve the conservation equations and use the constitutive models and equations of state to determine dynamic the material response.

The simulations of these tests were performed using the public domain version of the Lagrangian hydrocode DYNA3D originating from Lawrence Livermore National Laboratory, and an in-house developed SPH code. The Al7010 plate was characterised using an anisotropic plastic-hydrodynamic material model that was developed at Cranfield University. The model uses Hill's anisotropic yield criterion [2]:

$$f(\sigma_y) = \left[F(\sigma_y - \sigma_z)^2 + G(\sigma_z - \sigma_x)^2 + H(\sigma_x - \sigma_y)^2 + 2L\sigma_{yz}^2 + 2M\sigma_{zx}^2 + 2N\sigma_{xy}^2\right]^{\frac{1}{2}} - \sigma_{Yield} = 0$$

and has a strain rate dependent yield stress and hardening modulus. The constitutive equations are integrated using the tangent stiffness method. The spherical part of the stress tensor is calculated using an equation of state. A Grüneisen equation of state was used in all presented results. In order to model the spallation, which is clearly observed in the experimental results, a principal stress based spall criterion was used. This criterion detects spall if the maximum principal stress exceed a specified limit.

The characteristic of this plate impact problem is that it can be reduced to a 1-D wave propagation. Hence building an model is greatly simplified, both in the case of the finite elementanalysis and the SPH simulation. The model that was used for this simulation the three materials where modelled as rectangular bars. Symmetry planes where applied on all the sides. This will result in a 1D wave travelling along the length of the bar. The stress time histories where recorded in the elements at the back of the test specimen.

IV. Results and Discussion

In Figure 1 the simulated gauge traces at the impact velocity of 450m s^{-1} (at two times the HEL) are presented in which clear spall signals are resolved. The general pulse shape is in good agreement with experiment for both finite element and SPH simulations. A clear break in slope in the initial rising part of the curve, that is the HEL, can be seen. This occurs at 0.38 GPa and 0.37 GPa in the FE and SPH simulations respectively. When compared with the value measured in the measured experiment, 0.4 GPa, these values show good agreement with the experiment.

The Hugoniot stress levels are 1.28 GPa for the FE simulation, 1.30 GPa for the SPH simulation and 1.30 GPa in the experiment. Again the simulation results are in good agreement with the experiment. One can clearly see pull back signals in both traces which indicate spall. The measured value of the pull back signal (spall) in the experiment at 450 m s^{-1} is 0.31 GPa. The values of the pull back signal in the FE and SPH simulations are 0.2 GPa and 0.3 GPa respectively. There is a reasonable agreement for this value when using the FE model. In the case of the SPH simulation the value is exactly the same as the expariment. However the shape of the pull back signal and the stress levels at which it starts are quite different. Also, the pull back signal starts at a stress level of around 0.4 GPa in the simulations, while in the experiment the stress level is much lower at 0.2 GPa. This clearly indicates that simple spall criteria, such as a maximum principal stress criterion, are not capable of accurately predicting pull back signals.

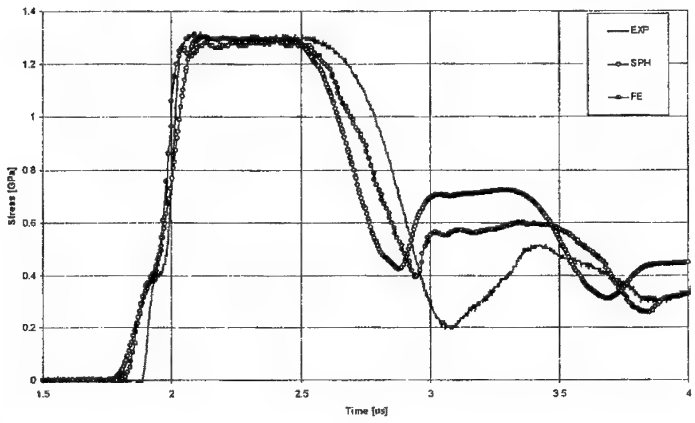

Figure 1.

V. Conclusion

Overall one can conclude that the SPH method is a viable alternative to FE for simulating this type of experiments. The only area where the FE simulations perform better than SPH method is in the wave propagation speed, which seems to be slightly overestimated in the SPH method. However, the SPH method has the extra advantages that it is easier to add new constitutive models, and that due to the meshless nature of the method it will be easier to incorporate complex material failure, and crack formation and propagation models.

References

[1] Z. Rosenberg, D. Yaziv, and Y. Partom, J. Appl. Phys. **51**, 3702 (1980).
[2] R. Hill, The Mathematical Theory of Plasticity, Oxford University Press, (1950)

Influence of Structural Factors on Strength of Ceramics and Mechanical Energy Dissipation at Dynamic Loading

V.A. Skripnyak, E.G. Skripnyak, A.S. Zhukov, T.V. Zhukova

Tomsk State University, Tomsk, Russia

Use of ceramic nano-powders allows to synthesize a ceramic materials with the required grain size and structural homogeneity. It is known, that static compressive strength, tensile strength, flexural strength and fracture toughness of modern nanocrystal ceramics approach to the strength characteristics of constructional metal alloys and steels. However, the mechanical behavior of nanocrystal ceramics at dynamic loading is weak investigated. The question about the ways of simultaneous increase of strength and dynamic fracture toughness of nanocrystal ceramics is open. Structural researches testify that at reduction of the grain sizes smaller than 0.1 microns the dislocation mechanisms providing accommodation of deformation of structural elements in polycrystalline ceramics are blocked. Under intensive pulse loading in homogeneous nanocrystal materials may be formed dissipative structures, that cause the macroscopic destruction of a material. In this case the cracks deflection mechanism may be not essential and ceramics will have low fracture toughness.

In this connection the study of influence of structural factors on mechanical behavior of ceramic materials have a practical interest.

In the represented report the theoretical forecasting of dynamic shear strength and spall strength of microcrystal and nanocrystal Al_2O_3, ZrO_2, SiC ceramics are submitted. Forecasting was received by means of computer modeling of mechanical behavior ceramics under plane shock wave loading with amplitudes up to 40 GPa. It was investigated the influence on the mechanical behavior of ceramics of the grain sizes, porosity, the average sizes of mesocracks and concentration of cracks.

The mechanical behavior of ceramic samples, is described within the framework of modification of continuum model [1] which is taking into account the structural factors on the macro -, meso- and microscopic levels. Mechanical behavior of ceramics is closely connected with of inelastic deformation at meso and microscopic levels. At test of ceramic materials under different temperatures in static conditions they behave as brittle ($T_0 / T_m < 0.2$) or semi-brittle solids ($0.2 < T_0 / T_m < 0.6$). But ceramics have high melting temperatures Tm. Therefore dislocations move only in the stress concentration region. The model assumes, that origination of structure defects occurs in the region of stress concentrators.

It was taken into account, that in real materials there are the concentrators of stresses on the macroscopic, mesoscopic and microscopic levels. The concentrators of stress on macro- and mesoscopic levels present the greatest danger for destruction of solid body. The mesoscopic concentrators of stress appear near the voids, cracks, solid phase's boundaries, grain boundaries, a crossings of shear bands.

In the model is used the G.C. Sih concept, that the nucleation of microcracks or their growth of the sizes can take place if the concentration of internal energy reach of some critical level. Amplitude of an elastic precursor corresponds to the critical level of concentration of internal energy at which microcracks may be nucleated.

Decreasing of a grain sizes and homogenization of ceramics structure, allows to lower stress concentration coefficient. In this case the Hugoniot elastic limits (σ_{HEL}) and appropriate dynamic strengths (Y) are increased. ($\sigma_{HEL} = -(1-\nu)\, Y/(1-2\nu)$, ν - Poisson factor).

The forecasting of dynamic strength for microcrystal and nanocrystal Al_2O_3, ZrO_2 ceramics and some experimental data are shown on Fig 1,2.

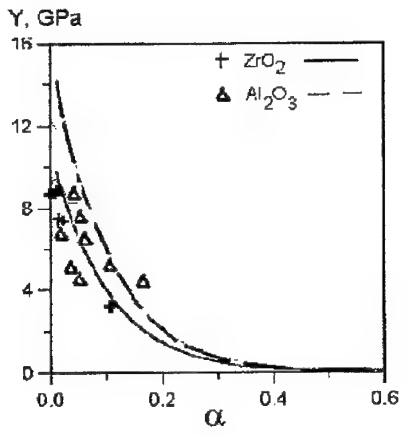

Fig 1. **Calculated dependence of dynamic strength on porosity of Al_2O_3 and ZrO_2 ceramics. Experimental data for Al_2O_3 [1-8], for ZrO_2 [9-11].**

The approximation of calculated stresses can be used for an estimation of dynamic strength of Al_2O_3 and ZrO_2 materials with different porosity and grain sizes.

$$Y(\alpha) = Y_o \exp(-\alpha/0.1),\ Y_0(d) = Y_{teor}(d/b)^{-0.1}, \qquad (1)$$

where Y_{teor} = 19.5 GPa for Al_2O_3, Y_{teor} =10.9 GPa for ZrO_2, b - the module of Burgers vector, b=4,76 10^{-8} cm for Al_2O_3.

For crystals with a cubic lattice the theoretical shear strength may be estimated as $\tau_{teop} = \mu_0^m/30$. If the hear module equal 94.12 GPa, τ_{teop} will be 6.274 GPa for ZrO_2. Dynamic strength Y in von Mises model is connected with shear stress by the ratio $\tau_{teop} = Y/\sqrt{3}$, therefore Y_{teor} will equal 10.9 GPa for FSZ (ZrO_2+Y_2O_3) ceramics. The corresponding maximum theoretical value of the σ_{HEL} is 19 GPa for FSZ ceramics. For Al_2O_3 ceramics the theoretical strength can be calculated as $\tau_{teop} = \mu_0^m/15$ and Y_{teor} will equal 19.5 GPa. Therefore, for Al_2O_3 the theoretical σ_{HEL} equal 27.8 Gpa.

Real values of σ_{HEL} will be much lower. Most near to theoretical value of Hugoniot elastic limit may be σ_{HEL} in single crystals of Al_2O_3 if the duration of a shock pulses are less than 50 ns.

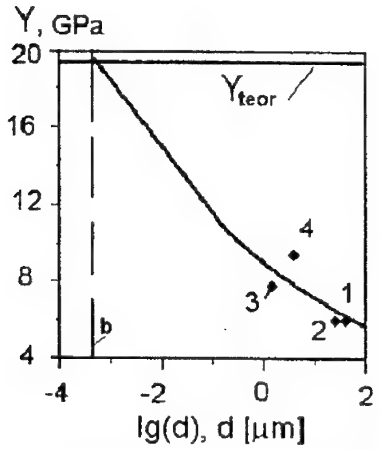

Fig. 2. **Dependence of dynamic strength polycrystalline Al_2O_3 ceramics on grain size. Experimental data 1,2-Lucalox [2], 3-MTU-JS-I [3], 4-D999 [4].**

At deformation of ceramic materials the dissipation of mechanical energy occur as a result of inelastic deformation and increase of surface energy of cracks. It is necessary to note that inelastic deformation of ceramics can be provided by the martensitic phase transformations besides the dislocation mechanisms. Ceramics possess a polymorphism if its crystal lattice have the lowered symmetry for example monoclinic, tetragonal etc. ZrO_2 ceramics has a 4 polymorph with monoclinic (m), tetragonal (t), cubic (c) and orthorhombic (o) crystal lattice. Martensitic transformation under loading of crystal m-t type can cause 5 % volume deformation and phase transformation t-c type cause 3 % deformation.

The model takes into account the inelastic deformation and dissipation of mechanical energy due to martensitic transformations. In the model the fraction of transformed material particles volume depends on grain size, the statistical distribution of shear stress at microscopic level.

Theoretical estimations of influence of the grain sizes and porosity on the dynamic strength and mechanical energy dissipation during high strain rate of ZrO_2 ceramics are received.

References

1. Skripnyak V.A., Skripnyak E.G. Computer modeling of mechanical behavior of constructional ceramics under shock loading // Proc. Int. Workshop New Models and Numerical Codes for Shock Waves Processes in Condensed Matter-1997. Oxford. UK: AWE Hunting - BRAE. V.1. 1997. P. 26.

2. Munson D.E. and Lawrence R.J. Dynamic deformation of polycrystalline alumina // J. Appl. Phys., 1979, V.50, N10, pp. 6272-6282.

3. Staehler J.M., Predeborn W.W., Pletka, B.J. The response of a high-purity alumina to plate-impact testing. In: High-Pressure Science and Technology - 1993. Eds.: S.C. Schmidt, J.W. Shaner, G.A. Samara and M. Ross. AIP Conference Proceedings, 1994, 309, pp. 745-748.

4. Murray N.H., Bourne N.K., Rosenberg, Z. (). Precursor decay in several aluminas. In: Shock Compression of Condensed Matter - 1995. Eds: Schmidt, S.C. and Tao, W.C. AIP Conference Proceedings 1996, 370, pp. 491-494.

5. Longy F., Cagnoux J. Plasticity and microcracking in shock-loaded alumina// J. Amer. Ceram. Soc., 1989. 72(6), pp. 971-979.

6. Ahrens T.J., Gust W.H., Royce E.B. Material strength effect in the shock compression of alumina// J. Appl. Phys., 1968. 39(10), pp. 4610-4616.

7. Gust W.H. and Royce E.B. Dynamic yield strength of B_4C, BeO, and Al_2O_3 ceramics. J. Appl. Phys., 1971.**42**, pp. 276-295.

8. Bartkovwski P., Dandekar D.P. Spall strength of sintered and hot pressed silicon carbide. In: Shock Compression of Condensed Matter - 1995. Eds: Schmidt, S.C. and Tao, W.C. AIP Conference Proceedings 1996. **370**, pp. 535-538.

9. Mashimo T., Nakamura A., Kodama M., Kusaba K., Fukuoka, K., and Syono, Y. Yielding and phase transition under shock compression of yttria-doped cubic zirconia single crystal and polycrystal // J. Appl. Phys., 1995. **77**(10), pp. 5060-5068.

10. Mashimo T., Nakamura A., Nishida M., Matsuzaki S., Kusaba K., Fukuoka K., Syono Y. Anomalous shock compression behavior of yttria-doped tetragonal zirconia // J. Appl. Phys., 1995. **77**(10), pp. 5069-5076.

11. Kipp M.E., Grady D.E. Shock compression and release in high-strength ceramics. In: Shock Compression of Condensed Matter 1989. Eds.: S.C.Schmidt, J.N. Johnson and L.W. Davison. Els. Sc. Pub. B.V., 1990, 377-380

Effect of Material Heterogeneity on the Shock Wave Profile of Composites in Plate Impact Tests

N. Chandra and A.M. Rajendran*

Department of Mechanical Engineering, Florid State University, USA
** US Army Research Office , RTP, North Carolina, USA*

In the study of shock wave propagation in solids, dispersion and attenuation play a critical role in determining the thermomechanical response of the media. These phenomena can be attributed to a number of nonlimealities arising from the wave characteristics, loading conditions, material heterogeneity (measured at various spatial scales ranging from nanometers to a few millimeters). The material nonlinear effects in general can be ascribed to impedance (and geometric)mismatch present at various length scales as often encountered in composite material systems.

Uniaxial strain experiments on the S-2 glass/polymer composite system display markedly different behaviour than that observed in monolithic metallic systems [Botelar, Rajendran and Grove 1999]. Stress profiles measured at various locations along the thickness direction in the plate impact experiments showed that the shock wave rise time increased with propagation in addition to the reduction of peak stress. In this work, we address the issue of shock wave rise time. A careful analysis of wave propagation in heterogeneous medium is carried out taking into account known values of elastic/acoustic properties of individual phases, fiber volume fraction and details of construction including lay-up sequence.

An analytical model has been developed to describe the scattering process (reflection/transmission) at various layer interfaces of multilayer composite system. FEM results are then used to compare the analytical predictions. These results show that the rise time can be a consequence of multiple internal reflections and wave dispersion occuring at the heteregeneous interfaces.

On the Transition from Rigid to Eroding Rod Penetration of Long Rods

Z. Rosenberg and E. Dekel

RAFAEL, Haifa, Israel

The penetration process of eroding rods into semi-infinite target has been investigated by many workers both experimentally and numerically. These works resulted in a deep understanding of the process of long rod penetration for the eroding rod case. The situation is much more complex for high strength rods which penetrate as rigid bodies at low impact velocities.

The purpose of the paper is to examine experimental data for high strength steel rods impacting semi-infinite Aluminum targets. Both Eulerien and Lagrangian numerical simulations were performed to follow the transition from rigid to eroding rods process. It is shown that material properties, such as strength to failure, are very important in order to simulate experimental results.

Ceramic Block Impenetrability to High Velocity Long Road Impact

F. Collombet[1], F. Malaise[2] and J.Y. Tranchet[3]

[1] Laboratoire de Génie Mécanique de Toulouse, IUT Paul Sabatier, Toulouse, France
[2] Centre d'Etudes Scientifiques et Techniques d'Aquitaine, Le Barp, France
[3] Cedocar, Service Prospective Analyse, Angoulême, France

It was recently showed that the applying of confinement near the impact area can lead to total erosion of the projectile without penetration in ceramic [Bless et al, 1992] [Malaise et al., 1999]. A phenomenological analysis of the conditions of ceramic "flow" in front of the rod gave the basis of a new modelling of ceramic behaviour [Tranchet et al., 2000]. The response of ceramic block to high velocity (1500 m/s) impact of a heavy metal alloy rod is numerically investigated. We study the possibilities and the limitations of the modelling.

The modelling is implemented in the Eulerian version of the explicit dynamic code OURANOS. This code is suitable to calculate the plastic flow of the rod and treat large displacements of fragmented ceramic. The experimental configurations are those described in [Malaise, 2000]. Two types of experiments are considered. The first experiment consists in an encapsulated rod impacting a silicon carbide block at 1500 m/s. The second one consists in an alone rod impacting the same ceramic block at the same velocity. We use bidimensional axisymetric mesh. The eulerian grid is made up 35 000 square cells whose sizes vary from 0.2 to 4 mm. The influence of the grid is discussed.

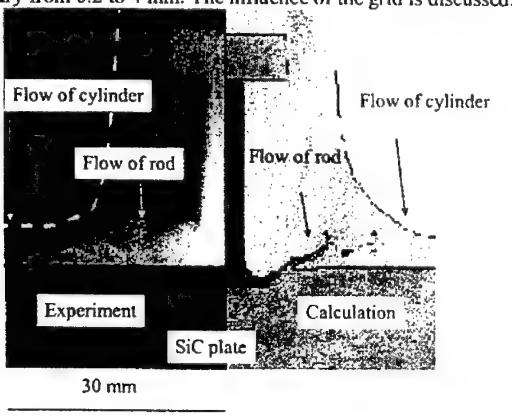

Figure 1: Experiment-calculation comparison at 20 µs after impact of the encapsulated rod onto a silicon carbide plate.

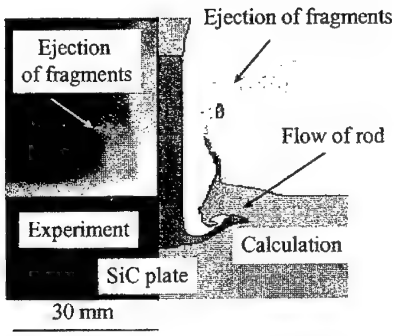

Figure 2: Experiment-calculation comparison at 20 μs after impact of the rod (alone) onto a silicon carbide plate.

Figure 1 and Figure 2 show comparisons between experiments and calculations, 20 μs after impact of the rod on the silicon carbide block. At this time, computation is in line with x-rays from tests. For the impact of the rod alone, the mechanisms of penetration, fragmentation of ceramic and ejection of fragments to the rear of projectile, are in good accordance with experiment. Penetration seems to take place in sequences such as those observed experimentally on boron carbide [Lundberg et al., 1998]. For the encapsulated rod, flow of matter takes place mainly in the radial direction. Moreover at this time, the depth of penetration of the rod alone is much more greater than for the encapsulated one. The effects of confinement on the penetration resistance of silicon carbide are restored by calculations. These comparisons validate qualitatively the modelling of ceramic response.

Nevertheless, some quantitative discrepancies remain between calculated and experimental total depths of penetration. These discrepancies can be explained on one hand, by the presence of mixed material cells at the interface, and on the other hand, by the need to describe the behaviour of the fragmented ceramic more precisely. The use of small cells reduces the discrepancies but not at all. More experimental data are necessary to better describe the behaviour of fragmented ceramic.

This type of modelling can be useful in the future in the analysis of the interface defeat mechanisms. Nevertheless, more efforts are needed theoretically and experimentally to quantify the influence of void content on the behaviour of the fragmented ceramic.

Acknowledgements: the authors would like to thank the Délégation Générale de l'Armement for funding this work.

References

[1] BLESS S. J., BEN-YAMI M., APGAR L., EYLON D., 1992, "Impenetrable targets struck by high velocity tungsten long rod.", Proc 2nd Int. Conf. on Structures under Shock and Impact, Portsmouth, UK, 16-18, June, 1992.

[2] MALAISE F., 1999, "Réponse d'une céramique à l'impact d'un barreau à grande vitesse (1500 m/s). Croisements essais dynamiques-modélisations numériques", thèse de l'Ecole Nationale Supérieure d'Arts et Métiers, n°1999-24.

[3] TRANCHET J. Y., MALAISE F., COLLOMBET F., 2000, "A numerical investigation of high velocity impact onto a ceramic block", 6th International Conference on Mechanical and Physical Behavior of Materials under Dynamic Loading, Krakow, Poland, *J. Phys. IV 10*, pp. 689-694.

[4] MALAISE F., TRANCHET J. Y., COLLOMBET F., 2000, "An experimental investigation of ceramic plate impenetrability to high velocity impact", 6th International Conference on Mechanical and Physical Behaviour of Materials under Dynamic Loading, Krakow, Poland, *J. Phys. IV 10*, pp. 589-594.

[5] LUNDBERG P., HOLMBERG L., JANZON B., 1998, "An experimental study of long rod penetration into boron carbide at ordnance and hyper velocities", 17th International Symposium on Ballistics, South Africa.

Void Formation During "Symmetric" Taylor Impact

D.D. Radford, S.G. Grantham, P.D. Church*, P.J. Gould*, W.G. Proud

Cavendish Laboratory, University of Cambridge, Cambridge, UK
** QinetiQ., Fort Halstead, Sevenoaks, UK*

Accurately predicting the deformation and failure of materials during ballistics events represents a major challenge for numerical simulations. As a results, a fully integrated approach between material testing, simulations and precise experiments is required. The approach adopted by our group is to represent the underlying physics in a simple manner, thereby capturing the major mechanisms, rather than attempting to simulate the vast complexity of the micro-mechanics (dislocations, etc.) at the meso-scale.

The methodology involves describing the material behaviour at the computational cell level and the failure process within the cell analytically, thereby linking the macroscopic and microscopic scales [1, 2]. Although this novel approach has been quite successful at predicting high rate deformation and fracture [3, 4], it is recognised that these algorithms must be exercised in order to understand the limits of applicability.

The "symmetric" version of the classic Taylor test [5] is widely used for this purpose and can be designed to produce fracture along the axis of the specimen. In the current investigation, symmetric Taylor experiments were performed on XM-Cu and modelled using the Goldthorpe path-dependent deformation [6] and fracture [1]. Comparing the results from the simulations to experimental data shows that the deformation model accurately predicts the deformation behaviour, but the fracture model overestimates the damage evolution. Through the use of a novel experimental arrangement, the actual time of void formation during impact has been quantified.

These results are compared to numerical predictions and recent developments of the fracture model are discussed.

References

1. Goldthorpe, B.D., J. Phys. IV France Colloq. C3 (EURODYMAT 97), 1997. **7**: pp. 705-710.
2. Church, P.D., T. Andrews, and B. Goldthorpe, in *Structures under Extreme Loading Conditions. PVP 394*, D.M. Jerome, Editor. 1999, ASME: New York. pp. 113-120.
3. Church, P.D., J. Macmahon, I. Softley, and C. Cameron, J. Phys. IV France Pr. 9 (DYMAT 2000), 2000. **10**: pp. 391-396.
4. Walley, S.M., P.D. Church, R. Townsley, and J.E. Field, J. Phys. IV France Pr. 9 (DYMAT 2000), 2000. **10**: pp. 69-74.
5. Taylor, G.I., J. Inst. Civil Eng., 1946. **26**: pp. 486-519.
6. **Gould, P.J., B.D. Goldthorpe, J. Phys. IV France Pr. 9 (DYMAT 2000), 2000. 10: pp.39-44.**

Numerical Modeling for Wave Processes after Non-Equilibrium Volume Energy Expansion in Elementary Cell of Heterogeneous Material

A.V. Ostrik, E.A. Romadinova

Institute of Problems of Chemical Physics, Chernogolovka, Russia

The main physical for calculation wave processes under volume energy expansion in elementary cell of heterogeneous material with dispersion filler is proposed. In numerical code we use implicit full-conservative finite-difference scheme, that let realize stationary solution. The solution of algebraic equations that are obtained after linearization of initial equations in finite-difference form by Newton method, is made by method of matrix running with main element choice by column. The results of calculation for heterogeneous material that consists of epoxy binder and filler of di-oxide tin or glass microsphere covered by wolfram are given here. There is the comparison for the data we obtained and the results that followed from the quasi-static model.

Under action of nanosecond x-ray radiation (XR) on condensed target intensive wave processes are developing in them and investigation of these processes has practical use [1-4]. In dependence of quantum energy E_{ph}, that determines characteristic size of energy absorption area, the physical pattern of radiation mechanical action pattern changes essentially [2, 3]. The volume energy expansion area under absorption of strong XR (10kev<E_{ph} ≤100kev) can reach centimeters or more. Meantime comparatively not high level of heating doesn't lead to intensive gas-dynamic processes but demands detailed consideration of heterogeneous structure of material, the existence of two-phase conditions, the porosity of components, the resistance of binder to shear and other peculiarities [4], that in the case of more high density of absorbed energy which is characteristic for soft XR action, is negligible.

I. Physical model

Wave processes in target forms in the result of thermomechanical action of radiation, the physical reason of which is the expansion of heterogeneous material (HM) under heating that is constrained by material inertness. If impulse continuance is small compare to the time of acoustic relaxation of volume energy expansion area(for nanosecond radiation and strong enough XR it's true? as a rule) then mechanical action of radiation can be considered gradually [5]. At the first step the adequation of pressure in elementary cell of HM of constant volume has place, because wave processes in the all area of energy expansion doesn't manage to develop . The second step correspond to the phase of wave processes and destructions in the whole HM. In this paper the numerical model for wave processes in the cell at the first step is purposed When the time of acoustic relaxation of each component of HM much more less of energy expansion time (the time of XR action), the processes of pressure establishment in the cell can be considered as quasi- static and wave movement can be neglected . [6]. But for big inclusions of HM filler and narrow XR impulse the pressure in the cell doesn't manage to establish during the time of energy expansion that leads to intensive wave processes. Spreading in the cell waves redistribute the energy between HM components and in the result after the wave attenuation the pressure may differ to the one followed from quadratic approximation.

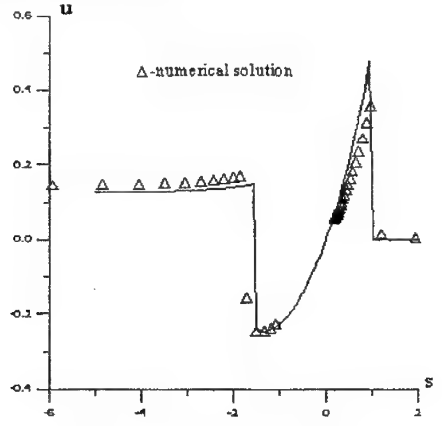

Fig. 1. Comparison with automodel solution

HM with dispersion filler which elementary cell consists of sphere inclusion inclosed by binder is considered (mass contains of filler in the cell and HM coincide). The boundary of cell is also taken to be spherical. Under action of strong XR the size of inclusions much less then energy expansion area thickness, that let us consider each component evenly heated in the cell bound and give spatial distribution of energy expansion in the cell by the only one parameter – the part of energy absorbed by the filler. As shown in [5] the influence of shear stress upon initial profile of pressure is negligible and waves in the cell can be described in hydro-dynamical approximation. So the problem resolves itself to the calculation system that contains one- dimension equations of gas dynamics in spherical coordinates for multi –layer cell. As volume density of energy expansion can be big enough [3] so for numerical

calculation of this system for describing phase transitions in HM components it's necessary to use wide – range equations of state (EOS).

As boundary condition the demand of incompressibility for cell is taken (radial shear at outer surface of the cell equal to zero). In the case of cored microshpere filler [7] the numerical modeling of wave processes in thick layer is quite delicate. To simplify the problem the behavior of microsphere is modeled by dynamic deformation of multi-layer elastic shell. At the boundary between filler and shell the demand of equality between radial shears and pressures is required.

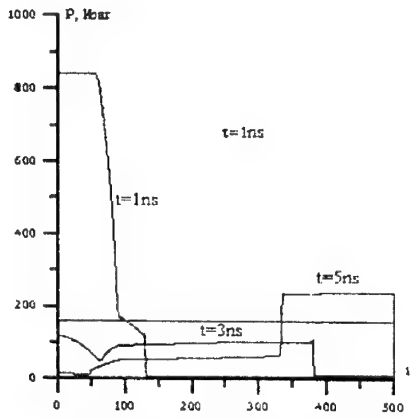

Fig 2 Compression wave propagation (1ns)

2. Numerical code

For numerical realization of HM elementary cell non-statical model we use implicit full-conservative scheme [8] for one-dimensional equation of gas-dynamics in LaGrange coordinates. The implicitly of taken scheme provides the possibility of reaching statical behavior for numerical method to compare the results with calculations by quasi-static methods. The solution of algebraic equations system with three-diagonal matrix, obtained after linearization of initial equations by Newton method in finite-difference form, on each temporary step is calculated by matrix running method with main element choice by column [9]. This method it correct for any definite system of equations (in contradistinction to common running method "diagonal prevalence" criterion isn't required) As well as finite-difference equations are written in matrix form, the conversion from one system of equations (physical model) to the other is quite simple and consists of the changes in calculation formulas of matrix and their orders. System of equation form doesn't influence the efficiency of given implicit finite-difference method. As numerical experiment shows high stability of the method provides correct calculation for even so difficult for finite-difference methods test , as the automodel problem of convergence to the center and reflection of spherical wave from it [8] (comparison results of numerical and analytical solution are presented on Fig 1 for automodel variables u and s) . The code is adapted for using the wide-range half-empiric EOS such as in [10] and tested on them. This EOS fulfils Bete- Wail's know requirements of matter normality out of two-phase area. Within the framework of the code the preliminary updating of EOS in two-phase area is provided [11].

3. The calculation results

HM that contains of epoxide-polyamide composition (binder) with high temperature capability and tin dioxide SnO_2 (dispersion filler), that absorbs radiation good was considered in numerical researches. The behaviour of these HM components was described by interpolation equation of state, in which pressure and specific inner energy represents sums of cold and hot components and Grunaizer

coefficient decrease when temperature and specific volume increase is considered. Process of compression waves propagation in elementary cell with HM specific energy expansion Q=10kDj/g and filler absorb energy part ε_f=0,8 is represented on Fig. 2, 3 (i-cell number). Filler dimension and its mass concentration are supposed a=10micron, X_f=20%. We may see for radiation time τ = 1ns pressure formation process has non-statical character and pressure profile may to defer from its quasi-statical value is indicated by plain line in Fig. 2.

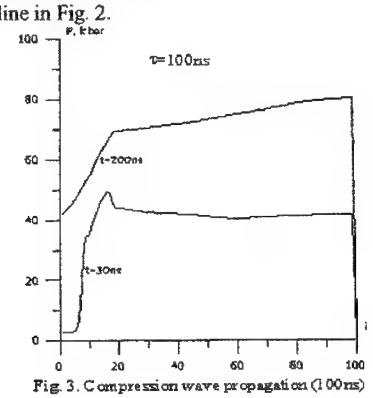

Fig. 3. Compression wave propagation (100ns)

However if radiation time is great (τ = 100 ns and in considered cell character acoustic times are 2ns, 9ns for filler and binder accordingly) this difference becomes inconsiderable and we may to estimate pressure profile by quasi-statical model [6,7].

References

1. Грабовский Е.В., Воробьев О.Ю., Дябилин К.С., Лебедев М.Е., Острик А.В., Фортов В.Е. *Генерация мощных ударных волн мягким рентгеновским излучением плазмы Z-пинча // ЖЭТФ, 1994. Т.60. Вып. 1. С.3-6.*

2. Лоборев В.М., Острик А.В., Петровский В.П., Чепрунов А.А. *Методы моделирования механического действия излучений на материалы и конструкции. Научно-технический сборник №1.–Сергиев Посад. ЦФТИ МО РФ, 1997. 75с*

3. Грибанов В.М., Острик А.В., Слободчиков С.С. *Тепловое и механическое действие рентгеновского излучения на материалы и преграды. Монография. Физика ядерного взрыва: В 2-х т. Том 2. Действие взрыва. –М.: МО РФ ЦФТИ, 1997. 256с.*

4. K.S. Kolesnikov, A.V.Ostrik, V.N. Bakulin *Numerical simulation for wave processes under X-ray action on heterogeneous material // Dynamics of Multiphase systems,Proceedings of International Conference on Multiphase Systems, held of occasion of the 60th Birthday of Academician Robert Nigmatulin, , 2000, Ufa,, RUSSIA, p. 359-364.*

5. Острик А.В., Острик Е.А. *Расчет давления при воздействии рентгеновского излучения на гетерогенный материал с пластическим связующим // Межотраслевой научно-технический журнал "Конструкции из композиционных материалов", 1999. Вып. 2. С.26-32.*

6. Острик А.В., Острик Е.А. *Численная модель квазистатического выравнивания давления в гетерогенном материале при воздействии на него излучения. / X Юбилейная международная конференция «Вычислительная механика и современные прикладные программные системы. Тезисы докладов.– Переславль-Залесский, 1999. С. 209-210.*

7. Острик Е.А. *Модель установления давления при импульсном объемном энерговыделении в гетерогенном материале с полидисперсным наполнителем /XVI Международная конференция «Воздействие интенсивных потоков энергии на вещество». Сборник трудов. Терскол, 2001. С.30-32.*

8. Волчинская М. И,,, Гольдин В.Я., Калиткин Н.Н., Самарский А.А.. *Сравнение разностных схем на тестах. Препринт №44. –М.: ИПМ, 1972. 20с.*

9. *Шаракшанэ А.А. Матричная прогонка с выбором главного элемента. Преп.,. №187.М.: ИПМ 1986. 24с.*

10. Сапожников А.Т., Першина А.В. *Интерполяционное уравнение состояния в области испарения // Вопросы атомной науки и техники. Сер. Методики и программы численного решения задач математической физики.-1984. Вып.2(16). С. 29-34.*

11. Куропатенко В.Ф. *Уравнения состояния в математических моделях механики и физики // Сборник научных трудов "Экстремальные состояния вещества" под ред. В.Е. Фортова, –М.: ИВТАН, 1991, с. 3-38.*

Erosion Failure Model for 3D Simulation of Perforation of Targets by a Group of High-Velocity Bodies

S.A. Zelepugin[1,2], V.N. Sidorov[2], E.B. Vidischeva[1,2]

[1] *Tomsk State University, Tomsk, Russia*
[2] *Department for Structural Macrokinetics, Tomsk Science Center, Tomsk, Russia*

The problem of high-velocity interaction of a group of several identical cylindrical bodies with a target is considered. Numerical simulation of damage accumulation in a sample is performed with an application of an active-type kinetic model of fracture. As a criterion of material erosion failure having place in the region of intensive interaction and deformation of contacting solid bodies, the critical value of specific energy of shear deformations is used.

One of complex problems of mechanics of deformable medium is the investigation of processes of interaction of several solid bodies with a target in conditions of high-velocity impact. This problem is connected with necessity of spacecraft protection against meteoroids in space. In [1, 2] the features of processes of interaction of two bodies with a plate in two-dimensional plane-strain statement were investigated numerically and the mutual influence of high-velocity particles on result of interaction was shown. However numerical modeling in plane statement especially of final stage of the process of deformation and fracture can give results qualitatively distinguished from three-dimensional experiment [3]. In the present paper the processes of high-velocity interaction of several solid bodies with a target are investigated numerically in three-dimensional statement [4].

The basic mathematical model employed in numerical code for solving high-velocity impact problems is based upon the set of differential equations of continuum mechanics that govern material flow. These equations are conservation of mass, momentum, and energy as well as a constitutive relationship that relates stress and strain increments to material properties. The set of equations describing time-dependent adiabatic motion of a compressible medium (in the case of both elastic and plastic deformation) taking into account the growth and accumulation of microdamages comprises the continuity equation, the equation of motion, the energy equation, and the equation that describes the variation of the specific volume of pores, respectivly [5]:

$$\frac{\partial \rho}{\partial t} + \operatorname{div}(\rho \mathbf{v}) = 0, \tag{1}$$

$$\frac{\rho dv_i}{dt} = \sigma_{ij,j}, \tag{2}$$

$$\frac{dE}{dt} = \frac{1}{\rho}\sigma_{ij}\varepsilon_{ij}, \tag{3}$$

$$\frac{dV_f}{dt} = \begin{cases} 0, & \text{if } |P_s| \le P^* \text{ or if } (P_s > P^* \text{and } V_f = 0) \\ -\operatorname{sign}(P_s) K_f (|P_s| - P^*)(V_2 + V_f), & \\ \quad \text{if } P_s < -P^* \text{ or if } (P_s > P^* \text{and } V_f > 0) & \end{cases} \tag{4}$$

Here $P^* = P_k V_1/(V_f + V_1)$, ρ is the density; v_i are the components of the velocity vector v; E is the specific internal energy, ε_{ij} are the components of the strain-rate tensor; $\sigma_{ij} = -(P+Q)\delta_{ij} + S_{ij}$ are the stress-tensor components; P_s is the pressure in the continuous component of the medium; $P = P_s(\rho/\rho_s)$ is the average pressure; Q is the fictitious viscosity; and K_f, P_k, V_1, V_2 are the material constants.

The material model includes the equation of state of the Mie-Grüneisen type that gives the pressure as a function of specific volume, internal energy, and specific volume of cracks, the deviatoric elastic constitutive relationships, von Mises yield criterion taking into account temperature effects, and

erosion failure model. The critical specific energy of shear deformations is used as a criterion of material erosion [4]. The current value of this energy is defined from relationship

$$\rho \frac{dE_{sh}}{dt} = S_{ij}\varepsilon_{ij}, \qquad (5)$$

where i, j = 1, 2, 3. The critical specific energy of shear deformations depends on the conditions of interactions and is a function of the initial impact velocity

$$E_{sh}^{c} = a_{sh} + b_{sh}\upsilon_0, \qquad (6)$$

where a_{sh} and b_{sh} are constants of the material. When

$$E_{sh} > E_{sh}^{c} \qquad (7)$$

in the computational cell near the contact boundaries, the cell is assumed damaged and the parameters in neighboring cells are corrected with regard for the principles of conservation laws.

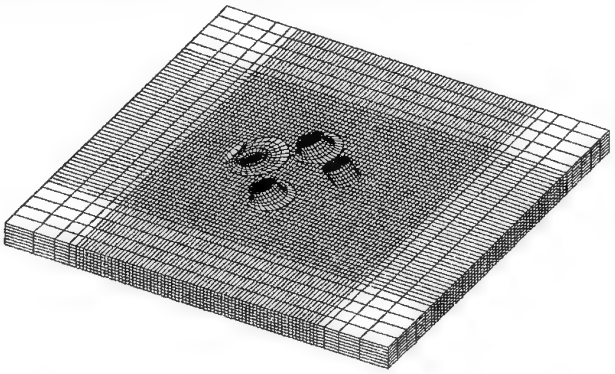

Figure 1. Stage in the group interaction process at an initial impact velocity of 2873 m/s, t = 3 μs.

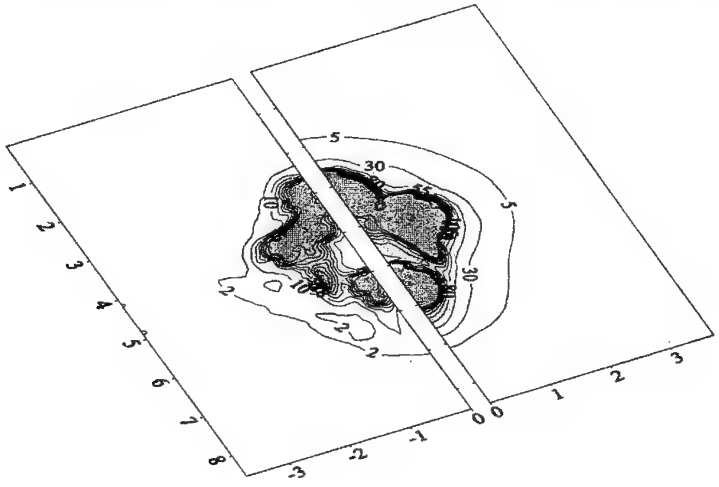

Figure 2. Contours of specific volume of pores (on the left with an interval ΔV_f – 8 cm^3/kg) and specific energy of shear deformations (on the right, ΔE_{sh} – 25 kJ/kg) along face surface of the target at 17 μs.

The problem of the interaction of four identical cylindrical impactors with a diameter and height of 6 mm with a target with a thickness of 8 mm is considered. The initial velocity of each impactor is of 2873 m/s and the angle is of 30^0. The material of interacting bodies is steel. For numerical solution of the problem the modified finite element method is used [6].

In Fig. 1 the stage of the process of group impact at 3 μs after beginning of the interaction is given. It illustrates the moment of the process when two intermediate impactors just begin to interact with the target, the last one on the right do not yet begin the interaction, while the first one penetrates the target. The process is accompanied by high plastic deformations, simulated also with the concept of failure of erosion type.

Figure 2 demonstrates mutual influence of the processes and formation of an integrated region of deformation and fracture in the target with centers relevant to each impactor. The region of deformation and failure appropriate to the last impactor, is a little away from integrated region owing to later beginning of impact and a little more initial distance between the particles. The additional center of microdamages between the last one and the average impactors stipulated by their mutual influence is observed.

References

1. Khorev I.E., Gorelski V.A., and Zelepugin S.A. Study of relaxation effects in a plate under synchronous contacting of two bodies with it // Applied Mechanics, no. 6, pp. 42-48, 1989. (in Russian).
2. Khorev I.E., Gorelski V.A., and Zelepugin S.A. Failure and relaxation effects in plates under synchronous contacting of two bodies with them // Problems of Strength, no. 7, pp 51-55, 1992. (in Russian).
3. Gorelski V.A., Zelepugin S.A., and Tolkachev V.F. Study of target perforation under nonsymmetric high velocity impact with the allowance for fracture and temperature effects // Bull. Acad. Sci., Mechanics of Solids, no. 5, pp. 121-130, 1994. (in Russian).
4. Khorev I.E., Zelepugin S.A., Konyaev A.A., Sidorov V.N., and Fortov V.E. Breaking Obstacles by a Group of High-Velocity Bodies // Doklady Physics, vol. 44, no. 12, pp. 818-822, 1999.
5. Zelepugin S.A. and Nikulichev V.B. Numerical Modeling of Sulfur – Aluminum Interaction under Shock-Wave Loading // Combustion, Explosion, and Shock Waves, Vol. 36, No. 6, pp. 845-850, 2000.
6. Gorelski V.A., Zelepugin S.A., and Smolin A.Yu. Effect of Discretization in Calculating Three-Dimensional Problems of High-Velocity Impact by the Finite-Element Method // Computational Mathematics and Mathematical Physics, vol. 37, no. 6, pp. 722-730, 1997.

Preserving Causality in Strongly Shearing Elastoplastic Flows

I.N. Gray

Atomic Weapons Establishment, Aldermaston, UK

In shear dominated flows, in the thermal softening regime of solid materials, the standard Prandtl-Reuss treatment of elastoplasticity results in the loss of the overall causal structure (hyperbolic character) associated with the material flow. This paper describes an elastic-viscoplastic constitutive model which exhibits specific strain rate sensitivite effects. The model is based on the idea of separating the rate sensitive and the strain hardening/thermal softening aspects of the an elastic material response into separate parallel processes. It provides a fullt conservative extension of the standard Prandtl-Reuss treatment used in hydrocodes and allows rate dependent overstress and stress relaxation effects relative to the plastic yield surface in stress deviator space. With this model the continuum equations preserve their hyperbolic character in the

thermal softening regime. The main issus relating to hydrocode implementation of the model are discussed.

Computer Simulation of Spall Fracture in Ceramics under Short Shock Impulses Loading

V.A. Skripnyak, E.G. Skripnyak, A.S. Zhukov, T.V. Zhukova

Tomsk State University, Tomsk, Russia

The propagation of shock impulses with duration from microsecond to several tens of nanoseconds and attenuation of their amplitude in single-phase polycrystalline ceramics, sapphire and ruby single crystals, nanocrystalline ceramic composites are investigated by numerical simulation method.

Deformation and fracture of ceramics closely connects with the evolution of material's structure. The relaxation of shear stress in constructional ceramics can be caused by set of physical mechanisms on meso- and micro-scale levels. The used model takes into account the kinetics of inelastic deformation caused by martensitic phase transformation, nucleation and motion of dislocation, nucleation of shear microcracks etc.

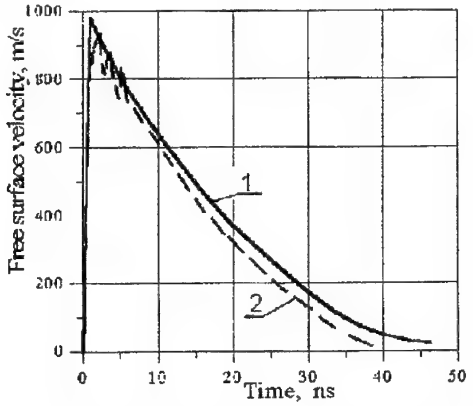

Figure 1. **Calculated (2) and experimental (1) profiles of free surface velocity of z-cut sapphire samples.**

The outcomes of simulation testify, that inelastic deformation can be negligible in the constructional elements from polycrystalline ceramics when the shock pulse amplitude is higher, than the Hugoniot Elastic Limit (HEL), if the impulses duration is comparable with time of relaxation corresponding to preferred physical mechanisms.

Strength of ceramics at dynamic loading depends from damage accumulation at meso- and macroscopic scale levels. The spall strength of polycrystalline ceramics at impulse loading with nanosecond duration is comparable to the theoretical strength at tension of the single crystals. In single crystals of Al_2O_3 (sapphire and ruby) and also in nonocrystalline ceramics based on Al_2O_3 and ZrO_2, the time of a fast relaxation of shear stress are about ten nanoseconds.

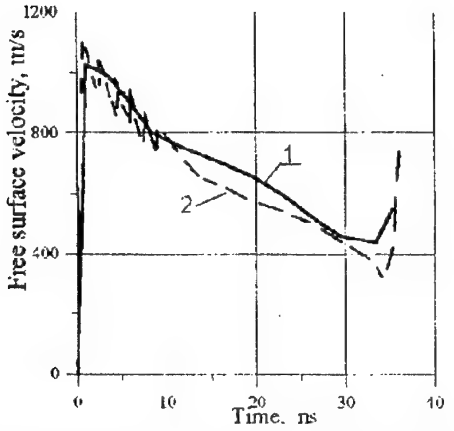

Figure 2. **Calculated (2) and experimental (1) profiles of free surface velocity of z-cut sapphire samples.**

The Al_2O_3 ceramics is capable to be practically elastic-deformed and the shear stress is compared to the theoretical shear strength, if the duration of pulse loading is not more than some tens nanoseconds. For impulse loading with duration of microsecond and amplitudes exceeding the HEL, inelastic deformation of ceramic materials can be caused by the growth of damages on meso-scale level. .

The results of simulation of high-power ion beam loading of sapphire plate [1] are shown in Fig.1 and Fig.2. The sample thickness in all case was 2,3 mm. In the first case there were no spall fracture, but the rising of impulse amplitude causes the spall fracture.

Obtained numerical results have satisfactory correlation with some of experimental data on shock pulses structures, spall strength and HEL in single crystals and few polycrystalline aluminum oxide ceramic materials. The numerical modeling showed that Hugoniot elastic limit of aluminum oxide polycrystalline ceramic much depends on meso-scale structure (porosity, average grain sizes, concentration and average sizes of penny shape cracks).

Numerical modeling of short pulses propagation in single crystal Al_2O_3 with metal base-plate on the rear surface of sample show the possibility of formation of very thin spall zone. The high level of spall strength value was obtained for z-cut sapphire in calculation of action of shock impulse with duration about 50 nanoseconds. The value was comparable with theoretical tensile strength of Al_2O_3 ceramics.

1. Kanel G.I., Razorenov S.V. // In High Pressure Science & Technology-1993. N.-Y. 1994.

Numerical Modeling of Strain Localization and Spall Fracture in Mesovolumes of Polycrystalline Materials under Shock Wave Loading

I.Yu. Smolin, P.V. Makarov, Yu.P. Stefanov, R.R. Balokhonov, V.A.Romanova

Institute of Strength Physics and Materials Science, Tomsk, Russia

Non-uniform development of plastic deformation and fracture is typical both for the high and slow rate loading. To describe this phenomenon in simulations one must take into account the main governing factors. Inhomogeneous inner microstructure of materials seems to be an evident reason. It should be taken into account in calculations. As a rule any material has hierarchical and complicated inner structure which evolve under loading. To take all this into consideration in modeling is a difficult problem. The aim of this work is to investigate numerically the influence of polycrystalline nature of metals in rather simple form on strain localization and multiple cracking under shock wave loading.

To solve this problem we consider mesovolumes of polycrystalline materials. Heterogeneity of a material structure is obviously taken into account through different mechanical properties of individual grains. Results of modeling formation of strain localization bands and rotation of mesofragments in the mesovolumes of a polycrystalline aluminum alloy under shock wave loading are discussed. Examples of modeling development of cracks in the mesovolume at spalling fracture are presented as well.

A mesovolume of Al 6061-T6 alloy containing large number of grains was chosen for numerical investigation. Its map is presented in Fig. 1(a). Different yield strengths were assigned for different grains indicated by different intensity of gray color in Fig. 1(a). Plane strain conditions were adopted. The symmetry boundary conditions were set on the mesovolume horizontal sides parallel to the x-axis. At the left side of the mesovolume the particle velocities obtained in calculation of 3 GPa plane shock wave propagation in the homogeneous material were set for the appropriate grid nodes during the calculation time. The right side was assumed to be free of stress.

The problems were solved by the finite difference method, use of the elastic plastic model of the medium and constitutive equations in the relaxation form were made. Patterns of stress, effective plastic strain, and also particle velocities distributions were registered while shock wave propagates into the mesovolume. Note that in the experiments the patterns of strain localization are registered after passing of the release waves and complete stress relaxation. In our calculations only origins of strain localization are revealed in the form of non-uniform distribution of plastic deformation in rather short period of time.

While a loading wave propagates into the material, the difference in the properties of its structural elements result in a non-uniform stress-strain state which the particle velocity field shown in Fig. 1(b) reflects very well. To make this non-uniform movement of particles visible, the particle velocities are presented as deflections of particle velocities in heterogeneous material from the corresponding velocities in the homogeneous material. It shows very well that the character of motion in the "plane" shock wave is complicated and out of one dimension. This is connected with different shear strength of different grains. So, in the system of coordinates moving with the shock wave the velocity field has a vortex nature. Centers of rotations correspond to the centers of individual grains or triple joints of grains.

Figure 1(c) displays the distribution of effective plastic strain in the volume under investigation.

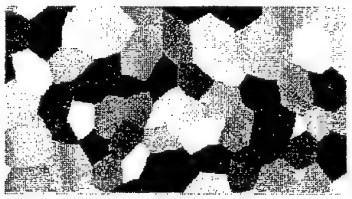

(a)

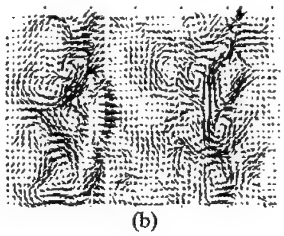

(b)

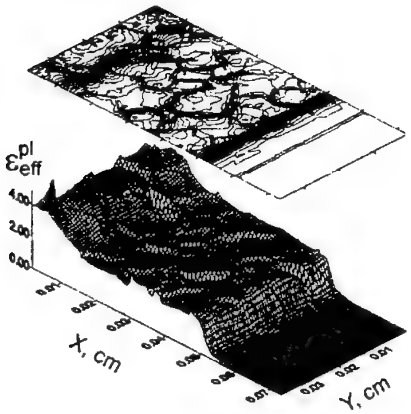

(c)

Figure 1. Simulation of shock and release wave propagation in a mesovolume of Al6061-T6: (a) polycrystalline map of the computation region, (b) velocity field, (c) contour lines and surface of plastic strain distribution.

In our numerical modeling of fracture, a crack is thought to propagate along the boundaries of computational grid cells, all of which are cohesive at the beginning. The crack growth is simulated by splitting the nodes of the computational grid and specifying the free-surface conditions on newly formed boundaries. The splitting of the grid nodes is realized providing the fracture condition is fulfilled. To simulate this process, we take both an instantaneous spallation criterion when the tensile stress becomes as much as a critical value in a local region:

$$\sigma \geq \sigma_0, \tag{1}$$

and a criterion which is based on the principle of linear damage accumulation

$$\int_{t_0}^{t_k} \left(\sigma_{eff} - \sigma_0\right)^{\lambda} \Phi^{-1} dt = 1, \qquad \sigma_{eff} > \sigma_0, \tag{2}$$

where Φ, σ_0, λ are material parameters.

Spalling cracks emerge in the region of the unloading wave generated upon reflection of the shock wave from the back free surface. The fracture of a heterogeneous medium at the mesoscale evolves as nucleation, growth, and coalescence of the multiple mesocracks. This process can therewith proceed simultaneously in different regions that is aided by a great number of stress concentrators. In heterogeneous materials, the intensity and duration of a pulse and the strength distribution among grains and grain boundaries govern the arrangement and orientation of cracks.

For the instantaneous spall fracture is located in a narrow region. Fig. 2 (a) depicts this pattern. When the damage accumulation criterion is used, the size of the fracture zone becomes wider as it depends on the pulse duration. Figure 2 (b) shows the distribution of mesocracks in the region where the heterogeneous material at issue fails completely. The non-simultaneous crack formation results in rotation of fragments attendant on the deformation of the material near the cracks. Part of the material in the fracture zone thus turns out to be completely fragmented.

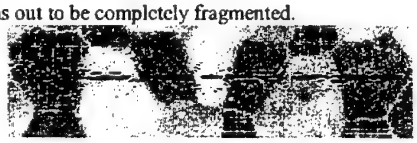

(a)

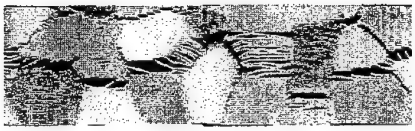

(b)

Figure 2. Fracture patterns in a mesovolume at spalling: (a) instantaneous fracture criterion is adopted; (b) damage accumulation is taken into account.

The difference in the yield and strength properties of the elements of the internal structure causes a host of cracks to emerge in the spallation zone. In calculations the parameters of the shock loading determine the fracture patterns at spallation. But in both cases a macrocrack is a result of coalescence of many mesocracks

Dynamics of Shear Stability Loss of Materials under Shock Wave Loading

V.A. Romanova, P.V. Makarov, R.R. Balokhonov, I.Yu. Smolin

Institute of Strength Physics and Materials Science, Tomsk, Russia

INTRODUCTION

An approach of physical mesomechanics, which has been developing by academician V.E.Panin's school [1,2] for about 10 yeas, considers a material under loading as a nonequilibrium self-organizing multilevel system. The bonding forces in the material under deformation are quite high and could not provide a simultaneous loss of shear stability over all cross section of the specimen. The plastic flow is thought of as a consecutive loss of shear stability on different scale levels: micro, meso and macro [2]. On the micro scale level the shear stability loss occurs in local zones of crystalline lattice that results in the dislocation generation, whereas on the meso scale level plastic shears generation in the local meso volumes of material results in formation of shear bands. The shear bands are main defects on the meso scale level. They appear near the stress meso concentrators of various physical nature [1,2] and provide a stress relaxation in the meso volumes. On the macrolevel a representative mesovolume loses the shear stability as a whole that corresponds to neck formation under quasistatic loading or, for instance, spalling effects under shock wave loading.

The main aims of the paper are (i) to construct phenomenological relaxation models to describe the shear stability loss of polycrystalline material under shock wave loading taking into consideration an evolution of dislocation continuum on microlevel and (ii) to formulate a criterion for beginning and development of plastic flow on the mesolevel, basing on the real physical processes, which occur in local meso volumes of material under loading.

MATHEMATICAL DEFINITION

To simulate the material deformation on various scale levels under shock wave loading we use a set of equations, which includes conservation laws and constitutive equations in relaxation form.

The subject under study is a mesovolume loaded by weak shock waves. In this case, heat effects are neglected and the medium may be considered as barotropic, that is, pressure $P = P(\rho)$ or $P = P(\theta)$,

where $\theta = \varepsilon_{ii}^e$, ρ is the mass density. Hence, the set of equations may be closed without the equation of conservation of energy (as the problems of dynamic elasticity). It is necessary, however, to note, that for this approach we have no information related to heat flow and temperature distributions. Based on the experimental data, equations of state have been constructed in [3] for a great number of materials. Constitutive equation for deviatoric stress in the relaxation form are as follows

$$\dot{\sigma}_{ij} = -\dot{P}\delta_{ij} + \dot{S}_{ij}, \quad \dot{S}_{ij} = 2\mu\left(\dot{\varepsilon}_{ij}^T - \frac{1}{3}\frac{\dot{V}}{V}\delta_{ij} - \dot{\varepsilon}_{ij}^p\right), \qquad (1)$$

where μ is the shear modulus; V is the specific volume; $\dot{\varepsilon}_{ij}^T$ are the total strain rates and $\dot{\varepsilon}_{ij}^p$ are the plastic strain rates.

The deformation processes under shock wave loading were simulated within one and two-dimensional formulations of the problem. Numerical solutions were performed in terms of Lagrangian variables using the finite-difference method of the second order of accuracy [1].

To define $\dot{\varepsilon}_{ij}^p$ the calculations of plastic flow on the micro- and mesoscale levels employed two various models:

* dislocation model for microdescription of plastic shears. Calculations were carried out within an one-dimensional formulation of the problem;
* 2D mesodescription of generation and propagation of shear bands on the mesolevel. We use here a new criterion of plasticity on the mesolevel.

MICROLEVEL DISLOCATION MODEL FOR CONTINUUM DESCRIPTION

For 1D formulation of the problem we can rewrite (1) in terms of main shear stress rate as follows: $\dot{\tau} = \mu(\dot{\varepsilon}_1^T - 2\dot{\gamma}^p)$. Here $\dot{\gamma}^p = \frac{1}{2}(\dot{\varepsilon}_1^p - \dot{\varepsilon}_2^p)$. Let us define the plastic strain rate as a flow of similar defects in the Orowan law: $\dot{\gamma}^p = |g| b N f v$.

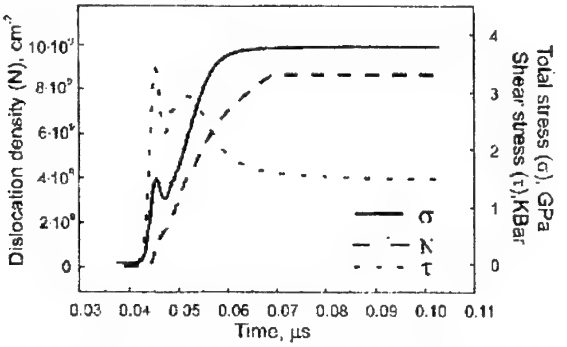

FIGURE 1. An evolution of dislocation density through the shock wave front of 3.7 GPa amplitude.

Since the movement of defects occurs mainly in the planes of maximum shear stress [4,5], the orientation factor $|g|$ in (2) is equal to 0.5. The expression for the dislocation density N was obtained in [6,7] and takes into account both the dislocation multiplication and heterogeneous dislocation nucleation, which occurs in areas of high gradient of shear stress. This model allows one to describe adequately an evolution of scalar dislocation density (Fig.1) through the shock and release wave fronts that results in a good agreement between the calculated and experimental data on elastic precursor decay and shock wave propagation.

MESO DESCRIPTION

To simulate the shear stability loss of representative mesovolume we solve 2D problem. For 2D and 3D calculations Eq. (1) is convenient to present in the form [9]

$$\dot{S}_{ij} = 2\mu\left(\dot{\varepsilon}_{ij}^{T} - \frac{1}{3}\frac{\dot{V}}{V} - \frac{1}{2\eta}\left(1 - \frac{\sigma_0'}{\sigma_{eff}}\right)S_{ij}\right). \qquad (3)$$

Here the viscosity function $\eta = \eta\left(\sigma_{eff}, \varepsilon_{eff}^{p}\right)$, where $\sigma_{eff} = 2\tau$ and $\varepsilon_{eff}^{p} = \frac{4}{3}\gamma^{p}$, was constructed forAL6061-T6 in [10], using the experimental data and profiles calculated by means of the above dislocation kinetics, and $\sigma_0' = \sigma_0'\left(\varepsilon_{eff}^{p}\right) = 2\tau_0'\left(\gamma^{p}\right)$ has a meaning of the current yield stress.

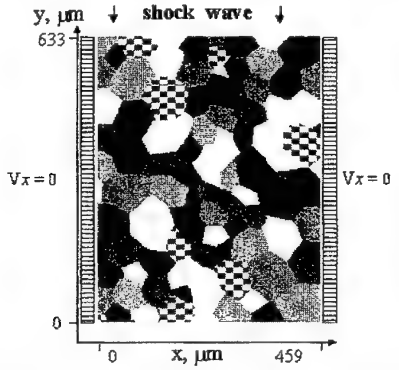

FIGURE 2. Schematic of mesovolume structures and boundary conditions for shock wave propagation

The subject under study is the polycrystaline mesovolume (Fig.2). We consider here the shock waves propagation of different amplitudes through the mesovolume, which is under all-round compression condition that corresponds to certain boundary condition (Fig.2). Calculations show that as the shock wave propagates away from the surface impacted, the shock front becomes progressively more gradual and wider due to development of plastic strain. Then the shock wave front involves mesofragments (grains and grain groups) as a whole into motion. The plastic strain on the mesolevel manifests itself as the rotation of mesostructure fragments and shear band formation (Fig.3.a).

To simulate plastic deformation mechanisms on the meso scale level, where stressed-strained state is essentially heterogeneous and plastic deformation develops in local zones [1,2], we have to take into account in the model a generation and development of plastic shears.

According to a great number of experimental results devoted to investigation of crystal plasticity on the mesolevel [1,2,9,10] there is a fact that generation of plastic shears in polycrystalline material occurs predominatingly from internal structure interfaces, for instance, free surfaces and grain boundaries. Basing on this fact we formulate a plastic flow criterion, that is a synthesis of conventional continuum approach and discrete one, which is widely used, for instance, in cellular automata method [1]. From this point of view a status of every element is consecutively defined for every step of calculation in accordance with some locally determined conversion rules, which control the cellular automata and can be written as: $\tilde{X}_{ij} = F\left(X_{ij}, \left\{X_q\right\}\right)$, (4)

where $\tilde{X}_{ij}$ are the current values of certain parameter of a net cell; X_{ij} are the values of the parameter for previous time step; $\left\{X_q\right\}$ is a variety of cells in the neighborhood of a i, j cell.

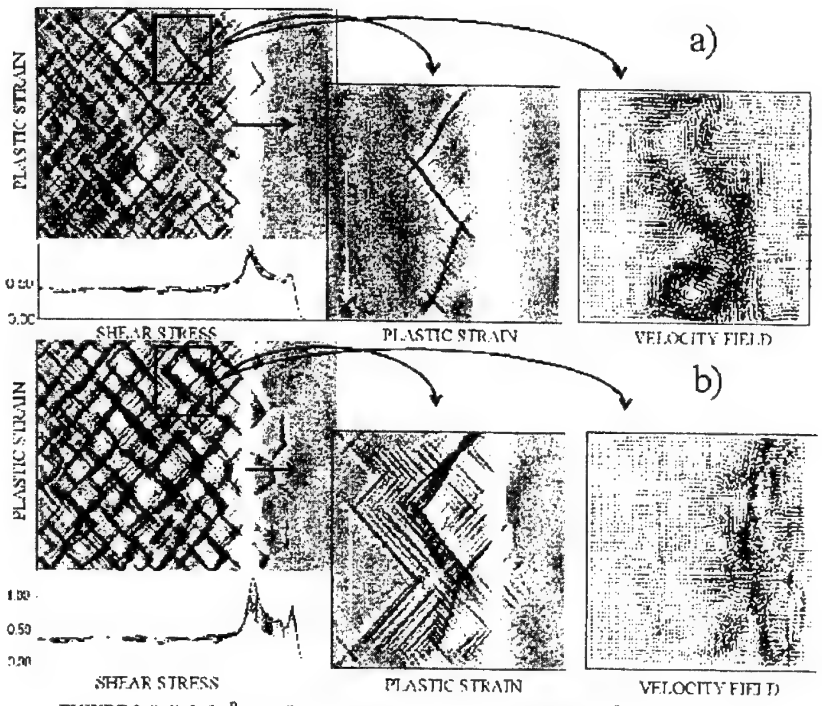

FIGURE 3. Relief of ε^p_{eff} profile of shear stress σ_{eff} and local pattern of ε^p_{eff} and velocity field for the case presented on Fig.2 and obtained using the conventional force yield criterion (a) and using new yield criterion (b).

In addition to well-known continuum force criterion we suggest a set of rules of elastic-plastic conversion for each net cell:

1) σ_{eff} has to achieve a critical value σ^*_0, which is different for various structure elements (free surface, grain, grain boundary, etc.). This condition is not sufficient.
2) Originally the plastic flow can arise only at the free surface or interfaces of crystal (grain boundary, boundary between the basic material and inclusion, coating, etc.), providing the condition 1 is fulfilled.
3) In other cells the plastic flow can arise if either σ_{eff} achieves theoretical shear strength σ^*_{cr}, or both the condition 1 is fulfilled and at least in one of the nearest cells an integral ε^p_{eff} has exceeded threshold value ε^p_{cr}.

Thus, when the rules 1,2,3 are fulfilled, there is a relaxation of shear stress in accordance with the law (3).

To compare the calculation results obtained, using different models, we carry out here the calculation of shock wave propagation through the representative mesovolume, which is presented in Fig.2. Figure 3.b shows deformation and velocity field patterns calculated, using the new criterion formulated above, to distinguish it from the type in Fig.3.a that uses maximum shear stress yielding criterion. It is clearly seen that the plastic strain in this case manifests itself as a local shear stability loss inside an individual grain that results in both higher level of shear stress and arising of many stretcher strain patterns, which form around grain boundaries and consecutively cover the grain.

CONCLUSION

To adequately describe the real shape of shock front and release wave on the macrolevel use was made of the dislocation model for defining the plastic strain rates. This model takes into account both dislocation multiplication and heterogeneous dislocation nucleation, which occurs in the areas of high shear stress gradient. Basing on this 1D calculation, we construct the relations for viscosity functions and use them to 2D simulate the deformation of representative mesovolumes. To simulate a generation and propagation of plastic shears, which are the main defects on the mesolevel, we formulate some additional rules to describe a beginning of plastic shears that allows one to model the formation of stretcher strain patterns inside an individual grain that results from high level of shear stress in shock front. This process corresponds to the local shear stability loss on the mesolevel.

References

1. *Physical Mesomechanics of Heterogeneous Media and Computer-Aided Design of Materials*, ed. by V.E. Panin, Cambridge Interscience Publishing, Cambridge, 1998.
2. Panin, V.E., *Russian Physics Journal*, ' 1, (1998).
3. Wallace, D., *Physical review B*. **22**, N4 1495-1502 (1980).
4. Gilman, J, «Microdynamical Theory of Plasticity», in *Microplasticity*, Metallurgiya, Publisher, Moscow, 1972, pp. 18-37.
5. Murr, L., and Kuhlmann-Wilsdorf, D., *Acta.Met.* **26**, 847-857 (1978).
6. Makarov, P.V., *J. Physics of Combustion and Explosion* **23**, ' 1, 22-29 (1987).
7. Makarov, P.V. Romanova, V.A. and Balokhonov, R.R., *Theoretical and Applied Fracture Mechanics* **28**, ' 2, 141–146 (1997).
8. Wilkins, M.L., *Methods in Computational Physics* **3**, 211-263 (1964).
9. Zhukova, T.V., Makarov, P.V., Platova, T.M., etc, *Physics of Combustion and Explosion*. **23**, ' 1, 29-35 (1987).
10. Makarov, P.V., Romanova, V.A., and Balokhonov, R.R., «Stress relaxation processes at mesoscale level in material mesovolume under shock wave loading,» in *New Models and Numerical Codes for Shock Wave Processes in Condensed Media-1998*, Conference Proceeding, 1998, pp. 860-867.
11. Malis, T., Lloyd, D.J., Tangri, K., *Physica status solidi(a)* **11**, '1, 275-286 (1972).
12. Murr, L.E., *Met. Trans.* Ser. A **6**, '3, 505-513 (1975).

Semiempirical Multi-Phase Equation of State for Carbon under Shock Loading

K. V. Khishchenko, V. E. Fortov, I. V. Lomonosov

Institute for High Energy Densities, Moscow, Russia

The description of the thermodynamic properties of matter over a wide region of the phase diagram is of fundamental as well as practical interest. The hydrodynamic simulation of shock-wave processes in condensed media calls for the equations of state for structural materials over the range from normal conditions to extremely high values of temperatures and pressures. Proper inclusion of phase transitions is important from the standpoint of numerical modeling of those processes.

We propose a new semiempirical equations-of-state model, which takes into account the polymorphs transformation, melting, evaporation and ionization effects. Wide-range equation of state for graphite–diamond–liquid carbon system is constructed on the basis of model developed.

Calculation results are compared with available experimental data in a broad region of the phase diagram. The most essential shock-loading and adiabatic-release experiments are described.

The multi-phase equation of state obtained can be used efficiently in calculations of the thermodynamic characteristics of carbon when solving applied problems.

Construction of Multi-Phase Equations of State

V.V. Dremov, A.L. Koutepov, E.E. Mironova, A.V. Petrovtsev, A.T. Sapozhnikov

Russian Federal Nuclear Center - Institute of Technical Physics, Chelyabinsk-70, Russia

Most of substances in the region of condensed state have rather complex phase diagram composed of liquid and solid phase polymorphous modifications stability regions.

When loading (static or dynamic) and subsequent release the substance undergoes phase transitions accompanied by sudden changes of density, energy absorption or release and etc.

Successful modeling of such processes requires three basic components: the computer code for continuum dynamics treatment; the multi-phase equation of state; the model of phase transitions kinetics.

Here we concern some aspects of the second component construction. Speaking of the multi-phase equations of state we restrict ourselves by the phase diagram region corresponding to condensed state leaving beyond phenomena of evaporation and ionization.

When constructing multi-phase EOS we take results of *ab-initio* calculations and experimental data in the regions of our interest as a ground.

It should be noted that information on the phase diagram layout obtained from experimental data is more or less reliable at low pressures. Degree of uncertainty grows as pressure and temperature increase. At high pressures and temperatures shock wave experiments are the only source of such information. Data on phase diagram in such experiments are shaded by kinetic processes, which in its turn depend on the condition of the experiment.

When constructing equations of state the physical models are used which may have rather complex mathematical form and can't be used directly in the continuum dynamics calculations. So, it is reasonable to transform the EOS into tabular form. Requirements to the tabular form become tougher so as small error in approximation of thermodynamic properties may lead to dramatic change in the phase diagram layout.

In the paper approaches to multi-phase equations of state construction have been considered. Helmholtz free energy for solid phases is written as a sum of several terms corresponding to static lattice potential, lattice phonon free energy, magnetic term and free energy due to thermal excitations of electrons. The last term instead of traditionally used square law is determined using Fermi-Dirac statistics and the one-particle spectrum of a crystal calculated for T=0K. Lattice contribution is described by Debay model or high-temperature expansion of Debay model and static potential is an approximation of ab-initio calculations and experimental data on static compression. To evaluate the equation of state for a liquid phase we used Grover model and variational perturbation theory. To enhance an efficiency of the equation of state use in continuum dynamics calculations it is converted into tabular form.

Equations of state of carbon, iron and chlorine substituted methane compounds are considered as the examples. Obtained results are in good agreement with thermophysical, phase boundary and shock wave measurements. Up-to-date ideas about layout of iron phase diagram at high pressures and temperatures have been discussed.

Mesoscale and Loading Properties of the Spall Strength of Copper

J. Cazamias, R. Minich, A. Schwartz

Lawrence Livermore National Laboratory, Livermore, CA, USA

We have carried out a systematic study to quantify the effects of specific microstructural features on the spall behavior of 99.999 (3 different grain sizes) and of [001] single crystal (pure and with silica inclusions) Cu. The samples were shocked with Cu flyers at velocities from 160 to 1,800 m/s using a 35-mm gas gun. VISAR measurements of the free surface velocity were used to characterize the spall pullback signal and details of the ringing.

The velocity time histories are modeled with an explicit 1-D finite difference hydrocode that includes *dislocation based rate dependent strength model*. The nucleation and growth of microvoids is modeled using a time dependent Landau-Ginzburg equation with void volume fraction as the order parameter. The Landau-Ginzburg free energy functional takes into account nucleation and growth and stress relaxation and also leads to a scaling relationship between stress and the order parameter.

The scaling exponents are chosen in the model to be consistent with experimentally observed spatial correlations of the order parameter. Grain size dependence is taken into account in the dislocation-based model through the athermal contribution to the flow stress.

Numerical Model for Simulation of Stress Relaxation in Solids

V.A. Bychenkov, L.V. Khardina

Russian Federal Nuclear Center, Snezhinsk (Chelyabinsk-70), Russia

Nature abhors shear stress. In absence of motion stress tensor relaxes to spherical one. This is the basic postulate governing the development of all models of solid kinetics. The widely known Maxwell model of elasto-plastic medium is among them. In absence of motion it can be written in the form:

$$\dot{\sigma}_{ij} = -S_{ij}/\tau, \qquad (1)$$

where σ_{ij} is stress tensor, S_{ij} – its deviator term, τ – relaxation time. Relaxation time is usually considered to be a constant. However, in recent models time is often and often a function of medium state (works of E.I. Ramensky, P.V. Makarov and others).

Another approach is proposed to formulate laws of solid behavior. It relies on analysis of data on kinetic strength theory, specifically, on concepts of the dilation thermofluctuation theory being developed by S.N. Zhurkov, V.A. Petrov (St. Peterburg) and A.A. Gornovoy (Snezhinsk). Consider a body subjected to tensile stress σ. The body is capable of withstanding the load σ during the time τ (σ). In compliance with Zurkov's classic kinetic equation it is written as

$$\tau = \tau_0 \exp\frac{U_0 - \gamma\sigma}{RT}, \qquad (2)$$

where T is temperature and τ_0, U_0, γ, R are constants. Following theoretical concepts of A.A. Gornovoy durability equation becomes more complicated with an implicit dependence of τ on σ[1]:

$$\ln\frac{\tau}{\tau_0} = \frac{T_0}{T}\left[\varepsilon - \frac{\sigma}{\sigma_0}\tau^{\beta}\right], \qquad (3)$$

where β is a constant and ε is density function. A.A. Gornovoy proposed a likewise equation for kinetics of elastic forerunner attenuation that has allowed description of some experimental data on behavior of metals. When differentiating Eq. (2) or (3) with respect to the time τ, it is easy to see that these equations describe free stress relaxation (in absence of motion and heat flow). Thus, we can write the relaxation equation in the form:

$$\sigma = \sigma(\tau,...), \qquad (4)$$

where the time τ should be considered as the time of stress relaxation from a maximum achievable value to the given value σ. One can easily see the kinetic equations (1) and (4) to differ qualitatively. Eq. (4) does not directly relate to pressure relaxation and is written in an algebraic form.

We propose that time-varying stresses be considered in the course of two parallel processes: deformation and relaxation. Deformation is described by laws of quasi-elastic change of stresses. Relaxation laws are formulated in the form (4) where σ is: ultimate tensile stress; or the 2-nd invariant of stress tensor; or pressure if medium is porous. Gradual destruction of material is described as a process of accumulation of microdamages.

Specifically, the flow law of stress tensor deviator in approximation of isotropic body can be written in the form of Prandtl-Rice:

$$\dot{S}_{ij} + \lambda S_{ij} = 2\mu\dot{e}_{ij}, \qquad (5)$$

where μ is shear modulus, $\dot{e}_{ij}$ - deviator of deformation rate tensor, λ – dissipation function, rotational term is omitted. Analysis of different kinetic models of shear strength displays that they all can be basically described by the flow law (5) with the dissipation function of one of the two forms:

$$\lambda = \dot{I} / J \tag{6}$$

or

$$\lambda = -\dot{J}_* / J_*, \tag{7}$$

where I, J are the second invariants of tensors of plastic deformation and stress rates, respectively, $J_*(t)$ is the law for free relaxation of J. Eq. (6) is typical for dislocation models while Eq. (7) is for thermofluctuation ones. Eq. (7) can be also written in the form:

$$\lambda = 1 / \tau(J_*), \tag{8}$$

where $J_*=J$. Eq. (8) can be also interpreted as the Maxwell model of elasto-plastic body with non-linear dependence of the relaxation time τ on state. To determine this dependence one can specifically use the dislocation concepts on kinetics of plastic deformation, then both the approaches (6) and (7) actually coincide.

VNIITF developed a technique for numerical simulations of 1D and 2D elasto-plastic flows [2,3]. It is used for dynamic problems of solid mechanics with typical times within $\sim 10^{-6} \div 10^{4}$ s. That is the reason why it is not necessary to determine the relaxation law for far times. We introduce a concept of quasistatic limits σ_0 (strength, fluidity, pressure in porous material) and assume satisfied the relaxation law of associated stress σ in the form

$$\sigma = \sigma_0 \cdot f_\sigma(\tau), \tag{9}$$

where $f_\sigma(\tau)$ is a decreasing function of the time τ. Thus, we assume valid separation of variables in the relaxation law: the quasistatic limit, which depends on pressure, temperature, plastic deformation and other thermodynamic parameters, is multiplied by the relaxation function, which depends solely on time. The simplest from of the relaxation function was derived to be as follows:

$$f_\sigma(\tau) = 1 + (\tau_0 / \tau)^{\beta}, \tag{10}$$

where τ_0 and β are constant and positive. Eq. (10) related to the relaxation law for tensile stress σ and the Beily destruction criterion

$$\int \frac{dt}{\tau(\sigma)} = 1$$

actually satisfy the empiric criterion of Tuler-Butcher [4]:

$$\int \left(\frac{\sigma - \sigma_0}{\sigma_0} \right)^{\gamma} \frac{dt}{\tau_0} = 1$$

Generally, the function $f_\sigma(\tau)$ should be tabulated. This specifically allows describing the law of superplastic deformation of metal alloys. An explicit difference scheme is used for elastic-plastic flows. It is similar to that one of the known Wilkins technique [5]. Stress calculating procedures are implemented in likewise manner. Fist we determine stress change in elastic approximation. Then the stresses exceeding values of quasistatic limits relax following the law (9). It should be noted that the allowance for stress relaxation kinetics places a restriction on step of the spatial mesh. The time of perturbation propagation through mesh must not exceed that of stress relaxation to the level of interest. Specifically, for the law (10) we can derive the following approximation of the step h:

$$h < \tau_0^{\frac{\beta}{\beta+1}}, \qquad (11)$$

where [h] = mm, [τ_0] = μs. Eq. (11) defines h to vary within the range from ~ 1 to 0.1 mm.

Figures 1,2 show calculated results that demonstrate the evolution of plane wave fronts in quartzite for different amplitudes of loading impulse and quasistatic and dynamic curves of porous iron compression.

Calculated results are in a good agreement with the experimental data available. Note rather complicated character of wave profiles. For the loading impulses lower than 10 -15 GPa, a three-wave configuration implements in general. Forerunner amplitude attenuates with distance. Forerunner is followed by the compression wave. Width of the plastic wave front is finite. Calculations were performed for the following values of parameters of the relaxation function (10):

- $\tau_0 = 2.5 \cdot 10^{-15}$ s, $\beta = 0.111$ that corresponded to the dynamic yield point for quartzite;
- $\tau_0 = 10^{-7}$ s, $\beta = 1$ that corresponded to the dynamic yield point for steel;
- The dynamic pressure limit in porous iron was described by a function somewhat more complicated than Eq. (10). We assumed $\beta \approx 0.1$.

The technique developed was successfully applied to some other dynamic problems, specifically, to describe the motion of spherical and cylindrical envelopes.

In conclusion it is necessary to note the following. Brittle destruction and deformation hardening of solids are simulating with the functional dependence of quasi-static yield stress vs. pressure, temperature and plastic deformation. Baushinger effect described by dependence of shear modulus vs. quasi-static yield stress, second invariant of stress tensor and loading characteristic.

References

1. A.A.Gornovoy, E.A.Kozlov, A.K.Muzyrya, E.V.Shorokhov, Rus. *J. Physics of Combustion and Explosion (FGV)* 1, 142-144 (1989).
2. V.A.Bychenkov, K.E.Vasilchenko, A.A.Gornovoy, Rus. *Problems of Atomic Science and Engineering (VANT), Series Mathematical Modeling of Physical Processes* 1-2, 9-12 (1995).
3. V.A.Bychenkov, V.F.Kuropatenko, L.V.Khardina, Rus. *News of the Chelyabinsk State University, Physics, Series* 6 1, 14-26 (1997).
4. Tuler F.R., Butcher B.M., *Int. J.Fract. Mech.* 4, 431-437 (1968).
5. Wilkins M., "Calculation of Elastoplastic Flows" in: *Computational Methods in Hydrodynamics,* Mir, Moscow, 1967, pp. 212-263.

SESSION "Mechanisms of Shock Wave Processes at Mesoscale-Level"

Chairmen:
M. Baer - Sandia National Laboratories, Albuquerque, USA
P. Makarov - Institute of Strength Physics, Tomsk, Russia

Physical Mesomechanics Approach as a New Base for Numerical Modeling of Plastic Flow and Fracture of Solids under Shock Wave Loading

P.V. Makarov

Institute of Strength Physics and Materials Science, Tomsk, Russia

By now Physical Mesomechanics of materials has been developed as a new scientific trend that considers plasticity and strength of solids on the base of taking into account their real internal structure.

This trend is based on advanced achievements in physics of plasticity, experimental and theoretical materials science and mechanics of solids.

Hierarchical models of plasticity and fracture of solids developed in the framework of the trend allow one to take into account effectively an internal structure of materials and to obtain both averaged macro-data and local values of parameters of deformed material.

Physical Mesomechanics approach, as applied to problems of shock wave loading of solids, makes it possible to study these problems on the different structural levels (micro, meso and macro). This approach allows us to take into consideration both the structural heterogeneity of different scales and fluctuations of flow parameters from the averaged macro data. This is required for the development of realistic dynamic theories of plasticity and fracture of shock wave loaded solids.

Physical Mesomechanics approach is based on the following main principles:

1) materials under loading are considered as hierarchically organized systems of structural elements of different scales, in which plastic deformation develops as a consecutive and interrelated process of the shear stability loss of materials at the different scale levels: micro, meso and macro;

2) primary mechanisms of plastic flow at the meso level are the formation of dissipative substructure, fragmentation of deformed materials and formation of new interfaces;

3) scheme of deformation at the meso level is "shear plus rotation", which provided by bulk structural elements of mesoscopic scales;

4) interfaces between structural elements play a key role in the nucleation and development of plastic shear at the mesolevel,

5) plastic deformation is considered as a relaxation process.

For the computer simulations of plastic flow in shocked solids these basic principles were used, as applied to existing models and to newly developed ones as well. Numerical technique used combines both continuum mechanics and discrete cellular automata methods.

Meso-level plays a crucial role in the Physical Mesomechanics approach. Objects of investigations are meso-volumes of deformed material, and all essential for simulation of plastic deformation elements of internal meso-structure (grains, grain boundaries, hard inclusions etc) are treated explicitly.

By this means the representative meso-volume is a macro particle of deformed material at the macro-level. The behavior of representative meso-volume under loading is equivalent to behavior of material as a whole. The deformation of structural elements at the meso-scopic scale is provided at the micro-level. Micro-level is a level of dislocation continuum in the presented approach. Plastic deformation is interpreted from a continuum view point at the micro-level. It is not the individual structure defects but dislocation continuum that falls under consideration. Such description is needed for the following simulation of plastic flow at the meso- and macro-levels.

The structure of shock wave fronts in metals is considered depending on grain sizes and their physical and mechanical characteristics. Also, studied are the other important features of shock wave loading: heterogeneity of plastic flow on the meso-level and localization of plastic deformation; rotations of different fragments (part of grains, whole grains, grain conglomerates); nucleation and development of localized plastic shears on free surfaces and different interfaces.

It is shown that the development of systems of conjugate bands of localized deformation of different power and the formation of blocks of different sizes are basic features of plastic deformation of polycrystalline materials. These processes begin already in front of shock wave and finish in unloading wave at the plastic spread of shock wave loaded material.

Towards Linking Mesoscale to Continuum Level Descriptions of Shock-Loaded Porous Materials

M.R. Baer

Sandia National Laboratories, Albuquerque, New Mexico, USA

Recent numerical simulations and experimental studies have revealed that highly structured waves are associated with impact-loaded heterogeneous materials. It is observed that shock response includes highly fluctuating states and localization effects due to the interaction of multiple waves and deformation at material boundaries. These features have also been experimentally observed using a line-imaging interferometer technique for impact onto a thin porous layer of granular sugar crystals. The focus of this study centers on interrogation of the extensive numerical data from mesoscale simulations. Detailed wave fields are probed using imaging and averaging techniques to determine statistical and mean properties of the shock fields. These methods provide distribution information that is needed toward developing new continuum-level descriptions of shock-loaded heterogeneous materials.

A ROLE OF ENERGY EXCHANGE IN MULTISCALE PROCESSES OF DYNAMIC PLASTICITY AND FRACTURE

YU.I. MESCHERYAKOV

Institute of the Mechanical Engineering Problems, Saint-Petersburg, Russia

Coupling between microstructure features of a material and its macroscopic response on impact is still poorly understood both qualitatively and quantitatively. This is due to commonly used wrong approach when one tries to link the resulting macroscopic response with the microstructure data obtained *after* dynamic loading. In reality, adequate modeling of dynamic processes should be based on the microstructure kinetics data obtained in real time, i.e. *during* dynamic processes. This requires that experimental technique at hand could register not only a macroscopic response of specimen on impact (such as the time-resolved free surface velocity profile) but also kinetic characteristics of internal structure, which provide a current information about scale and relative mobility of structure elements. Since the motion of structure elements in heterogeneous medium has a specifically stochastic nature, their kinetics should be interpreted in terms of a velocity distribution function or its statistical moments. The first statistical moment is known to be a mean mass velocity. It characterizes flux motion of medium with mean velocity u. Random character of the mass velocity reflects the second statistical moment – mass velocity dispersion D.

In considering the microstructure aspects of dynamic deformation it should be confessed that experimentally determinable kinetic characteristics to date are those belonging to the mesoscopic scale level which occupies an intermediate position between atom-dislocation and macrolevel. However, as distinct from the quasistatic situation, in dynamically loaded medium mesolevel cannot be considered as a completed structure. It is specifically transient structure where both a scale of structure element and energy capacity of mesolevel currently change. The latter assertion has important consequences which should be taken into account in deriving the criteria of dynamic fracture.

Firstly, in the well-known Grady's analysis of spallation [1] the process of dynamic fracture happens under steady conditions. Spallation is energetically permissible if the sum of kinetic and elastic energy is at least as large as the fracture surface energy. In accordance with [1], kinetic energy spent on spallation 15 times smaller than potential energy. However, experimental study of spallation performed in the present work and theoretical analysis [2] show that this assertion appears to be valid only for the steady processes. As for unsteady processes, the role of local kinetic energy in dynamic fracture may be increasingly important. There is experimental evidence that mean mass velocity at the plateau of compressive pulse may decrease by 30 - 50 % [3] . Owing to energy balance the increase of local kinetic energy leads to decrease of stored elastic energy, which is possible only in case of decreasing the local potential. This results in decrease the critical spall strength.

SESSION "Mechanisms of Shock Wave Processes at Micro-Level"

Chairmen:
V. Dremov - **Russian Federal Nuclear Center, Chelyabinsk-70, Russia**
T.Germann - **Los Alamos National Laboratory, USA**

Large-Scale Molecular Dynamics Simulations of Shock-Induced Plasticity, Phase Transformations and Detonation

T.C. Germann, B.L. Holian, K. Kadau, P.S. Lomdahl, J.-B. Maillet*

Los Alamos National Laboratory, Los Alamos, USA
**CEA/DIF, Bruyeres-le-Chatel, France*

Molecular dynamics simulations can be used to directly probe the response of matter to shock loading and unloading. Using modern computers, routine multimillion-atom simulations using realistic interatomic potentials are possible, providing insight into the underlying atomistic processes. A variety of shockwave phenomena in solids have been investigated, including plasticity, spallation, ejecta formation, diffusionless phase transformations (both solid-solid and melting), and detonations. We will discuss the capabilities and limitations of such simulations, focusing on two particular systems which we have recently studied: the bcc-to-hcp transformation of solid iron, and the shock-to-detonation behavior of model energetic materials.

The transformation pathway and kinetics of the alpha-to-epsilon polymorphic phase transformation of solid iron is found to depend strongly on the crystallographic orientation. Shock initiation in the [001] direction leads to a steady-state pattern of hcp twins a short distance behind the shock front, whereas the [011] direction forms a more complex and smaller-scale nanostructure which anneals over timescales much longer than the several picoseconds of our simulations. With the recent advances in ultrafast (sub-picosecond) X-ray diffraction of laser-shocked samples, direct experimental confirmation of this behavior using high-quality single crystal targets is hoped for in the near future. A more limited set of simulations have also been performed using polycrystalline samples, where heterogeneous nucleation at grain boundaries lowers the transformation threshold. How the averaging over grains and wave scattering off of grain boundaries lead to a steady-state in polycrystalline samples is an important open question which is currently being studied.

For the model "nanodetonics" system, we are using a REBO model potential describing a diatomic AB molecular crystal which can decompose by the exothermic chemical reaction 2 AB -> A2 + B2. We have investigated both homogeneous perfect-crystal behavior, including shock Hugoniots and critical width (2-D) or diameter (3-D) effects, as well as heterogeneous behavior such as hot spot initiation. Whereas point defects such as vacancies or isolated radicals have no apparent effect on the initiation threshold, a marked reduction in the critical pressure is found with even a single 10 nm diameter void. These simulations also give a great deal of insight into mechanisms by which void collapse can lead to initiation.

Molecular Dynamic Simulation of the Effect of High Rate Deformation upon Materials Microstructure

V.V. Dremov, M.S. Smirnova, A.I.Ryazanov*

Russian Federation Nuclear Center – VNIITF, Snezhinsk (Chelyabinsk-70), Russia
* *Russian Research Center "Kurchatov Institute", Moscow, Russia*

Microstructure response to dynamic loading may be very complicated. Here we present results of 3D molecular dynamic simulation of defects (vacancies and dislocations) generation in copper (fcc) and iron (bcc) samples put under high-rate deformation. Changes in mechanical properties as well as the defects generation rate as functions of the initial temperature and the strain rate have been investigated.

To investigate the processes we used samples constructed of up to 10^6 atoms arranged initially in fcc and bcc lattice having the form of parallelepiped $n_1a \times n_2a \times n_3a$, where a -- lattice constant. Various types of boundary conditions were used. The well-known Verlet leap-frog algorithm [1] was used for numerical integration of the motion equations. Embedded Atom Model (EAM) potential [2,3] describes the interaction between atoms.

We investigate the following types of dynamic loading: shock compression, stretching and shear. Dependence of microstructure response upon crystallite orientation relatively to loading axis was also of our concern.

It was found that when stretching at high deformation rate in the bulk of the sample once appeared vacancies tend to nucleate and grow in the form of almost spherical 'bubbles'. A vacancy should be formed before the 'bubble' starts to nucleate. Thermal fluctuations may provide the necessary atomistic mechanism of the vacancy generation in single crystal in the absence of grain boundaries and any other inoculants. The strain rate and boundary conditions affect the process as well. Fig.1 shows the fragment of the sample containing two 'bubbles' just before they merged in further evolution.

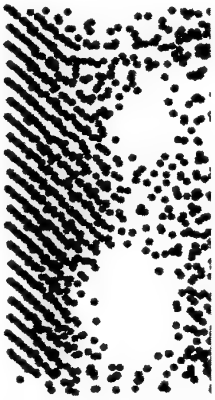

Figure 1. **Fragment of the copper sample.** Vacancies nucleation when stretching loading.

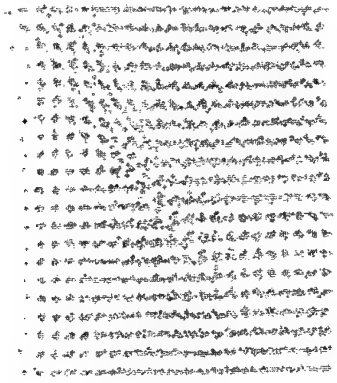

Figure 2. **Fragment of the copper sample.** Plastic deformation behind shock wave.

In numerical experiments on shock compression the fine structure of shock front has been investigated. Features of elastic-plastic transformations in fcc and bcc structures have been discussed. The fragment of fcc sample undergoing plastic transformation behind the shock wave is shown on the Fig.2. Generation rate of stacking faults as a function of strain rate has been investigated. Obtained results have been compared with those reported in [4,5] for fcc lattice with Lennard-Jones 6-12 potential.

References

1. D.W.Heerman Computer simulation methods in theoretical physics. Springer-Verlag 1986.
2. R.A.Johnson, Phys.Rev., B37 (8), p.3924
3. V.Shastry, and D.Farkas, Molecular Statics Simulation of Crack Propagation in alpha-Fe Using EAM Potentials , MATERIALS RESEARCH SOCIETY SYMPOSIUM PROCEEDINGS
4. B.L. Holian, P.S. Lomdahl, Science, v.280, pp.2085-2088.
5. T.C. Germann, B.L. Holian, P.S.Lomdahl, in Shock Compression of Condensed Matter –1999. Ed. by M.D. Furnish, L.C. Chhabildas and R.S. Hixon, pp.297-300.

Molecular Dynamics Simulation of the Melting Process of Some Metals in Strong Shock Waves

A.A. Selezenev, V.K. Golubev, A.Yu. Aleinikov, O.I. Butnev, R.A.Barabanov, B.L. Voronin

Sarov Open Computer Center, Sarov (Arzamas-16), Russia

Introduction

To determine and predict the melting point during the shock wave loading of metals is one of the most interesting and actual problems of shock wave physics. Along with experimental [1-4] and theoretical [5-9] methods of studying metal melting in shock waves (SW), the molecular dynamics (MD) modeling technique has a certain research potential [10, 15, 16]. The MD technique successfully combines the elements of numerical experiment with theoretical approach. Probably, it may be one of the alternative methods to study phase transitions in shock waves. A minimum number of assumptions (interaction potentials and equations of movement) accepted for the MD technique is also one of the advantages of this method.

For the first time the MD technique was used to study the SW structure within solid matter that is referenced in articles [11-13]. Besides, these publications describe the methodology of a numerical MD experiment to find out data on the structure of a shock wave jump. The initial intended use of the MD technique for investigation of solid matter melting in shock waves was made in the article [14]. Solid argon was taken as a testing material. In the article [14] it was obtained the dependence of temperature of shock-compressed argon upon the working pressure value. In publications [15,16] the MD technique was used to study the melting of such metals as Al, Cu, Pd, Pt. The dependence of melting temperature upon the static pressure value was calculated in these works for every metal. The numerically obtained dependencies of melting temperature upon the static pressure were compared with the P-U diagrams of shock compression of metals. Based on such a comparison there were determined the values of pressure and temperature behind the shock wave front at which the melting of metals took place. However, the approach of the works [15-16] does not take into account one particular feature of the process of shock wave compression. The condensed matter state behind the shock wave front may differ from the state of uniform volumetric compression. Just behind a planar shock wave front it is realized the state of one-dimensional strain, therefore a material elementary volume is subject to the effect of both normal and shear stresses [17]. In the work [9] it is shown that shear stress may influence on the parameters of material melting.

Numerical Experiment Formulation

As for the present work, the process of melting of such metals as Al, Cu, Pb, Pd, and Pt in shock waves was studied using the method of direct molecular modeling. Such an approach directly takes into account the influence of the particular features of shock wave compression upon the parameters of material melting. The computational MD cell presented a parallelepiped with the larger size which was equal to 35 periods of the crystal lattice and the transversal sizes which were equal to 10 periods. To verify the reliability of the results, the part of computations were performed using a larger cell, with the longitudinal and transversal sizes of 150 and 10 lattice periods respectively. The metal atoms were located in the nodes of a face-centered crystal lattice with the period corresponding to the metal state under normal conditions. The Morse potential was used for the description of interatomic interaction. The parameters of the potential were chosen coming out of the condition of correspondence between computational and experimental values of several physical properties of the materials [18]. In the work [19] it is shown that if the metal density increases under compression, the potential which was obtained using the embedded atom method is described quite well by the Morse potential. That is why the latter was chosen to describe the state of matter behind the shock wave front.

The shock wave was propagating along the direction of the larger parallelepiped's side (i.e. along the crystallographic direction {100}). It was generated by presetting the particle velocity of the atoms at one of the front surfaces of the considered parallelepiped. Along the directions perpendicular to the direction of SW propagation there were preset periodic boundary conditions. To calculate the parameters

of the matter state behind the shock wave front, in the computational MD cell there were marked out elementary volumes (containing 150-200 atoms). Within these volumes the following parameters were calculated: temperature, particle velocity, normal and tangential stresses, pressure, and the radial distribution function. The wave velocity was determined using the difference of arrival times for chosen elementary volumes and the initial distance between them. To determine the point of material melting in the shock wave, it was calculated the dependence of temperature of a shock-compressed material upon the material particle velocity in the shock wave. The analysis of the matter state behind the shock wave front was made with the help of the radial distribution function. In the work [20] it was demonstrated that the use of the radial distribution function in the context of MD modeling allowed an efficient analyzing of some features of condensed matter restructuring behind the shock wave front. In our calculations the plot of the radial distribution function also reflected the structural changes of the crystal lattice as well as disappearance of a far order in case that the material was melting behind the shock wave front.

The use of modern visualization tools [21] for the MD modeling allowed creating computer films, which serve to visualize and fix the process of material melting in shock waves.

MD Simulation Results

In the present work there were compared the computational and experimental D-U and P-U [22] diagrams obtained for the investigated metals. Fig. 1 illustrates the dependence of pressure in the shock-compressed aluminum upon the particle velocity obtained at MD modeling (markers). The pressure in the shock-compressed material was determined on the moving piston, which generated the shock wave. The solid line represents the dependence which was calculated on the base of the experimental D-U diagram from the work [22].

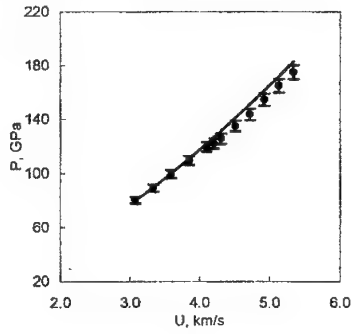

Figure 1. Dependence of shock-compressed aluminum pressure upon particle velocity.

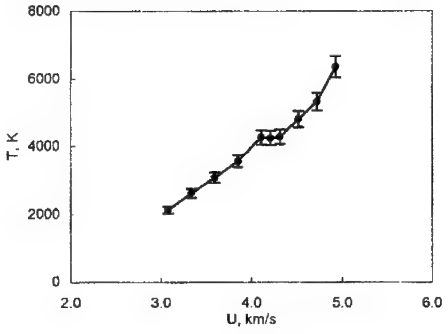

Figure 2. Temperature dependence of shock-compressedaluminum upon particle velocity.

To determine the melting temperature of the shock-compressed aluminum, it was calculated the dependence of the steady-state temperature behind the shock wave front upon the particle velocity. The obtained dependence is shown in Fig. 2. The characteristic salient point at the temperature dependence corresponds to the particle velocity value which is remarkable for the beginning of the aluminum melting.

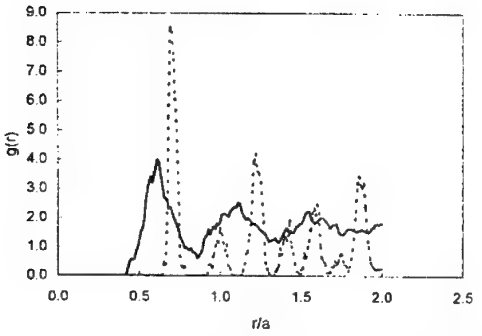

Figure 3. Radial distribution functions for aluminum under ambient conditions (the dotted line) and shock-compressed aluminum under the pressure of 135 GPa (the solid line).

Using the MD technique, there were calculated the radial distribution functions for aluminum under normal conditions (dotted line), as well as for aluminum behind the shock wave front (solid line) with the particle velocity of 4.62. km/s, which are shown in Fig. 3. The form of the radial distribution functions behind the shock wave front corresponds to the liquid state of aluminum.

In Fig.4 there are shown the frames from the computer film that was made on the base of modeling results. Fig. 4 reflects the configuration of the atoms within the marked out volumes of the MD cell when shock waves of different intensities pass through the cell.

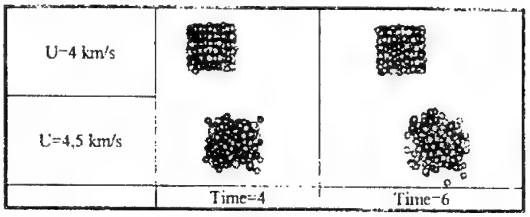

Figure 4. The character of atoms distribution within the marked out microvolumes behind SW front under the melting conditions and under preserving the lattice structure

Thus the analysis of the obtained results shows that the melting of aluminum in shock waves occurs in the particle velocity range of 4.1-4.3 km/s, which corresponds to the pressure range of 120-130 GPa and the computational temperature about 4100 K. The results of direct MD simulation do not contradict to well known experimental [3, 4] and theoretical [5, 6, 15] data. In the work [5] the thermodynamic analysis technique was used to show that aluminum melting in SW might be expected at the particle velocities of higher than 4 km/s that corresponds to the experimental data. In the works [6, 15] it was also theoretically revealed that the aluminum melting might be expected in the pressure range of 120-155 GPa. The experimental results [3,4] outline the melting interval for aluminum within the particle velocity range of 4.1-4.2 km/s. Thus the method of direct MD simulation of aluminum melting in the shock wave did not lead to a fixation of any tangible influence of the stress-strain state character upon the parameters of melting. The considered method was also used to determine the parameters of the shock wave induced melting for such metals as Cu, Pb, Pt, Pd. The MD results were compared to other well-known experimental and theoretical data.

References

1. Al'tshuler, L.. V.. Kormer, S. B., Bakanova, A. A. and Trunin, R. F., JETP **11**, 573 (1960). [in Russian]

2. Ternovoi, V. Ya., Fortov, V. E., Kvitov, S. V., and Nikolaev D. N., "Experimental Study of Lead Critical Point Parameters," in *Shock Compression of Condensed Matter-1995,* edited by S.C. Schmidt and W.C. Tao, AIP Conference Proceedings 370, New York, 1995, pp. 81-84.
3. Lalle, P., Courchinoux, R., "Melting on The Hugoniot," Ibid., pp.207-210.
4. Chhabildas, L. C., Furnish, M. D., and Reinhart, W. D., "Time-Resolved Wave-Profile Measurements at Impact Velocities of 10 km/s," in *SWCM –1998*, edited by A. L. Birukov at al., Conference Proceedings, Saint – Petersburg, 1998, pp. 192-195. [in Russian].
5. Urlin, V. D., JETP **49**, 485 (1965). [in Russian]
6. Moriarty, J. A., Young, D. A., and Ross, M., Phys. Rev. B **30**, 578 (1984).
7. Lomonosov, I. V., and Fortov, V. E., "Look Into Liquid Phase of Metal from the Equation of State: is There an Agreement between Shock-Wave and Isobaric-Expansion Data ?" in *Shock Compression of Condensed Matter-1995,* edited by S.C. Schmidt and W.C. Tao, AIP Conference Proceedings 370, New York, 1995, pp. 51-54.
8. Robinson, C. M., "A Multi-Phase Equation of State for Solid and Liquid Lead," in *SWCM-2000,* edited by A. Yu. Dolgoborodov at al., Conference Proceedings, Saint – Petersburg, 2000, p. 123. [in Russian].
9. Podurets, M. A., Teplofiz. Visok. Temper. **38,** 895-901 (2000). [in Russia].
10. Holian, B. L., Shock Waves **5**, 149-157 (1995).
11. Paskin, A., and Dienes, C. J., J. Appl. Phys. **13**, 1605 (1972).
12. Tsai, D. H., and McDonald K. A., J. Phys. Ser. C **6**, L171-L175 (1973).
13. Klimenko, V. Yu., and Dremin, A. N., Dokl. Akad. Nauk USSR **251**, 1379-1381 (1980).
14. Belonoshko, A. B., Science **275**, 955-956 (1997).
15. Jeong, Ji-W., Lee, In-H., and Chang, K. J., Phys. Rev. B **59**, 329-333 (1999).
16. Jeong, Ji-W., and Chang, K. J., J. Phys.: Condens. Matter **11**, 3799-3806 (1999).
17. Kanel, G. I., Rasorenov S. V., Utkin A. V., and Fortov V. E., *Shock Wave Phenomenon in Condensed Matter,* Yanus-K, Moscow, 1996, pp.76-78.
18. Golubev, V. K., and Selezenev, A. A., "The Use of Pairwise-Additive Interaction Potentials for Molecular Dynamics Calculation of Isothermal, Adiabatic and Shock Wave Compression of Metals," in *SWCM-2000,* edited by A. Yu. Dolgoborodov at al., Conference Proceedings, Saint – Petersburg, 2000, p. 157.
19. Johnson, R.A., Phys. Rev. B **37**, 3924-3931 (1988).
20. Klimenko V. Yu., and Dremin A. N., "Structure Relaxation in Shock Wave Front in Liquid" in *Detonation,* All Union meeting on Detonation Proceeding 2, Chernogolovka, 1981, pp. 108-111.
21. Segal, M., Akeley, K. and Leech, J., The OpenGL Graphics System: A Specification, Version 1.2.1. 1999. (http://www.opengl.org/developers/documentation/specs.html)
22. Al'tshuler, L. V., and Brusnikin, S. E., PMTF **28**, 134-146 (1987). [in Russian]

Stationary-Frame Atomistic Modeling of Shock-Induced Phenomena in Condensed Matter

S. Zybin [1], V. Zhakhovskii [2], M. Elert [1], C. White [3]

[1] U.S. Naval Academy, Annapolis, USA
[2] Osaka University, Osaka, Japan
[3] Naval Research Laboratory

A series of molecular dynamics (MD) simulations were performed to study an internal structure of shock waves in condensed matter using specially developed technique (V.V. Zhakhovskii, S.V. Zybin, K. Nishihara, and S.I. Anisimov, *Phys. Rev. Lett.*, vol. **83**, 1999, p.1175; *Suppl. Progr. Theor. Phys.*, vol. **138**, 2000, p. 223) within the shock front reference frame maintaining the shock front at rest in the computational box. This approach has shown significant advantage over a standard way of shock simulations within material (or piston) reference frame in accuracy of calculations of fine-grid shock profiles and distribution functions of flow variables. Besides, we also elaborated the ensemble-averaging technique in order to simulate non-steady shock induced phase transition accompanied by shock wave splitting. These time-averaging and ensemble-averaging techniques greatly reduce the statistical noise and allow us to simulate shock waves with a much smaller number of atoms then in a non-stationary approach.

Owing to these techniques, we were able to study in close details the orientation dependence of shock wave structure and elastic-plastic transition as well as oscillatory steady elastic shock in the Lennard-Jones solid. Furthermore, for a given shock velocity, the shock-induced melting transition in [110] and [111] directions differs from the [100] case where a metastable overheated state is developed

behind the front. We suggest that these effects could be explained by the orientation dependence of shear stress in the shock layer.

These techniques were also employed in a study of the shock wave structure and lattice transformation in a diamond perfect crystal using carbon reactive empirical bond order (REBO) potentials. The covalent bonding of diamond atoms significantly affects the mechanism of shock-induced elastic-plastic transformation and plays an essential role in the formation of graphite-like layered structures in the shock wave propagated along the [110] direction.

Besides, we also studied shock-induced chemistry in the hydrocarbons (methane and acetylene) under shock compression and spallation processes. The interatomic forces were introduced using a recently modified REBO potential with intermolecular interactions, termed the adaptive intermolecular REBO potential (AIREBO). We performed plane shock wave experiments and observed the chemical dissociation of methane and acetylene molecules in the shock layer, followed by polymerization into carbon chains for certain piston velocities. These results may be significant for the understanding of shock-induced chemical reactions.

Molecular Dynamic Valuations for Time of Reaction in Detonating HE

K.F. Grebyonkin, A.L. Zherebtsov, A.L. Kutepov, V.V. Popova

Russian Federal Nuclear Center - VNIITF, Snezhinsk (Chelyabinsk-70), Russia

The distribution of burning wave from " hot spots " is one of main processes, proceeding at shock-wave initiation of heterogeneous condensed HE. The reaction of HE in a wave of burning occurs at high pressure and temperatures(3-5 GPa and 3000 K for usual HE as HMX and RDX, and 10-20 GPa and 2500 K in low-sensitive HE as TATB), and there are no experimental data on times of reaction for such HE in these conditions. The extrapolation of HE rates of reaction, measured at smaller pressures and temperatures, can result in significant errors, therefore the valuations of HE time of reaction for the conditions, characteristic for distribution of burning wave, is an urgent problem.

The purpose of the presented work is the evaluation of HE time of reaction with the classic molecular dynamic method. The application of the classical approach for the evaluations is rather reasonable, as the temperature of media in this case is more or about the typical values of energy of oscillatory quantums of HE molecules. The calculations were conducted for nitromethane, as the elementary nitrite HE, the valuations of the other HE time of reaction was made by variations of dissotiation energy for C-N bond.

Method of calculations

Molecular modeling liquid nitromethane was based on the atom – atom calculation model, accounting the intermolecular interaction between A and B molecules as

$$E_{AB} = \sum_{i \in A} \sum_{j \in B} \left(E_{ij}^{[\exp-6]} + E_{ij}^{ele} \right),$$

where i and j atoms refer to the different molecules. The first component (6-exp Buckingham potential) describes atoms repulsion at close distances and van-der-Waalse attraction, the second component - electrostatic interaction.

The (6-exp) potential parameters, presented in different forms ,

$$E_{ij}^{[\exp-6]}(R_{ij}) = D_{0,ij}\left[\left(\frac{6}{6-\xi_{ij}}\right)e^{\xi_{ij}(1-R_{ij}/R_{0,ij})} - \left(\frac{\xi_{ij}}{\xi_{ij}-6}\right)\left(R_{0,ij}/R_{ij}\right)^6\right] \quad (1)$$

$$E_{ij}^{[\exp-6]}(R_{ij}) = -\frac{A_{ij}}{R_{ij}^6} + B_{ij}\exp\left(-C_{ij}R_{ij}\right) \quad (2)$$

were obtained from [1]). The potential parameters for atoms of different types were obtained from:

$$D_{0ij} = \left[D_{0ii} D_{0jj}\right]^{1/2} \qquad A_{ij} = \left[A_{ii} A_{jj}\right]^{1/2}$$

$$\xi_{0ij} = \left[\xi_{0ii} \xi_{0jj}\right]^{1/2} \qquad B_{ij} = \left[B_{ii} B_{jj}\right]^{1/2}$$

$$R_{0ij} = \frac{1}{2}\left(R_{0ii} + R_{0jj}\right) \qquad C_{ij} = \frac{1}{2}\left(C_{ii} + C_{jj}\right)$$

The distribution of electron density for an isolated nitromethane molecule was received from *ab initio* calculations by GAMESS code [2] using Hartri-Fock approximation and N21-3G basis. The optimization of molecule geometry was performed at the first stage. Then the calculation of electrostatic potential based on PDC (Potential Derived Charges) was conducted on ~1000 points within the molecule. The charges on atoms were chosen to reconstruct the best way the potential distribution within molecule. Table 1 presents the data for obtained charges. A root-mean-square deviation is 0.25 kcal/mol, and relative root-mean-square deviation - 3.2 %.

Table 1. Atomic charges for nitromethane molecule from GAMESS code calculations

Atom	C	N	O	H
Charge (in electron charges)	-0.3746	0.6898	-0.3872	0.1527

The molecular dynamic calculations were conducted with Tinker [3] code. The motion of 128 and 256 nitromethane molecules in a box with periodical boundary conditions was performed.

The comparison of nitromethane state parameters calculated with molecular dynamic method with the states (P,V,T), Hugoniot (see table 2) was performed to test the chosen method of calculations. The P(V)- dependense was obtained from experimental D-u ratio D=1.65+1.64u, and the temperature was calculated with modified Walsh - Christian method [5]., accounting the thermal capasity dependence[5].

Table 2.

Hugoniot			Our rezults		
P [GPa]	V [cc/g]	T [K]	P [GPa]	V [cc/g]	T [K]
5.1	0.59	643.6	5.1	0.59	640
7.7	0.55	821.9	7.6	0.56	820
10.4	0.53	1006.8	10.4	0.54	1000
16.3	0.50	1404.9	16.3	0.51	1400

The MD calculations (NPT ensemble) were conducted with time step 0.001 ps. The total time of modelind in these calculations was ~20-30 ps, that is enough for achievement of a system equilibrium state (see fig.1,2 presenting the density and pressure dependence on time of simulation).

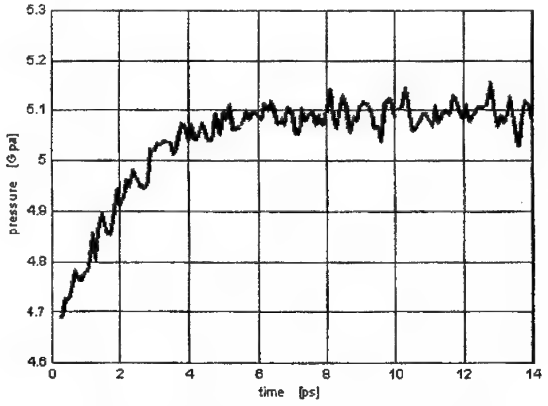

Figure 1. Pressure dependence on time of simulation.

The rather good agreement was achieved, and it validates the correctness of computational method.

It was assumed while performing the estimates of time for HE reactions (see for example – 6), that the limiting stage of HE decomposition is the break of (C-N) - bond, which is the weakest in the HE molecules formed on the base of nitro-compounds.

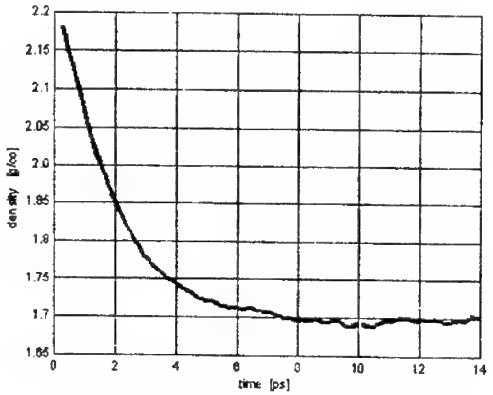

Figure 2. Density dependence on time of simulation
(Box of 128 nitromethane molecules, NPT – ensemble, P=5.1 GPa, T=640 K)

The calculations were carried for two values of C-N bond dissociation energy: 60 Kcal/mol and и 40 Kcal/mol for the box of 128 nitromethane molecules. The first case models nitromethane *per se*, as well as the low sensitive HE as TATB, and the second - the usial HE such as HMX and RDX [4]. The temperature and pressure (NPT – ensemble) were (P=10 GPa, T=2500 K) and (P=5 GPa, T=3000 K) correspondently, that is nearly relevant to the burning wave parameters in the observed cases.

The dependence of the number of dissociated molecules by C-N bond on time was obtained from the MD calculations. The condition of deleting these atoms on spacing interval at the distance 3A, that is the doubled length of C-N bond, was selected as the criteria of C-N bond breaking.

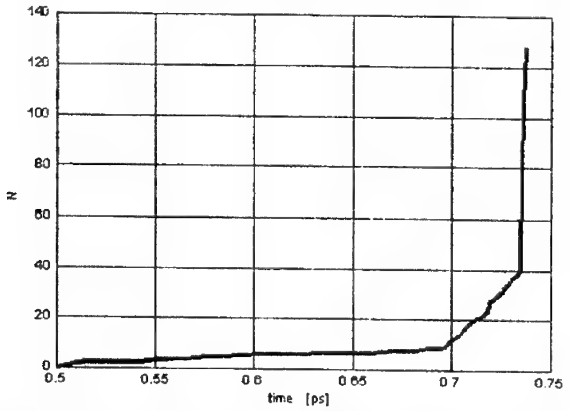

Figure 3. The dependence of the number of dissociated molecules on time for dissociation energy 40 kcal/mol. (NPT – ensemble, P=5 GPa, T=3000 K).

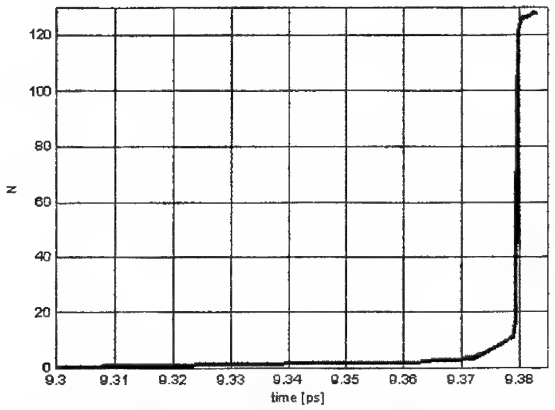

Figure 4. The dependence of the number of dissociated molecules on time for dissociation energy 60 kcal/mol. (NPT – ensemble, P=10 GPa, T=2500 K).

Fig.3 and 4 show the characteristic dependence of the number of dissociated molecules on time for two values of dissociation energy for P and T values, typical for the conditions of the wave of burning. Thus the characteristic times of HE decomposition in the wave of burning are about 0.5-1 ps for the usual HE such as HMX and RDX and ~10 ps for the low-sensitive HE TATB. The calculations were performed with time step 0.0001-0.0005 ps.

The obtained results are of particular interest for explanation of a reason for TATB low sensitivity and demonstrate, that the rate of burning wave propagation from hotspots in this case will be much lower, than for the usual explosives such as HMX and RDX.

References

1. S. Mayo, B. Olafson, W. Goddard DREIDING: A general force field for molecular simulation // *J. Phys. Chem.* 1990, **94**, pp. 8897-8909.

2. General Atomic and Molecular Electronic Structure System // GAMESS User's Guide// Department of Chemistry Iowa State University, 1983.

3. TINKER Software Tools for Molecular Design, 1997.

4. Charles L.Mader, Numerical modeling of detonation. M.: Mir, 1985.

5. Walsh J.M., Christian R.H. Equation of state of metals from shock wave measurement //*Phys.Rev.*, vol. **97**, N6, 1955.

6. Chaiken R.. The relations between pressure and temperature of shock compression and time of detonation delay in nitromethane. In *Detonation and HE*. M., Mir, 1981. pp. 220 - 235.

Molecular Simulation of Shocked Materials using Reactive Monte Carlo

J. K. Brennan, B. M. Rice

U. S. Army Research Laboratory, Aberdeen Proving Ground, USA

We demonstrate the applicability of the Reactive Monte Carlo (RxMC) simulation method[1,2] for calculating the shock Hugoniot of a material. The method requires inputting only the intermolecular potentials and the ideal-gas partition functions for the reactive species that are present. By performing Monte Carlo sampling of forward and reverse reaction steps, RxMC provides information on the chemical equilibria state including the density of the reactive mixture and the mole fractions of reactive species.

We illustrate the methodology for two simple systems (shocked liquid NO and shocked liquid N_2), where we find comparison with experimental measurements to be in excellent agreement.

Reactive Monte Carlo is shown to be a robust and efficient method for predicting shock Hugoniots. The method can be used to calculate the shock Hugoniot of materials for which no accurate equation of state is available, or when *a priori* knowledge of the species concentrations is lacking. Such a method would be a powerful tool in the development of novel energetic materials by allowing for the evaluation of the detonation performance of a notional material, while avoiding costly and time-consuming synthesis and measurements. Furthermore, multiple reactions can be simulated simultaneously in multiple phase systems, thus the method can be applied to the study of supercritical phase separation phenomena of shocked materials (see *e.g.*, 3-5). Other possible applications and extensions of the Reactive Monte Carlo method will be discussed.

Modeling High Speed Friction at Ductile Metal Interfaces

J.E.Hammerberg

Los Alamos National Laboratory, Los Alamos, NM 87545, USA

The modeling of deformation processes at sliding, compressed metal-metal interfaces is discussed from the point of view of multiple length- and time-scales. Large-scale atomistic simulations have demonstrated the importance of structural transformation and mechanical material mixing at high rates of deformation, leading to interfacial weakening and a decrease of the frictional coefficient with velocity at high velocities of relative motion.

At lower velocities, dislocation and phonon mechanisms predominate, which in certain cases may lead to an initial linear velocity dependence of the frictional force. Some of the limiting behaviors are amenable to simplified analyses, which will be presented.

The experimental situation for dynamical measurements of interfacial deformation at μsec time scales will be reviewed and some of the implications for macroscopic modeling in continuum materials dynamics computer codes will be discussed.

Modeling of the Structure of the Shock Wave Front in Solids

M.M. Kuklja [1], Yu. Skryl [2]

[1] Department of Mechanical Engineering, University of Maryland, College Park, USA
[2] *Institute of Mathematics and Computer Science, University of Latvia, Riga, Latvia*

THIS PAPER IS AN ATTEMPT TO SIMULATE THEORETICALLY THE STRUCTURE OF THE SHOCK WAVE FRONT IN SOLIDS. ANALYTICAL FORMULAE FOR THE WIDTH OF THE WAVE FRONT AND THE FRONT VELOCITY HAS BEEN OBTAINED. THE DISTRIBUTION OF PARAMETERS WITHIN THE FRONT STRUCTURE SUCH AS THE DENSITY, THE VELOCITY, THE TEMPERATURE, AND THE PRESSURE OF THE CRYSTALLINE MATTER ARE DERIVED AND ANALYZED. A COMPARASION BETWEEN THE ANALYTICAL RESULTS AND THE NUMERICAL CALCULATIONS IS DISCUSSED.

A VERY NARROW REGION WHERE ALL PARAMETERS OF MATTER (DENSITY, VELOCITY, TEMPERATURE, AND PRESSURE) ARE CHANGED SIGNIFICANTLY IS KNOWN AS THE STRUCTURE OF THE SHOCK WAVE FRONT. THE CALCULATION TECHNIQUE OF THE FRONT STRUCTURE HAS BEEN WELL ELABORATED FOR GASES. THE METHOD DEVELOPED ALLOWS ONE TO DEFINE THE PARAMETERS OF THE STRUCTURE, SUCH AS THE WIDTH OF THE WAVE FRONT AND THE FRONT VELOCITY. ALSO, THE METHOD PROVIDES INFORMATION REGARDING THE DISTRIBUTION FUNCTIONS OF ALL THE PARAMETERS OF A SUBSTANCE WITHIN THE SHOCK WAVE FRONT.

TO OUR BEST KNOWLEDGE, THEORETICAL STUDIES ON THE STRUCTURE OF THE SHOCK WAVE FRONT IN THE CONDENSED MATTER WERE NOT REPORTED SO FAR. THE LACK OF A CONSISTENT APPROACH TO THE DETERMINATION OF THE EQUATION OF

STATE (EOS) FOR THE CONDENSED MATTER IS THE MAIN REASON FOR THIS SITUATION. ONE OF THE POSSIBLE STRATEGIES TO PROCEED IS TO CHOOSE SOME FORM OF EOS, OBTAINED FOR A CRYSTAL, AND TRY TO DESCRIBE THE STRUCTURE OF THE SHOCK WAVE IN THE SOLID BY THE SAME TECHNIQUE AS WAS USED FOR THE GAS-PHASE.

THIS STUDY IS AN ATTEMPT TO DESCRIBE THEORETICALLY THE STRUCTURE OF THE SHOCK WAVE PROGRESSING IN THE SOLID. THE EQUATION OF STATE HAS BEEN CHOSEN FOR THE HMX ($C_6H_6N_6O_6$) CRYSTAL IN THE MIE-GRUNEISEN FORM. THEN, THE METHOD DEVELOPED FOR THE DESCRIPTION OF THE SHOCK WAVES IN THE GAS PHASE WAS APPLIED. IT IS SHOWN THAT THIS TYPE OF EOS IS QUITE SUITABLE FOR THE ANALYTICAL DESCRIPTION FOR THE STRUCTURE OF THE SHOCK WAVE FRONT IN SOLIDS.

Simulating Spallation in Polycrystalline Materials via Molecular Dynamics

A.M. Krivtsov

St.Petersburg State Technical University, St.Petersburg, Russia

One of the main challenges in use of molecular dynamics technique for simulating macroscopic behavior of materials is that all regular particles packings produce computer materials with anisotropic mechanical properties. If generally it is possible to choose interparticle potentials to obtain isotropic conditions for elastic moduli, there is no way to satisfy isotropic conditions for inelastic and strength properties. This can be the reason why molecular dynamics, which is widely used in modeling crystalline materials, still has limited applications in the case of homogeneous isotropic solids.

The approach, which allows bypassing this problem, is to construct polycrystal particle packings with random distribution of the monocrystal grains orientations. This method can produce isotropic computer materials, which can satisfy to very wide range of mechanical, thermodynamic and physical properties. Obviously this technique requires much more computer resources, since the elementary volume is now the monocrystal grain, containing itself hundreds of particles at least. Therefore the full-scale use of the polycrystal computer materials was started only recently, following the sharp increase in the power of the modern computers. Recent advances in nanotechnologies also stimulated molecular dynamics aided research in the area of nanocrystal materials [1].

In the presented work the plate spallation experiments where chosen to compare properties of mono and polycrystal computer materials. The plate impact experiments produce a simple deformation at very high strain rates, which makes these experiments to be essential tool for calibrating and validating material models that aspire to general applicability [2]. The history of molecular dynamics (MD) computer simulations of shock waves covers several decades, evolving to the point where weak-shock induced plasticity in the solid state can be studied [3]. Let us mention the detailed paper [4], where noticeable differences where obtained in spallation scenario between mono and polycrystal particle arrangements.

THE CURRENT WORK IS CONTINUATION OF THE INVESTIGATIONS [5, 6], WHERE INFLUENCE OF THE HETEROGENEITY CAUSED BY THERMAL MOTION IN MONOCRYSTALLINE MATERIALS ON THE SPALLATION PROCESSES WERE STUDIED. IN [5] IT WAS SHOWN THAT THIS KIND OF HETEROGENEITY COULD LEAD TO DRASTICALLY CHANGE IN THE SHAPE OF THE SPALL CRACK, INCREASING FINALLY THE SPALL STRENGTH OF THE MATERIAL. THE SIMULATION TECHNIQUE IS DESCRIBED IN [5], WHERE THE MOLECULAR DYNAMICS METHOD CLOSE TO [4] IS USED. MATERIAL IS SIMULATED BY 2D SET OF PARTICLES INTERACTING VIA PRESCRIBED POTENTIAL FORCES; SIMULATION IS MADE BY INTEGRATING NEWTON'S EQUATIONS OF MOTION FOR EACH PARTICLE. FOR THE SAKE OF SIMPLICITY THE STANDARD LENNARD-JONES 6–12 POTENTIAL IS USED TO DESCRIBE INTERACTION BETWEEN THE PARTICLES.

THE COMPUTATIONAL MODEL AT THE INITIAL STAGE IS PRESENTED IN FIG.1A. THE PARTICLES ARE ARRANGED IN TWO RECTANGLES, REPRESENTING IMPACTOR (BLACK) AND THE TARGET (GRAY). THE IMPACTOR IS PLACED WITH A SMALL GAP

FROM THE TARGET. IN FIG.1 THE PARTICLES ARE ARRANGED ON A TRIANGULAR LATTICE. THE ORIENTATION OF THE LATTICE IS THE SAME FOR THE IMPACTOR AND TARGET, WHERE ONE OF THE SIDES OF THE LATTICE TRIANGLES IS EXTENDED ALONG *Y*-AXIS. THE TOTAL NUMBER OF PARTICLES IS ABOUT 30 THOUSANDS. INITIALLY THE TARGET HAS ZERO VELOCITY, THE IMPACTOR HAS A CONSTANT VELOCITY DIRECTED TOWARDS THE TARGET, WHERE THE VALUE OF THE IMPACTOR VELOCITY IS ABOUT 20% OF THE WAVE SPEED IN THE CRYSTAL. FREE BOUNDARY CONDITIONS ON ALL BOUNDARIES ARE APPLIED. THIS IS DIFFERENT FROM [4], WHERE PERIODICAL BOUNDARY CONDITIONS WERE USED FOR THE *Y* DIRECTION. FREE BOUNDARY CONDITIONS ALLOW OBSERVING BOUNDARY EFFECTS, WHICH VARY SIGNIFICANTLY FOR DIFFERENT PARTICLES ARRANGEMENTS. THE THERMAL ENERGY OF THE PARTICLES MOTION (THAT IS PROPORTIONAL TO THE KINETIC ENERGY OF THE STOCHASTIC COMPONENT OF THE PARTICLES VELOCITIES) IS TAKEN TO BE NEGLIGIBLE WITH RESPECT TO THE KINETIC ENERGY OF THE IMPACTOR.

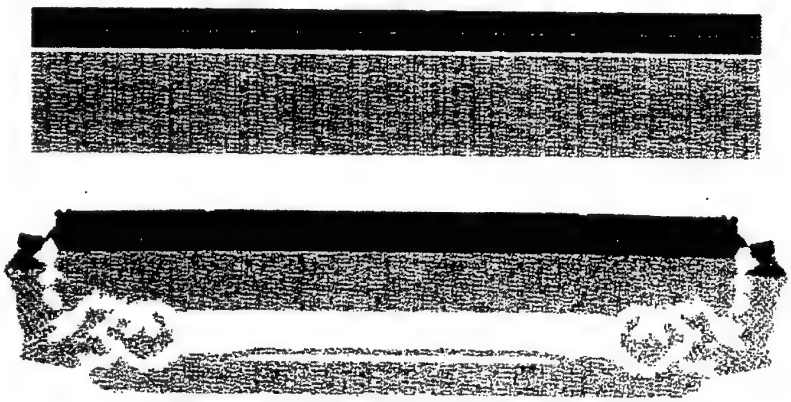

Figure 1. Spallation in monocrystal specimen: a) before impact, b) after impact.

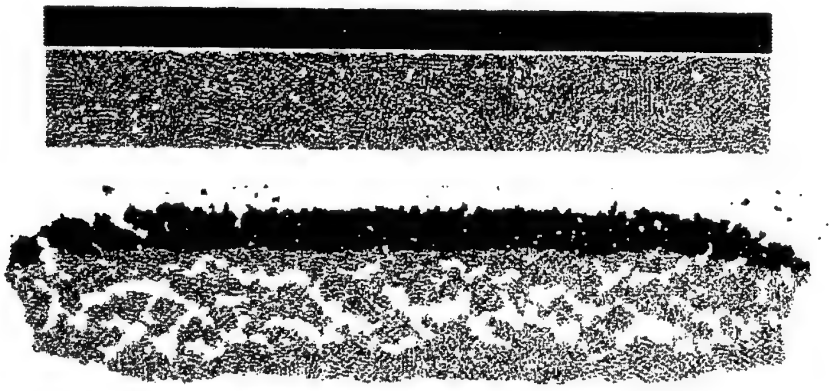

Figure 2. Spallation in polycrystal specimen: a) before impact, b) after impact.

The system configuration after spallation is shown in Fig.2a. From the figure it follows that the spall crack boundaries in the central part of the target are absolutely straight. This is result of the low thermal energy and coincidence between the impactor and target lattices. Multiply spallation is seen in Fig.1b, which sometimes occur for high impact velocities, such as the one used in the experiment. Specific fracture localization is well seen in the vicinity of the y boundaries. This is result of wave reflection from the free boundaries of the specimens.

Now let us see the results of the second impact experiment (Fig.2), where impactor is the same as before, but the target is prepared from the polycrystal material (Fig.2a). The material is obtained by the compression of monocrystal grains as described in [7]. The selected material posses significant porosity that was preserved to simulate plastic strains associated with pore collapsing, which can by of significant importance in spallation processes [8]. The result of the spallation experiment is shown if Fig.2b. Comparing Fig.1b and Fig.2b one can conclude that the fracture scenario is absolutely different for those two experiments. In the case of polycrystal target the x-width of the spallation zone is much higher, involving nearly the whole width of the target. This is in a good agreement with the conclusion from [4] that the defects due to the grain boundaries could diffuse the sharpness of the tensile shocks in the material. This is the similar result as was obtained in [5], where the diffusion of the shock wave sharpness was due to the thermal motion of the particles.

The thermal effect also explains that in the results from [4] the difference between the mono and polycrystal spallation was much lower then in the current experiments, since in [4] the considered initial thermal motion is much higher. Another reason why the effect of the polycrystalline packing is more significant in our case is that the sizes if the monocrystals are greater with respect to the width of the target. One more effect of the polycrystal packing is that the influence of the y-boundaries is much lower, then in the case of monocrystal. This is because the reflection of the shock waves from the grain boundaries prevents focusing of the fracture in some localized area, as it happens in Fig.1a. Another interesting result is that in the Fig.2 the damage of the impactor plate is much higher then in Fig.1, which is also due to heterogeneity of the shock wave front, produced by the granular structure of the target.

Summarizing the above it can be deduced that polycrystal computer materials can show in spallation experiments the behavior, which is strongly different from those for the monocrystals. The main feature of the polycrystals is smearing the shock waves due to heterogeneity of their granular structure. This leads to decreasing the localization effects, which are usual for ideal monocrystals. The similar effect (with the lower magnitude) can be produces by thermal motion of the particles in ideal crystals.

1. J. Schiotz, T. Vegge, F. D. Di Tolla, K. W. Jacobsen. Atomic-scale simulations of the me-chanical deformation of nanocrystal metals. *Physical Review B*, 1999, **60** (17), 11971–11983.
2. A. M. Rajendran, D. J. Grove. Modeling the shock response of silicon carbide, boron carbide and titanium diboride. International Journal of Impact Engineering, 1996, **18** (6), 611–631.
3. B. L. Holian. Atomistic Computer-Simulations of Shock Waves, *Shock Waves*, 1995, **5**(3), 149–157.
4. N. J. Wagner, B. L. Holian, A. F. Voter. Molecular-Dynamics Simulations of 2-Dimensional Materials at High-Strain Rates. *Physical Review A*, 1992, **45** (12), 8457–8470.
5. A. M. Krivtsov. Relation between Spall Strength and Mesoparticle Velocity Dispersion. International Journal of Impact Engineering, 1999, **23** (1), 466–476.
6. A. M. Krivtsov, Y. I. Mescheryakov. Molecular Dynamics Investigation of the Spall Fracture. *Proceedings of SPIE*, 1999, 3687, 205–212.
7. A. M. Krivtsov, M. Wiercigroch. Molecular Dynamic Simulation of Mechanical Properties for Polycrystal Materials. *Materials Physics and Mechanics*, 2001, **3** (1), 45-51.
8. A. M. Rajendran, M. A. Dietenberger; D. J. Grove. A Void Growth-Based Failure Model to Describe Spallation, *Journal of Applied Physics*, 1989, **65** (4), 1521–1527.

3D Effects in Molecular Dynamics Experiments on Spallation

I. M. Assatourova

St.Petersburg State Technical University, St.Petersburg, Russia

3D computer simulations require much more computational resources then 2D ones. Additional challenge is the visualization of the simulation results, which in 3D case arises in separate problem. From other hand, 2D simulations in many cases provide realistic results and can be used almost without lose of generality. The aim of this paper is to outline some specific features of 3D molecular dynamics simulation, which cannot be observed in 2D computer experiments. In the presented work the plate spallation experiments where chosen to compare 2D and 3D molecular dynamic simulations. The plate impact experiments produce a simple deformation at very high strain rates, which makes these experiments to be essential tool for calibrating and validating material models that aspire to general applicability [2].

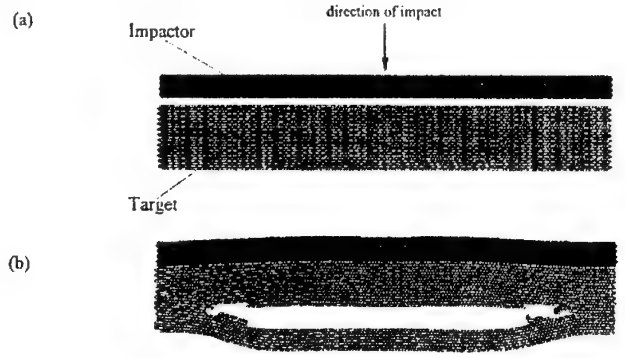

Figure 1. 2D spallation experiment: a) before impact, b) after impact.

The history of molecular dynamics (MD) computer simulations of shock waves covers several decades, evolving to the point where weak-shock induced plasticity in the solid state can be studied [3]. Let us mention the detailed paper on MD simulation of 2D spallation processes in mono and polycrystalline solids [4]. The current work is continuation of the investigations [5, 6], where 2D computer simulations of spallation processes where studied. The simulation technique is described in [5], where the molecular dynamics method close to [4] is used. Material is simulated by set of particles interacting via prescribed potential forces; simulation is made by integrating Newton's equations of motion for each particle. For the sake of simplicity the standard Lennard-Jones 6-12 potential is used to describe interaction between the particles.

2D computational model at the initial stage is presented in Fig.1a. The particles are arranged in two rectangles, representing impactor (black) and the target (gray). The impactor is placed with a small gap from the target. The particles are arranged on a triangular lattice. The total number of particles is about 5000. Initially the target has zero velocity, the impactor has a constant velocity directed towards the target. Free boundary conditions on all boundaries are applied. This is different from usual spallation tests ([4]), where periodical boundary conditions are usually applied for the direction, orthogonal to the direction of impact. Free boundary conditions allow observing boundary effects, which vary significantly for 2D and 3D cases. The thermal energy of the particles motion (that is proportional to the kinetic energy of the stochastic component of the particles velocities) is taken to be negligible with respect to the kinetic energy of the impactor. Fig.1b shows the system in the stage of the spall crack formation. The analogous 3D computational model is presented in Fig.2.

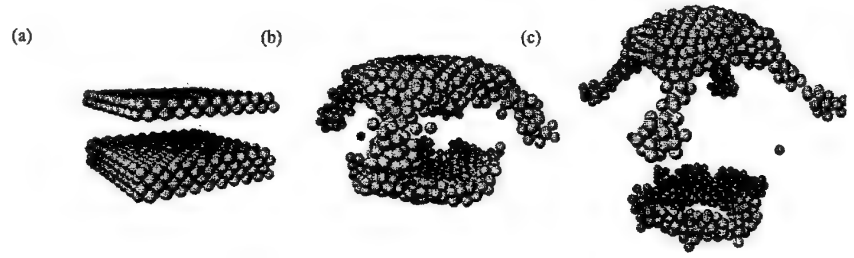

Figure 2. Sequential frames of the spallation process: a) before impact, b) during impact, c) after impact.

The particles are arranged in two parallelepiped plates, representing impactor (top) and the target (bottom). The particles are arranged on a face centered cubic (FCC) lattice. The total number of particles is about 1200. The relatively small number of particles is used in Fig.2 for better visualization of the model and to show clearly effects of discretization. Fig.2a, b, c show sequential frames of the spallation process. After impact the plates join, but in the middle of the thick plate appears a spall crack, which leads to separation of so called spall plate, which usually has same thickness as the thin plate. The boundary effect, which is especially strong near the corners of the plates leads to significant plastic deformation of these corners. Even more interesting is the deformation state in the spall plate, shown in Fig. 3a, b.

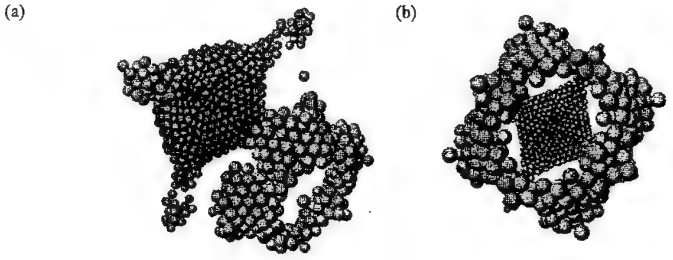

Figures 3a, b. The result of the spallation process from different directions of view.

In figures one can clearly see an axial hole, which is located in the center of the spall plate. This effect is a result of the shock waves focusing. These waves are reflected from the side faces of the plate; they move in the plane of the plate and form firstly an area of high compression, and immediately after — an area of strong tension in the center of the plate. This effect is well known for solid spheres subjected to a uniform surface shock, which leads to cavity forming in the center of the sphere [0]. Appearing of this central cavity in the spall plate is essentially 3D effect. This effect can be observed only for special values of impact velocity and proportions of the specimens. Fig.4 show another 3D experiment on spallation where the proportions of the plates differ from the previous experiment, which suppress appearance of the central hole in the spall plate. The total number of particles in Fig.4 is about 5000.

Fig.4. 3D spallation experiment, a) before impact, b) during impact, c) after impact.

The comparison of 2D and 3D computer experiments show that many general features of the spallation process, such as reflection of the shock waves from the free surfaces, development of the spall crack, and the velocity profile on the free surface are quite similar for 2D and 3D cases. The most important effects, which absolutely cannot be described by 2D models, are connected with reflection of the shock waves from the side surfaces and their localization in the center of the spall plate. These effects frequently appear in natural experiments on spallation, introducing specific disturbances in the results of measurements. Study of these phenomena on 3D computer experiments on spallation can give useful information, which cannot be obtained from 1D and 2D considerations.

References

1. M. Rajendran, D. J. Grove. Modeling the shock response of silicon carbide, boron carbide and titanium diboride. International Journal of Impact Engineering, 1996, **18** (6), 611–631.

2. L. Holian. Atomistic Computer-Simulations of Shock Waves, *Shock Waves*, 1995, 5(3), 149–157.

3. N. J. Wagner, B. L. Holian, A. F. Voter. Molecular-Dynamics Simulations of 2-Dimensional Materials at High-Strain Rates. *Physical Review A*. 1992, **45** (12), 8457–8470.

4. M. Krivtsov. Relation between Spall Strength and Mesoparticle Velocity Dispersion. International Journal of Impact Engineering, 1999, **23** (1), 466–476.

5. M. Krivtsov, Y. I. Mescheryakov. Molecular Dynamics Investigation of the Spall Fracture. *Proceedings of SPIE*, 1999, 3687, 205–212.

6. *Metals and minerals research in spherical shock-wave recovery experiments*, ed. by B. I. Litvinov (ONTI RFNC-VNIITF, Snezhinsk, 1996), in Russian.

SESSION
"Experiments in Support of Models Development for Inert Materials"

Chairmen:
J. Asay - **Sandia National Laboratories, Albuquerque, USA**
R. Dormeval - **CEA / Valduc, Dijon, France**

Recent Advances in High-Pressure Equation-of-State Capabilities

J.R. Asay, M.D. Knudson, C.A. Hall, J-P. Davis, D.L. Hanson, J.E. Bailey

Sandia National Laboratories, Albuquerque, NM, USA

The high-pressure equation-of-state (EOS) is typically determined with a variety of techniques, including planar explosive loading, two-stage light gas guns, and diamond anvil cells. These methods have been valuable in measuring thermodynamic properties over a large portion of the EOS. In particular, gas guns have become a standard laboratory technique for studying shock response and are typically used to determine the principal Hugoniot, which is the locus of end states achieved by steady shock compression. Shock pressures of several Mbar are easily obtained in high-impedance materials, such as tantalum. However, for many applications, it is necessary to extend shock compression to several tens of Mbar. In addition, a complete EOS is often needed, which requires that shock data be supplemented with other information, such as temperature measurements or off-Hugoniot response.

Recent developments in fast pulsed power techniques have been useful in achieving these two goals. In particular, the Z accelerator at Sandia National Laboratories, which develops about 22 million amperes of current on sub-microsecond time scales, is used to produce multi-Mbar shocks and to obtain continuous compression data. The accelerator is usually used in the "Z-pinch" mode in which cylindrically generated plasmas are accelerated to produce high photon energy x-rays that can be used to produce ablatively-driven shock waves for equation of state studies. The accelerator can also be operated in a direct current mode, in which magnetic pressure is applied continuously in time to a planar sample surface over time intervals of 100-300 ns and for strain rates of about 10^6 /s. In this configuration, peak pressures to 2 Mbar have been demonstrated for shockless loading conditions, with the possibility of extending this to several Mbar. The loading process produces nearly isentropic response of the material to be studied, so that the technique is useful in developing off-Hugoniot data for constructing a complete EOS.

The Isentropic Compression Experiment (ICE) has been used on a variety of materials to date for studying isentropic compression behavior to Mbar pressures, determination of mechanical properties such as compressive and tensile strength for shockless loading, and for detecting and determining dynamic phase transition boundaries and kinetics. The ICE technique has also been used to accelerate metal plates a few hundred microns thick and about 1 centimeter in diameter dto velocities exceeding 20 km/s. This method has been used to obtain absolute Hugoniot data on aluminum to 5 Mbar and relative Hugoniot data on aerogels and liquid deuterium to 700 kbar. An important advantage of the technique is that sample dimensions are relatively large, on the order of 1 mm thick, so that EOS accuracies are comparable to those achieved with conventional laboratory techniques, such as light gas guns.

The presentation will review these developments, including applications to phase transition studies, measurements of high-pressure isentropes and shock wave experiments to 5 Mbar with plate impact.

Hydrodynamic Features Experiments using Pulse Power Sources for Code/Data Comparisons

W. L. Atchison, R. Bowers, J. Guzik, and R. Kanzleiter

Los Alamos National Laboratory, Los Alamos, USA

The ATLAS Pulsed Power Facility began interim operations in October 2001. ATLAS is a capacitively driven pulsed power machine capable of generating peak currents between 16 and 30 MA with an 8 μs rise time. This driving current can be used to either compress metal cylinders in a Z-pinch configuration or accelerate thin liners to possibly as much as 10 km/s. Either direct compression, or impact and subsequent compression of a central target assembly provides physical data useful for validating hydrodynamic simulation codes in convergent geometries. One such series is the Hydro-Features (HF) experiments currently being conducted on ATLAS.

In this series, a 1 mm thick, 5-cm radius cylindrical aluminum liner is accelerated to a radial velocity between 4 and 6 mm/μs by the self-induced radial Lorentz force. Liner impact on a central target is used to drive a highly symmetric convergent shock into a well-diagnosed testing volume to provide data for hydrodynamic code validation. Target design and analysis was performed using the AMR Eulerian hydrodynamics code RAGE in 1-, 2-, and 3-dimensions. Since RAGE lacks MHD capabilities necessary to simulate the MHD drive, the one-dimensional Lagrangian MHD code RAVEN was used to simulate the drive bank and the shock motion following liner/target impact in one dimension. Initial target design for the HF series was based on experience gained during the Near Term Liner eXperiment (NTLX) series fired on Shiva Star at the Air Force Research Laboratory. A similar liner/target configuration was used for both the NTLX and HF experimental series. The one difference was the use of a Lucite central target in the NTLX series, while a water central target was used for the HF series. Data from NTLX showed very good agreement between calculated and measured shock locations with a slight 100 ns shift between computational and experimental data sources. Shock passage through the inner Lucite/Water testing volume produces an approximate doubling of the media density. This sharp density discontinuity allows visualization of subsequent shock motion. Comparison of the material interface behavior was generally good with some qualitative differences evident between simulation and measurements. Both experiments started with a series of characterization experiments, which examine a symmetric target arrangement with the inner testing volume aligned coaxially with the liner driver axis. As a first variation to this geometry, the inner core of the target is shifted by 4 mm from the liner driver axis. Variations in the shock velocity in the dissimilar materials produce off-center shock convergence.

A quantitative comparison between simulations and radiographic data of the shock and interface locations provides for code validation in convergent geometries. Comparison of data produced by other simulation codes will also be presented. Upon completion of the characterization experiments, additional targets are considered which examine issues relevant to more complex geometries.

Optical Properties of Solid and Fluids at High Shock Pressures

N.C. Holmes

Lawrence Livermore National Laboratory, Livermore, USA

A vital measure of the thermodynamics of shocked materials is the measurement of temperature. While simple in principle, for shocked metals with an optical depth of a few nm, this proves quite a challenging problem. Optical methods such as optical pyrometry may seem ideal, but one must know the optical emissivity of a surface or material at high pressures and temperatures, the optical properties of window used to maintain pressure at a surface, thermal transport effects, and so on. Studying these phenomena will lead to increased understanding of dielectric, transport, deformation, and state properties. In addition, the same problems can arise more generally in spectroscopic measurements of shocked materials. I will describe highlights of our current research in these areas, using examples in shocked α-Al_2O_3, LiF, D_2, and Fe.

Phase changes in Ni-Ti under shock loading

R. Hackenberg[1], D. Swift[2], K. Chen[3], J. Cooley[1], D. Paisley[2], D. Thoma[1], A. Hauer[4]

[1] *Materials Science and Technology Division, Los Alamos National Laboratory, USA*

[2] *Physics Division, Los Alamos National Laboratory, USA*
[3] *California Polytechnic Institute and State University, San Luis Obispo, USA*
[4] *Physics Division, Los Alamos National Laboratory, USA*

Introduction

The mechanisms of martensitic nucleation are still poorly understood, due in part to the high growth rate of martensitic product units. This study reports the results of dynamic laser shock-loading experiments with nanosecond stress pulses which may provide answers to these questions. Several Ni-Ti alloys are examined, with an emphasis on the phase changes that take place upon shock loading. Our interest in this system stems not just from the scientific goal of increasing the understanding of the phase changes in Ni-Ti, but also from the fact that the most widely used shape memory alloys are based on Ni-Ti [Otsuka98].

Sample preparation

Ingots of Ni-Ti binary alloys were prepared from high-purity elements by arc melting and then arc-casting into cylinders. Their nominal compositions were 50.0, 52.5, 55.4, 55.6 and 55.7 atomic % Ni. The ingots were homogenized at 1100°C for 50 hours and water quenched. Disc specimens of 6 mm diameter were cut from the ingots and ground and polished down to 100-125 microns thickness for the direct drive shots. For the symmetric impact experiments, 5 mm diameter full discs were used as flyer plates while 5 mm diameter half discs were used as targets.

Determination of the equation of state

A thermodynamically complete equation of state (EOS) is needed in order to understand the dynamic loading applied to a sample, and hence interpret the microstructure of recovered specimens. No relevant EOS for Ni-Ti alloys have been published, so we determined the EOS by theory and experiment.

Ab initio quantum mechanical equation of state

An *ab initio* EOS was calculated using quantum mechanics, by a variant of a method applied previously to several elements [Swift00,Swift01]. The frozen-ion cold curve was estimated for Ni-Ti in the CsCl structure by finding the ground state energy of the outer electrons with respect to *ab initio* pseudopotentials for Ni and Ti. The variation of Grueneisen's Gamma with compression was estimated from the cold curve by fitting functional forms and applying the Dugdale-Macdonald formula. Assuming a constant value for the specific heat capacity, a thermodynamically complete EOS was generated.

Because of the intrinsic limitations of the local density approximation used to represent the exchange-correlation energy of the outer electrons, the *ab initio* EOS overpredicted the lattice spacing at STP by ~1%. This discrepancy was corrected by adding a constant pressure offset to the EOS.

Laser-launched flyer experiments

The theoretical EOS was tested, and a basic constitutive model obtained, by performing laser-launched flyer experiments with laser Doppler velocimetry (VISAR) diagnostics. Flyers made from copper or Ni-Ti were mounted on a substrate consisting of PMMA coated with thin (~micron) layers of materials to absorb the laser energy, confine the plasma, and insulate the flyer from heating. The flyers were between 50 and 200 microns thick.

The TRIDENT laser at Los Alamos was used to launch the flyers. Pulses ~600 ns long in the infra-red were used, allowing the flyers to be launched without shocking up, spalling or significant ringing. Flyer speeds up to ~600 m/s were obtained.

The flyers were impacted against Ni-Ti targets, attached to PMMA windows. The target typically covered half of the area of the flyer, giving space for the flyer speed to be measured with the VISAR. The surface of the target - releasing into the window or into vacuum - was also monitored with the VISAR. Wave profiles at the surface of the target provided EOS and strength information. In the case of Ni-Ti flyers, the deceleration on impact with the window provided a point on the principal Hugoniot.

The EOS data obtained were consistent with the theoretical EOS, validating its use in the prediction of dynamic loading histories at different positions in the samples.

Shock and recovery experiments

Experiments were performed in which a set of Ni-Ti alloys covering a range of compositions were subjected to dynamic loading, then recovered and analysed to investigate the effect on the microstructure and phases present.

The samples used in these experiments were ~100 microns thick. Ten experiments were performed: two each on five different compositions.

Dynamic loading

The TRIDENT laser was used to induce pressure pulses by illuminating one surface of the sample directly. The pulse length in these experiments was 1.8 or 3.6 ns. The opposite surface of the sample was monitored using a line-imaging VISAR system. In most of the experiments, the sample was mounted on a sapphire window; in three experiments no window was used. The sample (and window, if used) was mounted in a clamp which held it around its entire edge. The window was intended to decelerate the shocked sample in an essentially 1D fashion, making it easier to correlate the loading history with the microstructure.

The *ab initio* EOS was used in hydrocode simulations to estimate the loading history experienced at each point in the sample. According to the simulations, the laser pulse produced a slowly-decaying triangular wave. Peak pressures were ~10 to 20 GPa.

Metallography

X-ray diffraction, optical microscopy, SEM and TEM were used to characterize phase distributions (i.e., B2 parent, martensite and intermetallic phases) in both the as-quenched (AQ) and shocked specimens; additionally, resistivity measurements were used on AQ samples.

The 50.0 Ni alloy showed the reverse transformation from B19' martensite to B2 upon shock loading, while the other alloys showed no martensite either in the as-quenched or shocked states; instead the amount of the Ni_4Ti_3 phase (present in the AQ state) changed after shock-loading in a manner dependent on alloy composition. These results are attributable to both the high Ni content of these alloys (preventing the formation of martensite in all but the 50.0 Ni alloys) and the significant temperature rise within the shocked region, which facilitate diffusional transformations involving Ni_4Ti_3.

Conclusions

The *ab initio* quantum mechanical method produced a complete EOS for Ni-Ti alloy in the CsCl structure. The EOS was tested against laser-launched flyer experiments, which were appropriate in terms of pressure range and time-scales for the direct-drive experiments.The direct-drive technique allowed samples to be loaded with nanosecond-scale pulses and recovered without undue disruption to the microstructure. Metallography revealed systematic variations in changes to the microstructure, which can be correlated with differences in composition and loading history.

Acknowledgements

We would like to acknowledge the contributions of the TRIDENT team, and of Andrew Forsman for his help in operating the line VISAR.

This project was funded under the LDRD-ER on Martensitic Phase Changes, FY 2000-2002. The LDRD program is funded under the auspices of the U.S. Department of Energy under contract W-7405-ENG-36.

References

Otsuka98 K. Otsuka and C.M. Wayman (eds) *Shape Memory Materials*, Cambridge (1998).

Swift97 D.C. Swift, *Ab fere initio equations of state for solids*, Proc 1997 APS Topical Conference on Shock Physics, held Amherst, Massachusetts, 28 Jul - 2 Aug 1997, AIP (1998).

Swift01 D.C. Swift, G.J. Ackland, A. Hauer and G.A. Kyrala, *First principles equations of state for simulations of shock waves in silicon*, Phys Rev B **64**, 214107 (2001).

Experimental Data on Dynamic Freezing in Tin

D.-P. Davis, J.R. Asay, D.B. Hayes, R.J. Hickman

Sandia National Laboratories, Albuquerque, USA

The isentropic ramp-wave loading technique developed at Sandia National Labs is a novel method to study the kinetics of phase transitions, particularly in regimes that are overdriven by shock loading techniques. The technique uses the Sandia Z and Saturn accelerators to produce magnetically driven planar ramp waves of 200-300 ns rise time in copper or aluminum, which then propagate into a material sample. An apparatus has been developed to provide a high-quality, high-purity molten tin sample pre-heated to 550-700 K. This sample is isentropically loaded to 100-250 kbar, driving it across the liquid–solid phase boundary. Velocity interferometry is used to measure time-resolved wave profiles at the interface between the molten tin and a window material (lithium fluoride or sapphire).

Preliminary experiments indicate that freezing under these dynamic conditions occurs on a time scale short enough to be detected using wave profile measurements. Results from a more comprehensive series of experiments, planned for April 2002, will be discussed.

Iron Sound Velocity and Preliminary Ellipsometric Data

J.H. Nguyen, N. Holmes

Lawrence Livermore National Laboratory, Livermore, USA

We measured sound velocity of shock compressed iron at pressures between 136 GPa and 400 GPa and observed indications of melting at 221 ± 3 GPa on the Hugoniot. The data follow an expected solid sound velocity curve up to 221 GPa and follow the liquid sound velocity curve upon completion of melting at 260 GPa.

In addition, we observed no solid-solid phase transition on the traversed Hugoniot, suggesting no new triple point or solid-solid phase boundary near 200 GPa.

In a parallel effort, we also designed and used a new miniaturized set-up to collect ellipsometric data in shock compression experiments. These data can be used to determine emissivities as well as optical constants at shocked conditions. Iron is among the metals we are studying with this technique.

High-Porous Shields in Hypervelocity Impact Studies

V.V. SILVESTROV

Lavrentyev Institute of Hydrodynamics, Novosibirsk, Russia

In the present paper, the author intends to draw attention of the researches working in the field of numerical simulations of impact phenomena to the three effects observed during high-velocity impact by spherical projectile on thin sheet. One of these effects is not widely known, though, it is not a new one; other effects are new. Last two effects were observed during impact on high-porous materials and found no explanation. Probably, these effects can be accurately explained using a detailed numerical simulation of the dynamics of impact by a high-velocity projectile on a shield and fragmentation of this projectile.

Experimental Setup. We studied experimentally the normal impact of a steel spherical projectile with diameter $d_p = 2$ mm and velocity $V_p = 2 \div 7.3$ km/sec on thin plates. The standard shields (used for comparison) were plates of duralumin; the other shields were plates of pressed copper fine powder (the size of a separate

grains is 10÷20 μm) with a density of $\rho_{\omega} = 2.2, 2.8, 4.0$ g/cc and a thickness of $t_b = 1 \div 2$ mm. After impact, the projectile breaks, and a cloud of secondary debris, consisting of fragments of the projectile and shield, develops behind it. To observe fragmentation and its results, we used a witness plate of soft duralumin. The cloud of debris strikes the witness plate thereby forming an ensemble of craters on the target surface. The number of craters and their sizes can attest the degree and character of fragmentation of impacting materials.

Using high porous metallic shields we pursued two main goals. Firstly, as the strength of these shields is close to zero, the temperature of shock heating reaches 10^4 K, and therefore, the fragments with sizes larger than powder grains are unable to be formed during impact, as a result, shield fragments cannot produce craters whose diameter exceeds 0.1 mm at maximum impact velocities. Therefore, we can assume that the craters with larger diameters were produced during impact by the fragments of a steel projectile. In the experiment, the craters with a size of 0.1÷4 mm were observed. Secondly, using shields made of physically inhomogeneous materials, we are able to study how this physical inhomogeneity affects threshold characteristics and a breakup pattern of the projectile.

The first effect is the formation of ***annular structure in crater field***. It is known that when a steel projectile impacts a thin aluminum shield with $t_b/d_p \le 0.5$ at a velocity of $V_p \ge 7$ km/sec, an annular structure is formed on the target surface. In this structure, the deepest craters are located in the annular zone nearby the center, not in the center of a crater field [Titov, 1968]. It has long been unclear what causes the formation of the above structure: the impact of projectile fragments or that of the shield debris from the peripheral area of the perforation hole.

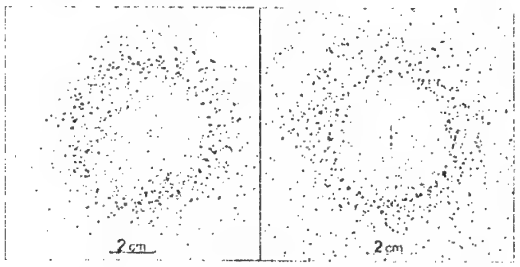

a - *D16*, 160 GPa *b* – *Cu*, 4 g/cc, 156 GPa

Figure 1. Witness plate patterns for an impact velocity of 7.3 km/sec, the annular structure.

Figure 1 shows pictures of crater fields for shields of duralumin and porous copper at $V_p = 7.3$ km/sec. Almost identical structures with the characteristic diameter 60÷70 mm are observed. These structures remain when the witness plate is placed from the shield at a standoff $S_0 = 75 \div 150$ mm and the structure diameter is proportional to S_0. However, in the case of a porous shield, most craters are formed by the projectile fragments with the characteristic size $s_f \approx 0.1 \div 0.2$ mm. Obviously, a specific radial dispersal of the largest projectile fragments originating from side and back surfaces of the spherical projectile is due to their interaction with an ellipsoid-shaped zone of high pressure, which exists into the projectile body near the projectile/target contact surface.

The second effect. It was found that at low impact velocities of 3÷5 km/sec, porous shields cause a better breakup of a steel spherical projectile than duralumin shields if ***impact pressures are equal*** and range from 30 to 100 GPa [Silvestrov et al, 2000]. Figure 2 shows a dependence of the maximum penetration depth for the debris fragments recorded on the witness plate on the impact pressure that was calculated in

a one-dimensional approximation by the equation of state for high-porous metals [Kormer *et al*, 1962].

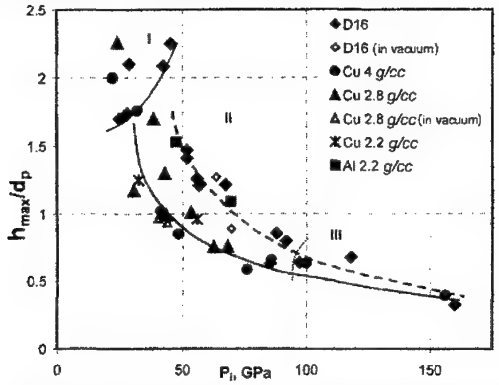

Figure 2. Maximum penetration depth versus the impact pressure for duralumin and porous shields. Region I denote the non-damage impacts.

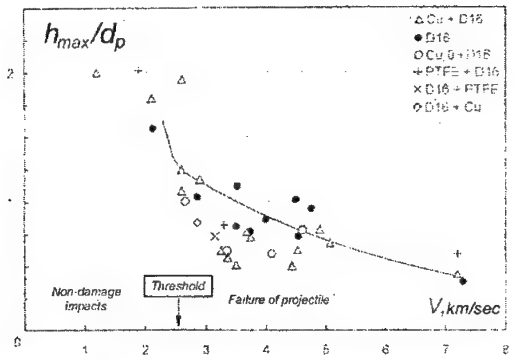

Figure 3. **Maximum penetration depth versus the impact velocity for double-layer shields.**

The threshold impact pressure decreases from 49 GPa (for duralumin D16) to 28 GPa in the case of high-porous copper shields even with the lower shield areal mass, and a greater radial dispersal of fragments in the debris cloud is observed. Probably, in this pressure range, a better breakup of the projectile is caused by the effects of the heterogeneous structure of a material for a high-porous shield, particularly, the effect of the high shield material temperature in the impact zone. However, in order to reach the same impact pressure for a porous shield, a higher impact velocity is required.

The third effect was noted when the protective properties of double-layer shields were being studied. One layer is of aluminum, and the other one is of copper powder with a density of 2.8 g/cc. Each layer is 1 mm in thickness. It was shown that the presence of a high-porous layer has a significant effect on the character of the projectile breakup and morphology of an observed crater field. Figure 3 shows the dependence of the penetration depth on the impact velocity. For porous copper/duralumin shields at impact velocities of $V_p \approx 3 \div 5$ km/sec, all points are

lower than for the aluminum shields 2 mm in thickness. Additionally, the decrease of maximal crater diameter and number of the large craters are observed. Hence, the double-layer bumper with the first layer made of low-pressed fine copper and the duralumin sheet as the second layer ruptures the steel projectile better than the duralumin bumper with the same thickness in the velocity range ~ 3÷5 km/s ***at equal areal mass and equal impact velocities*** [Silvestrov, 2001]. The order of layers is not important. With an increase in the impact velocity above 5 km/sec, the observed effects are lowered.

Thus, there are some probable reasons for the better crushing properties of high-porous layers. The first reason is the high temperature of shock heating of target material in the impact area and, hence, with the specific features of hydrodynamic rarefaction of the shield material from the impact side, for example, a cumulative ejection of the shield material in a vapor-liquid state into the projectile's side. Probably, in the shock-wave specificity of the interaction of the projectile with high-porous structures, for example, a multiple interaction of a projectile with powder grains.

The second reason is that in the case of double-layered shields, two shock waves with an increasing amplitude sequentially affect the projectile body under conditions of intensive unloading that is due to the small lateral size of the spherical projectile, and it can lead to a better breakup of the projectile. Under the first series of "shock loading-unloading" waves, not only large cracks that split a projectile body onto fragments are formed, but also fracture centers inside the fragments. Under the second series of the shock waves, these fracture nuclei activate and give rise to additional cracks that facilitate the greater splitting of projectile fragments.

Thus, using high-porous shields for studying hypervelocity impact on thin plates allowed to find out the origin for annular structure formation and to draw attention to using porous layers in the structure of anti-meteorite protection shields, which seems rather promising. Using available software codes, such as, for example, *AutoShield*, appear to be helpful in calculating hypervelocity impact for further simulating and qualitative explanations of the effects considered and also in testing the failure models under intensive dynamic loading.

Measurement of Shock Residual Temperature in Steel with Help of Phase Transitions in Zirconium and Titanium

A.M. Podurets, A.R. Kutsar

Russian Federal Nuclear Center-VNIIEF, Sarov (Arzamas-16), Russia

Measurement of temperature – one of the main thermodynamic parameters of the substance state, is of great experimental difficulty. Therefore more often the shock and residual temperatures are defined by calculations, using various equations of state. The basic experimental method of shock and residual temperatures measurement is the optical technique, best suitable for transparent materials. At temperature measurement in metals significant excess of experimentally obtained temperatures, in comparison with calculated ones, was frequently noticed, that is explained by elastic - plastic phenomena. In this work the new method of residual temperature estimation in metals is proposed, it can be used for equations of state testing.

The hysteresis of α-ω transformations in ***Ti*** and ***Zr*** is so great that the high pressure phases recover after removal of both static and dynamic pressures that allows to carry out studies of a phase structure and its dependence on conditions of loading.

As samples we used ***Zr*** and ***Ti*** disks with 16 *mm* in diameter and 1 *mm* in width. The samples were put in the recovered ampoules made of stainless steel X18H10T (24 *mm* in diameter and 16 *mm* in height) and loaded by plane shock waves with pressure amplitudes from 7 to 32 *GPa*.

The experiments were carried out at initial temperatures 0 and -180°C. The phase structure was determined using x-ray diffraction. Results of experiments are in Fig. 1.

From compression and unloading conditions, *P-T* diagram of ***Zr*** and ***Ti*** and temperature stability of phases at atmospheric pressure [1] we may conclude that the curve of ω-phase concentration in the recovered samples as a function of the pressure $\eta_\omega(P)$ should have three parts: raising, beginning at a

From compression and unloading conditions, *P-T* diagram of ***Zr*** and ***Ti*** and temperature stability of phases at atmospheric pressure [1] we may conclude that the curve of ω-phase concentration in the recovered samples as a function of the pressure $\eta_\omega(P)$ should have three parts: raising, beginning at a phase transition pressure, plateau (or maximum) and consequent lowering. This lowering is caused by the residual heating effect on ω-phase; it is known that at atmospheric pressure this phase is not stable and decomposes during heating, being transformed into stable α-modification.

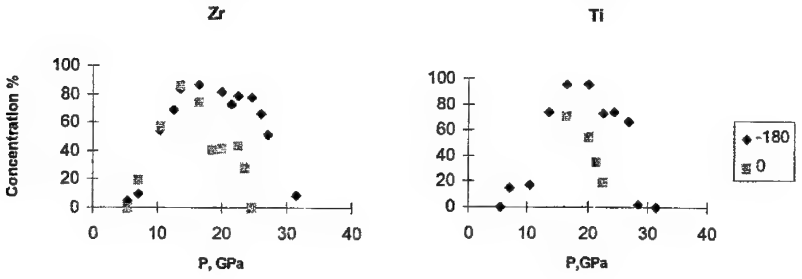

Figure 1: Concentration of the ω-phase in recovered samples $\eta_\omega(P)$ after shock loading at different initial temperatures.

The difference between dependencies $\eta_\omega(P)$ for titanium and zirconium is only in the value of pressure at which the ω-phase appears and disappears in the recovered samples.

Shock temperatures and residual temperatures after unloading, as a rule, are calculated with the help of equations of state, obtained from shock experiments data.

According to calculations using simple EOS, residual temperatures after loading to $P \leq 30$ *GPa* in materials of ampoules and samples should not exceed ~100°C. Obviously, that is not so, because in reality the ω-phase does not decompose at such temperature effect. Below we shall try, on the basis of obtained $\eta_\omega(P)$-dependencies and the data on temperature stability of the ω-phases, to restore actual residual temperatures, realized under conditions of our experiments.

So, above some pressure P^*, and consequently beginning with some residual temperature T_o, the high pressure phase in recovered samples completely decomposes, and its concentration becomes zero. It means that residual temperature also reaches some critical value T_0^*. Thus, by study of high pressure phase decomposition kinetics in laboratory conditions, it is possible to simulate the decomposition process in real conditions of sample cooling after loading and unloading. Basing on kinetics study and following decomposition modeling we obtained values of residual temperature in steel ampoules that were achieved in our experiments. The kinetics of ω-α transition was described by the Avrami equation.

The obtained values of residual temperature are much higher than values obtained by calculations (less than 90° at pressure up to 30 *GPa*). It is necessary to mark that the discrepancy in values of calculated and experimental residual temperatures in stainless steel of a similar composition was also found in [2] with use of the optical method.

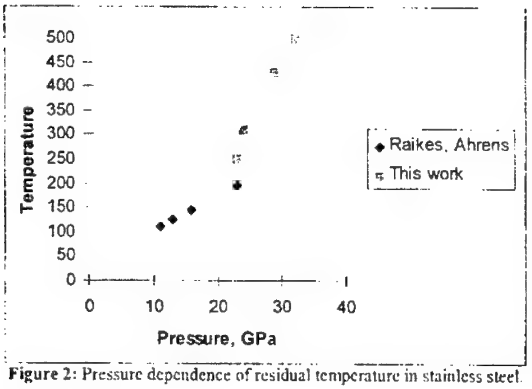

Figure 2: Pressure dependence of residual temperature in stainless steel.

[1] .., .., .., **213** (1973) 81-84.
[2] Raikes S.A., Ahrens T.J., *Geophys. J. R. Astr. Soc.* **58** (1979) 717-747.

A New Semi-Empirical 300 K Isotherm for Copper

J.C. Boettger, C.W. Greeff, J.D. Johnson

Los Alamos National Laboratory, Los Alamos, USA

Copper has a long history as one of the principal pressure standards available for use in equation of state work. There are at least three semi-empirical 300 K isotherms available for copper at this time[1-3], each obtained by approximately removing thermal effects from an experimentally determined Hugoniot. Each of these three standards is subject to its own set of limitations. The oldest and most commonly used copper standard is one published by McQueen, *et al,*[1] in a tabular form, for pressures ranging from 0 to 2.4 Mbar in increments of 0.1 Mbar. The second copper standard is a reduced Hugoniot that was used to calibrate the ruby fluorescence pressure scale[2], but is rarely used today due to its inaccessibility. The most recent copper standard was tabulated by Nellis, *et al,*[3] on a rather sparse mesh of pressures ranging from 0.95 Mbar to 10.0 Mbar and is typically used for pressures in excess of 2.4 Mbar.

In the present investigation, a new semi-empirical 300 K isotherm has been generated for copper as part of a global SESAME equation of state. For pressures up to about 3.5 Mbar, the 300 K isotherm was derived from shock data[4], using a Gruneisen function obtained with lattice dynamics from a theoretical phonon spectrum. At ultra-high pressures, the 300 K isotherm was required to asymptotically approach the Thomas-Fermi-Dirac limit. For intermediate pressures, the isotherm was required to smoothly switch between the two limits. The new 300 K isotherm is noticeably softer than that of McQueen, et al, due to the use here of a larger, more realistic Gruneisen parameter, but is in good accord with the copper standard used to calibrate the ruby fluorescence scale. For pressures between 2.4 Mbar and 10 Mbar, it is in rather good agreement with the tabulated pressures of Nellis, et al, except for their 10 Mbar point. The present isotherm agrees well with high precision electronic structure calculations for pressures ranging from 10 Mbar to 1 Gbar. The new 300 K isotherm should provide a good standard for pressures ranging from 0 to 10 Mbar.

1. R.G. McQueen, S.P. Marsh, J.W. Taylor, J.M. Fritz, and W.J. Carter, in *High Velocity Impact Phenomena*, edited by R. Kinslow (Academic, New York, 1970), p. 293.

2. P.M. Bell, J. Xu, and H.K. Mao, in *Shock Waves in Condensed Matter*, edited by Y.M. Gupta (Plenum Press, New York/London, 1985), p. 125; and references therein.

3. W.J. Nellis, J.A. Moriarty, A.C. Mitchell, M. Ross, R.G. Dandrea, N.W. Ashcroft, N.C. Holmes, and G.R. Gathers, *Phys. Rev. Lett.*, **60**, 1414 (1988).

4. A.C. Mitchell, W.J. Nellis, J.A. Moriarty, R.A. Heinle, N.C. Holmes, R.E. Tipton, and G. W. Repp, *J. Appl. Phys.*, **69**, 2981 (1991).

Temperature Dependence of the Shear Moduli of Copper and Stainless Steel 316 to 1.5 Megabars

D.L. Preston[1], R.S. Hixson[2], D. Hayes[2]

[1] *Applied Physics Division, Los Alamos National Laboratory, Los Alamos, USA*

[2] *Dynamic Experimentation Division, Los Alamos National Laboratory, Los Alamos, USA*

Hydrocode simulations of high strain rate solid flow require accurate models of plastic constitutive behavior. Most material strength models are based on the assumption that the flow stress scales with the shear modulus, G; hence the complete plastic constitutive relation requires a model of the density- and temperature-dependent shear modulus.

Longitudinal sound speeds on the shock Hugoniot can be accurately measured using the release wave overtake technique [*R.G. McQueen, J.W. Hopson, and J.N. Fritz, Rev. Scient. Instr. 53, 245 (1982)*]. Data exist for sound speeds in both copper and stainless steel 316 in the solid, liquid, and mixed phases. These data can be analyzed by assuming that the metal is on the equilibrium equation of state surface and that the plastic response is not time dependent [D. Hayes, R.S. Hixson, and R.G. McQueen, in *Shock Compression of Condensed Matter* – 1999, edited by M.D. Furnish, L.C. Chhabildas, and R.S. Hixson (American Institute of Physics, 2000)]. The Mie-Gruneisen equation of state that exactly produces the linear shock velocity – particle velocity Hugoniot $u_s = c_0 + s u_p$ is used for the solid phase. The product $\rho\gamma$ is assumed constant in the solid. The bulk sound speed on the Hugoniot for this Mie-Gruneisen equation of state is

$$c_{B,H} = c_0 \frac{1-\varepsilon}{1-s\varepsilon}\left[\left(1-\frac{\gamma\varepsilon}{2(1-\varepsilon)}\right)\frac{1+s\varepsilon}{1-s\varepsilon}+\frac{\rho\gamma\varepsilon}{2\rho_0}\right]^{\frac{1}{2}}. \qquad (1)$$

The shear modulus on the Hugoniot for an isotropic solid is obtained using

$$G_H = \frac{3}{4}\rho_H\left(c_{L,H}^2 - c_{B,H}^2\right), \qquad (2)$$

where $c_{L,H}$ is the measured longitudinal sound speed in the shocked state.

The shear moduli of copper and stainless steel 316 can be estimated to 10% accuracy along the melt curve by means of the Burakovsky-Preston (BP) melting relation which results from treating melting as a dislocation-mediated phase transition [L. Burakovsky, D.L. Preston, and R.R. Silbar, Phys. Rev. B **61**, 15011 (2000)]. The basic idea is that dislocations (and disclinations) suddenly proliferate at the melt point. A statistical mechanical description of this dense ensemble of dislocations yields the BP melting relation

$$T_m = \frac{c\,G(T_m)\,v_{WS}(T_m)}{4\pi \ln(z-1)} \ln\left(\frac{2.9}{\rho_D(T_m)\,b^2}\right) \qquad (3)$$

c is a geometric constant, z is crystal coordination number, $\rho_D(T_m)$ is dislocation density at melt, $v_{WS}(T_m)$ is the volume of the Wigner-Seitz cell at melt, and b is the magnitude of the Burgers vector. An analysis of melting data on 62 elements gave $\rho_D(T_m)b^2 = 0.61 \pm 0.2$, which amounts to only 17% uncertainty. For individual elements, $\rho_D(T_m)b^2$ is constant along the melt curve [L. Burakovsky, D.L. Preston, and R.R. Silbar, J. Appl. Phys. **88**, 6294 (2000)]. If the crystal structure does not change along the melt curve then Eq. (3) implies

$$G(\rho, T_m(\rho)) = G(\rho_0, T_m(\rho_0))\frac{\rho_0}{\rho}\frac{T_m(\rho)}{T_m(\rho_0)}, \qquad (4)$$

where ρ_0 is the zero-pressure mass density. Thus the experimental value of G at P=0 and the known melt curve can be used to calculate the shear modulus along the entire melt curve. For copper and stainless steel 316, $G(\rho, T_m(\rho))$ is determined to 10% accuracy.

To proceed we assume G is linear in T/T_m at fixed density

$$G(\rho, T) = G_0(\rho)(1 - \alpha(\rho)T/T_m(\rho)), \qquad (5)$$

from which follows

$$G(\rho, T_H(\rho)) = G(\rho, T_m(\rho))\frac{1 - \alpha(\rho)T_H(\rho)/T_m(\rho)}{1 - \alpha(\rho)}, \qquad (6)$$

where $T_H(\rho)$ is the Hugoniot temperature. Eq. (6) is used to obtain $\alpha(\rho)$ (provided $T_H << T_m$) given $G(\rho, T_H)$ as determined from analysis of sound speed measurements and $G(\rho, T_m)$ from the BP melting relation and the known melting curve.

We will discuss the release-wave measurements in copper and stainless steel 316, and the analysis of those data to determine the shear moduli on the Hugoniot. The BP melt relation, its accuracy, and its application to predicting the shear modulus along the melt curve will be considered next. We will then present our results for $\alpha(\rho)$. Finally, we will discuss the significance of ambiguous results at high pressure on the Hugoniot in terms of potential material response models.

Simulation of Small Spherical Particles Impacts on Fused Silica Targets

F. Malaise, I. Bertron, J-M Chevalier, R. Courchinoux

CEA/CESTA, Le Barp, France

Single impact damage of fused silica targets by small particles (0.55 mm diameter steel spheres) has been investigated experimentally and numerically. This study is applied to the prediction of damage induced when shrapnel strikes the debris shields of the Laser Megajoule chamber.

The particles were projected with a two-stage gas gun (MICA) at velocities up to 4000 m/s. Fused silica targets were placed normally to the direction of impact. The targets were recovered and polished after each experiment. Figures 1 and 2 show top view and sectioned view of the damage induced by the impact of a 0.55 mm diameter steel sphere at a velocity of 3670 m/s. On top view, we can see the crater

formed by the penetration of the sphere. On sectioned view, we can see cone, median and lateral cracks created during loading and unloading of the fused silica target.

An anisotropic damage model has been implemented in the 2D eulerian numerical code HESIONE [1][2][3]. Numerical results are presented in figure 3. The mechanisms of penetration, fragmentation of fused silica and initiation of cone, median and lateral cracks are in very good accordance with experiment. The size of the crater calculated with HESIONE is the same as the measured one. Nevertheless, some quantitative discrepancies remain between calculated and experimental size of damaged area. Efforts in modelling the propagation of cone and lateral cracks are essential to improve the numerical simulations.

References

[1] MALAISE F., BERTRON I., 2000, "Vulnérabilité d'un pare éclats de la chambre d'expériences du LMJ. Modèle de comportement dynamique de la silice fondue", CEA/CESTA/DEV/GEDT report, DO 361.

[2] RUBIN M. B., ATTIA A. V., 1990, "A continuum tensile failure model with friction", Lawrence Livermore National Laboratory Report, UCRL-ID-104759.

[3] BERTRON I., MALAISE F., 2001, " Vulnérabilité d'un pare éclats de la chambre d'expériences du LMJ. Implantation dans le code Hésione d'un modèle de comportement dynamique de la silice fondue", CEA/CESTA/DEV/GEDT report, DO 70.

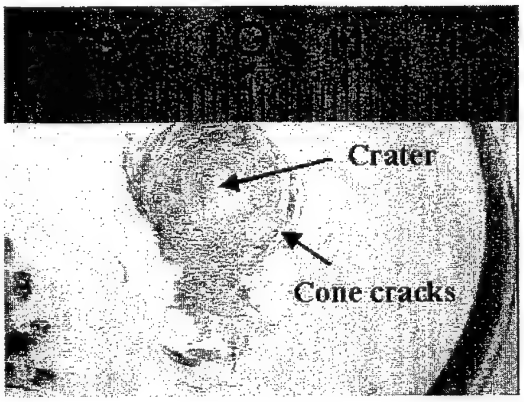

Figure 1. Top view of damage.

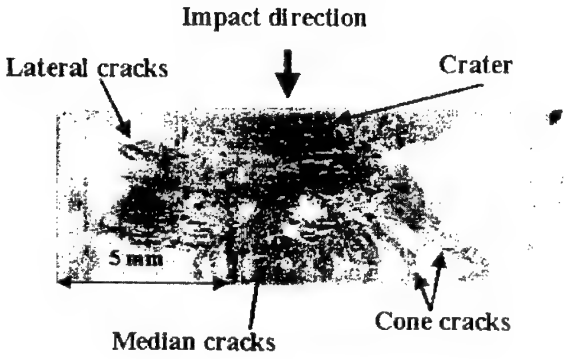

Figure 2. Sectioned view of damage.

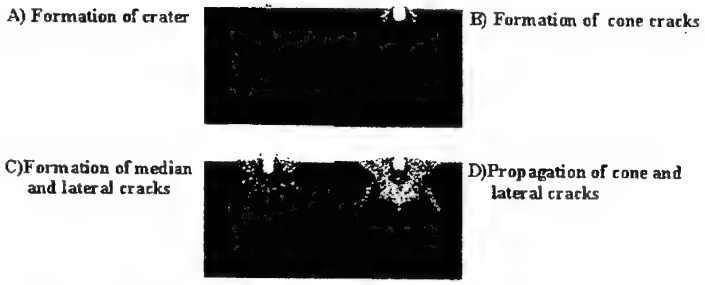

Figure 3. Numerical simulation of damage induced by the impact of a 0.55 mm diameter steel spherical particle on a fused silica target at a velocity of 3670 m/s (red area is anisotropically damaged).

Shock Wave Experiments Using a Pulsed Electron Beam to Study Copper and Molybdenum Thermoelastic Responses

F. Malaise, R. Courchinoux, B. Cassany, J-M Chevalier

CEA/CESTA, Le Barp, France

The thermoelastic behaviours of copper and molybdenum targets have been investigated experimentally and numerically using a pulsed source of electrons (3 Mev – 3kA – 60 ns duration).

Samples have been submitted to fluences up to 50 J/cm^2. The electron beam-target interaction generates an unstable shock wave that propagates through the sample and modifies the state of matter. The analysis of the thermoelastic response of a sample allows the effective Mie Grüncisen coefficient Γ_0 to be obtained [1]. Thermoelastic responses of copper and molybdenum have been studied by measuring the rear surface motion of target. Rear surface motion was registered by a differential laser interferometer (Michelson interferometer) mounted in the vicinity of the target chamber (Figure 1). The velocity is obtained by differentiating the displacement function f(x). The experimental set up is presented in figure 1. The assemblies of copper and molybdenum targets are respectively shown in Figure 2 and Figure 3.

The beam-target interaction has been analysed with numerical simulations of energy deposition and shock wave propagation. Mie Grüneisen equations of state (EOS) were constructed on the basis of published data. Comparisons between experimental and numerical results are shown in figures 4 and 5. Calculations correspond to a Mie Grüneisen EOS with $\Gamma_0 = 2$ for copper and with $\Gamma_0 = 1.6$ for molybdenum. The numerical simulations are in good agreement with experimental data.

Pulsed electron beam experiments are very interesting to obtain thermoelastic properties of materials. This method has been used to measure the Mie Grüneisen coefficient of materials of interest for CEA studies.

Acknowledgements

The authors want to thank J-L Rullier, D. Guilhem and T. Lefèvre for their contribution during the experiments.

References

[1] FORTOV V. E., EFREMOV V. P., KANEL G. I., MOROZOV P. V., DEMIDOV B. A., LOMONOSOV I. V., NI A. L., VOROB'EV O. YU, 1991, *Theoretical and experimental investigation of shock waves generated by high energy charged particle beams*, Proceedings of Conference Shock Compression of Condensed Matter.

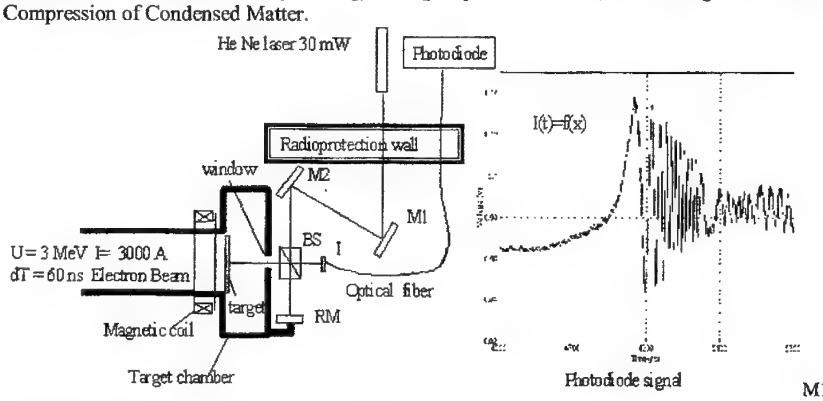

M1, M2 : Alignment mirrors
BS : Beam Splitter mounted on the target chamber
RM : Reference Mirror mounted on the target chamber
I(t) : Intensity
f(x) : Displacement

Figure 1. Experimental set-up.

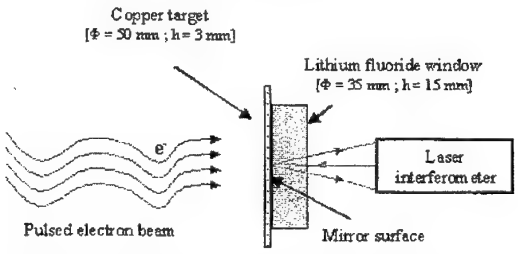

Figure 2. Experimental configuration with copper target.

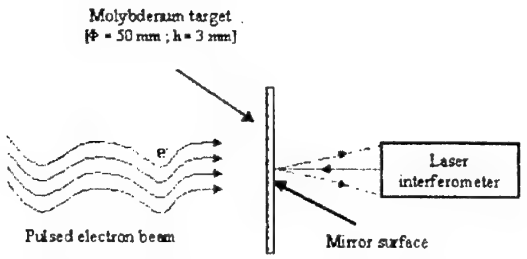

Figure 3. Experimental configuration with molybdenum target.

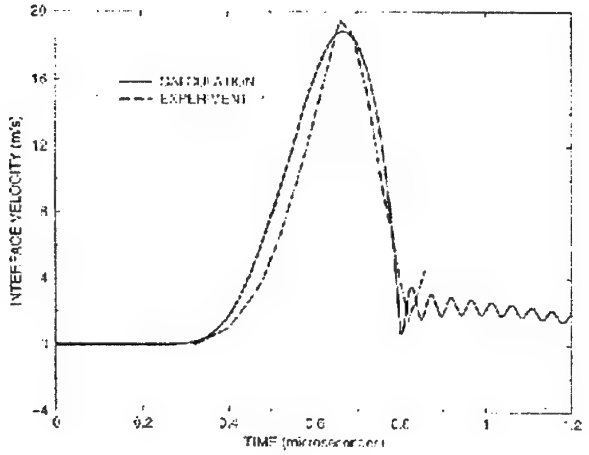

Figure 4. Comparison of experimental and calculated shock wave profiles at copper – lithium fluoride interface. The fluence of the pulsed electron beam is 50 J/cm^2.

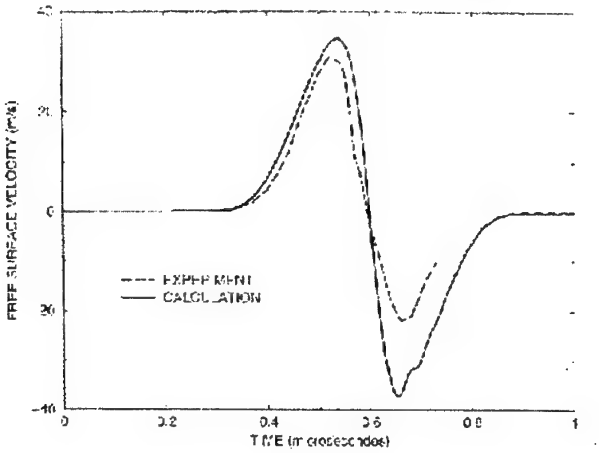

Figure 5. Comparison of experimental and calculated shock wave profiles at the rear face of molybdenum target. The fluence of the pulsed electron beam is 50 J/cm^2.

Program System SIRIUS for Studying and Testing Equations of State

L.F.Gudarenko, O.N.Gushchina

Russian Federal Nuclear Center-VNIIEF, Sarov (Arzamas-16), Russia

Equations of state are involved in application programs that implement various models describing compressible matter behavior under action of intense pulse loads. The equations of state are integrated into libraries for the operation to be more efficient. The program system SIRIUS (abbreviation of Russian *SIstema Rascheta i Issledovaniya Uravnenij Sostoyaniya* translated as *System for equations of state computation and study*).

The system contains:

- modules for isoline computation;
- modules for computation of intersection points of isolines calculated by various equations of state;
- modules for computation viewing;
- libraries of numerical methods used;
- libraries of equations of state;
- database of experimental data on properties of materials studied experimentally using shock waves.

The system is implemented in visual programming system Delphi using an object-oriented approach. The object-oriented model of the system involves more than seventy classes, principal of which are classes implementing numerical methods for equation system solution, the class of point computation on isolines, the equation of state class. Independent classes are developed for manipulation of thermodynamic functions and systems of units.

The modules for the isoline computation include an interface for setting initial data and a library of classes for the computation. The system SIRIUS can compute isobars, isochores, isotherms, isoenergets, Hugoniot and Poisson shock adiabats. The initial data setting interface allows selection of independent variables for the computation, setting a system of units, a variable at a step the computed data is to be output, making a list of TDF to be computed. The interface also allows setting initial independent variable approximations needed for numerical computations.

The modules for computation viewing implement the window interface, whose main window contains view toolbars and a bookmark set with computed data. The results are represented in the form of tables containing values of selected TDF. There is a capability to construct thermodynamic function graph series, plot experimental data from the database of experimental data or from text files.

The system SIRIUS can be employed to simulate experiments on studying material properties with the reflection method using the modules for computation of intersection points of isolines calculated by various equations of state. This allows both planning new experiments and more exact specification of previously obtained experimental data.

The following numerical methods are used in the system SIRIUS: the method for solution of Gaussian linear equation system with the major term selection, the Newtonian method for nonlinear equation system solution, and the method for numerical solution of differential equation systems with the rational extrapolation method. Each method is implemented as a separate class which can be used by any other application programs.

The database of experimental data on properties of materials studied experimentally using shock waves contains information about more than eight materials. The database involves data obtained by Russian and foreign investigators on shock and adiabatic compression of continuous and porous specimens as well as sound speed and rate of expansion of shock-compressed materials to air. The

database has the relational structure, the tables are implemented in the PARADOX format. The DBMS constitutes a widow interface allowing retrieval of needed material, scanning of data for selected material, construction of graphs, export of data to text files and graphs of curves computed in the system SIRIUS.

The libraries of equations of state include translated programs for computing thermodynamic functions (TDF) compiled in dynamically loaded library DLL. The mechanism of dynamic library loading allows using equation-of-state programs implemented in any languages. The libraries should be accompanies with text files with description of their contents and EOS characteristics. In the system SIRIUS, this information is compiled in the relational database. The database window interface contains the following fields: the list of all EOS, the list of constant sets for each EOS, the list of materials characterizing the constant set selected. For the selected EOS, it is possible to scan its characterization: passport, its description, if any, for the constant set selected.

It is suggested that in the future the range of problems solved with the system SIRIUS should be considerably extended, the algorithms for computing thermodynamic functions and service capabilities for computed data representation should be improved.

Thermodynamic Properties and Shock Compression of Strongly Coupled Plasma

P.R. Levashov[1], M. Bonitz[2], V.S. Filinov[1], V.E. Fortov[1]

[1]*Institute for High Energy Densities, Moscow, Russia*
[2]*Universität Rostock, Germany*

Thermodynamic properties of correlated Fermi systems attract the interest of scientists in many fields, including plasmas, astophysics, solids and nuclear matter [1]. However all present theories have practical difficulties. It is, therefore, important to use alternative approaches, such as quantum Monte Carlo simulation. This method allows for an efficient treatment of strong coupling phenomena. Nevertheless, there has been one major obstacle preventing efficient simulation of Fermi systems – the so-called sign problem resulting from summation over all permutations of the density matrix.

In this paper a different path integral representation is presented in which no sign problem appears [2]. The numerical simulation of strongly coupled hydrogen plasma considered as a subsystem of fermionic quantum electrons and a subsystem of classical protons is carried out. Calculated are dependencies of pressure and internal energy on degeneracy parameter at constant coupling parameters [3]. Different thermodynamic parameters are obtained on 6 isotherms between 10^4 and 10^7 K on temperature and from 10^{18} to 10^{28} cm^{-3} in density range. A number of interesting physical effects from pair distribution functions analysis appear in the simulations: formation of molecules at low densities of 10^{22} cm^{-3}, electron pairing at $5 \cdot 10^{26}$ cm^{-3}, proton crystallization at high densities of 10^{27} cm^{-3} [4]. The calculation of hydrogen shock hugoniot based on simulation results is performed. In the region of metal-insulator transition for hydrogen it is found a metastable behavior of pressure-density dependence on the isotherms 10^4 K and $2 \cdot 10^4$ K which vanishes at higher temperatures. Independent evaluations and experimental investigations indirectly confirm this fact. The results of our calculations are in a good agreement with other theories in the regions of their applicability.

1. Strongly Coupled Coulomb Systems, G. Kalman (Ed.), Pergamon Press 1998.
2. V. S. Filinov, P. R. Levashov, V. E. Fortov, M. Bonitz. In: Progress in Nonequilibrium Green's Functions, M Bonitz (Ed.), World Scientific 1999, P. 513.
3. V. S. Filinov, M. Bonitz, V. E. Fortov, JETP Letters **13**, 245 (2000).
4. V. S. Filinov, V. E. Fortov, M. Bonitz, D. Kremp, Phys. Let. A **274**, 228 (2000).

SESSION
"Experiments in Support of Detonation Models Development"

Chairmen:
W. Proud - **University of Cambridge, Cambridge, UK**
P. Urtiew - **Lawrence Livermore National Laboratory, USA**

Thermal Cook-Off of an HMX Based Explosive: Pressure Gauge Experiments and Modeling *

P.A. Urtiew, J.W. Forbes, C.M. Tarver
F. Garcia, D.W. Greenwood, K.S. Vandersall

Lawrence Livermore National Laboratory, Livermore USA

Safety issues related to thermal cook-off are important for handling and storing explosive devices. Violence of event as a function of confinement is important for prediction of collateral events.

There exist major issues requiring of understanding of the following events: (1) transit to detonation of a pressure wave from a cook-off event, (2) sensitivity of HMX based explosives changes with thermally induced phase transitions and (3) the potential of a metal fragment accelerated by a cook-off reaction, creating a reaction in a neighboring explosive device by its impact.

Results of cook-off events of known size, confinement and thermal history allows for development and/or calibrating computer models for calculating events that are difficult to measure experimentally.

*This work was performed under the auspices of the United States Department of Energy by the Lawrence Livermore National Laboratory under Contract No. W-7405-ENG-48

Anomalous Detonation Velocities Following Type II Deflagration-to-Detonation Transitions

M.J. Gifford & J.E. Field

Cavendish Laboratory, Cambridge University, Cambridge, U.K.

Early experiments identifying type II deflagration-to-detonation transitions (DDT) in ultrafine pentaerythritol tetranitrate (PETN) and cyclotrimethylene trinitramine (RDX) showed that the detonation velocities in these materials were significantly different from predictions based on the initial density of the charge. The detonation velocity in the PETN was found to be substantially higher following a type II DDT than a shock-to-detonation transition (SDT) in pristine material. By contrast, the detonation velocity of the ultrafine RDX following a type II event was lower than for the SDT charges.

Subsequent experiments have been carried out to measure variation in temperature, pressure and charge geometry during type II DDT events and so determine the nature of the charge prior to the outbreak of detonation. A further series of experiments have been performed in which the initial conditions are altered to emulate aspects of the state of the material prior to a type II DDT. The results of these experiments have allowed a hypothesis for the change in detonation velocity to be constructed.

Effect of HMX Polymorphous Transformations after Thermal Treatment on Its Sensitivity to Impact Treatment

O.L. Ignatov, V.N. Lashkov, V.N. Lobanov, A.V. Strikanov, A.N. Shestakov

Russian Federal Nuclear Centre – VNIIEF, Sarov (Arzamas-16), Russia

HMX is one of the most powerful high explosives, it possesses high heat stability and big crystal density. HMX withstands the exposure at the temperature of 200°C during 8 hours 30 minutes, and the temperature of 220°C during 2 hours [1]. HMX crystals exist in four modifications (α, β, γ, and δ), which are stable in different temperature intervals and differ in crystal density and sensitivity to mechanical effects [2, 3, 4]. HMX heating-up at the temperature of 180°C ensures its complete transition from β-modification to metastable δ - modification.

The present report represents the results of research of polymorphous transition in HMX using the method of differential scanning calorimetry. The difference in the initial polymorphous transition temperature for macrocrystalline and microcrystalline HMX has been shown. The polymorphous transition in microcrystalline HMX starts at the temperature about 10 degrees higher as compared to the macrocrystalline HMX. It has been experimentally demonstrated that after heating-up of HMX, which leads to its polymorphous transition to δ-modification, it remains highly sensitive to friction during a long period of its storage at room temperature (over five years). During first 48-72 hours the reverse polymorphous transition to a mixture of stable and metastable phases takes place in HMX bulk.

The sensitivity of macrocrystalline and microcrystalline HMX to friction after heating-up, which leads to its polymorphous transition to δ-modification, can be compared to sensitivity of TNRS and lead azide [5]. At the same time the character of HMX explosive transformation considerably differs from priming explosives. The mechanical effect excites a detonation process in priming explosives, and the one excites a flash without detonation in HMX.

References

1. L.V. Dubnov, N.S. Bakharevich, A.I. Romanov. Industrial explosives. Moscow: Nedra, 1988.
2. E.Yu. Orlova. Chemistry and technology of high explosives. Leningrad: Khimiya, 1981
3. E.Yu. Orlova, N.A. Orlova, V.F. Zhilin at al. Oktogen – heat resistant explosive. Moscow: Nedra, 1975.
4. V.N. Lashkov, V.N. Lobanov, S.A. Klimov, O.L. Ignatov, A.V. Kiselyov. Polymorphous transformations in oktogen. The materials of international conference "Shock waves in condensed mediums", Russia, Saint Petersburg, October 8-13, 2000 r.
5. L.I. Bagal. Chemistry and technology of priming explosives. Moscow: Mashinostroyeniye, 1975.

A Laser-Accelerated Flyer System

M.W. Greenaway, W.G. Proud, J.E. Field

Cavendish Laboratory, University of Cambridge, Cambridge, UK

A system has been developed for the production of miniature aluminium flyer plates using a Nd:YAG laser. These flyer plates have been found to achieve velocities in excess of 8 km/s and have been successfully impacted onto the secondary explosives pentaerythritol tetranitrate (PETN) and hexanitrostilbene (HNS) to induce detonation. High-speed streak photography has been used to observe the integrity of the flyers and the detonation event.

Sensitivity studies have been conducted to establish the threshold optical energy required to launch a flyer of sufficient velocity to produce a detonation. The effect of the density of the charge has been investigated and an optimum can be found. PETN is more sensitive than HNS to this stimulus; complete experimental details and results are given.

Isothermal Equations of State of Energetic Materials Using X-ray Diffraction Methods

S.M. Peiris, T.P. Russell

Naval Surface Warfare Center, Indian Head, USA

Introduction

Energetic materials such as explosives and propellants react at high pressure and temperature. Therefore, their reaction rates, energy output and reaction products all depend on the phase or structure of the material at that high pressure and temperature. Good hydrocodes are built on reliable experimental data that are directly measured under the conditions of the reaction, rather than extrapolated from ambient conditions using several assumptions. Therefore, we compress energetic materials to static high pressure in diamond anvil cells, heat them to high temperature using built-in heat coils, and study their high-pressure, high temperature phases and structures using powder x-ray diffraction, Raman and IR vibrational spectroscopy. This presentation will focus on results from the diffraction studies on ammonium perchlorate (AP), FOX-7, NaN_3 and HMX.

The diamond anvil cells used in these studies to generate high pressure are Merrill-Basset cells mounted with Type-IA diamond anvils. The sample is placed in the 0.25-0.5 mm diameter hole drilled in a metal gasket. Finely ground powders of each energetic material are loaded in to the gasket hole, along with an in-situ pressure calibrator. Energy-dispersive and angle-dispersive x-ray diffraction experiments are carried out at the B1 and B2 lines of the Cornell High Energy Synchrotron Source (CHESS), at Cornell University in Ithaca, NY, USA. A solid-state Ge detector or an image plate is used to collect x-ray diffraction patterns for 12-30 minutes at each pressure. The d-spacing (d) of each diffraction peak is estimated and "indexed" according to the JCPDS card for that material [1].

If a diffraction pattern can be indexed to the known structure of that material, average unit cell parameters including unit cell volumes can be obtained. The volume (actually V/V_0, where V_0 is the volume at 1 bar or atmospheric pressure) thus obtained at each pressure is used to determine the compression of the material. Isothermal thermodynamic parameters are calculated by fitting both the Birch-Murnaghan (BM) [2], and Vinet et al.'s Universal (VU) [3], equations of state (EOS) to the data.

Further, the material is compressed and then heated to different constant temperatures. X-ray diffraction patterns obtained at a set high temperature and various pressures yield an Isotherm. Subsequently by setting different temperatures we can obtain isotherms at different temperatures. This method also enables us to calculate thermal expansion of the material under compression at different pressures.

Results

Ammonium perchlorate (NH_4ClO_4 or AP) is THE most widely used energetic material. There are only 3 studies of AP at high pressure and each of these studies report a single phase transition at occurring at different pressures, disagreeing with each other. Our results indicate the existence of two high-pressure phase transitions in AP, which helps eliminate these disagreements. Under hydrostatic conditions, the first transition starts at about 0.9 GPa with the appearance of a few extra peaks within the room-pressure diffraction pattern. The second transition starts at 2.9 GPa with a drop in diffraction intensity followed by an entirely new pattern of diffraction peaks by 3.0 GPa. This new phase above 3.0 GPa is stable to 5.6 GPa. The pressure-volume data obtained to 0.9 GPa were used to generate an isothermal (room temperature) equation of state yielding a bulk modulus of 15.2±0.3 GPa for the ambient-pressure phase.

FOX-7 (diaminodinitroethylene or DADNE) is a new energetic material. Our data indicates that the ambient pressure monoclinic structure of FOX-7 is stable to 4.0 GPa. The pressure-volume data obtained to 4.0 GPa yielded an isothermal room temperature bulk modulus.

We have also studied the β to δ phase transition of HMX using compression to 2.5 GPa and heating to 250°C. We notice that the β to δ phase transition at this pressure, is at a slightly higher

temperature than the 165°C observed upon heating at ambient pressure. All this and data obtained for other compounds will be discussed.

[1] Joint Committee on Powder Diffraction Standards, currently named International Center for Diffraction Data.
[2] Birch, F., *J. Geophys. Res.* **83**, 1257-1268 (1978).
[3] Vinet P., Ferrante, J., Smith, J. R., Rose, J. H., *J. Phys. C: Solid State Phys.* **19**, L467-L473 (1986).

Shock Propagation and Instability Structures in Compressed Silica Aerogels

W. M. Howard, J. D. Molitoris, M. R. De Haven, A. E. Gash, J. H. Satcher

Lawrence Livermore National Laboratory, Livermore, USA

We have performed a series of experiments examining shock propagation in low density aerogels. High-pressure (~100 kbar) shock waves are produced by detonating high explosives. Radiography is used to obtain a time sequence imaging of the shocks as they enter and traverse the aerogel. We compress the aerogel by impinging shocks waves on either one or both sides of an aerogel slab. The shock wave initially transmitted to the aerogel is very narrow and flat, but disperses and curves as it propagates. Optical images of the shock front reveal the initial formation of a hot dense region that cools and evolves into a well defined micro-structure.

Structures observed in the shock front are examined in the framework of hydro-dynamic instabilities generated as the shock traverses the low-density aerogel. The primary features of shock propagation are compared to simulations, which also include modeling the detonation of the high explosive, with a 2-D Arbitrary Lagrange Eulerian hydrodynamics code The code includes a detailed thermochemical equation of state and rate law kinetics. We will present an analysis of the data from the time resolved imaging diagnostics and form a consistent picture of the shock transmission, propagation and instability structure.

The Effect of Al_2O_3 Phase Transitions on Detonation Properties of Aluminized RDX

S.B. Victorov

Moscow State Engineering Physics Institute, Moscow, Russia

Introduction of aluminum into a condensed high explosive (HE) can improve its detonation performance, but modeling this phenomenon encounters a number of difficulties. A detailed review on detonation behavior of aluminized HE is given in [1], the accompanying theoretical difficulties are also discussed there. The key theoretical question is whether or not the Al reacts in the reaction zone or at a later time. We hope that a way, suggested in the present work and derived from thermodynamic computations taking into account a possibility of the Al_2O_3 phase transitions behind the detonation front, will help us answer this key question.

In this work we compute the detonation velocity and other Chapman–Jouguet (CJ) parameters of RDX/Al mixtures by using our thermochemical TDS code.

It is assumed that molecules of fluid detonation products (N_2, N, H_2O, CO_2, CO, NH_3, NO, CH_4, O_2, O, H_2, H, and OH) interact via a spherically symmetric, modified Buckingham (Exp-6) potential. For strongly attracting molecules (H_2O and NH_3), temperature-dependent Exp-6 potentials are used. The like-pair Exp-6 parameters were determined mostly by matching both experimental Hugoniot data and available results of static experiments. Unlike-pair intermolecular interactions are described by non-additive Exp-6 potentials that do not follow classical Lorentz–Berthelot combination rules. The improved

vdW1f model, which is used in this work to describe a multicomponent Exp-6 fluid, is assumed to be enough accurate. The HMSA/MC equation of state (EOS) [2], derived from the hypernetted-mean spherical approximation (HMSA) integral equations for pair distribution functions [3], is employed to calculate the excess thermodynamic properties of an effective vdW1f fluid. This EOS accurately reproduces the results of Monte Carlo and molecular dynamics simulations.

The following six species are considered as possible condensed detonation products of RDX/Al mixtures: graphite and diamond nanoparticles, solid and liquid Al, and solid and liquid Al_2O_3. Carbon nanoparticles are treated by an approach described in [4]. Semi-empirical EOS of condensed Al and Al_2O_3 were calibrated by matching available thermal and shock-wave data. For liquid Al_2O_3 there is a lack of any high-pressure experimental data so that the EOS parameters were chosen to match the density of the known atmospheric isobar as well as high-pressure values estimated from the solid EOS and the melting point data.

The obtained EOS of solid and liquid Al_2O_3 predict that the melting temperature of Al_2O_3 significantly increases as pressure increases. It reaches, e.g., 4400 K at 15.5 GPa (we remind ourselves that the known melting temperature is 2327 K at 1 atm). Hence, detonation of powerful HE may produce the solid Al_2O_3 at high initial densities of HE due to relatively low CJ temperatures and high CJ pressures. The liquid Al_2O_3 may be produced in detonation products at low initial densities of HE, where its CJ temperatures are higher and CJ pressures are lower, and the solid-to-liquid phase transition, i.e. Al_2O_3 melting, may affect the detonation properties at intermediate initial densities of HE.

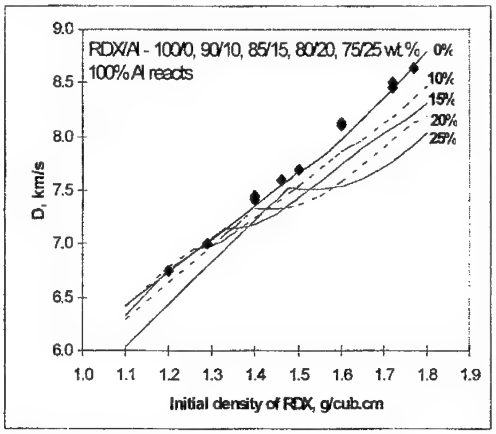

Figure 1. D vs $\rho_{0,RDX}$ for RDX/Al mixtures with different Al content. Points are the experiment for pure RDX. Lines are the results calculated by TDS. Al completely reacts.

Detonation velocities, D, of RDX/Al mixtures with different content of Al (from 0 to 25 wt.%) computed under the assumption of equilibrium (Al completely reacts in the reaction zone) are presented in Fig. 1 as plots vs the initial density of RDX, $\rho_{0,RDX}$. At $\rho_{0,RDX} < \rho_{0,RDX,*}$ (where $\rho_{0,RDX,*} = 1.26$, 1.34, 1.41, and 1.48 g/cm^3 for mixtures containing 10, 15, 20, and 25 wt.% Al, respectively) detonation occurs in the usual (CJ) mode, the detonation products contain liquid Al_2O_3. In the regions $\rho_{0,RDX,*} < \rho_{0,RDX} < \rho_{0,RDX,*}+\Delta\rho_{0,RDX,*}$, the Al_2O_3 phase transition (solidification) in detonation products makes detonation occur in the anomalous mode with the CJ condition failure, much as the graphite-to-diamond transition causes the anomalous detonation mode for carbon-rich HE [5,6]. At $\rho_{0,RDX} = \rho_{0,RDX,*}$ corresponding to the beginning of the anomalous detonation region, the D vs $\rho_{0,RDX}$ slope has a break that could be detected experimentally. In the case of the anomalous detonation, the detonation wave has an unusual two-front structure. The first front (i.e. the detonation front), as it usually is, corresponds to the end of the reaction zone, but in distinction to the usual (CJ) mode of detonation the CJ condition of the

equality between the sound velocity and the local particle velocity is not satisfied here. Nevertheless, the first front propagates stably and its velocity is measured as the detonation velocity.

The detonation products contain the solid Al_2O_3, there is no the liquid Al_2O_3 here. The Al_2O_3 melting begins immediately behind the detonation front. A rarefaction wave behind the detonation front contains the sonic surface (the second front), where the sound velocity is equal to the local particle velocity. The Al_2O_3 melting is finished before the second front and at the sonic surface the detonation products contain the liquid Al_2O_3, there is no the solid Al_2O_3 here. The length of the anomalous detonation region, $\Delta\rho_{0,RDX,*}$, diminishes as the Al content decreases: $\Delta\rho_{0,RDX,*} = 0.07$, 0.11, 0.17, and 0.26 g/cm^3 for mixtures containing 10, 15, 20, and 25 wt.% Al, respectively. At $\rho_{0,RDX} > \rho_{0,RDX,*}+\Delta\rho_{0,RDX,*}$ detonation again occurs in the usual (CJ) mode, the detonation products contain solid Al_2O_3.

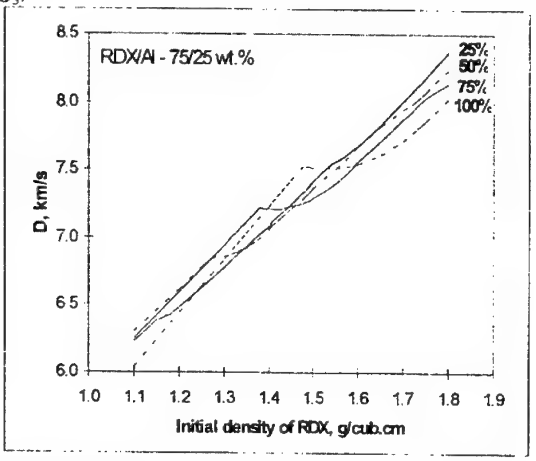

Figure 2. Calculated D vs $\rho_{0,RDX}$ for RDX/Al-75/25 wt.% mixtures. Each curve is labeled with the value of the Al reacted fraction, wt.%. 100% means that Al completely reacts.

The effect of the degree of Al oxidation on the detonation velocity of the RDX/Al-75/25 wt.% mixtures is shown in Fig. 2 for four values of the reacted fraction of Al: 25, 50, 75, and 100 wt.%. The curve labeled 100% corresponds to the complete Al oxidation and is the same as in Fig. 1. Table 1 shows how $\rho_{0,RDX,*}$ decreases and $\Delta\rho_{0,RDX,*}$ diminishes as the reacted fraction of Al decreases.

The presented results make it possible to explain some experimental observations. Firstly, D of high-density HE is known to decrease upon Al introduction, the effect is the more prominent the finer the Al particles, sometimes D reduces even more significantly than upon introduction of inert particles instead of Al. This is due to the formation of solid Al_2O_3 in detonation products. If the Al remains as non-reacted, the decrease of D is much poorer as seen in Fig. 2. The smaller are the Al particles, the easier is their oxidation and the greater is the fraction of solid Al_2O_3. Secondly, in low-density charges, D also diminishes, but to a much lesser extent, the detonation pressure features a weak maximum at 10-15 wt.% Al. This is due to the formation of liquid Al_2O_3 in detonation products of low-density HE, our calculations show that the decrease of D would be much more significant if the products contain the solid Al_2O_3 instead of the liquid one.

We suggest careful experiments on the D vs $\rho_{0,HE}$ dependencies for HE/Al mixtures containing about 20-30 wt.% fine Al particles, choosing explosives with relatively small content of carbon to avoid the significant effect of the graphite-to-diamond transition on D. These experiments should reveal whether a break in the D vs $\rho_{0,HE}$ slope occurs due to the Al_2O_3 phase transition. If such a break will be detected, it means that Al reacts in the reaction zone to a rather large extent, the measured values of $\Delta\rho_{0,HE,*}$ will help us evaluate the Al reacted fraction. If a break in the D vs $\rho_{0,HE}$ slope will not be detected for, say, RDX/Al mixtures, one should choose another HE which differs from RDX in the CJ temperature

values, e.g., nitroguanidine whose CJ temperature is significantly lower than that of RDX. This will allow one to cover a wider range of thermodynamic states in finding the region of the Al_2O_3 phase transition. In any case, such experiments will help us refine the EOS of liquid Al_2O_3 which cannot currently be viewed as enough reliable due to lack of high-pressure data for this species.

Table 1. The location of the beginning, $\rho_{0,RDX,*}$, and the length, $\Delta\rho_{0,RDX,*}$, of the anomalous detonation region for RDX/Al-75/25 wt.% mixtures

Reacted fraction of Al, wt.%	0	25	50	75	100
$\rho_{0,RDX,*}$, g/cm^3	–	1.16	1.28	1.38	1.48
$\Delta\rho_{0,RDX,*}$, g/cm^3	0	0.04	0.10	0.17	0.26

References

1. *Ermolaev B.S., Khasainov B.A., Baudin G., Presles A.-N.* Behavior of aluminum in detonation of high explosives. Surprises and interpretations. // Chem. Phys. Reports. 2000, V. 18, No. 6, P. 1121.

2. *Fried L.E., Howard W.M.* An accurate equation of state for the exponential-6 fluid applied to dense supercritical nitrogen. // J. Chem. Phys. 1998, V. 109, No. 17, P. 7338.

3. *Zerah G., Hansen J.-P.* Self-consistent integral equations for fluid pair distribution functions: Another attempt. // J. Chem. Phys. 1986, V. 84, P. 2336.

4. *Victorov S.B., Gubin S.A., Maklashova I.V.* An equation of state and detonation properties of hydrazine–nitromethane liquid mixtures. // Shock Waves. 2001. To be published (in 2001).

5. *Victorov S.B., Gubin S.A.* Influence of solid carbon phase transitions on detonation parameters of high explosives: anomalous mode of detonation. Int. Conf. «Shock Waves in Condensed Matter», 12–17 July 1998, St.Petersburg, Russia, P. 94.

6. *Victorov S.B., Gubin S.A., Maklashova I.V., Sumskoi S.I.* Structure of rarefaction wave for TNT detonation products. 12th Symp. Combustion and Explosion, 11–15 September 2000, Chernogolovka, Russia, Part 2, P. 88.

7. *Ermolaev B.S., Khasainov B.A., Baudin G., Presles A.-N.* Behavior of aluminum in detonation of high explosives. Surprises and interpretations. // Chem. Phys. Reports. 2000, V. 18, No. 6, P. 1121.

8. *Fried L.E., Howard W.M.* An accurate equation of state for the exponential-6 fluid applied to dense supercritical nitrogen. // J. Chem. Phys. 1998, V. 109, No. 17, P. 7338.

9. *Zerah G., Hansen J.-P.* Self-consistent integral equations for fluid pair distribution functions: Another attempt. // J. Chem. Phys. 1986, V. 84, P. 2336.

10. *Victorov S.B., Gubin S.A., Maklashova I.V.* An equation of state and detonation properties of hydrazine–nitromethane liquid mixtures. // Shock Waves. 2001. To be published (in 2001).

11. *Victorov S.B., Gubin S.A.* Influence of solid carbon phase transitions on detonation parameters of high explosives: anomalous mode of detonation. Int. Conf. «Shock Waves in Condensed Matter», 12–17 July 1998, St.Petersburg, Russia, P. 94.

12. *Victorov S.B., Gubin S.A., Maklashova I.V., Sumskoi S.I.* Structure of rarefaction wave for TNT detonation products. 12th Symp. Combustion and Explosion, 11–15 September 2000, Chernogolovka, Russia, Part 2, P. 88.

LAST MOMENT PAPERS

Shock-Induced Chemical Reaction in Al/S Mixture

A.Yu. Dolgoborodov, M.F. Gogulya, M.N. Makhov, M.A. Brazhnikov, V.E. Fortov*

Institute of Chemical Physics, Moscow, Russia
**Institute for High Energy Densities, Moscow, Russia*

Previous studies have shown that shock-induced reactions in solid materials could occur in microsecond time-scale. This has allowed one to suppose that such reactions could proceed in self-sustaining regime in non-explosive mixtures. Pyrometric studies of high density sulfur mixtures with Al, Mg, Ti showed significant temperature increase (500 K – 1000 K) in comparison with shocked crystal sulfur within first 50 ns of shock loading. For Al/S mixtures, complicated pressure histories were observed. The profiles, possibly classified as detonation-like, could be explained by formation of the products, e.g. aluminum sulfide, with larger specific volume than initial components. Temperature-time histories at contact with LiF windows and pressure-time profiles in bromoform placed behind the Al/S samples (thickness = 3 - 3.5 mm) are shown in Fig. 1 and 2.

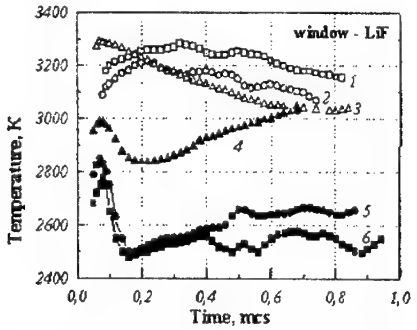

Figure 1. Temperature-time histories at contact Al/S with LiF windows. 1, 6 - Al/S 35/65 P – 33,0 (40,7) GPa; 2, 5 - Al/S 55/45 P – 34.6 (40,3) GPa; 3, 4 - Al/S 75/25 P – 36.4 (39,8) GPa; open symbols Al flake (PP-1), closed - Al coarse (630-1000 μm). P - calculated pressure in incident (reflected) waves without reaction.

There were performed experiments on search of self-sustaining detonation-like regime in Al/S mixture varying both density and components' ratio. It was obtained that, in samples (porosity 7-10%) 40 mm in diameter, shock wave generated by booster charge had decayed within 5 mm of sample thickness. Detonation-like process was observed in Al/S mixture with porosity about 70%. It was initiated by low-dense AP/PMMA mixture in steel tube with internal diameter of 30 mm. Insignificant variation in mixture density or in intensity of initiating pulse resulted to the either shock wave decaying with formation of compacted mixture consisting of products and reagents or to the low-velocity burning. The best result was obtained for pyrotechnic Al powder mixed with sulfur (40/60) at density of 0.72 g/cm^3 when initiated by AP/PMMA (97/3) booster. Measured velocity of the process was 1.3 km/s.

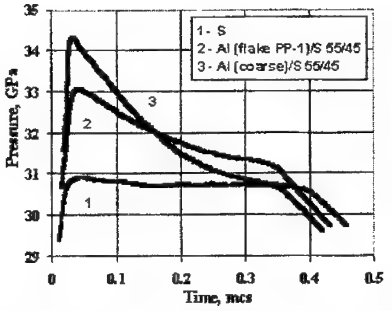

Figure 2. Pressure-time profiles in bromoform placed behind the Al/S samples. (Shock wave created by duralumin flyer plate (velocity = 3.6 km/s, thickness = 2 mm).

Stability of the observed process in Al/S mixture depends on structure and porosity of mixture, sizes of particles, and initiation impulse. It could occur in the narrow limits of variation of mixture density and intensity of initiating impulse. So, on the one hand, weak initiator doesn't generate the necessary amount of reaction centers required for self-sustaining regime; in this case the process would transform to a burning. On the other hand, relatively strong initiating impulse over-compacts the mixture. Thus the conditions for reagents mixing and interaction are degraded. It results to the decrease of energy release and shock wave decaying. The influence of strong initiation is similar to "over-initiation" observed for commercial explosives. Conceptually, the effect of charge density can be explained in the same manner. Its increase results to the enhancement of the shock wave velocity. More powerful shock wave needs for lager energy release that is higher reaction completeness within so-called detonation zone. Effective time of components interaction is limited by the rarefaction arriving to this zone. One can suppose that in this case the effective time will diminish. That means that self-sustaining regime decays. Moreover, density increase deteriorates reagents mixing and reaction growth.

The experiments demonstrate principal ability for detonation-like processes to occur in solid non-explosive mixtures. It is anticipated that experimentation currently in progress will lead to clearing the conditions under which reactions in solids are able to propagate in detonation regime.

Computational Analysis of Actinide and Lanthanide Compressibility and Structure at High Pressures

B.A. Nadykto, O.B. Nadykto

Russian Federal Nuclear Center - VNIIEF, Arzamas-16 (Sarov), Russia

The actinide structure study with both theoretical-computational and experimental methods is being given much attention to. This is because the electronic structure in these elements is most complex and competition between a large number of close energy levels of electrons in atoms of these materials leads to unexpected and frequent changes in material properties under a relatively low external effect.

Much experimental material on compressibility of the materials at high pressures has been accumulated. Experiments on static compression of materials in diamond anvils using synchrotron radiations for x-ray diffraction analysis allowed tracking a change in the crystalline structure with

increasing pressure for many materials. The shock-wave methods continue to provide very useful information on changes in material properties at high pressures.

The analysis of experimental curves $P(\rho)$ detects non-monotonicities which indicate material property changes under pressure. When the material crystalline structure does not change, these non-monotonicities can be explained only with a change in electron structure of solid atoms (i.e. electron redistribution between inner and outer shells). The electron structure can also change with a simultaneous change in crystalline structure (i.e. atom positions in the crystal lattice).

Different behaviors of light actinides (before Am) and heavy actinides (after Am) are attributable to different nature of f electrons in the materials. The high density of light actinides and the parabolic nature of the curve of ionic radii as a function of the atomic number for light actinides are commonly believed to be due to the delocalized nature of 5f electrons in the elements and their involvement in bonding in solid. In heavy actinides, 5f electrons are considered localized (i.e. localized in the inner shell) and making no contribution to the atom bonding in solid.

There is belief that compression of an element with localized 5f electrons leads to their delocalization which should result in a higher equilibrium density and higher bulk modulus. In addition, the compression is believed to lead to energy band expansion and prevalence of high-symmetry crystalline structures.

The available experimental data seems to suggest that this explanation is inadequate. ε-phase plutonium clearly contradicts this explanation, when the bulk modulus decreases by a factor of 4 with increasing density compared to the previous phase (δ phase). Another example is the recent experimental data on americium compression by a high pressure up to P=100 GPa [1]. The transition from phase AmI to phase AmII and AmIII leads to a change in the slope of P(V) curve corresponding to a severe decrease in the bulk modulus (more than by a factor of 2) instead of the predicted increase and to increase in equilibrium volume for these phases. Besides, despite the different crystalline structure of the phases AmII and AmIII, their P(V) curve can be described with a single curve with the same bulk modulus, B_0=13.3 GPa, and equilibrium density, ρ_n=11.9 g/cm^3. An abrupt increase in the bulk modulus in americium occurs in the transition to phase AmIV. Most experimental data points for this phase lie on the computational curve with B_0=82 GPa and ρ_n=18.7 g/cm^3. However, three upper experimental data points abruptly deviate from the computational curve and are described with parameters B_0=340 GPa and ρ_n=24.2 g/cm^3. This change suggests a significant rearrangement of the electron structure of the outer electron shell under pressure. Note that the experimental data on thorium and uranium compressibility also indicate existence of a similar hard phase (with B_0=400 GPa) at pressure higher than 100 GPa.

Lanthanides also display a transition under pressure to other electron states, and the transitions can hardly be explained by exclusive influence of f electrons. Experimental data [2] infers that at pressure higher than 100 GPa in cerium there is high-pressure phase with B_0=316 GPa and ρ_n=11.5 g/cm^3 (with atomic volume of cerium being close to that of thorium and uranium high-pressure phases). A qualitatively similar behavior can be observed in barium, in which there are no f electrons, but which undergoes several phase transitions, including without crystalline structure change, under pressure. The appearance of hard phases at high pressures is characteristic of many elements, and here there is no any specific effect of f electrons.

References

1. Lindbaum A., Heathman S., Litfin K. at al. // Phys. Rev. 2001. Vol. B63. 214101.
2. Vohra Y.K., Beaver S.L., Akella J. et al. // J. Appl. Phys. 1999. Vol. 85, N 4. P. 2451.

A Modified Taylor Impact Test in Combination with Numerical Simulations – a New Approach for Obtaining Material Properties under High Dynamic Loads

I. Rohr, H. Nahme, K. Thoma

Fraunhofer Institut für Kurzzeitdynamik, Ernst-Mach-Institut, Freiburg, Germany

There is an increased demand for improved material models and their input data when modelling materials under static and dynamic loads. The knowledge of exact model parameters over a broad strain rate range is therefore a case of absolute necessity. One technique often used for evaluation and validation of model parameters for numerical models is the taylor impact test where strain rates in excess of 10^4 s^{-1} and high strains can occur. In this test a sample which has typically cylindrical symmetry is fired against a rigid wall. Normally from post-impact measurements of the deformed specimen (e.g. geometric size of the outer shape, micro-hardness measurements) conclusions about the material data as e.g. dynamic yield stress are drawn. Nevertheless it has to be mentioned that these post-impact measurements can be very complicated (sample have to be catched softly to give no secondary deformation for inverse tests, very exact measurement of micro-hardness, final length etc.) and gives only informations taken from the final state of the sample and not during the impact process.

In this paper special attention is given to a modified taylor impact test with VISAR (Velocity Interferometer System for Any Reflector) - technique which allows us to determine dynamic material data due to a measurement of the rear side movement of the sample. In comparison to common taylor impact test analysis the major advantage of the method used here is that we measure the dynamic material data from the velocity-time plot which is recorded instantaneous during deformation process and not after the whole impact process from the distorted sample. Therefore additional advantages in this test method arise when it is combined with numerical simulations: With the measured velocity-time signal of the elastic wave propagations at rear side and the final shape of the specimen enhanced validation calculations of the conducted test can be made. This can be used for a better evaluation and development of the model used in the numerical simulations.

In this paper a modified Taylor impact test with VISAR-technique is presented. The rear side movement of a high strength steel 35 NiCrMoV109 under impact loading was measured by means of this modified taylor impact test with VISAR-technique. The investigated impact velocities were 214 - 611 m/s. The investigated velocity range covers both, pure elastic-plastic deformation and elastic-plastic deformation with failure yielding to a shortening of the cylindrical sample. The dynamic yield stress, strain and strain rate have been determined according to elasto-plastic theory. The experimental data were used in hydrocode simulations to reproduce the experimental tests. A numerical variation of model parameters in the simulations show a high sensitivity of the calculated velocity-time profile which is useful for model calibrations. This leads to the conclusion that this modified taylor test in combination with numerical simulations is an important experimental tool for determination of dynamic material data on the one hand and for model improvement and development on the other hand.

About the Mechanical Stability of Crystalline Systems

B.S. Bertyaev, V.I. Igoshin*

Samara State Technical University, Samara, Russia
** Physical Institute (Samara Branch) of Russian Academy of Sciences, Samara, Russia*

The stability of the "crystal-boundary" system is considered in the framework of the two-level model [1] with Fe and carbon steel as the examples under the conditions of the shock-and-wave application of load. As the subsystems forming the whole system the α-phase with its boundary and the γ-phase are considered. The internal pressure in the subsystems under the pulsed loading has been calculated. The calculations show that the pressure of repulsion between the particles in the α-phase 6.7 times as large as the pressure on the boundary in the region of temperatures of the phase transition in Fe and carbon steel [2]. Under the conditions of the pulsed loading these values become smooth. It follows from the balance equation regarding the static pressure in the "crystal-boundary" system that as the source of the negative pressure in crystalline α-phase serves the boundary. It is worth to note that the pressure of repulsion between the particles of the crystalline α-phase is higher than the pressure of contraction on the side of the boundary.

The analysis of the balance equation regarding the pressure on the boundary shows that as the source of the negative pressure on the boundary serves the crystalline phase. The negative pressure on the boundary from the side of the crystal of the α-phase is higher, than the value of the repulsion pressure

between the particles on the boundary. Therefore, that makes sense to assume the possibility of overlapping the external electronic shell, the collectivization of electrons and the appearance of the conduction. It is indirectly confirmed by the change of resistance in the manganin sensors under the pulsed loading.

In the framework of the model under consideration the equation for compressibility B and modulus of the all-round compression M has been obtained for the α -phase, boundary and γ -phase, namely:

$$B=M^{-1}=\frac{d\zeta}{dp}-\frac{v}{kT}(\zeta+\zeta^2),$$

where ζ is the relative percentage of the vacant volume, p is the internal thermal pressure in the subsystems, v is the volume per one particle, k is the Bolzman constant, T is the temperature of the system. The results of calculation of the values of B and M for α -phase (α index), boundary (k index) and γ -phase (γ index) in Fe and Y8 steel are shown in the Table 1.

It turned out, that the compressibility of the boundary 15.5-16.5 times as large as the compressibility of the crystalline α -phase. This circumstance is not taken into consideration in the modern theoretical models. It is revealed that mechanical stability of the "crystal-boundary" system is determined by the interaction between atoms of the crystalline phase and atoms of the boundary. The lack of the stability and the air of the transformation are stipulated by the nature of transition of particles from one subsystem to the second subsystem and depend on the value and sign of the outer pressure.

Table 1. The values of $B\alpha$, B_k, $B\gamma$, $M\alpha$, M_k, $M\gamma$ in Fe and Y8 steel

Substance	$B\alpha$, Pa^{-1}	B_k, Pa^{-1}	$B\gamma$, Pa^{-1}	$M\alpha$, Pa	M_k, Pa	$M\gamma$, Pa
Fe	$9.517\ 10^{-12}$	$1.57\ 10^{-12}$	$3.156\ 10^{-12}$	$1,05\ 10^{11}$	$6.37\ 10^{9}$	$3.168\ 10^{10}$
Y8 steel	$1.398\ 10^{-11}$	$2.19\ 10^{-10}$	$4.169\ 10^{-11}$	$7.15\ 10^{10}$	$4.566\ 10^{9}$	$2.40\ 10^{10}$

References

1. Bertyaev B.I. Bulletin of Samara State Technical University, Series: Physico-mathematical Sciences, Issue 9, Samara: SamSTU, 2000, pp. 191-196.
2. Bertyaev B.I. International conference: III Kharitons topical scientific Readings "Extreme states of substance. Detonation. Shock waves", Sarov, Russia, 2001, pp.92-93.

Bistability of Polyatomic Molecules Internal Degrees of Freedom States in the Relaxation Zone behind Shock and Detonation Waves Front

L.V. Katkovsky, A.I. Birjukov*

Institute of Applied Physical Problems, Minsk, Belarus
** Institute of Information, Moscow, Russia*

It is well known, that the energy exchange processes which include highly excited vibrational states of molecules influence the structure of shock and detonation waves in gases and solids. Intra- and intermolecular relaxation affects as on the distribution function of vibrational states of final explosive products, and on macro parameters (the decomposition and chemical reaction rate constants depend on temperature and pressure) of the decomposition of molecular products of explosion in a detonation wave. The appearance of relaxation instability in reaction zone behind shock and detonation waves is connected with the formation of products with a superequilibrium energy content of vibrational states.

By the numerical modeling we have revealed the phenomenon of the bistability of vibrational states in polyatomic gas (particularly, in mixture of CO_2 and N_2), if alongside with relaxation processes, the resonance absorption and multiple scattering of radiation in molecular rotational-vibrational bands is taken into account. The indicated phenomenon consists of the fact, that the quasistationary distributions of molecules vibrational states (or vibrational temperatures) depend on the direction of approaching to a

quasi-stationary state: from greater densities to smaller ones or in the opposite direction (shock wave or rarefaction wave, for example).

In the first case (moving from greater densities to smaller ones) the spatial profiles of vibrational temperatures are monotonic and correspond to excitation both coupled, and antisymmetric modes (in case of CO_2 and N_2 molecules), in the second case (moving from smaller densities to greater ones, this is as in shock wave) the spatial profiles of vibrational temperatures in some modes (in the coupled mode of CO_2, for example) are nonmonotonic and correspond to deexcitation (in relation to translational temperature). Furthermore, in the second case, the further successful increase of matter density behind shock wave front, leads, at definite density value, to the jump changes of vibrational state spatial distribution temperatures with subsequent smooth relaxation to equilibrium distribution. It means, that second type solution can pass into the equilibrium solution only through nonequilibrium "phase transition".

The phenomenon mentioned above arises due to strong nonequilibrium states in the system "radiation - substance", appearance of nonlinear effects, which lead to the bistability of vibrational temperature distributions. The detected phenomenon can play an important role for description of energy exchange processes between translational and internal degrees of freedom of molecules and analysis of flow dynamics behind shock and detonation waves front.